SYNTHESIS OF SOME NEW PYRROLE DERIVATIVES AND INVESTIGATION OF THEIR BIOLOGICAL EFFECTS

Master's Degree Thesis

Shoruq Ahmed Omar NAJI

Eskişehir 2023

SYNTHESIS OF SOME NEW PYRROLE DERIVATIVES AND INVESTIGATION OF THEIR BIOLOGICAL EFFECTS

Shoruq Ahmed Omar NAJI

MASTER'S DEGREE THESIS

Department of Pharmaceutical Chemistry

Supervisor: Prof. Dr. Ahmet Çağrı KARABURUN

Eskişehir

Anadolu University

Graduate School of Health Sciences

June 2023

FINAL APPROVAL FOR THESIS

This thesis titled "Synthesis of Some New Pyrrole Derivatives and Investigation of Their Biological Effects" has been prepared and submitted by Shoruq Ahmed Omar NAJI in partial fulfillment of the requirements in "Anadolu University Directive on Graduate Education and Examination" for the degree of Master of Science (MS) in Pharmaceutical Chemistry Department has been examined and approved on 29/05/2023.

Committee Members		**Signature**
Member (Supervisor)	: Prof. Dr. Ahmet Çağrı KARABURUN	……
Member	: Prof. Dr. Şeref DEMİRAYAK	……
Member	: Prof. Dr. Leyla YURTTAŞ	……

Prof. Dr. Gülşen AKALIN ÇİFTÇİ

Director

Graduate School of Health Sciences

ÖZET

YENİ BAZI PİROL TÜREVLERİNİN SENTEZİ VE BİYOLOJİK ETKİLERİNİN İNCELENMESİ

Shoruq Ahmed Omar NAJI
Farmasötik Kimya Anabilim Dalı
Anadolu Üniversitesi, Sağlık Bilimleri Enstitüsü, Haziran 2023
Danışman: Prof. Dr. Ahmet Çağrı KARABURUN

Enflamatuvar tepki, potansiyel zarara karşı çok önemli bir koruyucu mekanizma görevi gören karmaşık bir biyolojik süreçtir. Bu sürecin merkezinde prostaglandinleri sentezleyen siklooksijenaz (COX) enzimleri, özellikle COX-1 ve COX-2 alttipleri rol almaktadır. Bilimsel bilgiyi ilerletme arayışımızdaki bu çalışmada, COX enziminin potansiyel inhibitörleri olarak yeni pirol türevlerini tasarlayıp sentezleyerek bu alana katkıda bulunmayı hedefledik. Amaç, enzimin aktivitesini modüle etmek için daha güçlü moleküller keşfetmektir. Yaklaşık 3000 bileşikten oluşan sentez kütüphanemizi tarayarak olası aktif maddeleri kısa zamanda ve etkin şekilde belirledik. Bunun yanı sıra sentezlenen bileşikler ve (COX-1/-2) enzimleri arasındaki karmaşık etkileşimi daha derinden anlamak amacıyla gelişmiş yerleştirme çalışmaları ve kantitatif yapı-etki ilişki (QSAR) analizlerinden yararlandık. Sonuç olarak elde ettiğimiz QSAR verileri doğrultusunda sentez yolumuzu belirledik. Özellikle, **5e** ile birlikte **5b**, **4g**, **4l**, **4h** ve **4k** bileşikleri, COX enzim aktivitesinin güçlü inhibitörleri olarak tespit edilmiştir. Bu en son bulguların, yalnızca bilimsel keşiflerin geleceğine yeni bir bakış sağlamakla kalmayıp, aynı zamanda COX enzim inhibitörleri olarak pirol türevlerini kullanan yeni anti-enflamatuvar ilaçların potansiyel gelişimine yönelik daha fazla araştırmanın yolunu açacak önemli bir katkısı olacağını düşünüyoruz.

Anahtar Sözcükler: COX-1 ve COX-2 inhibitörleri, Pirol türevleri, Antienflamatuvar maddeler, Valide moleküler docking çalışmaları, QSAR.

ABSTRACT

SYNTHESIS OF SOME NEW PYRROLE DERIVATIVES AND INVESTIGATION OF THEIR BIOLOGICAL EFFECTS

Shoruq Ahmed Omar NAJI

Department of Pharmaceutical Chemistry

Anadolu University, Graduate School of Health Sciences, June 2023

Supervisor: Prof. Dr. Ahmet Çağrı KARABURUN

The inflammatory response is a complex biological process that acts as a crucial protective mechanism against potential harm. At the center of this process, cyclooxygenase (COX) enzymes that synthesize prostaglandins, especially COX-1 and COX-2 subtypes, play a significant role. In this work, as aimed to advance scientific knowledge, to contribute to this field, new pyrrole derivatives were designed and synthesized as potential inhibitors of the COX enzyme. Our goal was to discover more potent molecules to modulate the enzyme's activity. By scanning our synthesis library consisting of approximately 3,000 compounds, we identified potential active substances in a short time and effectively. Additionally, we benefited from advanced docking studies and quantitative structure-activity relationship (QSAR) analyses to further understand the complex interaction between the synthesized compounds and (COX-1/-2) enzymes. As a result, we determined our synthesis path in line with the QSAR data we obtained. In particular, compounds **4g**, **4h**, **4k**, **4l**, **5b** and **5e** have been identified as potent inhibitors of COX enzyme activity. We believe that these latest findings will make an important contribution, not only providing a new perspective for scientific discoveries, but also paving the way for further research towards the potential development of new anti-inflammatory drugs using pyrrole derivatives as COX enzyme inhibitors.

Keywords: COX-1 and COX-2 inhibitors, Pyrrole derivatives, Anti-inflammatory agents, Validated docking studies, QSAR.

ACKNOWLEDGEMENT

I would like to take this opportunity to offer my most sincere appreciation to everyone who assisted me in achieving the goal of successfully defending my thesis. To begin, I would like to express my deepest gratitude to ALLAH for all of the blessings that have assisted me in reaching this point in my life. Without these blessings, I would not be where I am today.

My advisor, Professor Dr. Ahmet Çağrı KARABURUN, has been an unwavering resource for both direction and support throughout the entirety of my research, and I would like to take this opportunity to express my gratitude to him. It was of great assistance to me that he gave me permission to take part in the Erasmus program in Italy. During my time there, I was able to expand my knowledge of computational research into drug design and development while working under the supervision of Professor Maraingela Agamennone. This was possible thanks to the opportunity I had during my time there. In particular, I would like to call attention to the fact that she was able to supply me with the data that I required.

Sincere gratitude is extended to my colleague, Dr. Asaf Evrim EVREN, who has been of great assistance to me in a variety of different capacities throughout the course of my work. In each of these roles, I've been able to accomplish much more than I could have on my own. Throughout the entirety of the work that I have been doing, he has been an extremely helpful resource for me. I also want to thank Associate Professor Dr. Begüm Nurpelin SAĞLIK for her work on biological studies. I want to thank Mrs. Betül AYDIN for her help with chemical analysis of the manufactured products.

I would like to take this opportunity to thank YTB for providing me with a scholarship that enabled me to earn my master's degree. Before I go much further, I want to express my most heartfelt gratitude to my sister, Asil NAJI, whose unwavering support has served to serve as a driving force in keeping me motivated throughout the entirety of this journey. For inspiring me to continue my education and for supporting me as I work to make a name for Palestine in the academic field during my academic journey outside, I have my MOTHER to thank more than anyone else. I have the utmost debt of gratitude toward her. In closing, I would like to extend my heartfelt appreciation to every single member of my family for the unflinching love and support they have shown me throughout my life.

29/05/2023

STATEMENT OF COMPLIANCE WITH ETHICAL PRINCIPLES AND RULES

I hereby truthfully declare that this thesis is an original work prepared by me; that I have behaved in accordance with the scientific ethical principles and rules throughout the stages of preparation, data collection, analysis and presentation of my work; that I have cited the sources of all the data and information that could be obtained within the scope of this study, and included these sources in the references section; and that this study has been scanned for plagiarism with "scientific plagiarism detection program" used by Anadolu University, and that "it does not have any plagiarism" whatsoever. I also declare that, if a case contrary to my declaration is detected in my work at any time, I hereby express my consent to all the ethical and legal consequences that are involved.

Shoruq Ahmed Omar NAJI

TABLE OF CONTENTS

LIST OF TABLES

Page

LIST OF FIGURES

Page

LIST OF ABBREVIATIONS

ADME	: Absorption, distribution, metabolism, elimination
AA	: Arachidonic acid
^{13}C-NMR	: Carbon nuclear magnetic resonance
COX	: Cyclooxygenase
DMSO	: Dimethyl sulfoxide
DMSO-d_6	: Deuterated dimethyl sulfoxide
ddH_2O	: double-distilled water
Ex/Em	: Fluorescence excitation/emission
GI	: Gastrointestinal
HRMS	: High resolution mass spectroscopy
HBA	: Hydrogen bond acceptor
HBD	: Hydrogen bond donor
THF	: Tetrahydrofuran
TLC	: Thin layer chromatography
TMS	: Tetramethylsilane
UV	: Ultraviolet light
Log S	: Aqueous solubility
SI	: Selectivity index
m	: Multiplet
M.P.	: Melting point
m/z	: Mass/charge
TXA_2	: Thromboxane A_2
PGH_2	: Prostaglandin H_2
HHT	: Hydroxyheptadecatrienoic acid
MW	: Molecular weight
PGI_2	: Prostaglandin I_2
LOX	: Lipo-oxygenase
No. V	: Number of Violations (Lipinski's rule)
HTS	: High throughput screening
PNS	: Peripheral nervous system

ppm	: Part per million
q	: Quartet
PDB	: Protein Data Bank
RT	: Room temperature
SD	: Standard deviation
t	: Triplet
d	: Doublet
IR	: Infra-red
IT	: Ion trap
TPSA	: Topological polar surface area
IUPAC	: International Union of Pure and Applied Chemistry
J	: Coupling constant
LCMS	: Liquid chromatography-mass spectrometry
Log P	: Octanol/water partition coefficient
DLS	: Drug-likeness score
ESI+	: Electrospray ionization- positive ion mode
pIC_{50}	: The negative log of the IC_{50} value
RMSD	: Root Mean Square Deviation
IFD	: Induced-Fit Docking
IC_{50}	: Inhibition concentration
NSAIDs	: Non-steroidal anti-inflammatory drugs
PGs	: Prostaglandins
^{1}H-NMR	: Proton nuclear magnetic resonance
RDD	: Rational drug design
SAR	: Structure activity relationship
TLC	: Thin layer chromatography
3D	: Three dimensions
2D	: Two dimensions

1. INTRODUCTION

Inflammation is a crucial process that helps defend the body fight off injuries or microbial infections. The immune response is a crucial mechanism that facilitates the elimination of harmful stimuli and promotes the healing of injured tissues. Acute inflammation is a component of the adaptive immune system, which serves as the first line defense against foreign invaders and potentially harmful molecules. However, chronic inflammation can result from a variety of diseases, including cancer, progressive neurological disorders, and heart disease [1]. The four well-known symptoms of inflammation are redness, pain, swelling, and heat. Chemical mediators released by the circulatory system, inflammatory cells, and injured tissues support the inflammatory response, including vasoactive amines, peptides, and eicosanoids [2]. The enzyme cyclooxygenase metabolizes arachidonic acid (AA), which also participates in the production of of proinflammatory prostaglandins (PGs). PGs sensitize nociceptors and nerve endings in the periphery, sending pain signals to the brain. Prostaglandins such as prostaglandin E2 increase the permeability of blood vessels and magnify the effects of other inflammatory mediators, causing hyperalgesia and localized inflammation by activating afferent C fibers, leading to increased blood flow and localized edema resulting from acute inflammation [3]. Prostaglandins are also involved in the regulation of blood flow to the kidneys, protection of the stomach lining, and prevention of excessive bleeding by stimulating platelet aggregation (Figure 1.1). The underlying biochemical mechanism of action for both the therapeutic effects and side-effects of NSAIDs is the blocking of cyclooxygenase [4].

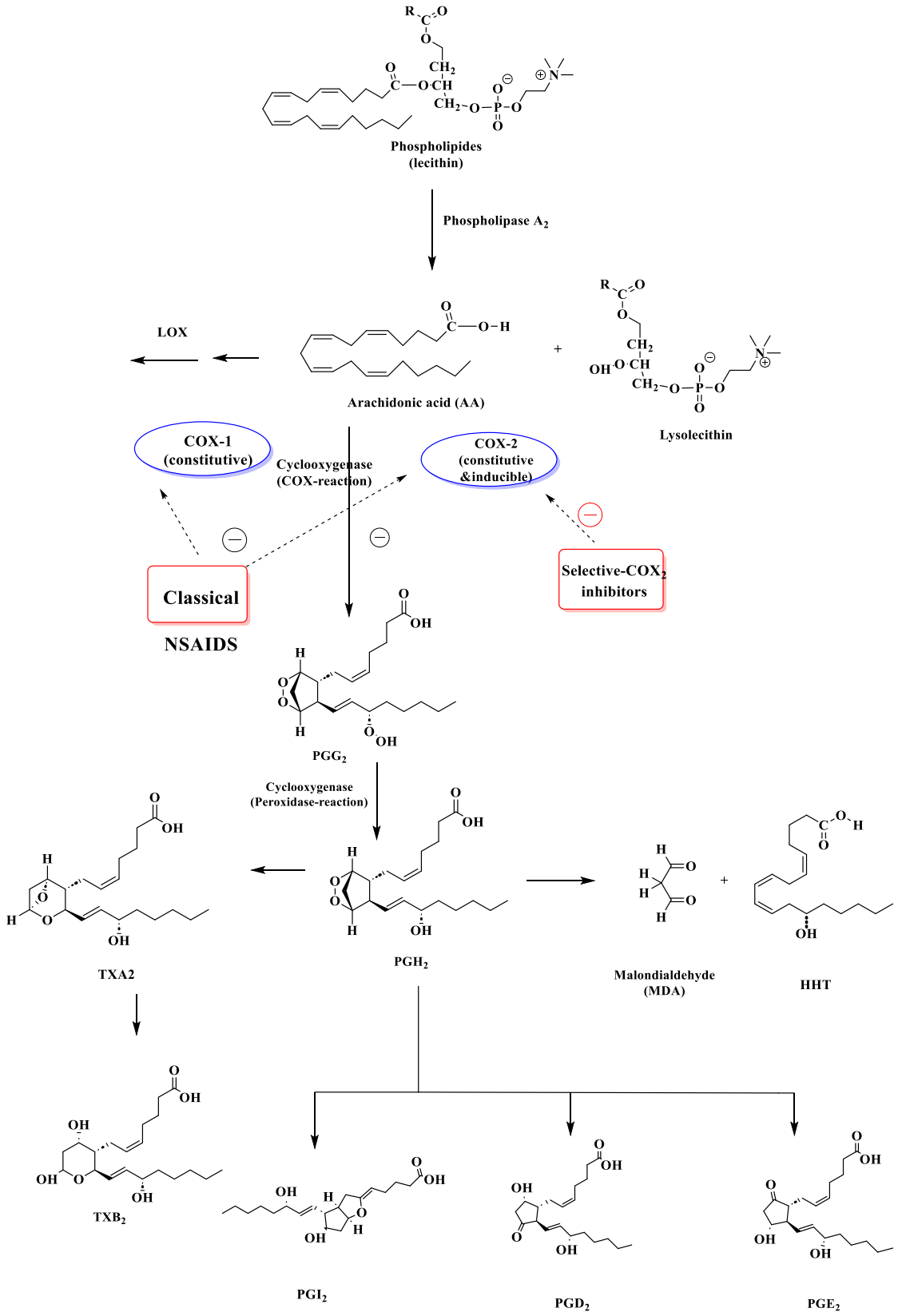

Figure 1.1. *Simplified arachidonic acid cascade and roles of COX-1 and COX-2*

During the early 1990s, a research team led by Needleman, Simmons, and Herschman discovered an inducible variants of the COX-1 and COX-2 isoforms which they resposible to convert arachidonic acid into related prostaglandins [5, 6]. While COX-1 is always present and involved in homeostatic processes, The expression of COX-2 is stimulated in response to physiological stimuli and plays a role in pain and inflammation mediation. Both COX-1 and COX-2 are inhibited by Nonsteroidal anti-inflammatory drugs (NSAIDs), which results in anti-inflammatory and analgesic effects. While COX-2 inhibition is necessary for NSAIDs to exert their therapeutic effects, COX-1 inhibition leads to dangerous gastrointestinal complications, such as Lesions and hemorrhage, which can be fatal if untreated. A higher risk of morbidity may be present in patients with these lesions. The hypertensive and renal side effects of NSAID use are particularly dangerous for patients with impaired renal function. A decrease in prostaglandin production, which regulates the flow of blood through the kidneys, can lead to water retention, hypertension, and even renal failure. Additionally, NSAIDs cause bronchoconstriction, which can result in asthma attacks. This effect is brought on by a switch in metabolism from the cyclooxygenase pathway to the 5-lipoxygenase pathway, which results in less PGE2 (a substance that dilates the airways) being produced. When the 5-lipoxygenase pathway rather than the obstructed cyclooxygenase pathway is used to metabolize arachidonic acid, leukotrienes, which are bronchoconstrictors, are created [7, 8].

In fact, minor lesions or more serious accidents like bleeding, perforation, or obstruction result from blocking COX-1, which Its expression is an innate characteristic of the gastric mucosa It is involved in the generation of prostanoids that promote gastric mucosal protection [9]. Researchers have created drugs that specifically inhibit COX-2 activity and introduced to the market as a means of avoiding the potential for adverse effects caused by inhibiting COX-1. However, rofecoxib and valdecoxib were taken off the market due to an exponential increase in thrombotic events with prolonged use [10, 11]. However, some evidence has explored the chemical structure of rofecoxib to the establishment of cardiac side effects. Rofecoxib's propensity to generate a reactive metabolite that can react with the nucleophilic groups of a wide variety of biological molecules to cause structural damage to cells raises the possibility that adverse cardiac events are not a class-related side effect [12].

In light of these issues, scientists are working hard to develop new NSAIDs with the same anti-inflammatory and analgesic effects as existing ones, but without the associated side effects. This research is crucial because NSAIDs are frequently utilized to treat patients with chronic painful symptoms or inflammation conditions. However, because of the risks of long-term use, it is essential to identify less risky alternatives [13, 14]. More effective oxide (NO) donors (NO-releasing coxib) less side effect on gastrointestinal system (GI) and improved cardiovascular effects have been recently the subject of invistigation [15].

1.1. Breaking news about the development of NSAIDs

NSAIDs have been used as first-line drugs for pain and inflammation since 1897. NSAIDs like phenylbutazone and indomethacin have a long history of study and development; for example, JR Geigy discovered phenylbutazone in 1946 and Merck & Co discovered indomethacin in the 1960s [16]. Phenylbutazone used to be widely prescribed, but its serious side effects, including agranulocytosis and bone marrow suppression, peptic ulcers, and bleeding, led to its demise [17]. The United Kingdom is credited with developing ibuprofen in the 1950s and 1960s. After aspirin [18], it was the second NSAID to be made available without a prescription. The success of ibuprofen prompted many drug companies to investigate and develop new NSAIDs with a wide range of chemical and biological properties. Some conventional NSAIDs, as depicted in Figure 1.2, inhibit both COX-1 and COX-2, two distinct forms of cyclooxygenase, which has a number of drawbacks, including gastrointestinal and ulcerogenic side effects, which restrict their use [19].

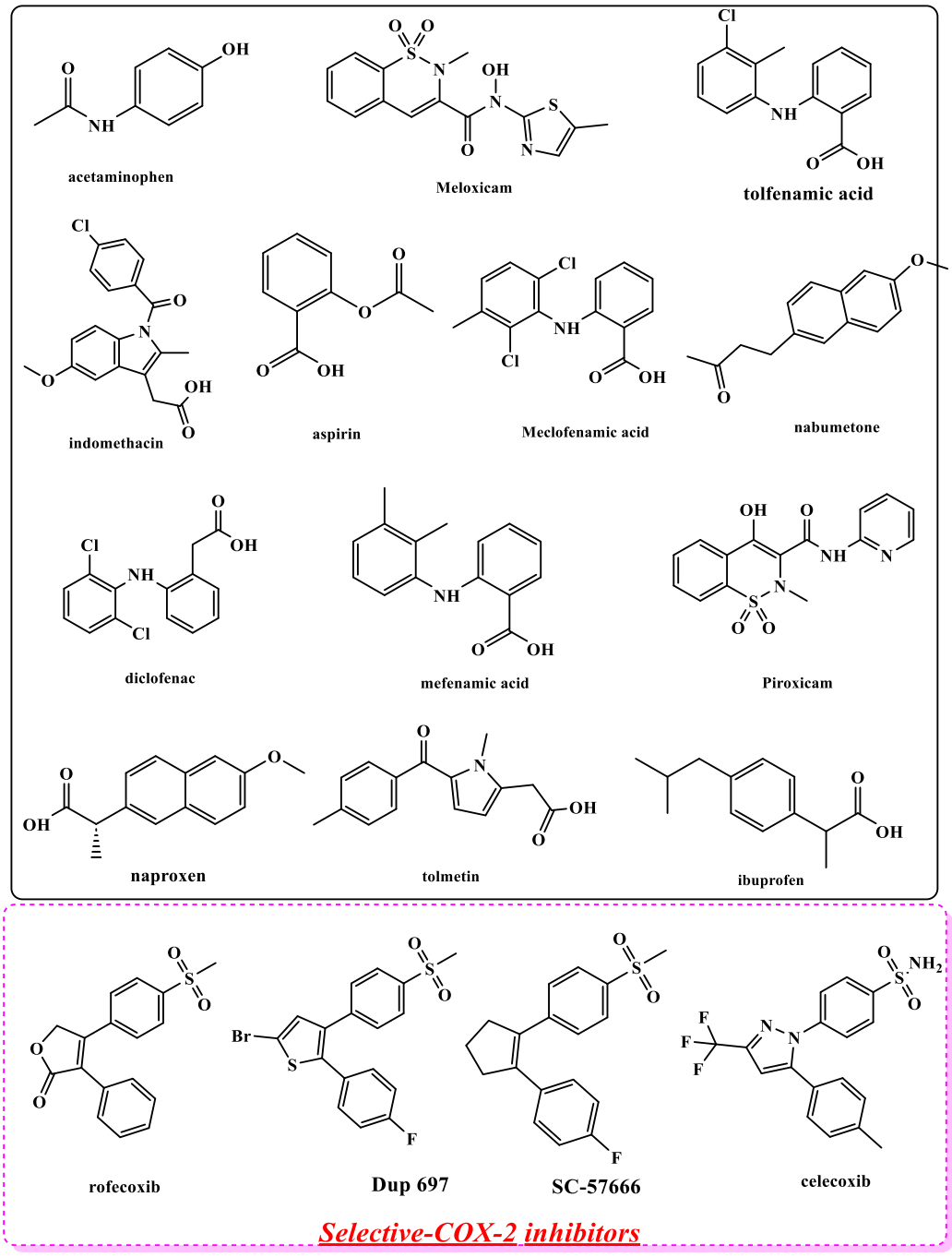

Figure 1.2. *Structure of some clinically approved NSAIDs*

In fact, it is challenging to create drugs that specifically target COX-2 without affecting COX-1, due to their shared cellular expression and sequence homology [20]. New drug candidates can be effectively designed through molecular hybridization. Celecoxib and rofecoxib are currently used as COX-2 inhibitors, but they both have negative effects on the heart [21]. Common NSAIDs with a pyrrole nucleus at their structure are of particular interest [22, 23]. Tolmetin, ketorolac, indomethacin,

acemetacin, and etodolac are all pyrrole nucleus moieties that fall into this category [24, 25]. These compounds inhibit the production of prostaglandins by blocking either COX-1 or COX-2. A few examples of these compounds' structures are shown in Figure 1.3.

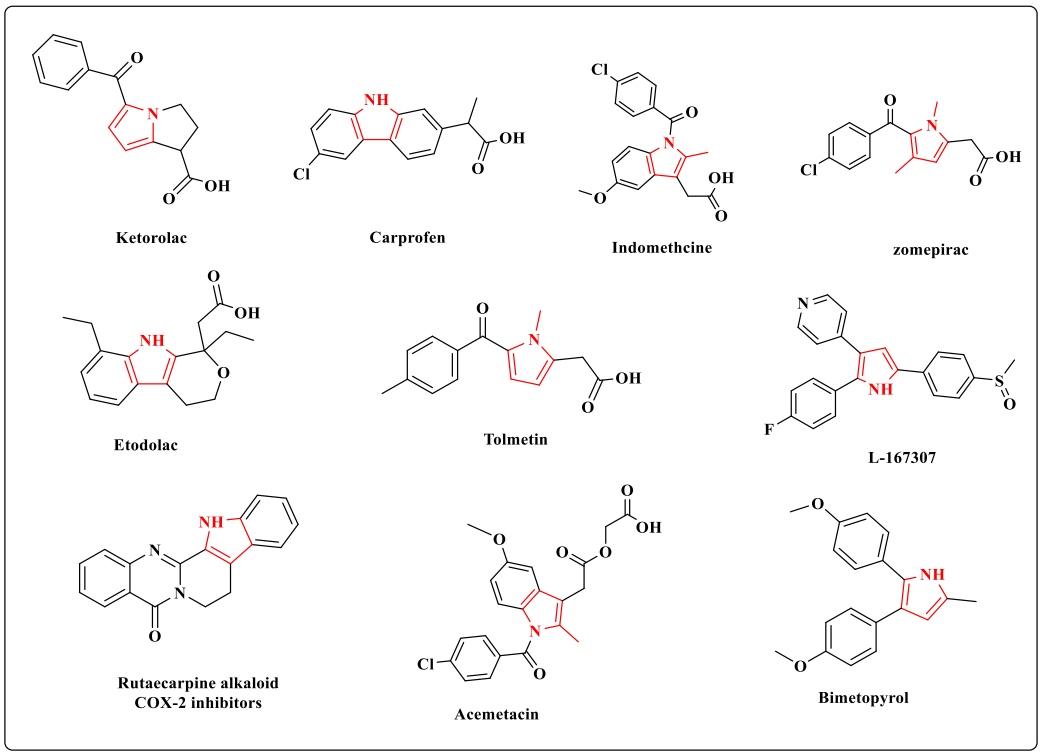

Figure 1.3. *NSAIDS containing pyrrole nucleus moieties*

Two well-known pyrrolylacetic acid-derived NSAIDs include tolmetin and zomepirac, with IC_{50} values of 2.1 μM and 1.2 μM for human COX-2, respectively. Despite their usefulness, their potential for inducing long-term side effects means they should be used with caution [26, 27]. Pharmaceutical companies make extensive use of N-pyrrolcarboxylic acids because of its many beneficial biological properties and because some of its compounds have been identified as highly effective COX-2 inhibitors [24, 28]. Recently, several studies have been published describing the development, synthesis, and anti-inflammatory efficacy of a new class of anti-inflammatory agents containing pyrrole carboxylic acid with application to COX inhibitors. We set out to develop COX-1/COX-2 inhibitors that struck a balance between the two enzymes by fusing the structural features of conventional COX-2 inhibitors including the key chemical ingredients for inhibiting COX-1.

Given the known anti-inflammatory strength of zomepirac and tolmetin, identified by the presence of pyrrolylarylketone (Figure 1.3), and the selective COX-2 inhibition of 1,2-diaryl pyrroles (Figure 1.2), our research efforts were aimed at developing a method for producing substituted 2-[3-(Ethoxycarbonyl)-2-methyl-5-(substituted phenyl)-1*H*-pyrrol-1-yl] alkanoates (Figure 1.4). Our attention was directed towards design, synthesis, and evaluation of novel pyrrol carboxylic acid derivatives, which possess both an acidic group for anti-inflammatory effects and 2-methylpyrrole pharmacophores that act as COX inhibitors. We aimed to investigate the effect of the substituted phenyl group, taking into consideration its significant size and ability to interact with the hydrophobic pocket. Docking studies were conducted to investigate the anti-inflammatory activity of the synthesized compounds and understand how they might bind to the COX-1 and COX-2 active sites. Additionally, we employed FB-QSAR to establish the relationship between inhibitory activity and 3D pharmacophoric characteristics, thus providing valuable insights for the development of COX-1 and COX-2 inhibitors. Figure 1.4 illustrates our meticulously devised approach for the targeted compounds.

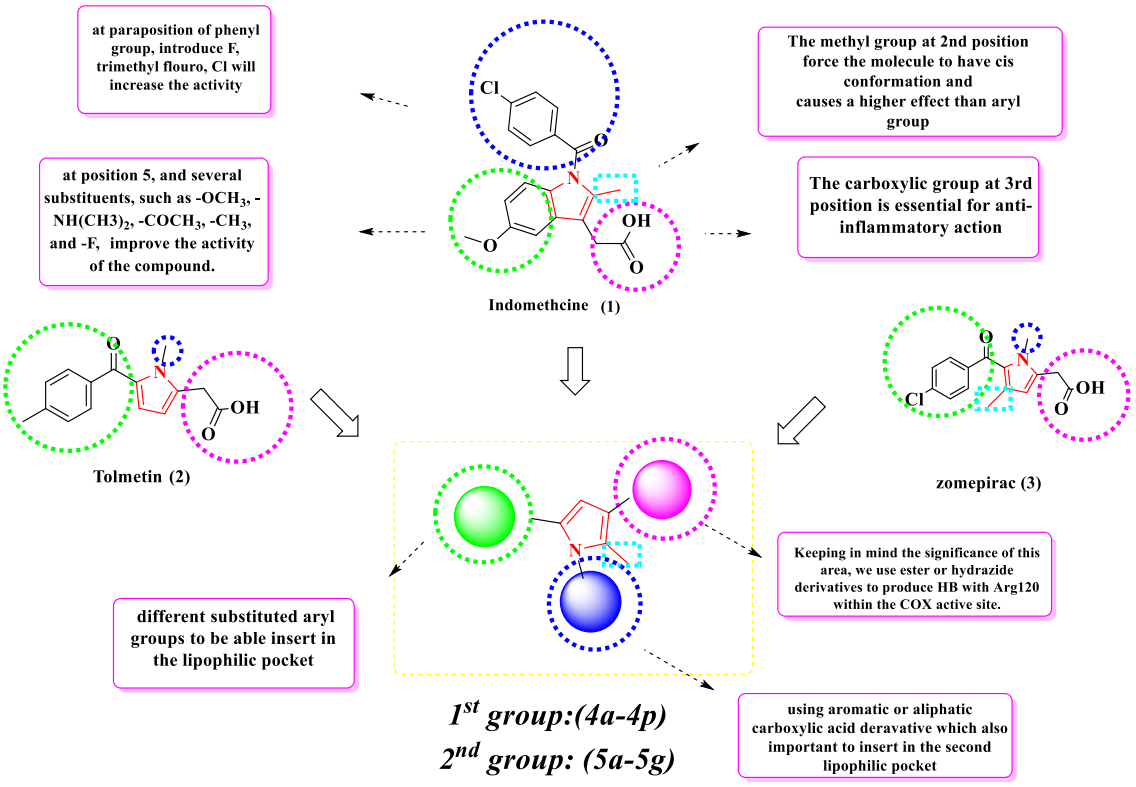

Figure 1.4. *Presentation examples of indomethacin (1), zomepirac (2), tolmetin (3), designed compounds (**4a-4p** and **5a-5g**) and the development of novel COX-inhibitors*

2. LITERATURE REVIEW

2.1. Pyrrole

2.1.1. Chemistry

Pyrrole (C_4H_5N) is a heterocyclic aromatic compound that has garnered considerable interest in the field of organic chemistry due to its unique structure and versatile chemical reactivity. It contains a five-membered ring with four carbon atoms and one nitrogen atom. Pyrrole does not have isomers, but its tautomeric forms are interconvertible by hydrogen atom migration (Figure 2.1). The nitrogen atom in pyrrole is slightly acidic due to the delocalization of its lone pair of electrons into the aromatic ring. This delocalization makes pyrrole a weaker base compared to other nitrogen-containing compounds, but it can still react with various electrophiles such as alkylating agents, acylating agents, and other carbonyl-containing compounds. Additionally, the pi electrons of the aromatic ring in pyrrole can undergo various types of reactions, such as electrophilic aromatic substitution and nucleophilic addition, making pyrrole a versatile building block in organic synthesis. Pyrrole and its derivatives have been used in various applications, including as intermediates in the synthesis of pharmaceuticals, agrochemicals, and natural products. Additionally, pyrrole-containing compounds have shown promising results as antitumor, anti-inflammatory, and antibacterial agents. The diverse range of reactivity and potential applications of pyrrole make it an essential component in organic chemistry research [29].

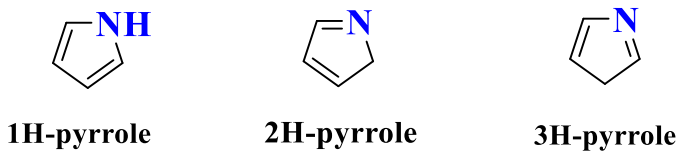

Figure 2.1. *Pyrrole tautomers*

2.1.2. Classical approaches for pyrrole synthesis

One of the crucial aspects of developing pharmaceuticals based on pyrrole is their synthesis, particularly the synthesis of polysubstituted pyrroles. Over the last decades, there are many methods for synthesizing pyrrole compounds in laboratory routes [30]. The traditional approaches, including the Hantzsch [31], Barton-Zard reaction [32], Van

Leusen pyrrole synthesis [33], Piloty–Robinson pyrrole synthesis [34], Paal-Knorr and Knorr reactions [35], allow the condensation of carbonyl compounds and amines, resulting in poly-substituted pyrroles [36]. Classic synthesis routes for producing poly-substituted pyrroles are summarized in Figure 2.2.

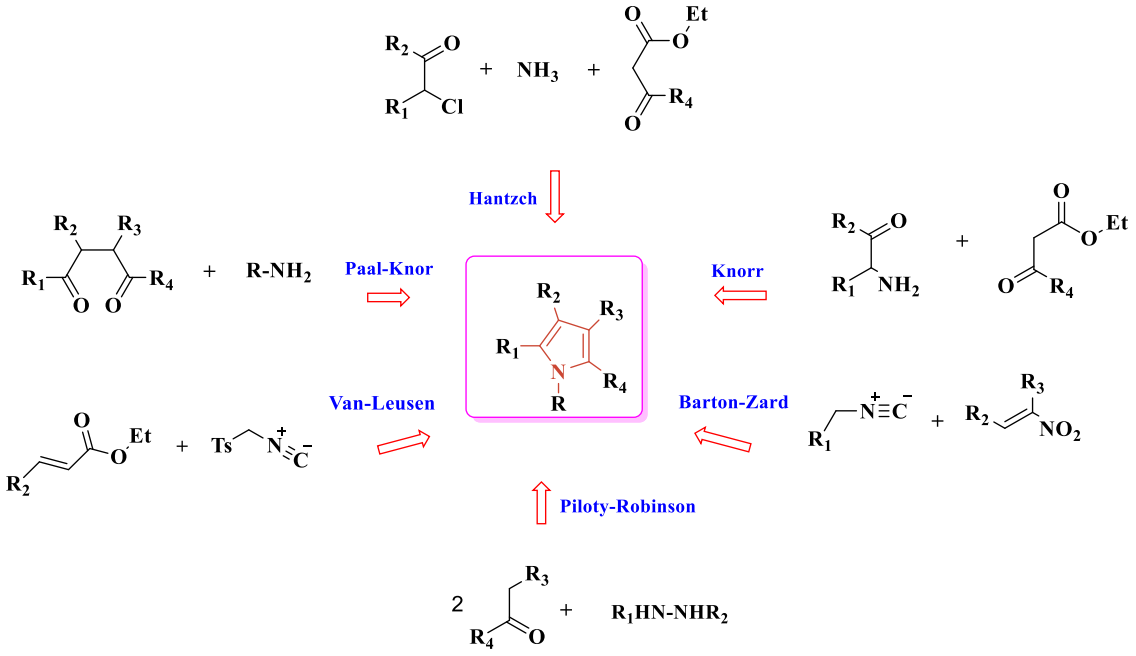

Figure 2.2. *Classic approaches to access polysubstituted pyrroles*

2.1.2.1. Hantzsch method pyrrole synthesis

Hantzsch is a multicomponent reaction [36].This method synthesizes ester-substituted pyrrole [37]. This technique involves heating a primary amine with a combination of α-haloketone and beta-keto ester in equal amounts. The ester undergoes a transformation into an enaminone or enamino ester **1**. The initial intermediate combines with the α-halo carbonyl component to generate the C-alkylated intermediate **2**. Subsequently, the C-alkylated intermediate undergoes cyclocondensation, resulting in the formation of the final product 3. This process involves the loss of a molecule of water (Figure 2.3).

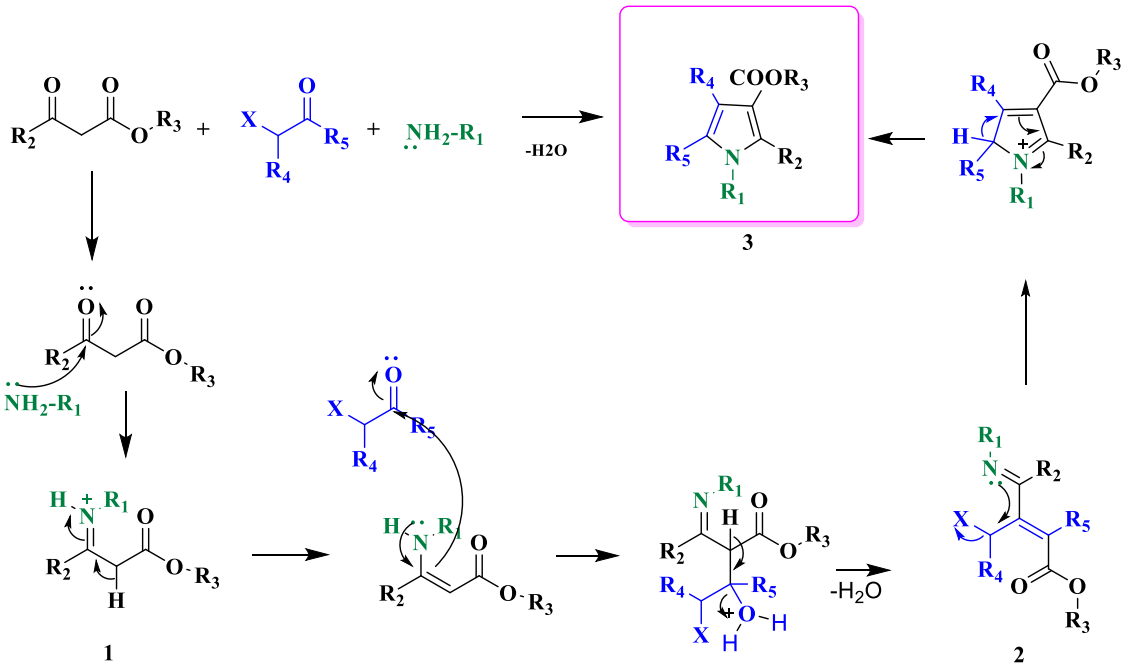

Figure 2.3. *The most widely accepted pathway for the Hantzsch pyrrole synthesis reaction*

2.1.2.2. Paal-Knorr pyrrole synthesis

In this synthesis, a reaction between a 1,4-dicarbonyl compound and either ammonia or a primary amine takes place. The reaction is typically run under protic or Lewis acidic conditions [35, 38]. It produces a polysubstituted pyrrole, but with using ammonium hydroxide or acetate (as reported by Paal) produces an N-unsubstituted pyrrole (Figure 2.4) [39].

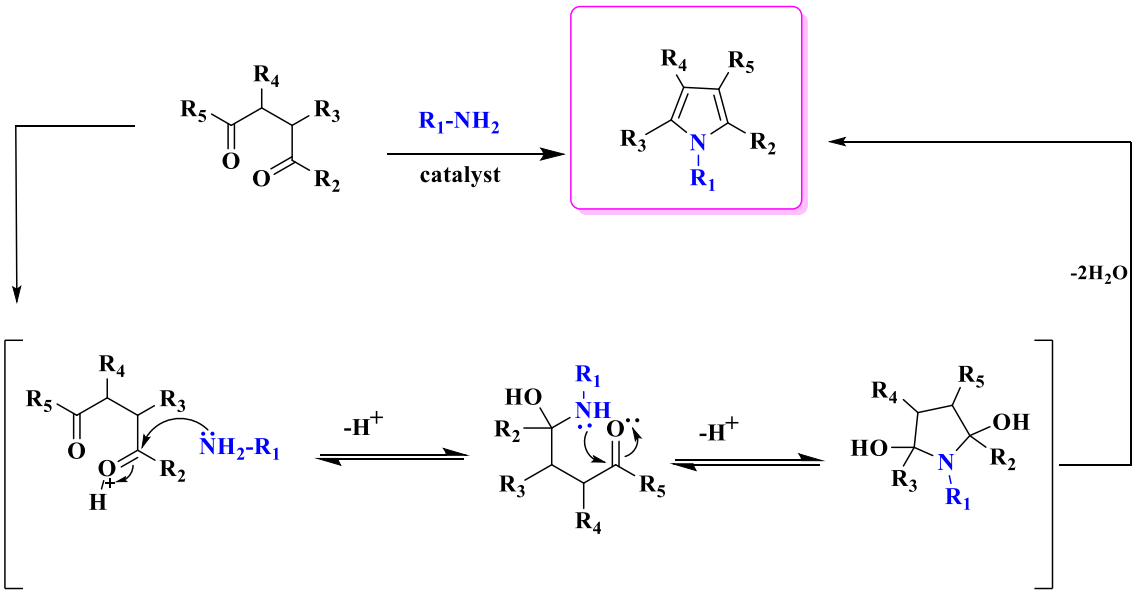

Figure 2.4. *Mechanism for the Paal-Knorr pyrrole synthesis*

2.1.2.3. Knorr pyrrole synthesis

This widely used reaction involves the condensation of an α-aminocarbonyl with a ketocarbonyl. To obtain tetra-substituted pyrroles, the reaction is heated under acidic conditions using acetic acid as the solvent [40]. The process entails the condensation of an aminoketone **4** with a α-carbonyl compound **5**, resulting in the formation of the corresponding imine **7**, Subsequently, an enamine is produced through a tautomeric equilibrium **8** that can be cyclized *via* nucleophilic attack on the carbonyl group in the intermediate. Finally, dehydration and tautomerization generate N-H substituted pyrroles **6** as presented in (Figure 2.5).

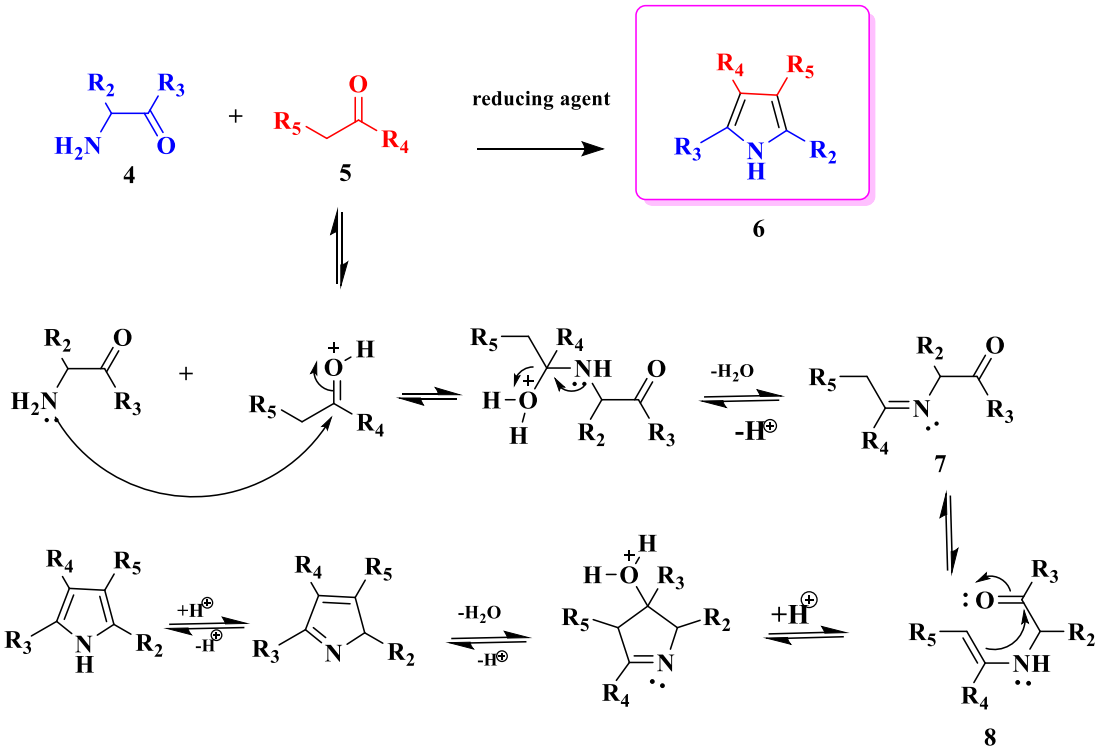

Figure 2.5. *Mechanism for the Knorr pyrrole synthesis*

2.1.3. Pharmacological profile

Serve as crucial structural elements in many bioactive compounds and useful building blocks in natural product and material science synthesis. Their synthesis has

always been a major research area in synthetic chemistry, and many methods have been developed [41]. Pyrrole is synthetic, but its analogs are found in vitamin B12, bile pigments bilirubin and biliverdin, and other natural products [42]. The pyrrole and pyrrolidine moieties can be found in some currently available drugs, while other drugs are still in the research and development phase [43]. which contributes further to its wide activities that include antimicrobial [44], antipsychotic [45], antiviral [46], anti-inflammatory [47], anti-oxidant and antidiabetic activity [48, 49], as well as anticancer [50] and anticonvulsant activity [51]. Figure 2.6 introduces possible drugs based on the structural classes of pyrroles introduces possible drugs based on the structural classes of pyrroles.

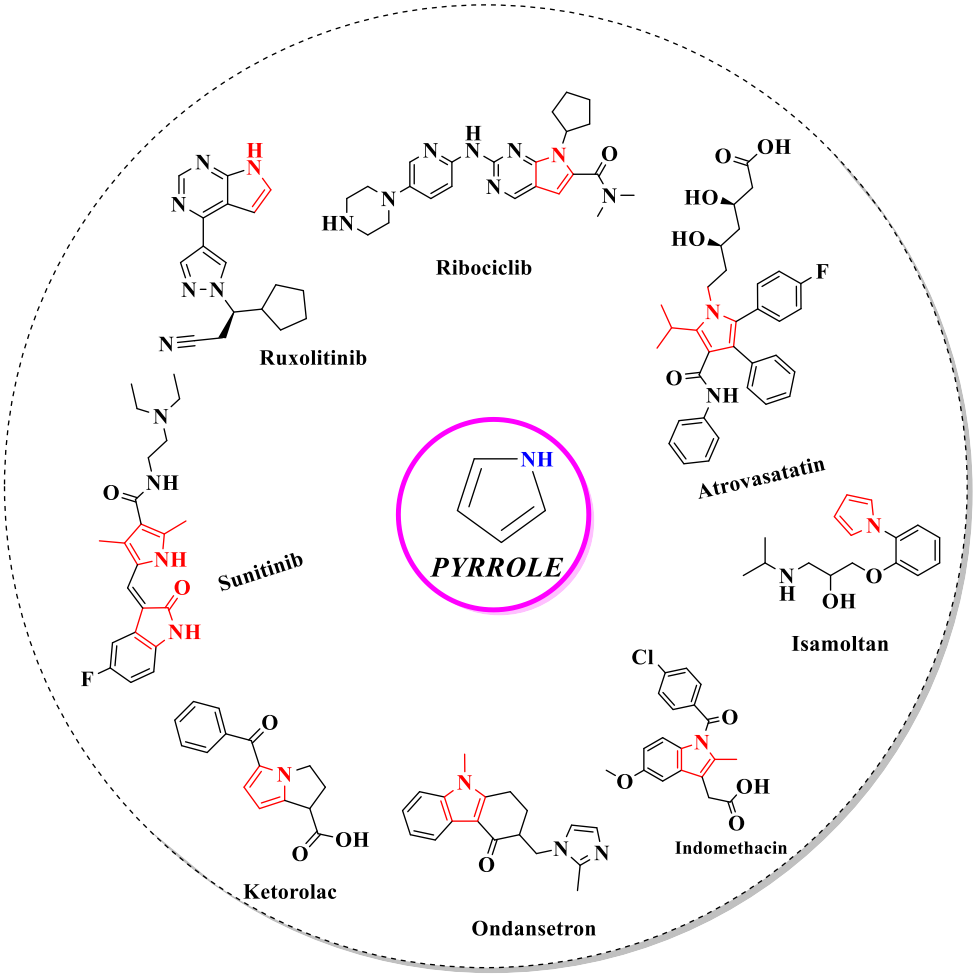

Figure 2.6. *Clinical drug candidates based on pyrrole-nuclus analogus*

2.1.3.1. Novel anti-inflammatory activity from lead compounds: a structural literature review

The search for effective anti-inflammatory agents has long been a focus of medicinal chemistry research. In recent years, there has been a growing interest in exploring the potential of lead compounds in the development of new anti-inflammatory drugs. This section, will provide a literature review that focuses on the structural characteristics of lead compounds with anti-inflammatory activity, with the aim of identifying key features that contribute to their effectiveness. By examining the existing research in this area, we hope to gain a better understanding of the underlying mechanisms of anti-inflammatory activity and guide the design of future lead compounds with improved therapeutic potential.

P. Januario et al. cite ketoprofen as a standard pharmaceutical. It has been suggested that a mechanism of action superior to that of common NSAIDs can be achieved by preparing a series of benzophenone derivatives joined to a thiazole group and demonstrating anti-inflammatory activity through inhibition of both prostaglandins and neutrophils [52]. Later, Shaukath A. Khanum et al. presented yet another benzophenone analogue, this one involving N-phenyl acetamide derivates; Moreover, in another study, he synthesized benzophenone-N-ethyl piperidine ether analogues; none of these compounds exhibited any appreciable side effects in comparison to nonsteroidal anti-inflammatory drugs like indomethacin and naproxen Figure 2.7 [53].

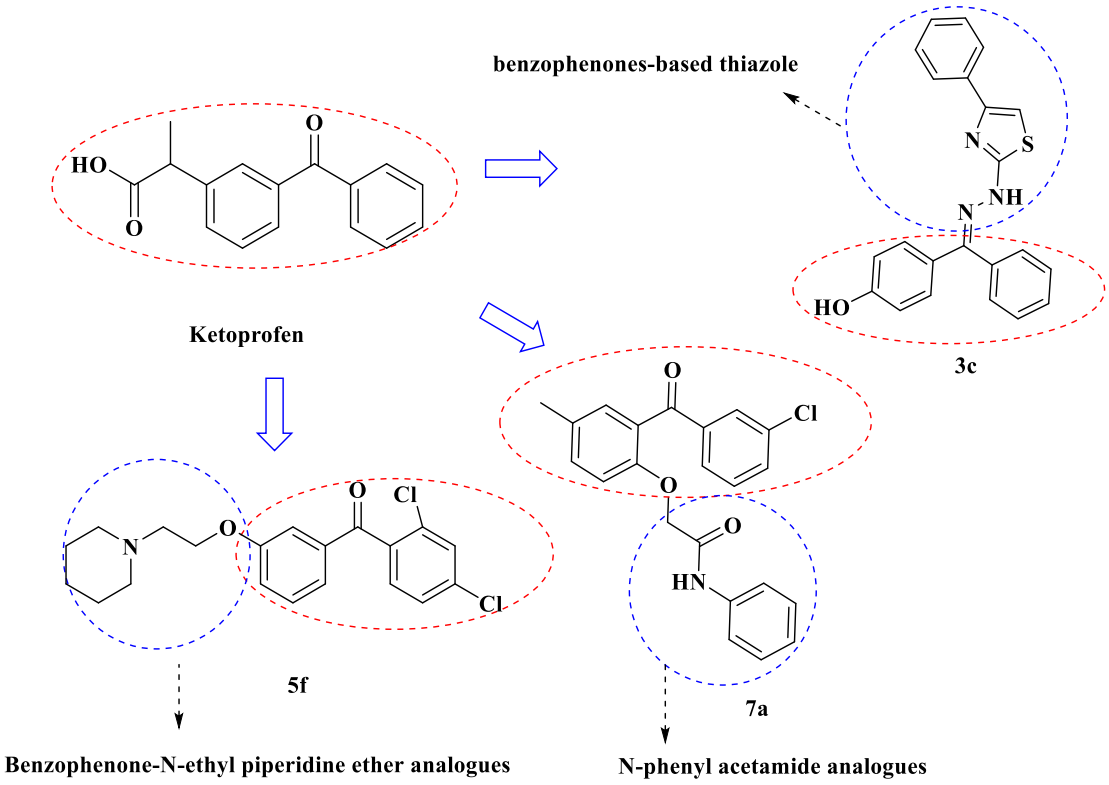

Figure 2.7. *Creating a series of benzophenone derivatives based on ketoprofen*

Küçükgüzel et al. replaced the carboxylic acid group of diflunisal with substituted triazoline thiones **4c** exhibited the highest anti-inflammatory activity (73.03%) whereas diflunisal, the drug used as standard, has been found less active (24.16%) [54]. Sadik Al Mekhlafi et al. synthesis a new anti-inflammatory agent compound **1** on the replacement of ibuprofen's carboxylic group with an amide group linked to a thiadiazole thus produce with less ulcer effect Figure 2.8 [55].

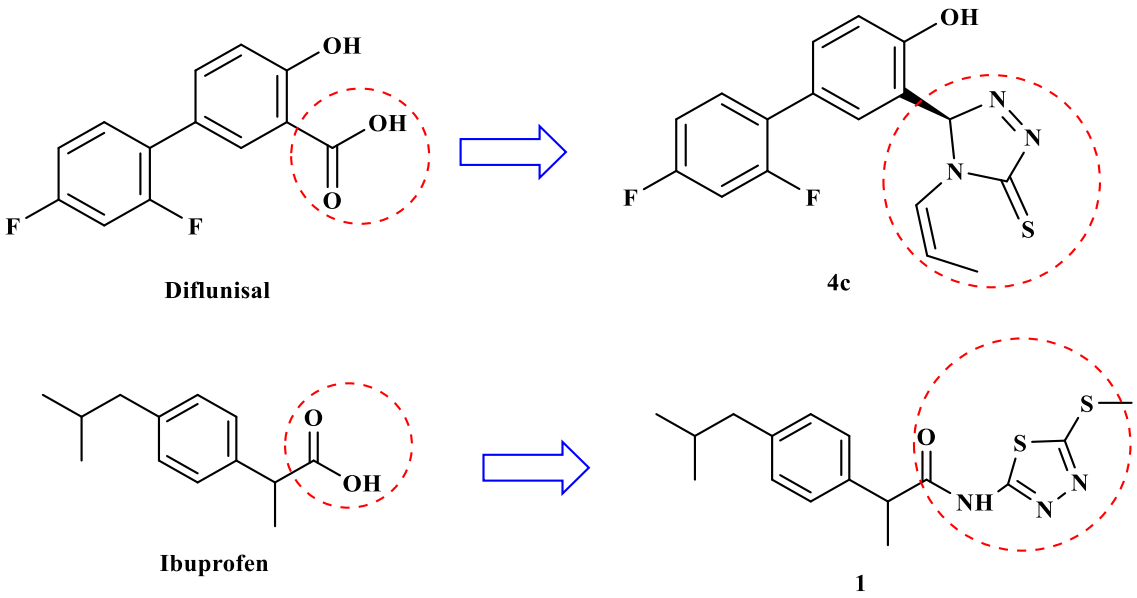

Figure 2.8. *Improved anti-inflammatory activity through: Carboxylic acid group substitution in Ibuprofen and Diflunisal*

Substituted 1*H*-pyrazolyl-thiazolo[4,5-d]pyrimidines were developed by Bekhit et al. using the diaryl heterocycle derived from celecoxib as a starting point. The pyrazole ring is linked to the thiazolo[4,5-d]pyrimidine ring system at position 4 and compound **12a** was synthesized and exhibited systemic anti-inflammatory activity with IC_{50} 7.56 µM and % 72.4 protection comparable to that of indomethacin (% 75.9 protection). However, it is 20% less effective than indomethacin when compared at the same dose [56]. Then, B. P. Bandgar et al. using the same scaffold of pyrazole with introducing the 3-benzamidocarbazole analogus, were reported as an inhibitor of production and synthesis PGE2 and the compound **5c** with two methoxy substituted in aryl ring exhibited a potential anti-inflammatory % Inhibition (88.34- 24.25) µM for COX-2 and COX-1 respectively [57]. Additionally, Zhen Zhang et al. Also using another hereosystem with introducing thiazole derivatives compound **E26** [58] whereas, Eman K.A. Abdelall et al. synthesis other analogus with using pyrazolopyrimidine scaffold and compound **13a** showed higher activity (IC_{50} =0.10 - 0.11 µM range) with respect to celecoxib (IC_{50} = 0.049 µM) Figure 2.9 [59].

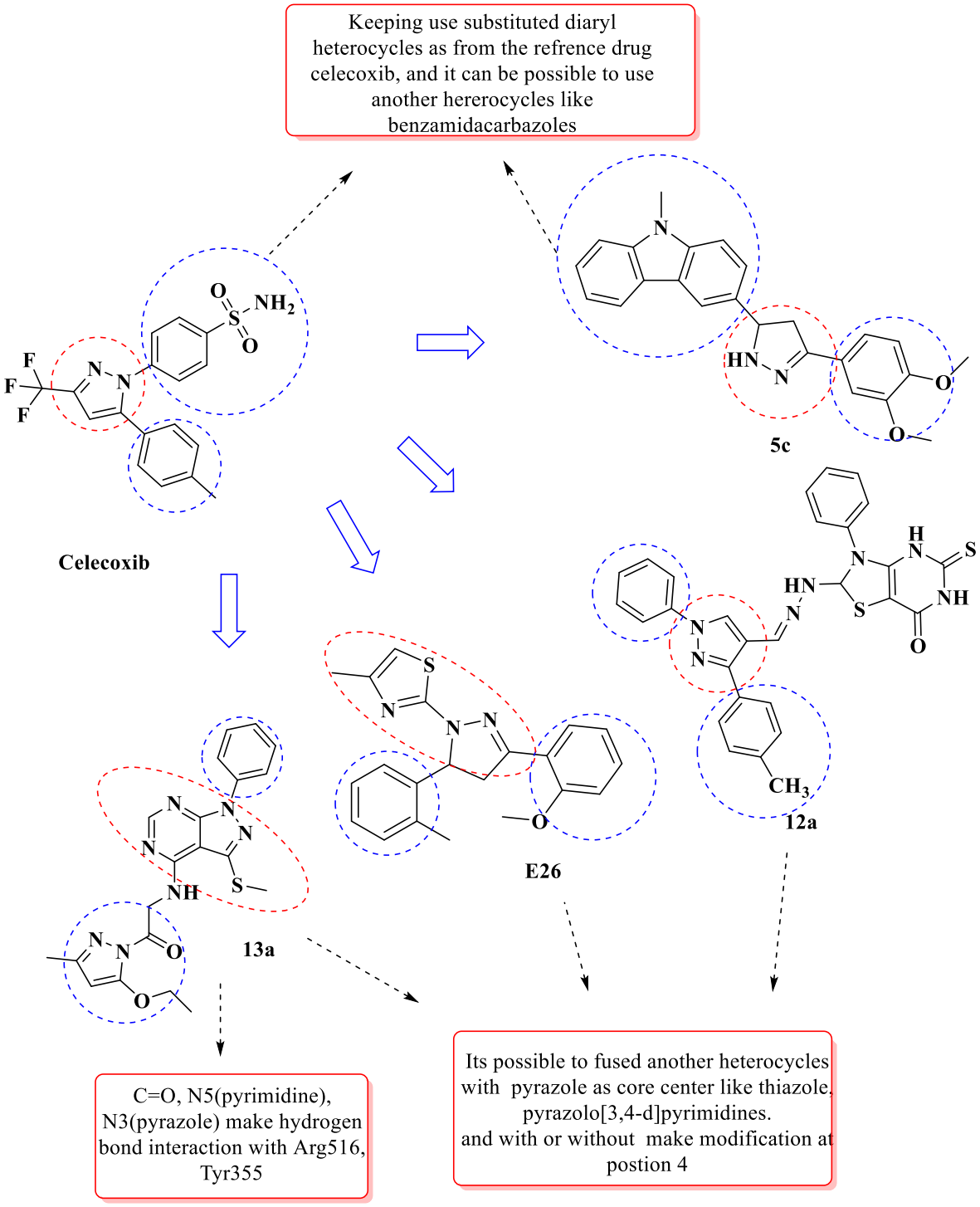

Figure 2.9. *Recent advances in pyrazole-based anti-inflammatory agents: Scaffold substitutions and activity comparisons*

Lynch et al. inspired from oxicams (piroxicam) which characterised by the 4-hydroxy benzothiazine heterocycle and the presence of carboxyamide substituent at the 3rd position of the benzothiazine ring, synhesis carboxamino-1,3 thiazole derivatives

containing N, N dimethyl amino phenyl moieties compound **4** showed anti-inflammatory activity across a concentration range of (10^{-2} - $5x10^{-4}$) M [60].

Ukrainets et al. The structural analogs of piroxicam, in which the sulfo and amino groups in the benzothiazine cycle are arranged reciprocally and produce compound **4d** by the "flip-flop drugs" methodology which are more potent than Lornoxicam by their anti-inflammatory properties [61]. In addition M. Szczęśniak-Sięga et al. Using the same scaffold of benzothiazine, and different linker between thiazine and piperazines nitrogens are: three-carbon aliphatic linker **6b** and series two-carbon with a carbonyl group linker (**7b** using acetoxy linker) showing different activity toward COX-1 and COX-2 (Figure 2.10) [62].

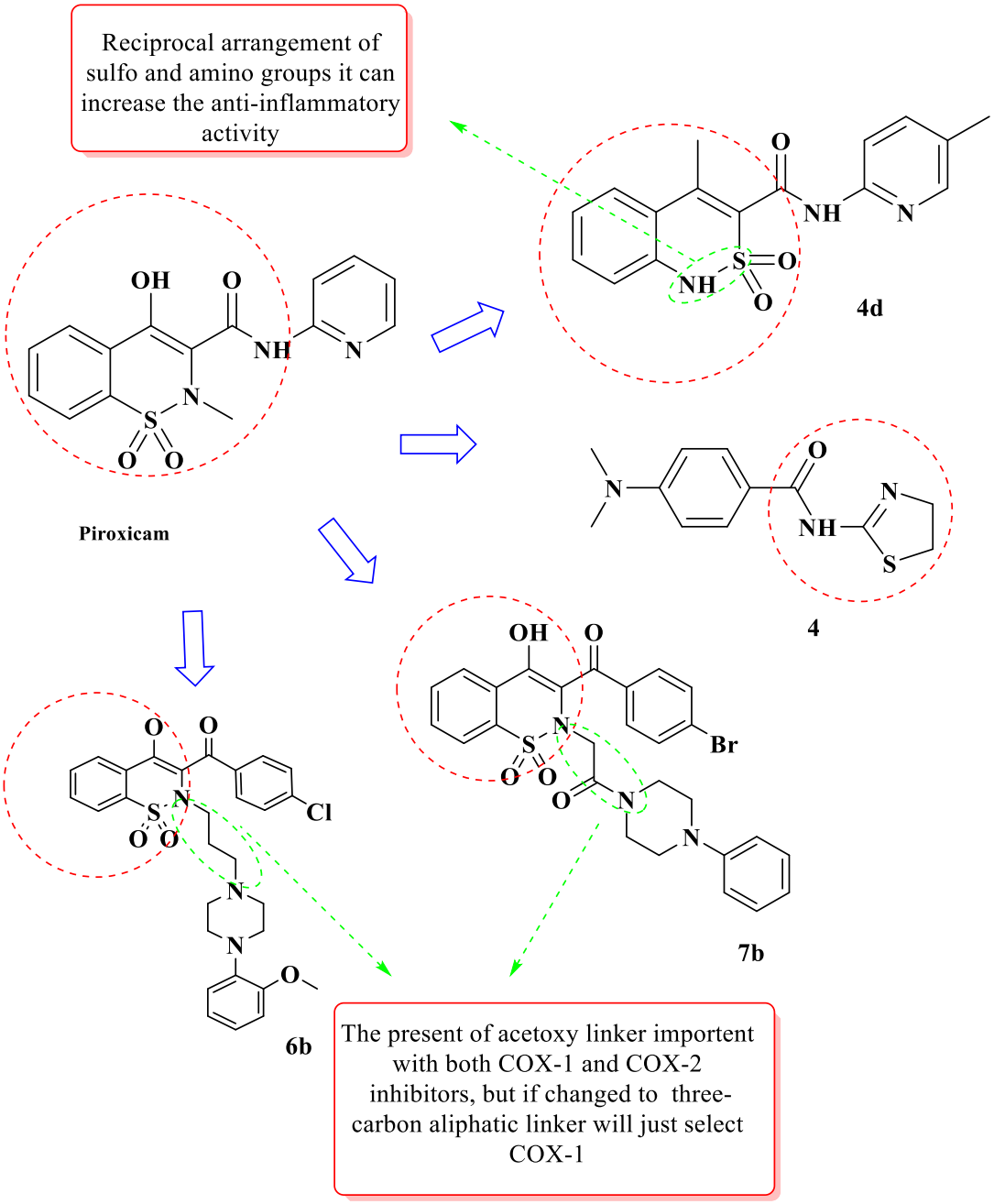

Figure 2.10. *Exploring the anti-inflammatory activity of benzothiazine-based derivatives: Substitutions and linker variations*

New evidence suggests that mPGES-1 is aviable therapeutic target for the creation of safe and effective anti-inflammatory medications. These compounds belong to a new class of selective benzoxazole piperidine carboxamides that are effective when taken orally [63]. Arhancet et al. synthesis compound **12** which is the result of structural activity optimization using cyclohexyl carbinols on lead **5**, then Introduction of

fluoroalkyl and aryl substituents at the C_6 of the benzoxazole ring led to the discovery of compound **PF-4693627** and was chosen to participate in a clinical trial (Figure 2.11) [64].

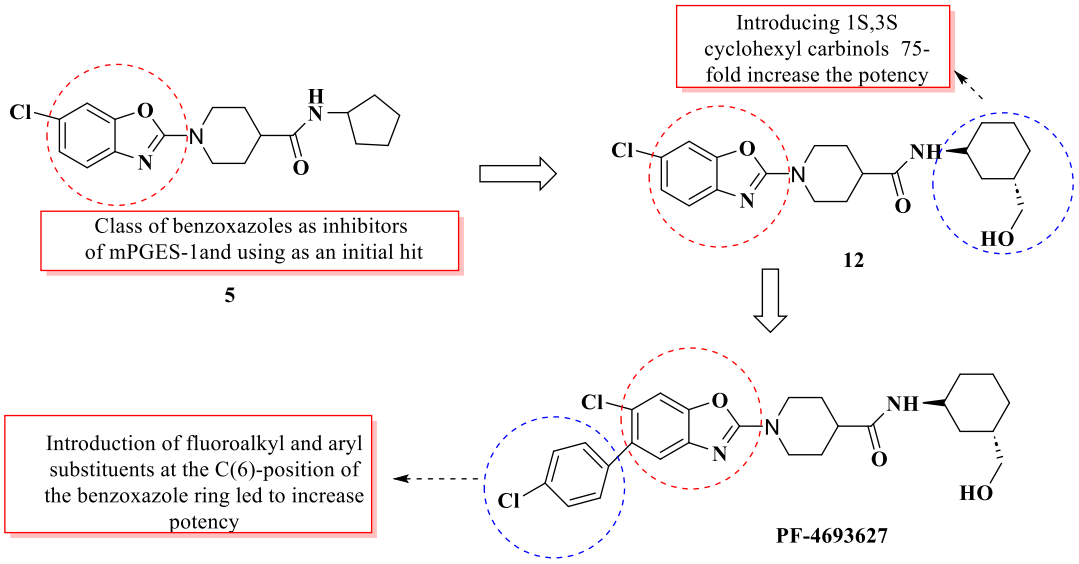

Figure 2.11. *Development of benzoxazole piperidine carboxamides as selective mPGES-1 inhibitors for anti-inflammatory therapy*

Minju Kim et al. synthesize a series of phenylsulfonyl hydrazide derivative by conducting both computational and physical HTS with the Korean Chemical Bank's reference collection and compound **1** (IC_{50} = 5700 nM against PGE2 production) was the most promising , After further optimization, the active lead compound **8n** (IC_{50} = 4.5 and 6.9 nM) was found, which is 30–150 times more effective than MK-886 in a cell-free assay against mPGES-1 enzyme (IC_{50} = 70 nM) [65], following that Park et al. contious the previous working and made some modification to generatea new potent phenylsulfonyl hydrazide (**7d**; IC_{50} = 0.06 μM against PGE_2) [66]. Following the introduction of these intriguing hydrazide groups and their potential anti-inflammatory effects, numerous research projects have attempted to incorporate hydrazides into their designs. Here are a few instances: VinutaKamat et al. synthesize some hydrazides linked to pyridine-containing thiazole in order to create powerful bioactive scaffolds. This process produced the compound **5i**, which had the highest IC_{50} value [67] and Pallavi et al. synthesis **10e** showed the highest IC_{50} value for COX-1 and COX-2 SI inhibition (Figure 2.12) [68].

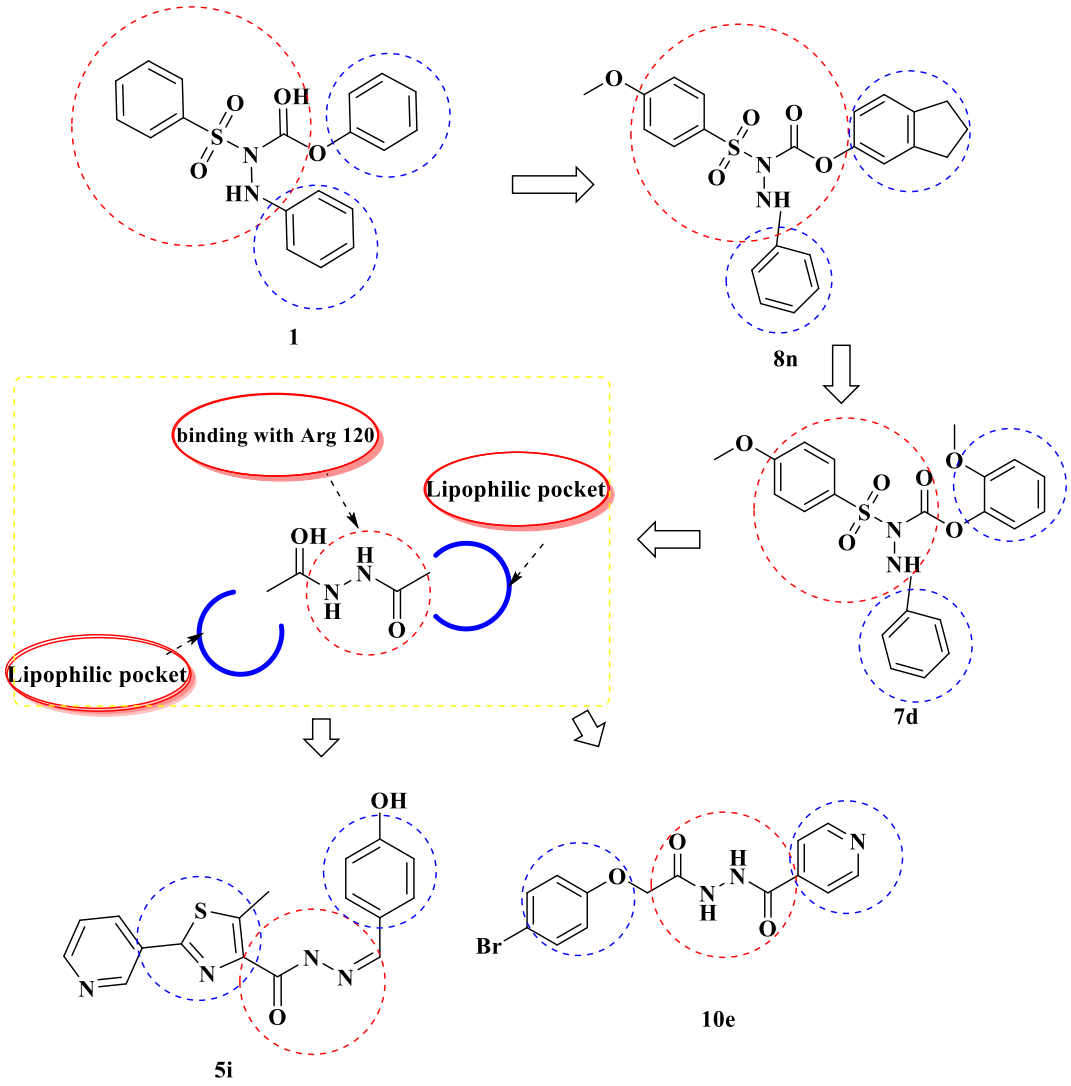

Figure 2.12. *Exploring the anti-inflammatory activity of phenylsulfonyl hydrazide derivatives and their potential as novel therapeutic agents for inflammatory diseases*

Conjugating NSAIDs with cleavable moieties is a common strategy for hiding the free carboxylic acid and boosting GI tolerance, as has been widely reported in the literature. The invention takes by Sahu et al. the advantage of the fact that amino acids are present in many foods and are not toxic until consumed in large quantities by covering up the NSAIDs' free carboxylic acid and synthesizing numerous ester and amide prodrugs, whereas Mahfouz et al. using *N*-hydroxymethylsuccinimide (HMSI) and *N*-hydroxymethylisatin (HMIS) as promotions to lessen their toxicity to the gut and increase their bioavailability (Figure 2.13) [69, 70].

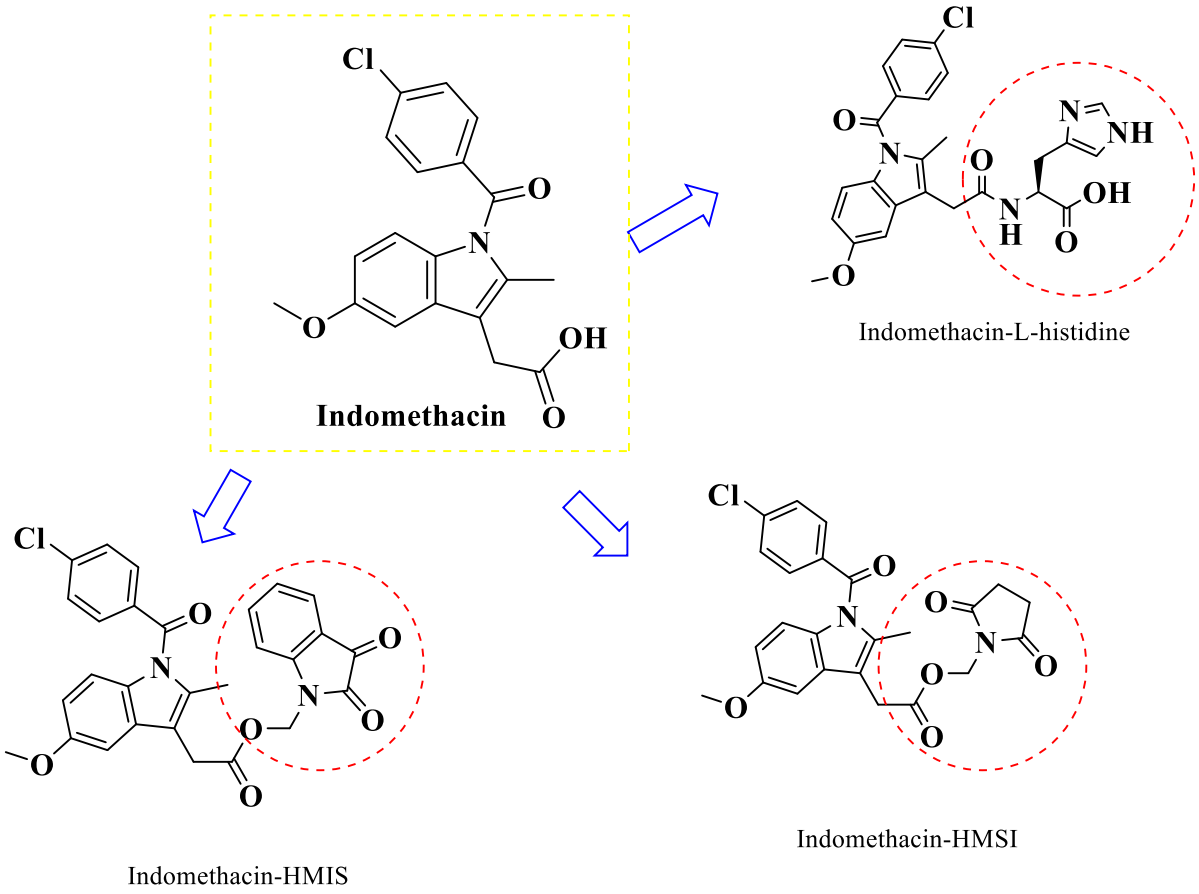

Figure 2.13. *Prodrugs: Strategies for enhancing GI tolerance of NSAIDs*

2.1.3.2. Literature review of pyrrole nucleus with anti-inflammatory activity

Pyrrole, as a noteworthy ring structure, has been discovered to have a wide range of biological processes; this ring ranges from one type of biologically active compound to another. In comparison to previous reviews that focused on the importance of pyrrole and its analogs from 2015 to 2021, Here, we take a look at the most up-to-date research concerning the therapeutic potential of pyrrole analogs, including their anti-inflammatory effects.

Hayashi et al. reported a novel of substituted 2-(pyridin-2-yl)indol-3-acetic acid analogues was prepared, constructed, and tested to locate selective and potent COX-2 inhibitors that could be used to treat inflammatory diseases as shown in Figure 2.14 . The most active compound, which has a floro substitute at position 6, demonstrated 70% inhibition against carrageenan-induced oedema in the foot of SPF/VAF SD rats, as expected, and its respective COX-2 inhibition selectivities were 86.5-fold higher than

those of the 5-fluoro analogue and those of the 5-fluoro-6-chloro analogue (26.4 - 9.73) fold, respectively [71].

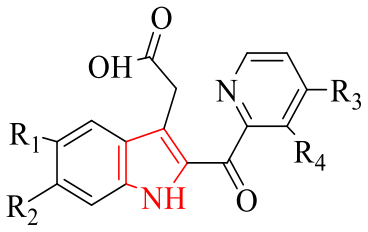

Figure 2.14. *[2-{[(4-Substituted or 4,5-disubstituted)-pyridin-2-yl]carbonyl}-(5- or 6-substituted or 5,6-disubstituted)-1H-indol-3-yl]acetic acid (R_2 =F, R_3= Me for the most active canditadtes)*

Said Fatahala et al. reported synthesis of pyrrolopyridine and pyrrolopyridopyrimidine analogs as anti-inflammatory agents. Their findings shows that diclofenac and pyrrolopyridines both significantly inhibit IgE while having good anti-inflammatory effects. Compared to the standard medication diclofenac in tests for their effects on cytokines (specifically, IL-1, TNF-), CRP, histamine, and immunoglobulin E (IgE), the most active derivative as shown in (Figure 2.15) had an IC_{50} value on Histamine, IgE, CRP, IL1-β, TNF-α are 0.784 ± 0.016 (µg/L), 1.5 ± 0.28 (IU/mL), 6.6 ± 0.80 (mg/L), 11.58 ± 0.42 (ng/L), 31.1± 0.10 (pg/mL) repectively {Said Fatahala, 2017 #9}.

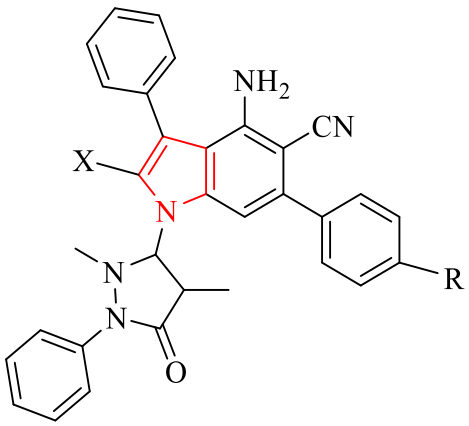

Figure 2.15. *4-Amino-5-cyano-2-substituted-phenyl-3-phenyl-6-(substitutedphenyl)-1-(1,5-dimethyl-3-oxo-2-phenyl-2,3-dihydro-1H-pyrazol-4-yl)-1H-pyrrolo[2,3-b]pyridine.(X= Ph, R= H,-OCH_3 for the most active compounds)*

Reale et al. synthesized a new series of chemical compounds called 1,5-diarylpyrrol-3-sulfur analogs and evaluated their ability to reduce inflammation. Moreover, studies involving molecular modeling indicate the most active compounds as shown in the Figure 2.16. Additionally, the invitro studies of the presented canditates are revealed that inhibited 32.6 ± 3.9 % at a dose of 10 mg/Kg [72].

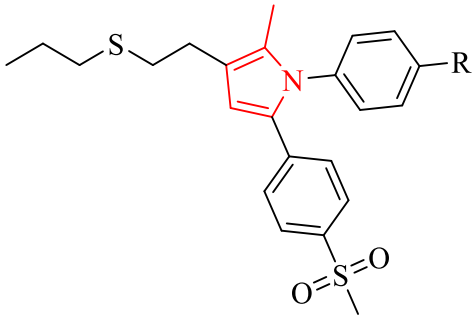

Figure 2.16. *1-(Substitued phenyl)-2-methyl-5-(4-(methylsulfonyl)phenyl)-3-(2- (propylthio)ethyl)-1H-pyrrole. (R= H,F for the most active canditates)*

Szczukowski et al. described the synthesis of a new group of chemical compounds that are pyrrolo[3,4-d]pyridazinone analogs with 4-aryl-1-(1-oxoethyl)piperazine attached. They also tested the anti-inflammatory activity of these compounds. The most potent of the synthesized compounds as shown in Figure 2.17, with a mean IC_{50} (658.7 μM) shows promising anti-inflammatory and anti-oxidant activity by inhibiting cyclooxygenase with higher specificity for the COX-2 isoenzyme [73].

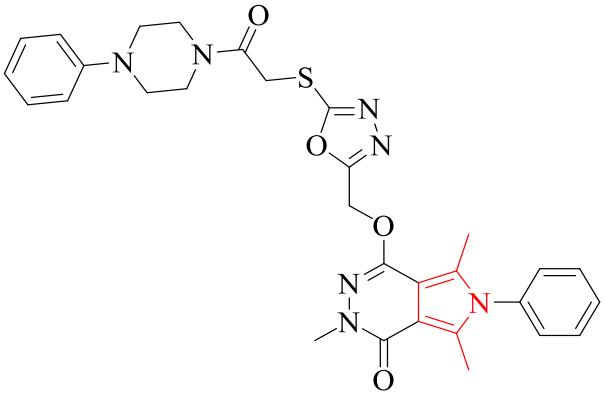

Figure 2.17. *3,5,7-Trimethyl-1-[[2-[2-oxo-2-(4-phenylpiperazin-1-yl)ethyl]sulfanyl-1,3,4-oxadiazol-5-yl]methoxy]-6-phenyl-pyrrolo[3,4-d]pyridazin-4-one*

Harrak et al. designed a series of 1,4-benzodioxine derivatives and pyrrole-related compounds (Figure 2.18). Compound **b** (showed the highest enzyme inhibition, with an

IC_{50} of 5.8 M-roughly 17 times higher than that of ibuprofen whereas compound **a** an also demonstrated superior inhibitory action against carrageenan-induced oedema, with an IC_{50} of 34 M [74].

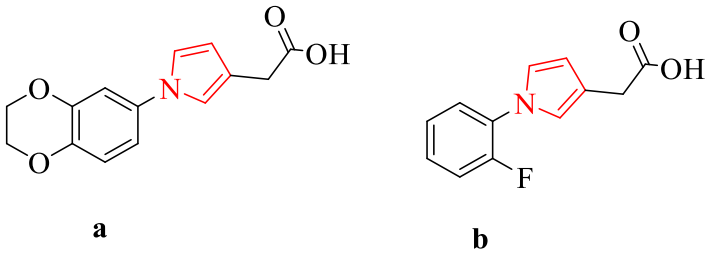

Figure 2.18. *(a) 2-[N-(2,3-Dihydro-1,4-benzodioxin-6-yl)-pyrrol-2-yl] acetic acid, (b) 2-(N-(2-Fluorophenyl)pyrrol-3-yl) acetic acid*

Paprocka et al. synthesize *1H*-pyrrole-2,5-dione derivatives and the result show that dimethyl pyrrolamido pyridine carboxamide analogues (Figure 2.19). These compounds may have the potential to suppress the production of IL-10, as they were observed to exhibit significant inhibition of this target at concentrations of 50 µg/mL or 100 µg/mL (with inhibition ranging from 71% to 95%). Notably, the level of inhibition achieved by these compounds was higher than that of ibuprofen (which resulted in inhibition of 57% and 77% at the same concentrations) [75].

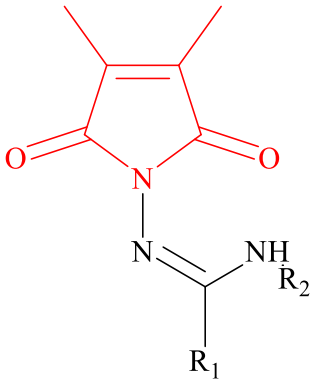

Figure 2.19. *3,4-Dimethyl-1H-pyrrole-2,5-dione derivatives (for the most active one is R_1= 4-C_5H_4N, R_2= C_6H_5)*

Josef et al. synthesize benzoylpyrrolopyrrole carboxylic acid series of compounds displayed potent anti-inflammatory and pain-relieving properties (Figure 2.20). It was found that p-methyl derivative of 5-Benzoyl-1,2-dihydro-3*H*-pyrrolo[1,2-α] pyrrole-1-carboxylic acid was found to have an ED_{50} (6mg/ kg per day) and 4-vinylbenzoyl

derivatives were found to be most potent with ED_{50} (3mg/ kg per day) being equivalent to indomethacin in 7 day rat assays [76].

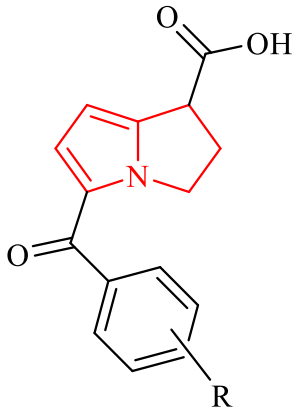

Figure 2.20. *5-Aroyl-1,2-dihydro-3H-pyrrolo[1,2- α] pyrrole-1-carboxylic acids and related compounds (for most actives when R= CH_3 or CH_2=CH)*

Samar said et al. synthesize pyrrolopyridines and pyrrolopyridopyrimidines from aminocyanopyrroles , and the final substances' capacity to reduce the production of inflammatory cytokines in vitro and decrease inflammation in vivo was examined. The biological findings indicate that cyano-pyrrolopyridine analogs has 36.33% reduction in inflammation (Figure 2.21) [77].

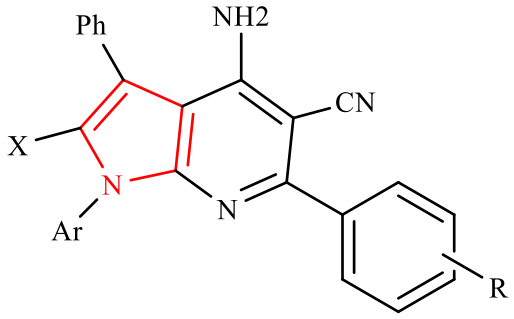

Figure 2.21. *4-Amino-5-cyano-3-phenyl-6-(4-methoxyphenyl)-1-(1,5-dimethyl-3-oxo-2-phenyl-2,3-dihydro-1H-pyrazol-4-yl)-1H-pyrrolo[2,3-b]pyridine*

Twenty-four chalcones of pyrroles were synthesized by Mohd Faudzi et al., who reported their anti-inflammatory effects on IFN-gamma/LPS-induced RAW 264.7 macrophage cells by inhibiting the production of NO and PGE_2. In addition, the crystal structure and the molecular studies support these findings. The IC_{50} values for nitric oxide

and PGE_2 production in LPS/IFN- stimulated RAW2647 cells were 12.1 ± 1.5 μM and 0.5 ± 1.5 μM, respectively, and the compound were not cytotoxic at the measured concentrations Figure 2.22 [78].

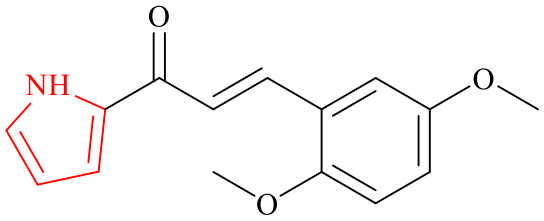

Figure 2.22. *(E)-3-(2,5-dimethoxyphenyl)-1-(1H-pyrrol-2-yl)prop-2-en-1-one*

Wilkerson et el. reported the synthesis of 1,2-diarylpyrroles as shown in Figure 2.23 which was associated with inhibition of the inducible isoform of COX. However, the compound with sulfonyl methyl substitution at para position on phenyl ring exert the most potent in both COX-1 and COX-2 with an IC_{50} value of 267 μM and more than 300 μM respectively [79, 80]

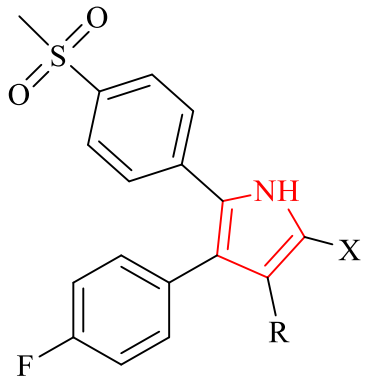

Figure 2.23. *2-Substituted and 2,3-disubstituted-4-(4-fluorophenyl)-5-[4-(methylsulfonyl)phenyl]-1H-pyrroles.(R=Br,Cl,SO_2Me for the most active compounds)*

Khanna et al. recognize the efficacy of substituted 4,5-diarylpyrroles as described by Wilkerson et al. [79, 80] and changing the order of the replacements of aryl groups, they obtained the compounds shown in Figure 2.24. However, the one with the flouro group at para position on the phenyl ring with (COX-2, IC_{50} = 60 nm) and selective (COX-1/COX-2 =>1700) inhibitor is the most promising. Furthermore, the fluoro group can be replaced by H, CF_3, or CH_3 groups in order to generate compounds with high efficacy and selectivity [81].

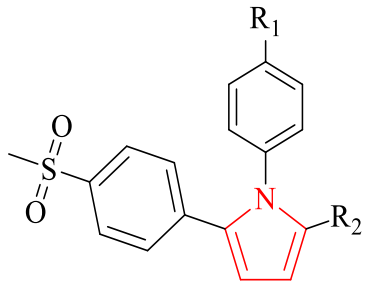

Figure 2.24. *1-(Substituted phenyl)-2-substituted-5-[4-(methylsulfonyl)-phenyl]-1H-pyrrole. (R1=F, R2=Me of the most active compound)*

Luong et al. endorsed the skeleton of zomepirac to obtain pyrroleacetate selective inhibitors by exchange the carboxylic acid group of zomiperac with a pyridazinone moiety offered a potent and selective set of inhibitors (Figure 2.25). The compound has an IC_{50} of 0.6 μM in COX-2 and IC_{50} of 1000 μM in COX-1. The compound has an ED_{30} of 3.3 mg/kg and an ED_{40} of 2.9 mg/kg in the rat CFE and adjuvant arthiritis models, respectively [20].

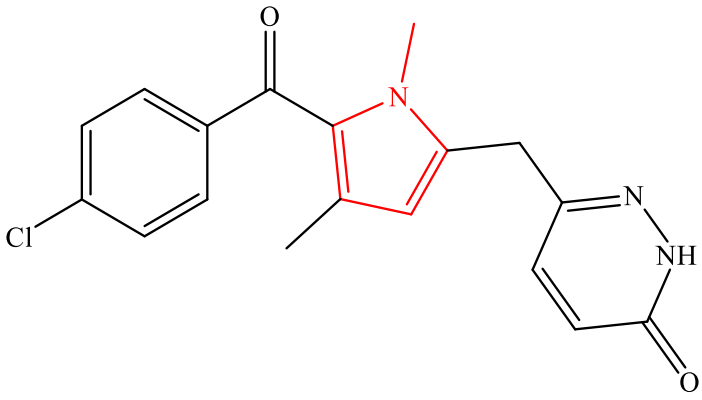

Figure 2.25. *6-((5-(4-Chlorobenzoyl)-1,4-dimethyl-1H-pyrrol-2-yl)methyl)pyridazin-3(2H)-one*

Battilocchio et al. inspired of the work by Khanna et al. [81]. They successful in developing a class of diarylpyrroles that have undergone biological and pharmacological testing. The findings demonstrate the compounds in (Figure 2.26) with the standout compound having two flouro groups at position 3,4 on phenyl ring proving to have exceptional anti-nociceptive activity even at dose 1 mg/Kg (36% reduction) and being able to reduce writhes by 60% after administration at 40 mg/Kg comparable to celecoxib [82].

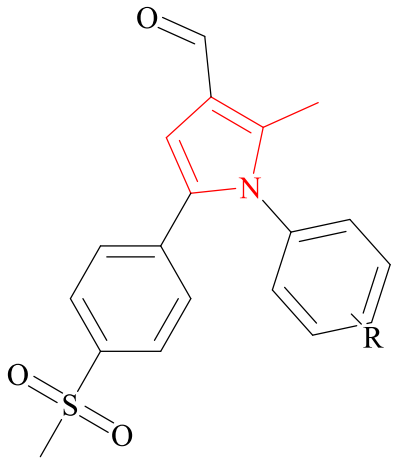

Figure 2.26. *2-Methyl-5-[4-(methylsulfonyl)phenyl]-1-[3,4-difluoro-phenyl]-1H-pyrrole-3-carboxaldehyde. (R= 3,4 diflouro of the most active compound)*

More recently, Redzicka et al. reported design, synthesis, and anti-inflammatory activity of *N*-substituted 3,4-pyrroledicarboximides and the inhibitory activity against COX-1 and COX-2 has been shown for all of the synthesized compounds. Figure 2.27 illustrates the most effective compound against COX isoforms, with IC_{50} values of 94.17 ± (0.04) μM and 61.46 ± (0.02) μM of COX-1 and COX-2 repectively [83].

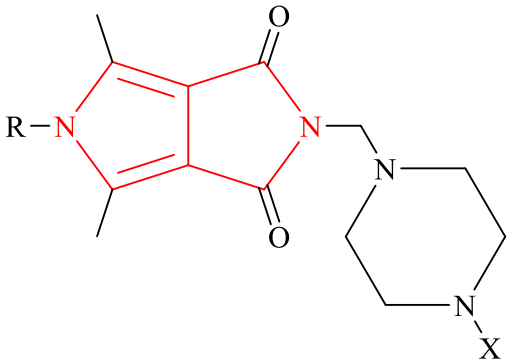

Figure 2.27. *4,6-Dimethyl-5-(substituted)-2-[4-(substituted)-1 piperazinyl]methylpyrrolo[3,4-c]pyrrole-1,3(2H,5H)-dione. (R= 3-ClPh, X= 4-BrPh for the most active compound)*

3. MATERIALS

3.1. Chemicals

2-Bromo acetophenone	: Sigma-Aldrich, Germany
2-Bromo-(2`-benzofuran)ethanone	: Sigma-Aldrich, Germany
2-Bromo-2`,4`-dichloro acetophenone	: Sigma-Aldrich, Germany
2-Bromo-2`-acetonaphthone	: Sigma-Aldrich, Germany
2-Bromo-3`,4`-dichloro acetophenone	: Sigma-Aldrich, Germany
2-Bromo-4`-chloro acetophenone	: Sigma-Aldrich, Germany
2-Bromo-4`-cyano acetophenone	: Sigma-Aldrich, Germany
2-Bromo-4`-fluoro acetophenone	: Sigma-Aldrich, Germany
2-Bromo-4`-methoxy acetophenone	: Sigma-Aldrich, Germany
2-Bromo-4`-methyl acetophenone	: Sigma-Aldrich, Germany
Acetone	: Sigma-Aldrich, Germany
Chloro acetyl chloride	: Sigma-Aldrich, Germany
Chloroform	: Merck, Germany
DMSO-d_6	: Merck, Germany
Ethyl acetate	: Sigma-Aldrich, Germany
Glacial acetic acid	: Sigma-Aldrich, Germany
Methyl alcohol	: Sigma-Aldrich, Germany
Petroleum ether	: Sigma-Aldrich, Germany
Sodium acetate	: Sigma-Aldrich, Germany
TLC silica gel 60 F_{254}	: Merck, Germany
Toluene	: Sigma-Aldrich, Germany
Sodium metal	: Merck, Germany

3.2. Instruments and Tools

Electronic balance	: Shimadzu, Libror EB-330 HU, Japan
Magnetic based heater stirrer	: Heidolph, MR 3003, Germany
Mass spectrometer	: Shimadzu, LCMS-IT-TOF, Japan
Melting point detector	: Mettler Toledo-MP90 Melting Point System, Germany
Nuclear magnetic resonance spectrometer	: Bruker, UltraShield 400 MHz, USA
Rotary Evaporator	: Heidolph, 4000/G3, Germany
Ultraviolet lamp	: Camag, Cabinet, Switzerland

4. METHODOLOGY

4.1. Database library preparation and developing field-based QSAR (FB-QSAR) model

To show how the filters we've built work, and what kind of impact they have on the chemical landscape, we need to put them through their paces. We consulted the ChEMBL database (https://www.ebi.ac.uk/chembl/ ; Accessed date: July 10, 2022). The CHEMBL database yielded the identifiers 4275 and 9521 for COX-1 and COX-2, respectively (CHEMBL code: CHEMBL 221, CHEMBL 230). After determining the IC_{50} values (log $IC_{50} \geq$ 6.00) for COX-2, we used the ligand filter in maestro to narrow the list down to only those compounds with own tetra-substituted pyrrole mioties, ultimately identifying 477 compounds. These compounds were then docked and minimized in Maestro using the Glide plugin before being imported into the 3D Field-Based QSAR interface for further study. The FB-QSAR model was developed with default settings using a Partial Least Squares (PLS) factor of 5, and the training set was arbitrarily set to 75% of the data. Parameters like R^2, Q^2, Pearson correlation coefficients (Pearson-r), stability, RMSE, F, and P values were examined to evaluate the FB-QSAR model's reliability and validity [84]. These parameters' thresholds were validated based on the following criteria: The value of the dissimilarity between R and Q should be less than 0.1. In addition, the Pearson correlation coefficients ($|r_c|$) had to have an absolute value of 0.3 or higher [85]. Subsequently, the results generated from the FB-QSAR model were utilized in the design and synthesis of our targeted compounds.

4.2. Synthetic Methods

4.2.1. Method A: Synthesis of ethyl acetoacetate sodium salt (1)

The ethyl 3-oxobutanoate sodium salt **(1)** was prepared by reacting an equimolar amount of acetoacetate ethyl ester (2.8 ml, 21.90 mmol) with Na metal (0.5 g, 21.7 mmol) at 0 °C for 5 days in the presence of anhydrous toluene (Figure 4.1).

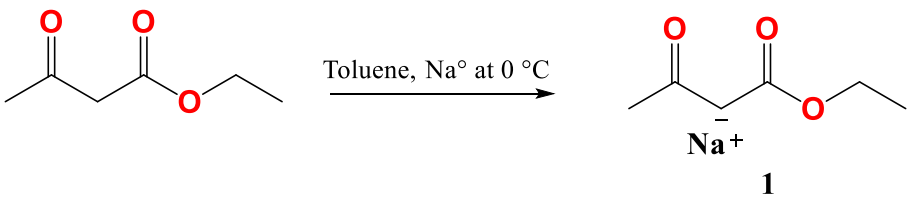

1

Figure 4.1. *Preparation of ethyl acetoacetate sodium salt*

4.2.2. Method B: (Bromination) : Synthesis of substituted bromo-acetophenones (2)

For the bromination step, solution of bromine (1.2 equivalent) in glacial acetic acid was added drop by drop to a stirred solution of substituted acetophenones in glacial acetic acid with just two drops of hydrobromic acid 6-8 hours at 0 °C (Figure 4.2).

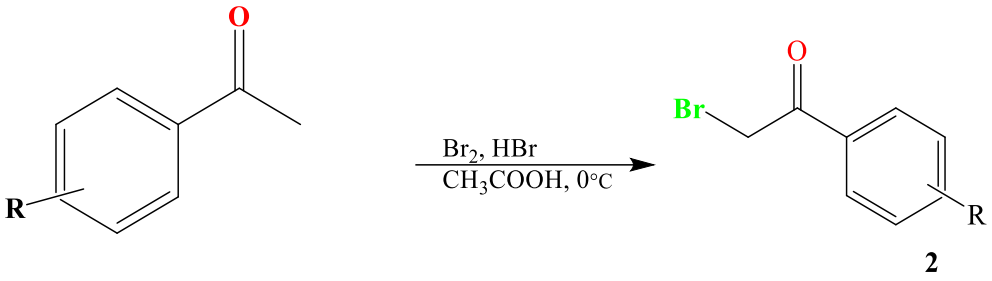

Figure 4.2. *Bromination of acetophenone derivatives*

4.2.3. Method C: Synthesis ethyl 2-acetyl-4-oxo-4-(substituted phenyl) butanoate (3)

By using substituted-bromo acetophenones **(2)** as the nucleophilic reagent, the salt ethyl acetoacetate sodium salt **(1)** is transformed into compound **(3)**. The toluene used as a solvent was evaporated after the reaction was finished. The residue was washed with water and filtered to create the desired output, as shown in (Figure 4.3).

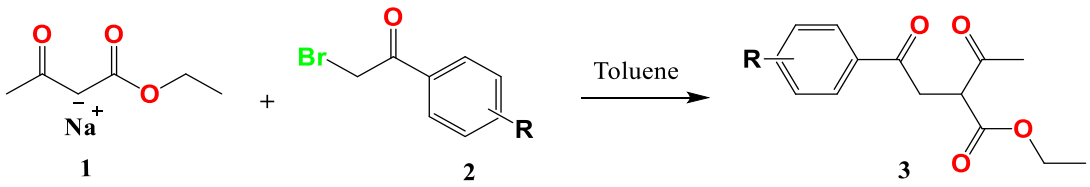

Figure 4.3. *Synthesis of ethyl 2-acetyl-4-oxo-4- (substituted phenyl) butanoate*

4.2.4. Method D: Synthesis of 2-[3-(ethoxycarbonyl)-2-methyl-5-(substituted phenyl)-1*H*-pyrrol-1-yl]substituted carboxylic acid (4a-4p and 5a-5g)

Pyrrole ring was closed under Paal–Knorr conditions by refluxing equimolar amounts of amino derivatives (2 equivalent) and ethyl 2-acetyl-4-oxo-4-(substituted phenyl) butanoate (**3**) in glacial acetic acid for 12- 24 hours (Figure 4.4). The reaction was monitored using TLC, the reaction was worked-up with using iced water and the precipitated product was extracted with using ethyl acetate.

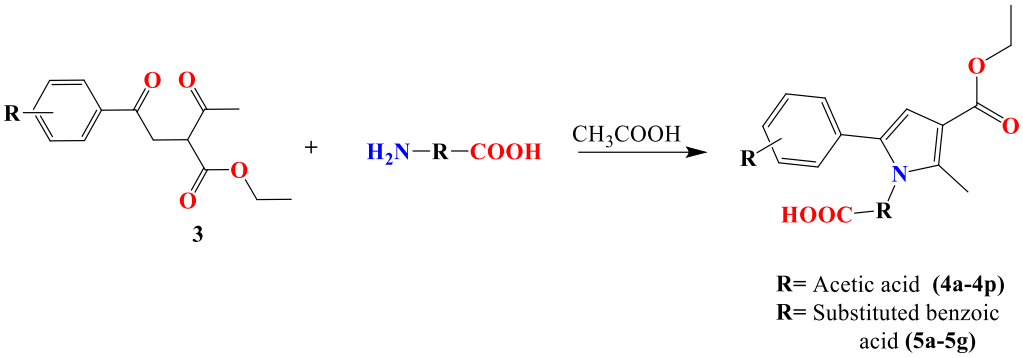

Figure 4.4. *Synthesis of 2-[3-(ethoxycarbonyl) -2-methyl-5-(substituted phenyl) -1H-pyrrol-1-yl]substituted carboxylic acid*

4.3. Thin Layer Chromatography (TLC) Studies

Throughout the synthesis processes and reaction monitoring, TLC applications were utilized. In order to extract reaction medium samples, we used capillary tubes and then diluted them in ethanol before applying them to aluminum plates coated with silica gel 60 F_{254}. These plates were then placed in a mobile phase consisting of ethyl acetate/petroleum ether mixtures of varying polarity (9:1, 3:1, and 1:1) to monitor the reaction's development. To ensure accurate tracking, diluted samples were collected at predetermined intervals and then spotted onto the plates using capillary tubes, followed by vertical placement within a closed chamber containing the corresponding mobile phase. UV illumination at 254 nm and 366 nm was used to view the TLC plates, which allowed for polarity-based separation of the sample's components, resulting in distinct retention factors Rf and spots. This technique provided precise regulation of the reaction, leading to optimal outcomes.

4.4. Melting Points Determination

In order to determine the melting points of the synthesized compounds, small amounts of each were meticulously placed into separate capillary tubes. Once sealed by burning off one end, the samples were inserted into the Mettler Toledo-MP90 Melting Point System, where they were gradually heated until reaching their respective melting points. Throughout the process, the device recorded the melting points of the samples at regular intervals. The resulting data was analyzed and compiled to determine the precise melting points of each compound. This technique allowed for accurate measurements of

melting points, enabling a deeper understanding of the chemical properties and qualities of the synthesized compounds.

4.5. Chemical Spectral Analysis

4.5.1. Infra-red spectrometry (IR)

In order to obtain a comprehensive understanding of the synthesized compounds, the Shimadzu-IR Affinity-IS was utilized to record their IR spectra. An attenuated total reflection (ATR) chamber was selected as the ideal instrument to measure the interaction between infrared radiation and 10 mg of each compound, resulting in high-quality spectra. The data obtained from the spectra was then plotted with wave number cm^{-1} against transmittance percent, which allowed for the identification of the various peaks. Advanced computer algorithms were employed to detect and precisely pinpoint the location of each peak, providing valuable information about the chemical composition and structure of the synthesized compounds. By utilizing this cutting-edge technology, we were able to gain a deeper understanding of the properties and characteristics of the synthesized compounds, allowing for more accurate conclusions to be drawn about their potential applications.

4.5.2. Proton nuclear magnetic resonance spectrometry (^{1}H-NMR)

The synthesized compounds were analyzed using ^{1}H-NMR spectroscopy to provide insight into their chemical structure. For this purpose, Bruker 300 MHz and 400 MHz NMR spectrometers were utilized with tetramethylsilane (TMS) serving as the internal standard. The solution of the final synthesized compounds was dissolved in 0.5 ml of either DMSO-d_6 or ethanol, and the ^{1}H-NMR spectra were recorded.

The NMR technique provides information about the chemical environment of each proton in a molecule, allowing for the determination of its structure. The peak locations and shapes provide information about the types and number of protons present in the molecule, as well as their relative positions. By interpreting the spectra obtained from the synthesized compounds, we were able to determine the number and position of protons in each compound, providing insight into their chemical structure.

Using NMR allowed us to confirm the success of our synthesis reactions and to determine the purity of the final compounds and making accurate conclusions about their potential applications.

4.5.3. Carbon nuclear magnetic resonance spectrometry (^{13}C-NMR)

The ^{13}C-NMR spectroscopy technique was utilized to gain a deeper understanding of the structural characteristics and properties of the synthesized compounds. This technique involved the use of Bruker 75 MHz and 100 MHz NMR spectrometers, which were equipped with tetramethylsilane (TMS) as the internal standard. The synthesized compounds were dissolved in 0.5 ml of either DMSO-d_6 or ethanol, and the resulting solutions were used for the analysis.

The ^{13}C-NMR spectra provided insight into the carbon atoms within the synthesized compounds. By measuring the chemical shifts of the carbon atoms and comparing them to the TMS reference peak, the functional groups and molecular connectivity of the synthesized compounds were identified. The spectra were obtained by irradiating the samples with radiofrequency radiation at the resonant frequency of the carbon atoms in the sample, causing the atoms to absorb energy and transition between energy levels.

4.5.4. High resolution- mass spectrometry (HR-MS)

Mass spectrometry is an effective analytical method utilized for determining the molecular mass, chemical structure, and composition of a compound. In our study, we utilized liquid chromatography attached to a hybrid ion-trap and time-of-flight mass spectrometry (LCMS-IT-TOF) device manufactured by Shimadzu in Kyoto, Japan. This device utilizes electrospray ionization-positive ion mode (ESI+) to record mass spectra.

To record mass spectra, we first dissolved the final synthesized compounds in either acetonitrile or methanol. These solutions were then injected into the LCMS-IT-TOF device, which ionized the compounds and separated them based on their mass-to-charge ratio (m/z). The device then recorded the mass spectra by measuring the ion current as a function of m/z.

The LCMS-IT-TOF device provides accurate and precise mass measurements, allowing us to identify the molecular weight of the synthesized compounds. Additionally, the device can be used to determine the chemical structure of the compounds by fragmenting the ions and analyzing the resulting spectra. This information is essential for determining the identity and purity of the synthesized compounds, as well as for identifying potential impurities or byproducts.

4.6. Determination of COX-1 & COX-2 Inhibitors Activity

The study conducted an evaluation of synthesized pyrrole carboxylic acid derivatives to determine their capacity to block the COX enzyme. To measure the production of PGG_2, fluorometric analysis was utilized. The inhibitory effects of these compounds on both COX-1 and COX-2 enzymes were thoroughly examined using the BioVision COX-1 and COX-2 Inhibitor Screening Kits manufactured by Milpitas, CA, USA [86] . These kits consist of COX enzymes, COX assay buffer, COX probe, and COX cofactor (all in DMSO), arachidonic acid, NaOH, and selective inhibitors such as celecoxib and indomethacin, which target COX-1 and COX-2 enzymes. Remarkably, the study discovered that several compounds exhibited promising inhibition of both COX-1 and COX-2 enzymes, highlighting their potential as anti-inflammatory agents.

4.6.1. Preparation of components of COX-1 & COX-2 kits

To execute the inhibition assay, the constituents of the kit were prepared in the following manner. Initially, the COX-1/COX-2 enzyme solutions were created by reconstituting the lyophilized powder present in the kit with 110 µL of ddH_2O. Then, a diluted COX cofactor was formed by combining COX assay buffer (398 µL) and COX cofactor (2 µL). The arachidonic acid/NaOH solution was diluted by adding 5 µL of arachidonic acid and 5 µL of NaOH, followed by the addition of 90 µL of ddH_2O. These solutions were merged to generate the reaction mixture (80 µL) for each well. The reaction mixture comprised COX assay buffer (76 µL), COX probe (1 µL), diluted COX cofactor (2 µL), and COX-1/COX-2 enzyme solution (1 µL). Subsequently, the test compounds (10 µL) were added to the solution, and the mixture was incubated for 5-10 minutes at 25 °C. To halt the reaction, 10 µL of diluted arachidonic acid/NaOH solution was added to each well. The fluorescence (Ex/Em = 535/587 nm) of the samples was then measured kinetically at 5-minute intervals using a BioTek-Synergy H1 multimode microplate reader (BioTek Instruments, Inc., Winooski, VT, USA). The assay was performed in quadruplicate with a blank and control, and all inhibitor concentrations were tested. The mean ± standard deviation (SD) of the percentage inhibition results were calculated, and the IC_{50} values were determined by plotting the percentage inhibition versus the log concentration using GraphPad 'PRISM' software (version 5.0). Moreover, the selectivity index (SI) was computed by dividing the $IC_{50(COX\text{-}1)}$ by the $IC_{50(COX\text{-}2)}$.

4.7. Molecular docking

To investigate the effects of the new pyrrole derivatives on COX-1 and COX-2, we applied computational protocols, this may involve performing molecular docking calculations and optimizing the structures of the resulting complexes. The objective of our study was to investigate the potential interaction mechanisms of these inhibitors in the binding sites of both COX-1 and COX-2. Glide grid [87] was computed for some probe atoms or rotable groups to assess the optimal inhibitor-macromolecule interaction regions. To determine whether Schrödinger maestro software [88] is a suitable approach for studying the binding mode of the pyrrole carboxylic acid derivatives in both COX-1 and COX-2 binding sites, a preliminary calculation was performed. Specifically, we used the crystallographic complex between COX-1 and COX-2 protein with indomethacin as a control structure to identify the best run parameters and ensure successful docking of flexible pyrrole carboxylic acid derivatives within the COX-1 and COX-2 active sites. This approach helped us explain the observed effects of the pyrrole derivatives and gain a better understanding of their potential as inhibitors for both COX-1 and COX-2.

4.7.1. Selection and validation of COX-1 & COX-2 proteins for studying the interaction of inhibitors

To study the interactions of inhibitors with COX-1 and COX-2 proteins, we selected homospaines proteins for our calculations. These proteins have a similar structure, making it easier to compare the interactions of inhibitors between COX-1 and COX-2. [89]. We used criteria such as the availability of a full amino acid sequence and differences in bound small molecules or conformational states of the binding regions to select high-resolution crystal structures from the Protein Data Bank (PDB) (www.pdb.org;).To validate the selected structures, we employed a re-docking procedure and measured the RMSD. This approach helped ensure that the crystal structures accurately represented the binding modes of the inhibitors, and that our calculations would yield reliable results. Overall, our selection and validation process were aimed at improving the accuracy and reliability of our computational studies and increasing our understanding of the potential of new COX-1 and COX-2 inhibitors for medical applications.

4.7.2. Preparation of COX-1 and COX-2 proteins

To perform computational studies on COX-1 and COX-2 proteins, we downloaded their protein structures from the Protein Data Bank (PDB) in "pdp" format. We used Maestro's Protein Preparation Wizard [90]. To refine the structures by removing crystals and water molecules, adding hydrogen atoms, and minimizing the macromolecular structure to optimize the positions of hydrogen atoms and eliminate strains. These steps were crucial to ensure that the protein structures were suitable for reliable results.

For COX-2 dimers (5-F1a), the heme group is a crucial component of the active site, so we retained it during the preparation process. However, to simplify our calculations, we focused only on chain A and its components, while removing all components within chain B, including solvents and other heteroatoms. This selection was based on the fact that chain A and chain B are identical in COX-2 dimers. On the other hand, COX-1 (6-Y3C) protein does not contain a heme group or crystal ligand, and it is not a metalloprotein. Therefore, standard protein preparation procedures were sufficient to refine its structure for computational studies. Overall, our preparation process aimed to accurately represent the active sites of COX-1 and COX-2 proteins and ensure that our computational studies yield reliable results.

4.7.3. Induced fit molecular docking (IFD) of selected protein

In this study, we utilized induced fit molecular docking (IFD) to accurately predict the binding interactions between the ligand and the COX-1 and COX-2 proteins. The IFD protocol is a powerful tool that considers various factors to produce reliable and precise docking results. This includes the ability to dock the ligand into the correct binding site, predict the conformation of the ligand when docked into the protein, account for the flexibility of the protein and the ligand, and consider the electrostatic or van der Waals interactions between the protein and the ligand [91]. The IFD simulation also takes into account the conformational changes that occur in the protein upon binding to the ligand, providing a more accurate representation of the binding site and the critical interactions that stabilize the protein-ligand complex [92].

To perform IFD calculations, we utilized the module present in Maestro, which integrates the Glide docking capability with Prime homology modeling, to customize the protein for ligand binding. We centered the grid in the stem region on the reference ligand "indomethacin" for both COX-1(6-Y3C) and COX-2 (5-F1a) proteins and applied default

settings for the remaining parameters. This allowed us to generate reliable docking poses for each ligand and obtain a more detailed understanding of the ligand-protein interactions. By utilizing the IFD protocol, we were able to generate accurate and reliable docking results for our study.

4.7.4. Generation of binding site grids from induced fit docking simulation

In the previous section (**4.7.3**), we performed induced fit molecular docking (IFD) simulations to predict the binding interactions between the ligand and the COX-1 and COX-2 proteins. The resulting IFD simulations were used to generate grids that provide valuable information about the protein's binding site, including key residues, critical interactions, and the overall shape of the site. The grid generation process involved selecting specific amino acid residues and centering the grid at their location, with a grid spacing of 12 Å [93]. The grids were generated based on the induced conformation of the protein, which accounts for both the protein's shape and the formation of new interactions with the ligand. For the COX enzymes, we chose the following amino acid residues: THR94, Tyr355, Tyr385, Ser353, Tyr348 and Ser530. These residues were within a 20-radius grid box centered at X = 18.1, Y = 51.98, and Z = 17.42. Using this binding site grid, we docked new tetra substituted pyrrole derivatives for further study. These grids will be useful for understanding the interactions between the ligands and the proteins and can aid in the development of new drugs with improved binding affinity and selectivity.

4.7.5. Ligand preparation

In this section, we will describe the process of preparing these compounds for molecular docking simulations. The structure of all designed compounds was generated with the Build tool in Maestro and then prepared through Ligprep at physiological pH (7.4±1.0) with a force field of OPLAS4. This process allowed for effective assignment of bond orders and incorporation of hydrogen atoms into the structures. The PRCG minimization algorithm was used to minimize the resulting structures while maintaining a convergence gradient of 0.05.

To enhance the accuracy of the results, we applied a conformational search using a combination of mixed torsion and low mode sampling techniques. This involved searching for different possible conformations of the molecules that are energetically favorable and accessible. These techniques were applied to identify the most stable and

low energy conformation of the ligands. Overall, the ligand preparation process was essential for obtaining reliable and accurate docking results. It ensured that the ligand structures were correctly and consistently prepared for the subsequent molecular docking simulations.

4.7.6. Ligand docking in both COX-1 and COX-2 protein

This section utilizes molecular docking to assess the binding affinity of compounds that were identified and synthesized through QSAR, and subsequently found to exhibit activity towards the COX-1 and COX-2 binding sites. The docking was carried out using the Glide flexible ligand docking software in Standard precision (SP) mode, and all docking factors were kept as default. The docking calculations were carried out without any bonding restraints. Monte Carlo algorithm was used to generate the ligand poses, which provided a detailed description of the orientation and position of the ligands relative to the receptors, as well as their core conformations [94]. We docked the designed pyrrole carboxylic acid compounds in both COX-1 (6-Y3C) and COX-2 (5-F1a) proteins. The ligand efficiency of these molecules in binding to COX-1/2 proteins was predicted based on the Glide docking score. This step is crucial in understanding the binding interactions between the synthesized compounds and the COX proteins, which can aid in the development of new drugs with improved binding affinity and selectivity.

4.7.7. Molecular dynamics study (MDS)

In addition to molecular docking, MD simulations were conducted to assess the dynamic stability of the ligand-receptor complexes. To ensure the reliability of the hits identified from the docking analysis, MD simulations were carried out for a duration of 100 ns. For this purpose, we employed the Desmond application [95], utilizing the OPLS3e force field from the Schrodinger Suite and the three-point (TIP3P) water model as a transferable intermolecular potential. To optimize the complex, an energy minimization process was performed. The system was neutralized by introducing Na^+ and Cl^- ions, and a dynamic condition was established with the addition of 150 mM NaCl. Subsequently, the molecular dynamics simulation was executed to capture the dynamic behavior of the ligand-receptor complexes over time. Several key parameters, including the radius of gyration (Rg), root mean square fluctuation (RMSF), and root mean square deviation (RMSD), were calculated using the Desmond application. These parameters

provide valuable insights into the structural dynamics and stability of the ligand-receptor complexes, aiding in the characterization of their binding interactions and facilitating the development of novel drugs with improved binding affinity and selectivity.

4.8. Physicochemical, Drug-Likeness, Pharmacokinetic and Toxicokinetic Properties Prediction

Clinical trials and regulatory approval are stringent processes, and only about 20% of drugs make it to the market due to a small number of compounds with optimal pharmacokinetic and toxicokinetic properties [96]. Low bioavailability leads to poor absorption, rapid elimination, and hepatic clearance, which pose challenges to drug development [97]. Thus, early drug development must consider a compound's absorption, distribution, metabolism, excretion, and toxicity (ADMET) descriptors to evaluate safety and potential efficacy. In this study, Qikprop (Schrödinger, LLC, New York, NY, USA) was utilized to assess the ADMET profiles and drug likeliness of all the compounds and standards. Lipinski's Rule of Five, which mandates a molecular weight (MW) $\leq$ 500 Dalton, $\leq$ 5 hydrogen-bond donors (HBD), hydrogen-bond acceptors (HBA) $\leq$ 10, and a log (octanol/water) partition coefficient (log P) < 5, was used to assess the drug-likeness of the compounds. Any compound that violated more than one of Lipinski's Rule of Five was excluded. Furthermore, the allowable range of rotatable bonds was limited to between 0 and 15.

5. RESULT AND DISCUSSION

5.1. Designing Promising New Compounds using FB-QSAR Model

The FB-QSAR model demonstrated reliability and high accuracy in predicting COX-2 inhibitor activity, with the steric field having the most significant impact on activity, followed by the electrostatic and hydrophobic fields. The model's insights were utilized to design promising new compounds, and the top **22** most active compounds predicted by a FB-QSAR model were selected for synthesis and testing. In addition, the FB-QSAR model was used to predict the activity of compounds identified from *in-vivo* studies. Meanwhile, contour maps were generated for the different fields using PLS factor 5 to investigate the effects of various structural features on the anti-inflammatory activity of indomethacin. Yellow steric contours denoted that large clusters did not promote anti-inflammatory activity, while green contours indicated that large groups were beneficial. Blue outlines in the electrostatic field showed that the addition of an electrostatic group would increase activity, while red contours indicated that the addition of an electronegative group would also be beneficial. Hydrophobicity, as indicated by yellow contours, correlates positively with anti-inflammatory activity, while white contours indicated the opposite. In the hydrogen bond donor field, blue-violet contours indicated that hydrogen bond donors would increase activity, while cyan contours indicated that increasing hydrogen-bond donors would not be appropriate for anti-inflammatory activity. The red areas of the diagram represented regions where an increase in the hydrogen bond acceptor would improve activity, while magenta contours indicated the opposite. Figure 5.1 summarizes the indomethacin structure-activity relationship (SAR) using the drug's contour maps. Based on the findings of the FB-QSAR analysis, the COX inhibition activity of indomethacin is influenced by several factors, ranging from strong to weak properties, including steric effects, hydrogen bond acceptor (HBA) effects, hydrophobic effects, electrostatic effects, and hydrogen bond donor (HBD) effects. The results indicate that the configuration of the indole ring at the N1 position should have a steric group, such as an acyl or alkyl group and negative electrostatic effect. Additionally, at the 5^{th} position, a steric group with a negative electrostatic effect (such as C=O or OH) is preferred. On the other hand, the presence of a methyl group at the 2^{nd} position does not have a steric effect, but it is predicted to have a positive electrostatic effect and act as an HBD group according to the model. Furthermore, a small steric group and a strong negative electrostatic group, such as a carboxylate group (CH_3COOH or C_6H_5COOH),

are recommended at the 3rd position of the indole ring, similar to the acetic acid group in indomethacin. Moreover, the inclusion of hydrophobic groups at the 4th, 5th, 6th, and 7th positions (except for potential HBA groups) is expected to enhance the activity of indomethacin in COX-2 inhibition. Figure 5.2 displays the molecular modifications implemented in synthesized compounds (**4a-4p** and **5a-5g**). While the methy groups at position 2 remained unchanged, modifications were introduced at positions 1, 3, and 5. At position 1 small and large hydrophobic groups containing both hydrogen bond acceptor (HBA) and hydrogen bond donor (HBD) features were added via the carboxyl group. Position 3 was modified with an ester group that also functions as an HBA and HBD. To maintain the hydrophobic and electrostatic effects of the region, large hydrophobic groups like Phenyl, and naphthyl and biphenyl were added at position 5. In addition to these substituents, a thiophen group was also used as a hydrophobic substituent to replace or supplement the phenyl group. These modifications were incorporated in the design and synthesis of compounds (**4a-4p** and **5a-5g**).

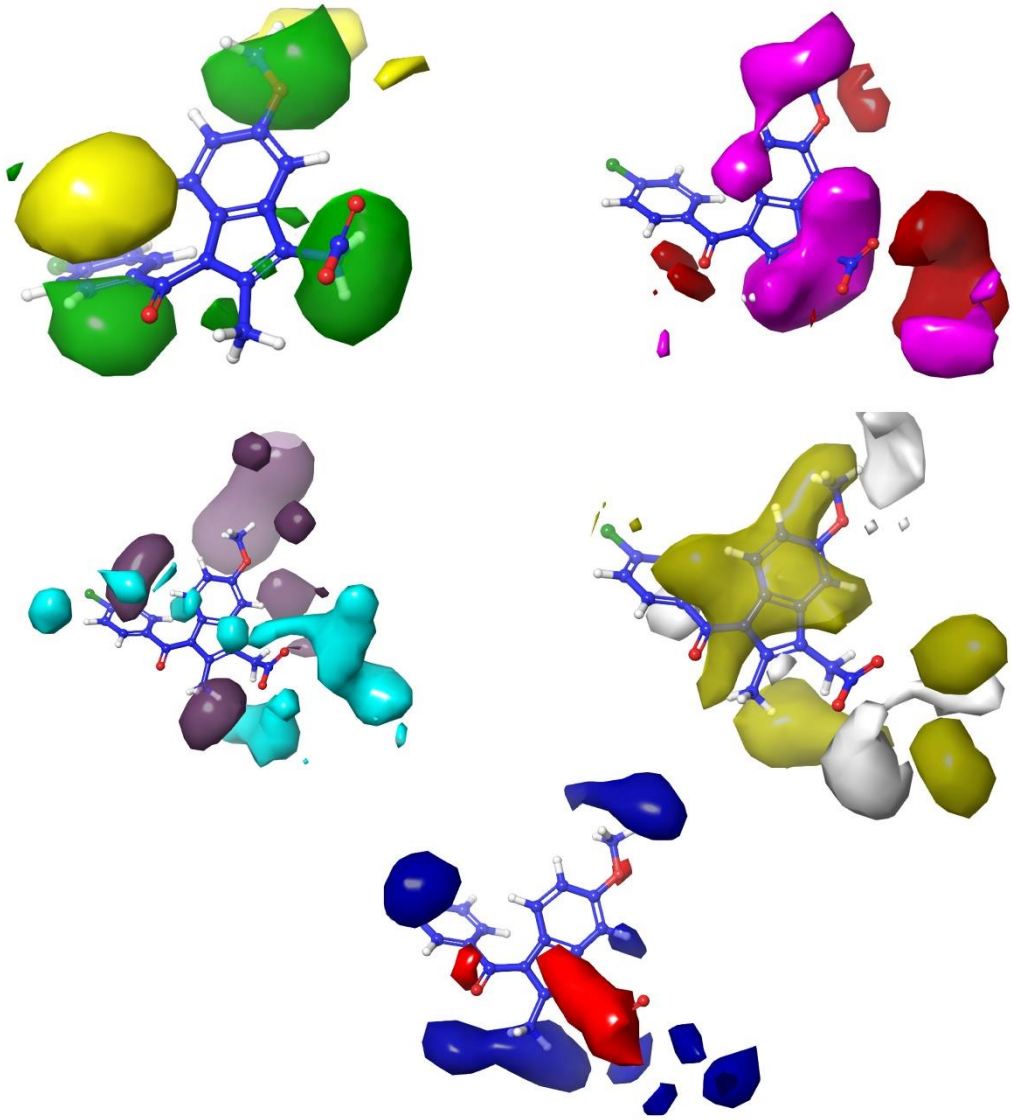

Figure 5.1. *3D Visualizations of indomethacin contour maps: steric* (positive effect (+): green, negative effect (_): yellow), electrostatic (+: blue, -: red), hydrophobic (+: yellow, -: white), HBA (+:red, -:magenta), and HBD (+:blue-violet, -: cyan), respectively

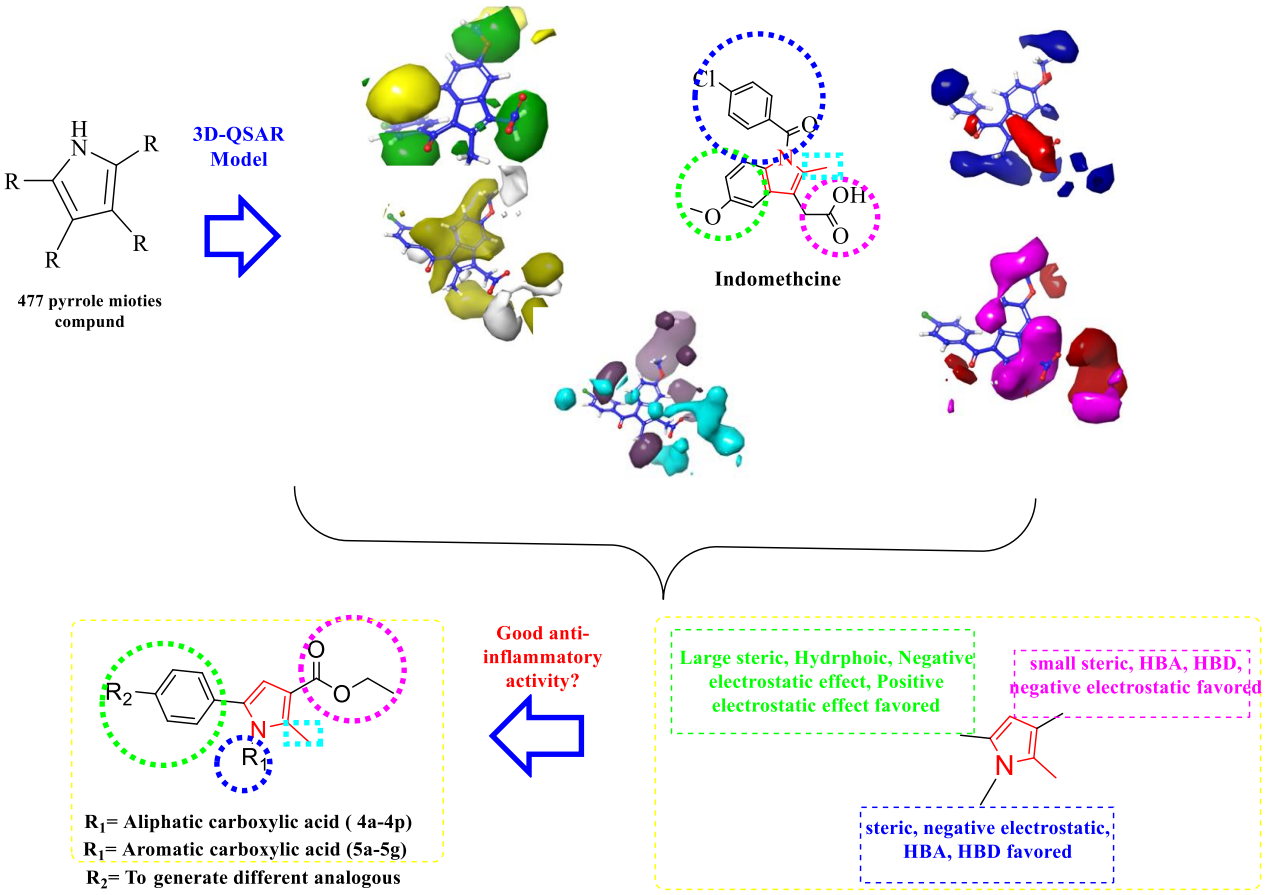

Figure 5.2. *The 3D-QSAR model driven design of target compounds (**4a-4p** and **5a-5g**)*

5.1.1. Evaluation of the FB-QSAR model for predicting COX-2 inhibitor activity

The reliability of the final model (**Model 5**) for predicting the COX-2 inhibitor activities of compounds was assessed using various statistical parameters, such as R^2, Q^2, Pearson^{-r}, stability, RMSE, F, and P values. The values obtained for each parameter fell within the acceptable ranges specified in Table 5.1 of the article's methods section, indicating that the model is both reliable and capable of producing accurate predictions in both internal and external environments. This suggests that the model could be a valuable resource for medicinal chemists seeking to develop safer and more effective drugs.

The outcomes of the FB-QSAR study are presented in Table 5.2. The results showed that the steric field had the most significant effect on the COX-2 inhibitor activity of compounds, accounting for 19.4% of the observed variance, while the electrostatic field accounted for 11.3%. The CoMSIA model, which builds on the CoMFA model, includes additional fields, such as the hydrophobic and hydrogen bond fields. The

hydrophobic field was found to have a substantial effect on the antibacterial activity of the compounds, accounting for 33.7% of the observed variance, while the steric field, electrostatic field, hydrogen bond acceptor field, and hydrogen bond donor field accounted for 19.9%, 15.1%, 13.4%, and 17.8%, respectively. These results provide insights into the factors that influence the COX-2 inhibitor activity of compounds and could aid in the rational design of more potent and selective COX-2 inhibitors.

In Figure 5.3, a linear graph is presented to plot the experimental and predicted values of COX-2 inhibitor activities for all the compounds. The experimental values were obtained through laboratory experiments measuring the inhibitory activity of each compound against the COX-2 enzyme. These values were extracted from the Chembl database, a publicly available repository of bioactivity data. The predicted values, on the other hand, were generated through an FB-QSAR model that used the compounds' chemical structures as inputs to predict their COX-2 inhibitory activities. The linear graph in Figure 5.3 provides a tool for evaluating the performance of the FB-QSAR model in predicting COX-2 inhibitory activities. The x-axis represents the experimental values, while the y-axis represents the predicted values. Each data point on the graph corresponds to a single compound, and the position of the point indicates the degree of agreement between the predicted and experimental values. Data points close to the diagonal line, which represents perfect agreement between the predicted and experimental values, indicate a higher level of accuracy for the model.

By comparing the experimental and predicted values, the accuracy of the FB-QSAR model can be assessed, and areas for improvement can be identified. This information is valuable for guiding the design and development of new COX-2 inhibitors with improved activity and selectivity.

Table 5.1. *The FB-QSAR model's verification values*

#FACTORS	SD	R2	STABİLİTY	F	P	RMSE	Q2	PEARSON-R
1	0.5032	0.6581	0.997	338.7	7.17^{-43}	0.49	0.6812	0.8266
2	0.4138	0.7700	0.992	293.0	1.39^{-56}	0.41	0.7792	0.8845
3	0.3547	0.8320	0.985	287.2	3.87^{-67}	0.37	0.8192	0.9068
4	0.3179	0.8658	0.979	279.1	2.66^{-74}	0.37	0.8196	0.9083

5	0.2905	0.8886	0.969	274.5	5.36^{-80}	0.37	0.8219	0.9090

Table 5.2. *Gaussian (steric, electrostatic, hydrophobic, HBA, and HBD) effects are observed in FB-QSAR results.*

#FACTORS	Steric	Electrostatic	Hydrophobic	HBA	HBD
1	0.3308	0.0660	0.1673	0.1456	0.1153
2	0.2523	0.0901	0.2025	0.1620	0.1340
3	0.2152	0.0975	0.2216	0.1538	0.1445
4	0.1986	0.1056	0.2279	0.1455	0.1534
5	0.1948	0.1135	0.2270	0.1435	0.1459

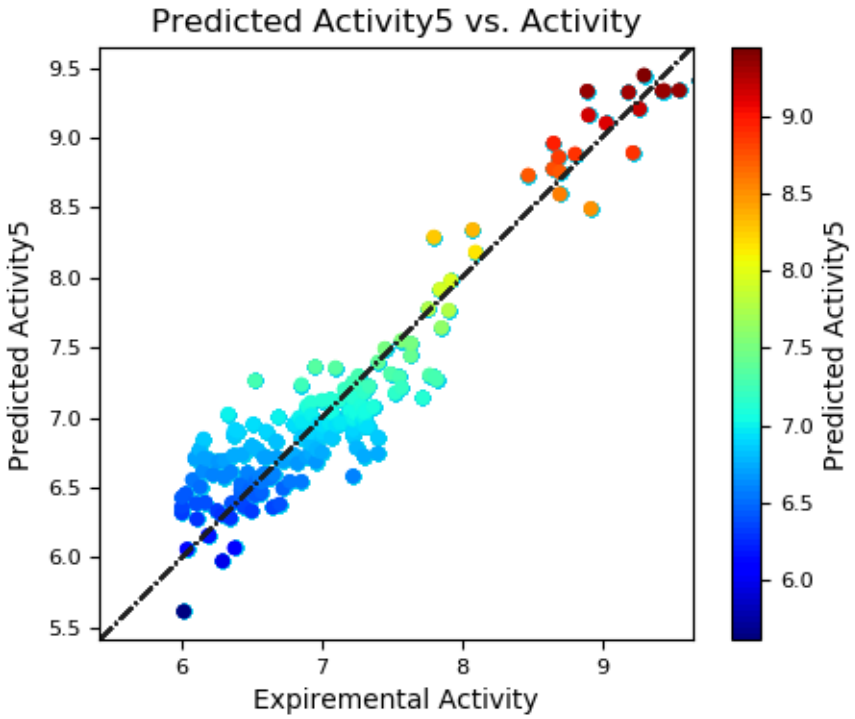

Figure 5.3. *The linear diagrams of the COX-2 FB-experimental QSAR's and predicted* pIC_{50}

5.1.2. FB-QSAR models predict structurally synthesized compounds (4a-4p and / 5a-5g)

The study aimed to use FB-QSAR models to predict the activity of structurally modified compounds (**4a-4p** and **5a-5g**) and reference anti-inflammatory drugs with a specific focus on their COX-2 inhibitory activity. The experimental and predicted pIC_{50} values were compared and compiled in Table 5.3, using the ideal model, factor 5, for predictions. The results showed that several synthesized compounds exhibited higher inhibitory activity against COX-2 compared to the reference drugs. For example, compound **4h** had a predicted pIC_{50} value of 7.11 and compound **4m** had a pIC_{50} value of 6.62, both higher than that of ibuprofen and Nimesulide (6.44 and 6.20, respectively), which are reference drugs listed in Table 5.3.

On the other hand, all the benzoic acid derivatives showed lower predicted and experimental activity towards COX-2 compared to the reference drugs. These findings suggest that the acetic acid analogs exhibit greater activity towards COX-2, which is supported by the results obtained from the fluorometric methods used to measure the activity. Table 5.3 also includes experimentally validated pIC_{50} values obtained using BioVision's kit protocol for COX-2 inhibitory activity [98, 99]. Among the reference drugs, celecoxib had the highest predicted pIC_{50} value of 7.26, followed by Ibuprofen (6.44) and Nimesulide (6.20). The experimentally measured pIC_{50} values for celecoxib, Nimesulide, and Ibuprofen were 6.87, 5.77, and 5.27, respectively, using our model, indicating good agreement between the experimental and predicted values, and validating the model.

In summary, the study demonstrated the potential of FB-QSAR models in predicting the activity of novel compounds for drug discovery. The synthesized compounds exhibited promising COX-2 inhibitory activity, with some compounds showing higher activity than the reference drugs. The experimentally validated pIC_{50} values provided further support for the reliability of the FB-QSAR model in predicting COX-2 inhibitory activity.

Table 5.3. Active compounds against inflammation predicted by FB-QSAR and confirmed experimentally.

Compounds	Predicted activity[5]	Experimental Activity*	compounds	Predicted activity[5]	Expiremental Activity*
4h	7.1136	7.0411	**5d**	5.9243	> 5
4k	5.9243	6.9665	**5a**	5.5925	> 5
4l	6.1436	6.8446	**4m**	6.6225	> 5
4g	6.0261	6.7258	**4n**	6.0661	> 5
5b	5.5926	> 6	**4d**	6.4691	> 5
5e	5.5925	> 6	**Celecoxib**	7.2610	6.87
5f	5.9612	> 6	**Ibuprofen**	6.4498	5.27
4c	5.4850	> 6	**Nimesulide**	6.2041	5.77
4i	6.1678	> 6			
5g	5.3411	> 6			
4e	6.1800	> 6			
5c	5.3848	> 6			

{(*): Rapid and Reliable Test for Identifying COX Enzyme Inhibiting Compounds (BioVision's kit protocol), ([5]): predection activity with using FB-QSAR model 5}.

5.2. Synthesis Of The Targeted Compounds

5.2.1. Synthesis of ethyl 2-acetyl-4-oxo-4-(substituted phenyl) butanoate (3)

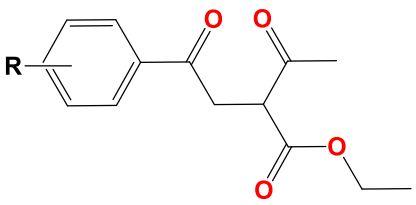

3

Figure 5.4. *Molecular structure of compound (3)*

Ethyl 2-acetyl-4-oxo-4-(substituted phenyl) butanoate was synthesized according method C.

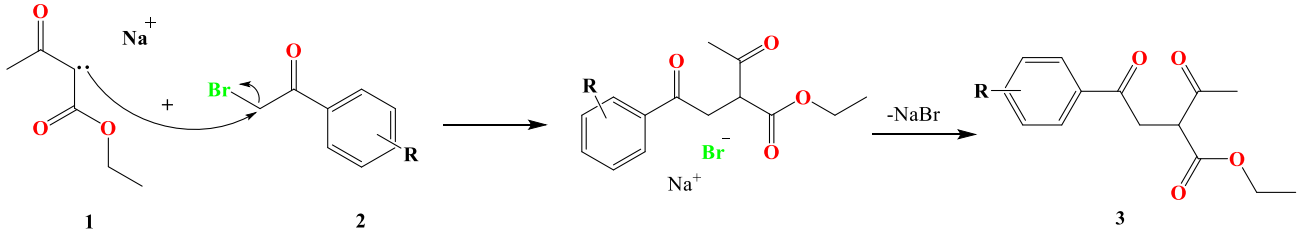

1 **2** **3**

Figure 5.5. *Schematic representation of method C mechanism*

5.2.2. Synthesis of 2-[3-(Ethoxycarbonyl)-2-methyl-5-(substituted phenyl)-*1H*-pyrrol-1-yl]substituted carboxylic acid (4a-4p and 5a-5g)

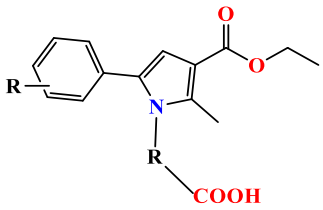

R= Acetic acid dev. **(4a-4p)**
R= Substituted benzoic acid dev. **(5a-5g)**

Figure 5.6. *Molecular structure of compound (**4a-4p and 5a-5g**)*

2-[3-(Ethoxycarbonyl)-2-methyl-5-(substitutedphenyl)-1*H*-pyrrol-1-yl]substituted carboxylic acid (**4a-4p & 5a-5g**) were synthesized according to method D.

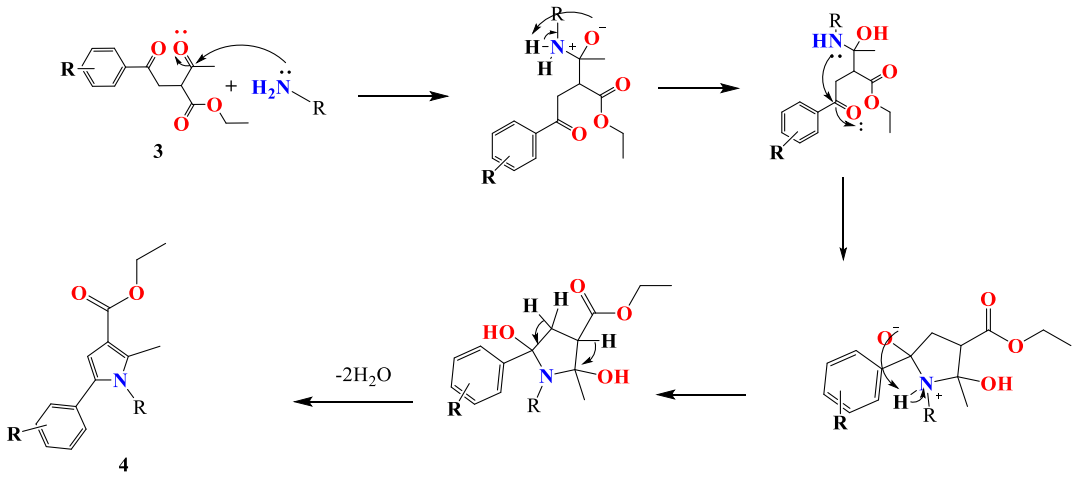

Figure 5.7. *Schematic representation of method D mechanism.*

5.2.2.1. 2-(3-(Ethoxycarbonyl)-2-methyl-5-phenyl-1H-pyrrol-1-yl)acetic acid

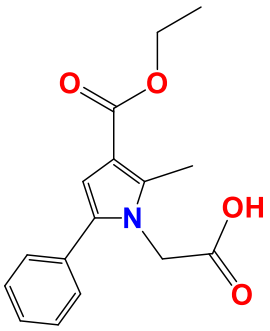

Figure 5.8. *Molecular structure of compound* ***4a***

Synthesized according to method **D**, experimental melting point: 190-191ºC, 75% yield percent.

^{1}H-NMR (400 MHz, DMSO-d_6; δ, ppm): 1.25 (3H, t, *J*= 7.07 Hz, -CH_2-**CH_3**), 2.45 (3H, s, pyrrole-**CH_3**), 4.18 (2H, q, J_1=7.05 Hz, J_2= 14.08 Hz, -**CH_2**-CH_3), 4.62 (2H, s, **CH_2**-COOH), 6.42 (1H, s, **CH**-pyrrole), 7.29 (2H, d, *J*= 7.72 Hz, Ar-**H**), 7.37 (1H, t, *J*= 6.78 Hz, Ar-**H**), 7.42 (2H, t, *J*= 7.12 Hz, Ar-**H**).

^{13}C-NMR (100 MHz, DMSO-d_6; δ, ppm): **):** 11.52 (-pyrrole-**C**H_3), 14.89 (-CH_2-**C**H_3), 46.60 (-**C**H_2-COOH), 59.31 (-**C**H_2-CH_3), 109.27 (Pyrrole-**C_4**), 111.76 (Pyrrole-**C_3**), 128.16 (Phenyl-**C_4**), 128.98 (Phenyl-**$C_{2,6}$**), 129.23 (Phenyl-**$C_{3,5}$**), 132.29 (Phenyl-**C_1**), 133.92 (Pyrrole-**C_2**), 137.79 (Pyrrole-**C_5**), 164.89 (**C**O-O-Et), 170.42 (**C**OOH).

HRMS (-m/z): $[M+H]^+$: For $C_{16}H_{17}NO_4$ calculated molecular weight: 288.1216; found: 288.1230.

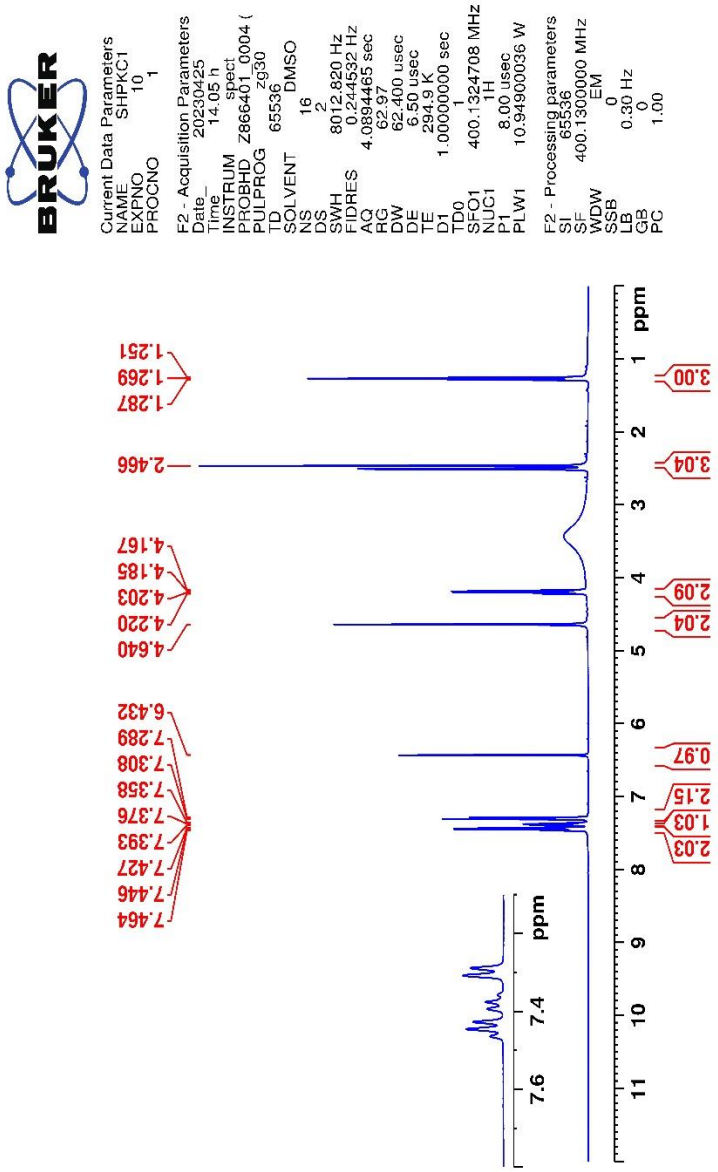

Figure 5.9. *^{1}H-NMR spectrum of the compound **4a***

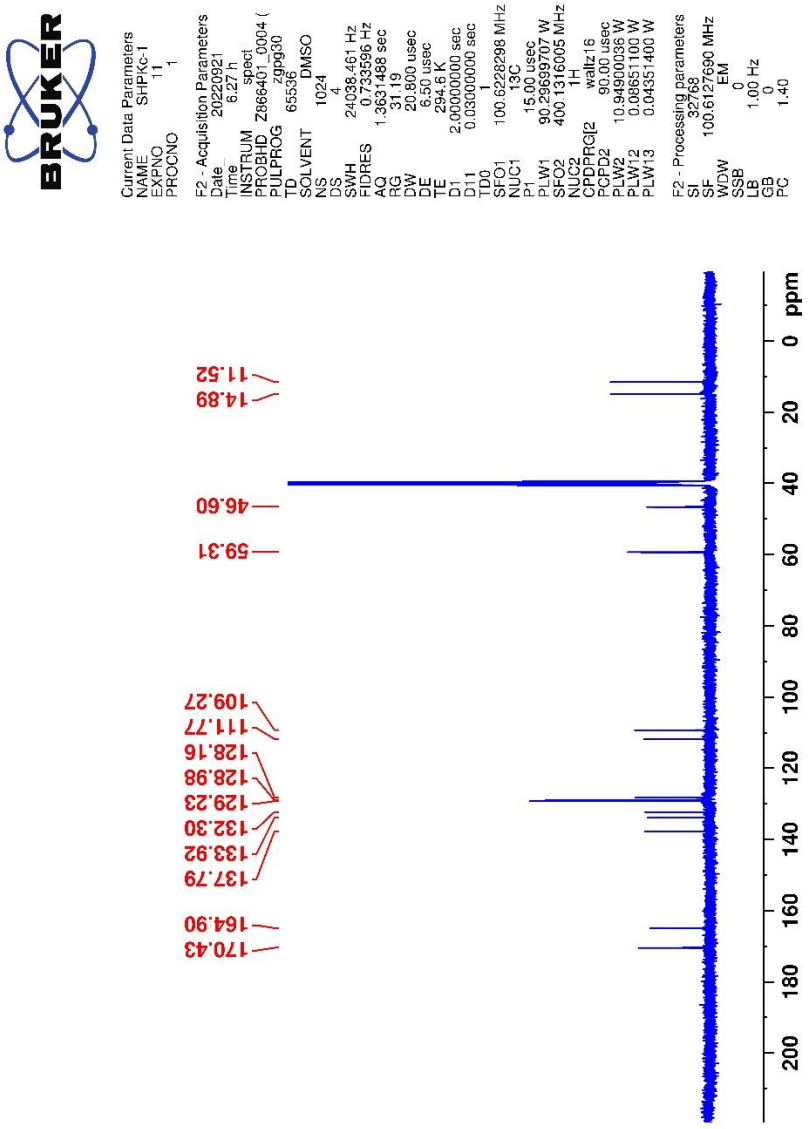

Figure 5.10. *^{13}C-NMR spectrum of the compound* ***4a***

Formula Predictor Report - SHPKC1-2_352.lcd

Page 1 of 1

Data File: C:\LabSolutions\Data\Analiz\Asaf\SHPKC1-2_352.lcd

Elmt	Val.	Min	Max	Elmt	Val.	Min	Max	Elmt	Val.	Min	Max	Elmt	Val.	Min	Max	Use Adduct
H	1	0	30	O	2	0	4	S	2	0	0	Ru	2	0	0	H
C	4	0	30	F	1	0	0	Cl	1	0	0	Pd	2	0	0	
N	3	0	5	P	3	0	0	Br	1	0	0	I	3	0	0	

Error Margin (ppm): 5
HC Ratio: unlimited
Max Isotopes: 3
MSn Iso RI (%): 10.00

DBE Range: 5.0 - 25.0
Apply N Rule: yes
Isotope RI (%): 1.00
MSn Logic Mode: AND

Electron Ions: odd
Use MSn Info: yes
Isotope Res: 9000
Max Results: 50

Event#: 1 MS(E+) Ret. Time : 2.533 Scan# : 381

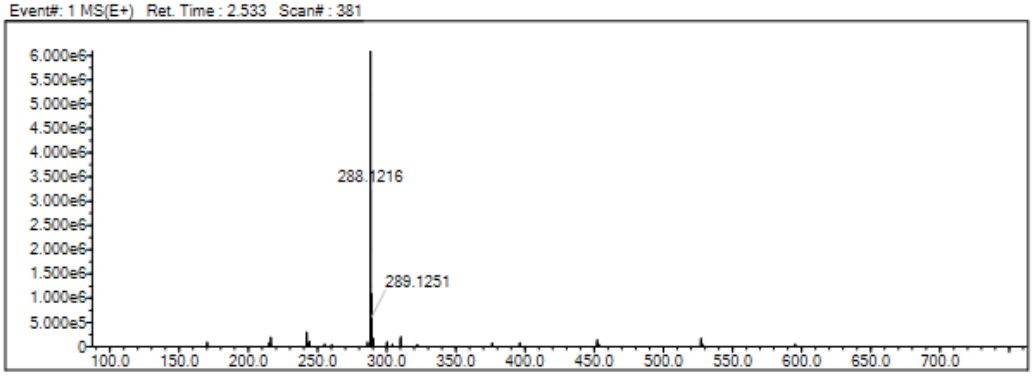

Measured region for 288.1216 m/z

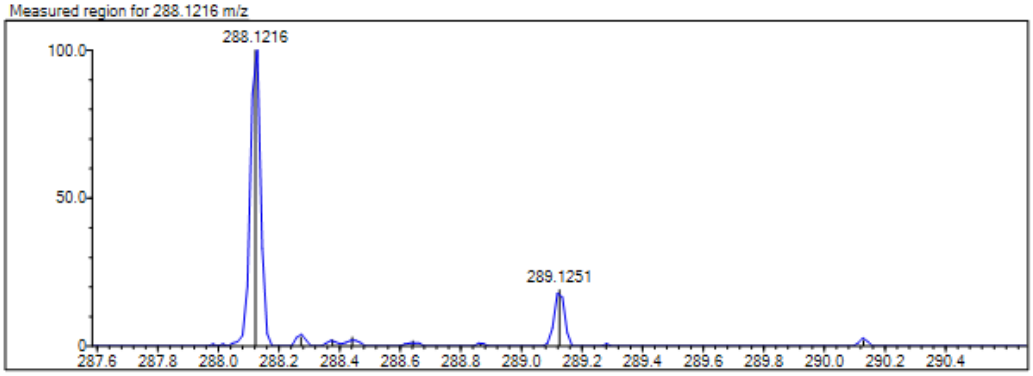

C16 H17 N O4 [M+H]+ : Predicted region for 288.1230 m/z

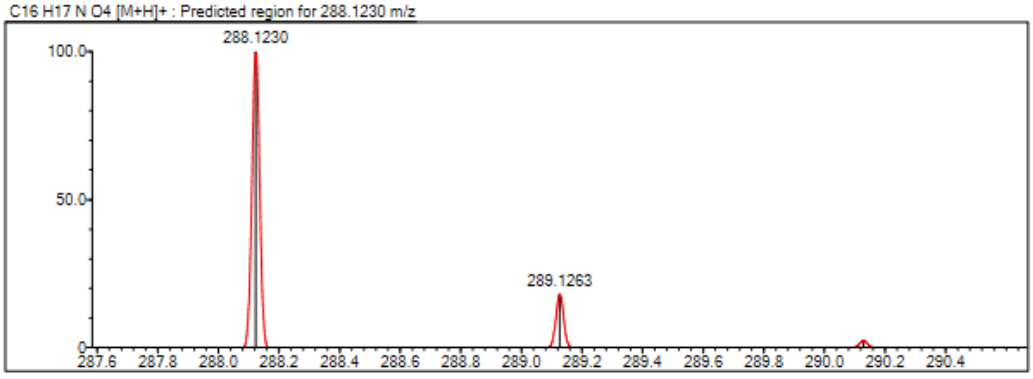

Rank	Score	Formula (M)	Ion	Meas. m/z	Pred. m/z	Df. (mDa)	Df. (ppm)	Iso	DBE
1	87.30	C16 H17 N O4	[M+H]+	288.1216	288.1230	-1.4	-4.86	96.62	9.0

Figure 5.11. *Mass spectrum of the compound* ***4a***

5.2.2.2. 2-[3-(Ethoxycarbonyl)-5-(4-methoxyphenyl)-2-methyl-1H-pyrrol-1-yl]acetic acid

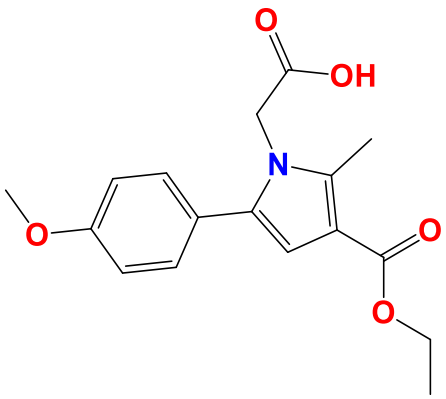

Figure 5.12. *Molecular structure of compound **4b***

Synthesized according to method **D**, experimental melting point: 250-251ºC, 65% yield. present.

^{1}H-NMR (400 MHz, DMSO-d_6; δ, ppm): 1.25 (3H, t, *J*= 7.10 Hz, -CH_2-**CH_3**), 2.58 (3H, s, pyrrole-**CH_3**), 3.77 (3H, s, -O-**CH_3**), 4.05 (2H, s, **CH_2**-COOH), 4.15 (2H, q, J_1=7.05 Hz, J_2= 14.3 Hz, -**CH_2**-CH_3), 6.25 (1H, s, **CH**-pyrrole), 6.93 (2H, d, *J*= 8.34 Hz, Ar-**H**), 7.33 (2H, d, *J*= 8.29 Hz, Ar-**H**).

^{13}C-NMR (100 MHz, DMSO-d_6; δ, ppm): 11.79 (-pyrrole-**C**H_3), 14.99 (-CH_2-**C**H_3), 49.86 (-**C**H_2-COOH), 55.55 (-O**C**H3), 58.88 (-**C**H_2-CH_3), 107.57 (Pyrrole-**C_4**), 110.33 (Pyrrole-**C_3**), 114.24 (Phenyl-**$C_{3,5}$**), 125.69 (Phenyl-**$C_{2,6}$**),130.33 (Phenyl-**C_1**), 133.48 (Pyrrole-**C_2**), 137.23 (Pyrrole-**C_5**), 158.85 (Phenyl-**C_4**), 165.46 (**C**O-O-Et).

HRMS (-m/z): $[M+H]^+$: For $C_{17}H_{19}NO_5$ calculated molecular weight: 318.1332; found: 318.1336.

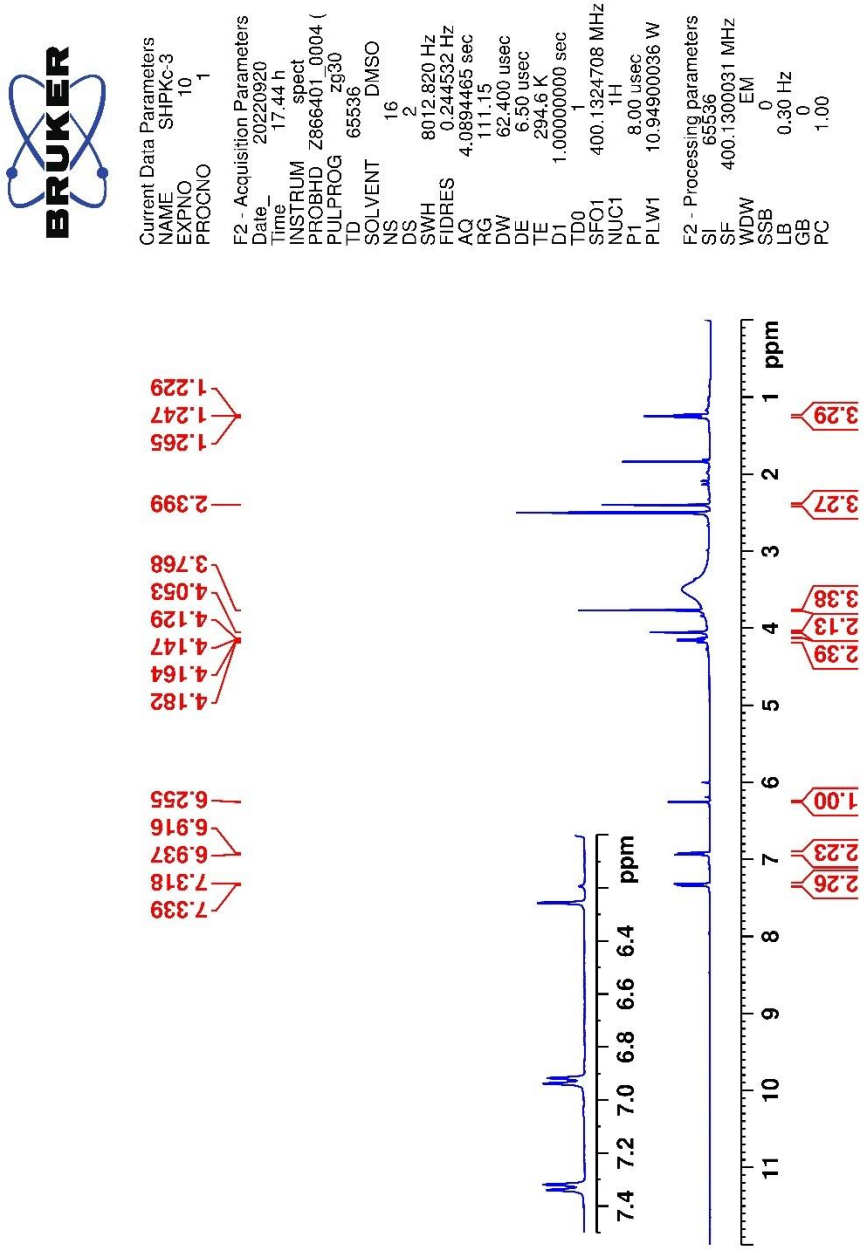

Figure 5.13. *[1]H-NMR spectrum of the compound **4b***

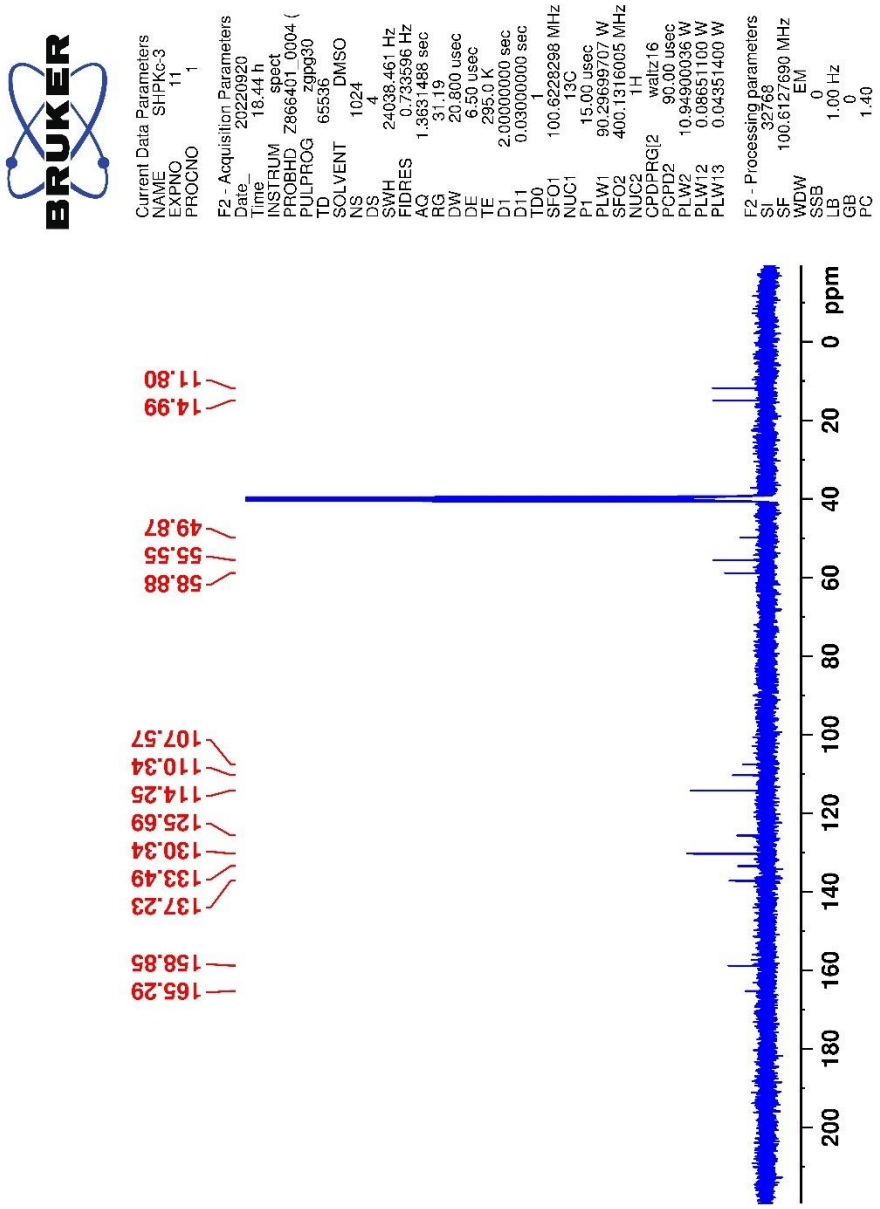

Figure 5.14. *^{13}C-NMR spectrum of the compound **4b***

Formula Predictor Report - SHPKC3_314.lcd

Data File: C:\LabSolutions\Data\Analiz\Asaf\SHPKC3_314.lcd

Elmt	Val.	Min	Max	Elmt	Val.	Min	Max	Elmt	Val.	Min	Max	Elmt	Val.	Min	Max	Use Adduct
H	1	0	30	O	2	0	5	Cl	1	0	0	I	3	0	0	H
B	3	0	0	F	1	0	0	Br	1	0	0					
C	4	0	32	P	3	0	0	Ru	2	0	0					
N	3	0	6	S	2	0	0	Pd	2	0	0					

Error Margin (ppm): 5
HC Ratio: unlimited
Max Isotopes: 3
MSn Iso RI (%): 10.00

DBE Range: 5.0 - 25.0
Apply N Rule: yes
Isotope RI (%): 1.00
MSn Logic Mode: AND

Electron Ions: odd
Use MSn Info: yes
Isotope Res: 9000
Max Results: 50

Event#: 1 MS(E+) Ret. Time : 2.613 Scan# : 393

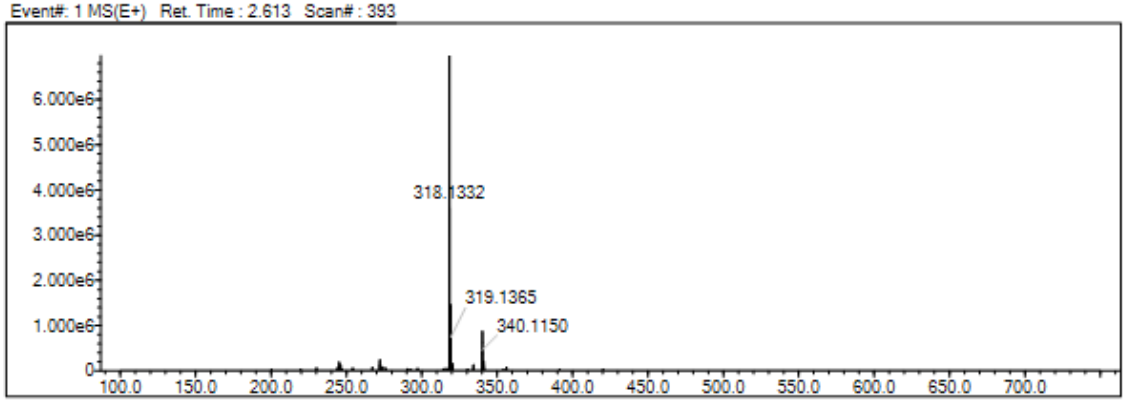

Measured region for 318.1332 m/z

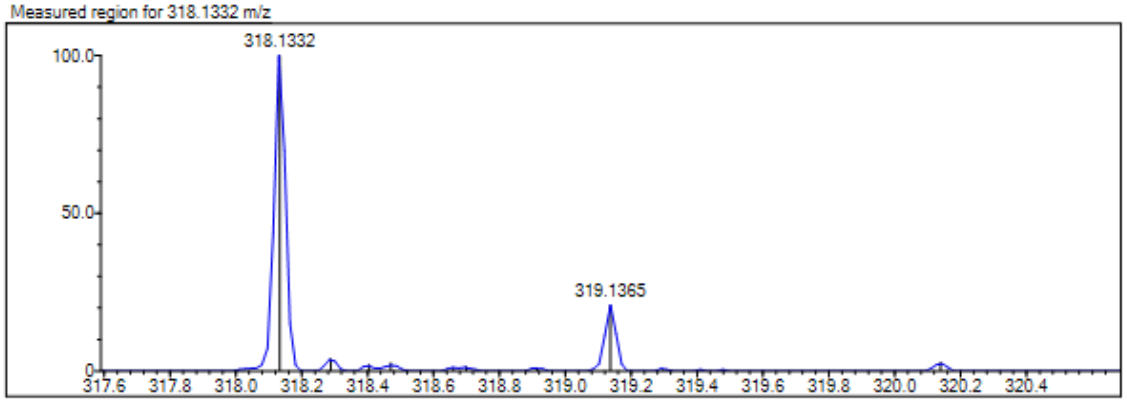

C17 H19 N O5 [M+H]+ : Predicted region for 318.1336 m/z

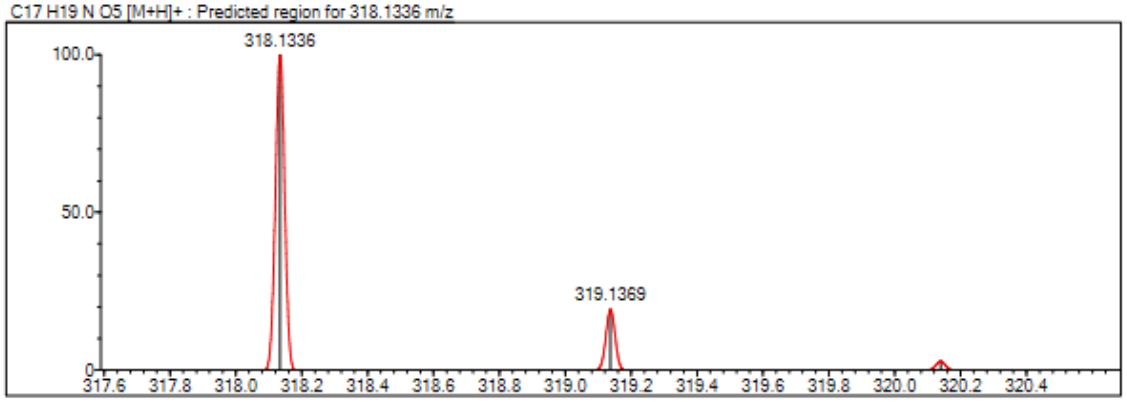

Rank	Score	Formula (M)	Ion	Meas. m/z	Pred. m/z	Df. (mDa)	Df. (ppm)	Iso	DBE
1	87.14	C17 H19 N O5	[M+H]+	318.1332	318.1336	-0.4	-1.26	87.71	9.0

Figure 5.15. *Mass spectrum of the compound* ***4b***

5.2.2.3. 2-[3-(Ethoxycarbonyl)-5-(4-fluorophenyl)-2-methyl-1H-pyrrol-1-yl]acetic acid

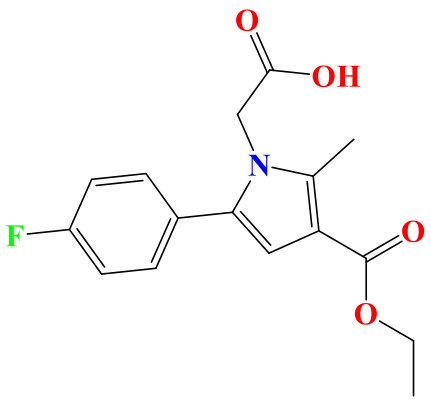

Figure 5.16. *Molecular structure of compound* ***4c***

Synthesized according to method **D**, experimental melting point 160-161 ºC, 85% yield percent.

^{1}H-NMR (400 MHz, DMSO-d_6; δ, ppm): 1.25 (3H, t, *J*= 7.06 Hz, -CH_2-**CH_3**), 2.42 (3H, s, pyrrole-**CH_3**), 4.17 (2H, q, J_1=7.05 Hz, J_2= 14.1 Hz, -**CH_2**-CH_3), 4.44 (2H, s, **CH_2**-COOH), 6.38 (1H, s, **CH**-pyrrole), 7.24 (2H, t, *J*= 8.66 Hz, Ar-**$H_{3,5}$**), 7.34 (2H, t, *J*= 5.65 Hz, Ar-**$H_{2,6}$**).

^{13}C-NMR (100 MHz, DMSO-d_6; δ, ppm) 11.57 (-pyrrole-**C**H_3), 14.90 (-CH_2-**C**H_3), 47.52 (-**C**H_2-COOH), 59.22 (-**C**H_2-CH_3), 109.11 (Pyrrole-**C_4**), 119.38 (Pyrrole-**C_3**), 115.91, 116.12, (Phenyl-**$C_{3,5}$**), 129.02 (Phenyl-**C_1**), 131.08, 131.16 (Phenyl-**$C_{2,6}$**), 132.75 (Pyrrole-**C_2**), 137.69 (Pyrrole-**C_5**), 160.85 (Phenyl-**C_4**), 164.95 (**C**O-O-Et), 170.52 (**C**OOH).

HRMS (-m/z): $[M+H]^+$: For $C_{16}H_{16}NO_4F$ calculated molecular weight: 306.1130, found: 306.1136.

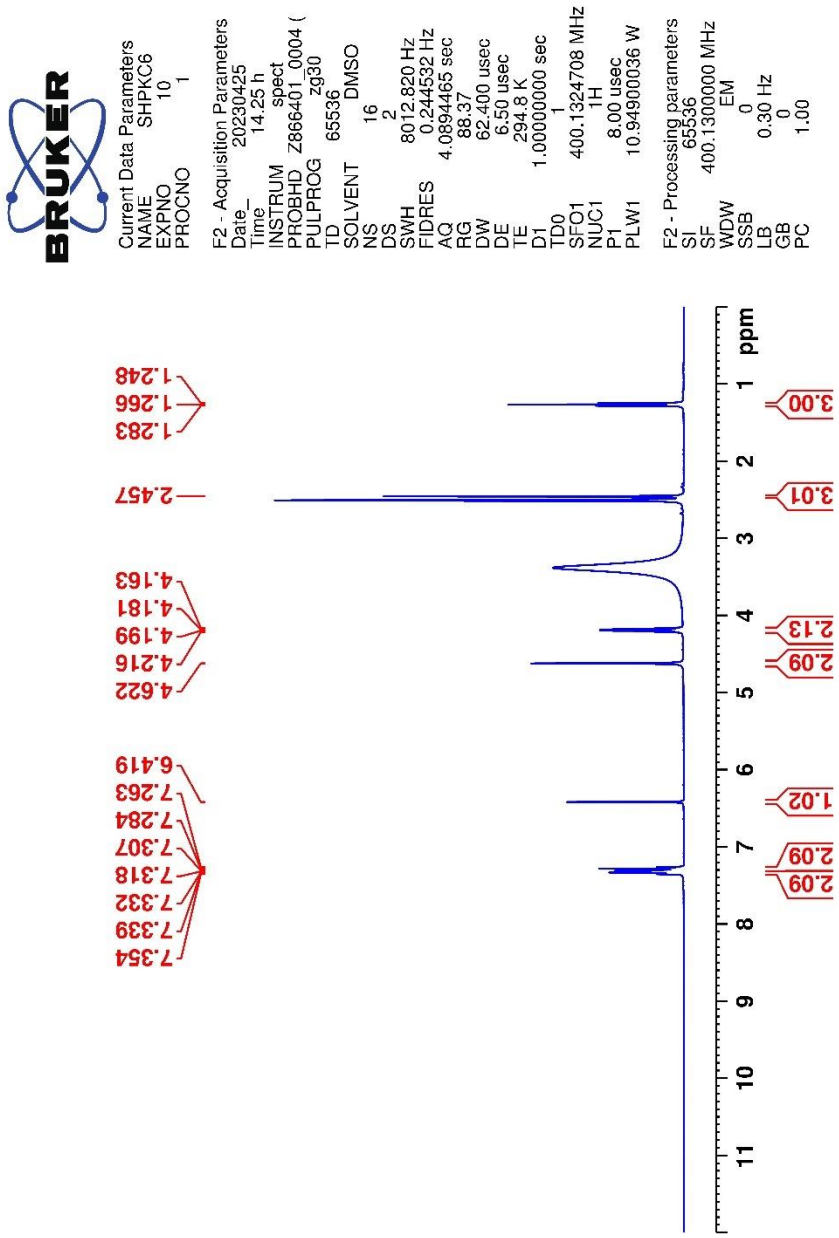

Figure 5.17. *[1]H-NMR spectrum of the compound **4c***

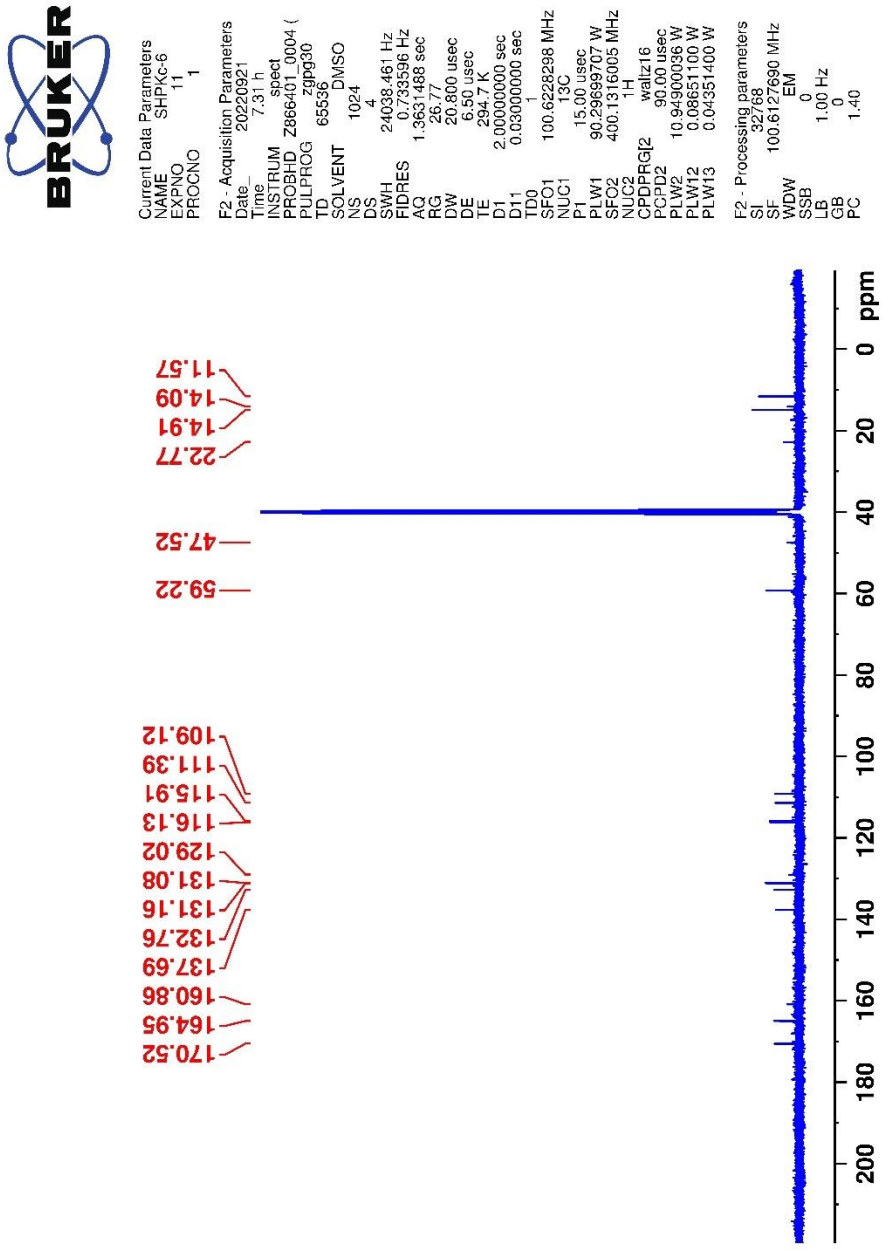

Figure 5.18. *^{13}C-NMR spectrum of the compound **4c***

Formula Predictor Report - SHPKC6-2_353.lcd

Page 1 of 1

Data File: C:\LabSolutions\Data\Analiz\Asaf\SHPKC6-2_353.lcd

Elmt	Val.	Min	Max	Elmt	Val.	Min	Max	Elmt	Val.	Min	Max	Elmt	Val.	Min	Max	Use Adduct
H	1	0	30	O	2	0	4	S	2	0	0	Ru	2	0	0	H
C	4	0	30	F	1	1	1	Cl	1	0	0	Pd	2	0	0	
N	3	0	5	P	3	0	0	Br	1	0	0	I	3	0	0	

Error Margin (ppm): 5
HC Ratio: unlimited
Max Isotopes: 3
MSn Iso RI (%): 10.00

DBE Range: 5.0 - 25.0
Apply N Rule: yes
Isotope RI (%): 1.00
MSn Logic Mode: AND

Electron Ions: odd
Use MSn Info: yes
Isotope Res: 9000
Max Results: 50

Event#: 1 MS(E+) Ret. Time : 2.573 -> 2.573 Scan# : 387 -> 387

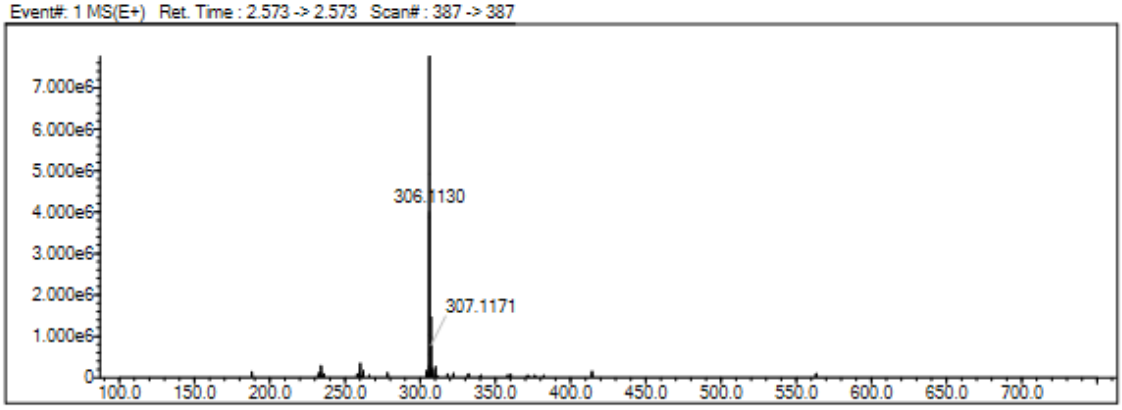

Measured region for 306.1130 m/z

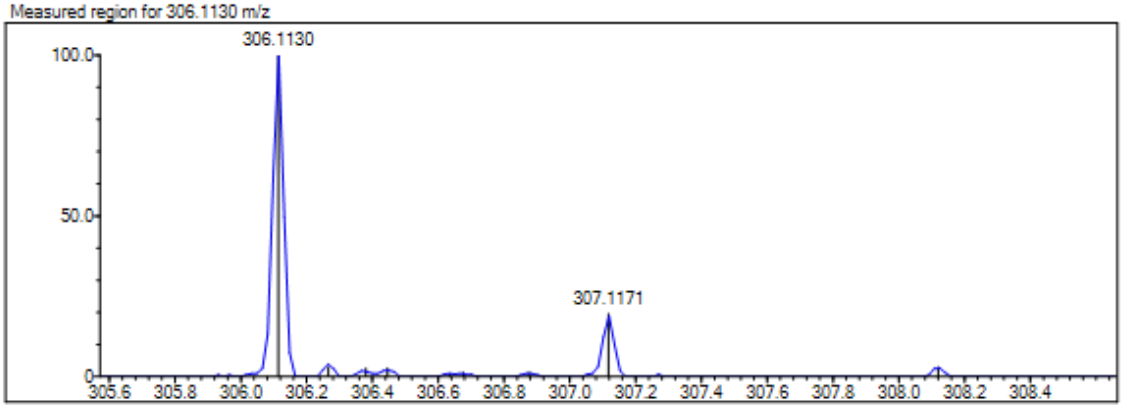

C16 H16 N O4 F [M+H]+ : Predicted region for 306.1136 m/z

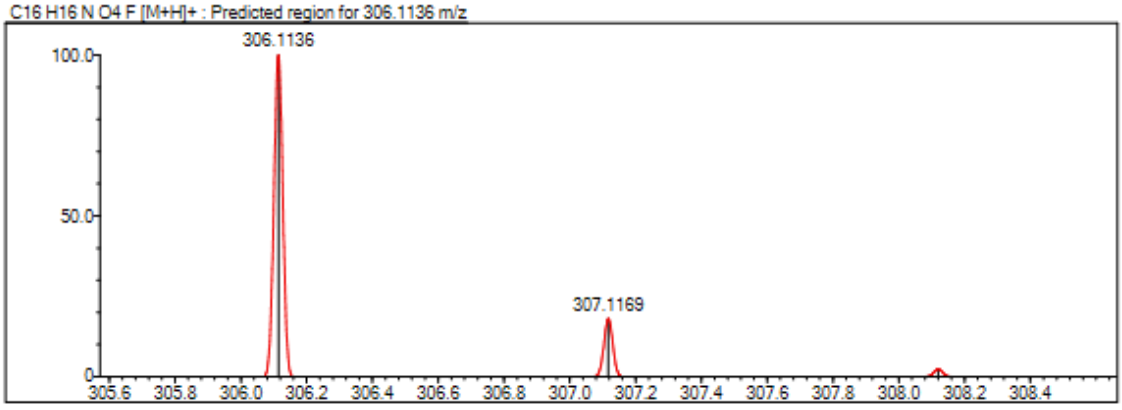

Rank	Score	Formula (M)	Ion	Meas. m/z	Pred. m/z	Df. (mDa)	Df. (ppm)	Iso	DBE
1	97.60	C16 H16 N O4 F	[M+H]+	306.1130	306.1136	-0.6	-1.96	100.00	9.0

Figure 5.19. *Mass spectrum of the compound* ***4c***

5.2.2.4. 2-[5-(4-Chlorophenyl)-3-(ethoxycarbonyl)-2-methyl-1H-pyrrol-1-yl]acetic acid

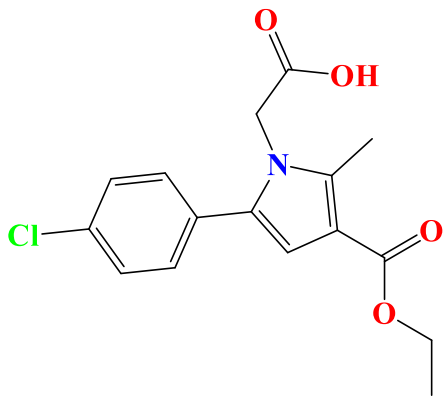

Figure 5.20. *Molecular structure of compound **4d***

Synthesized according to method **D**, experimental melting point: 210-211ºC, 63% yield percent.

^{1}H-NMR (400 MHz, DMSO-d_6; δ, ppm): 1.25 (3H, t, *J*= 7.07 Hz, -CH_2-**CH_3**), 2.43 (3H, s, pyrrole-**CH_3**), 4.17 (2H, q, J_1=7.06 Hz, J_2= 14.14 Hz, -**CH_2**-CH_3), 4.58 (2H, s, **CH_2**-COOH), 6.44 (1H, s, **CH**-pyrrole), 7.31 (2H, d, *J*= 8.08 Hz, Ar-**$H_{2,6}$**), 7.47 (2H, d, *J*= 8.06 Hz, Ar-**$H_{3,5}$**).

^{13}C-NMR (100 MHz, DMSO-d_6; δ, ppm) 11.52 (-pyrrole-**C**H_3), 14.88 (-CH_2-**C**H_3), 46.88 (-**C**H_2-COOH), 59.34 (-**C**H_2-CH_3), 109.69 (Pyrrole-**C_4**), 111.83 (Pyrrole-**C_3**), 129.23 (Phenyl-**$C_{2,6}$**), 130.65 (Phenyl-**$C_{3,5}$**), 131.22 (Phenyl-**C_1**), 132.63 (Phenyl-**C_4**), 132.84 (Pyrrole-**C_2**), 138.13 (Pyrrole-**C_5**), 164.82 (**C**O-O-Et), 170.41 (**C**OOH).

HRMS (-m/z): $[M+H]^+$: For $C_{16}H_{16}NO_4Cl$ calculated molecular weight: 322.0829; found: 322.0841.

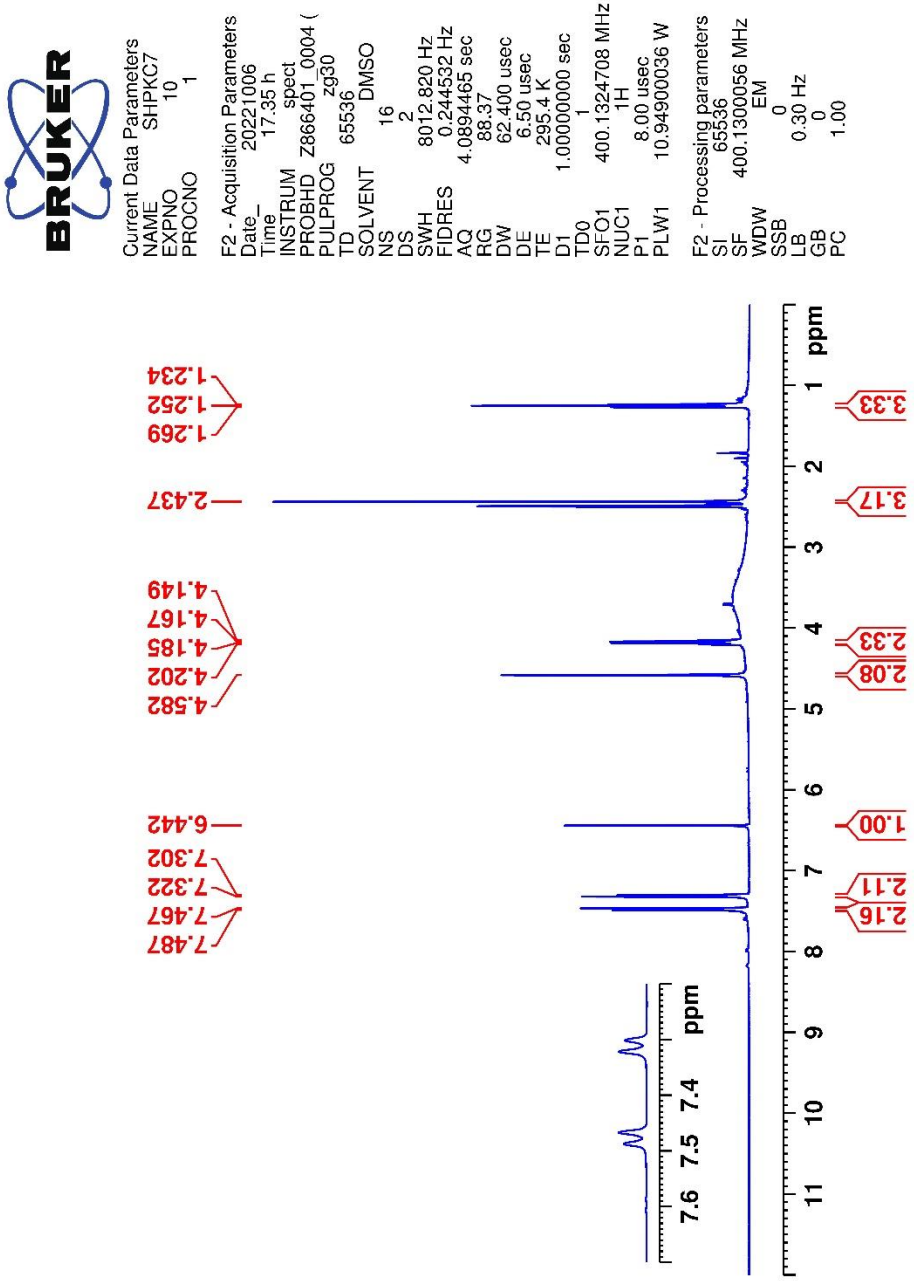

Figure 5.21. *[1]H-NMR spectrum of the compound* ***4d***

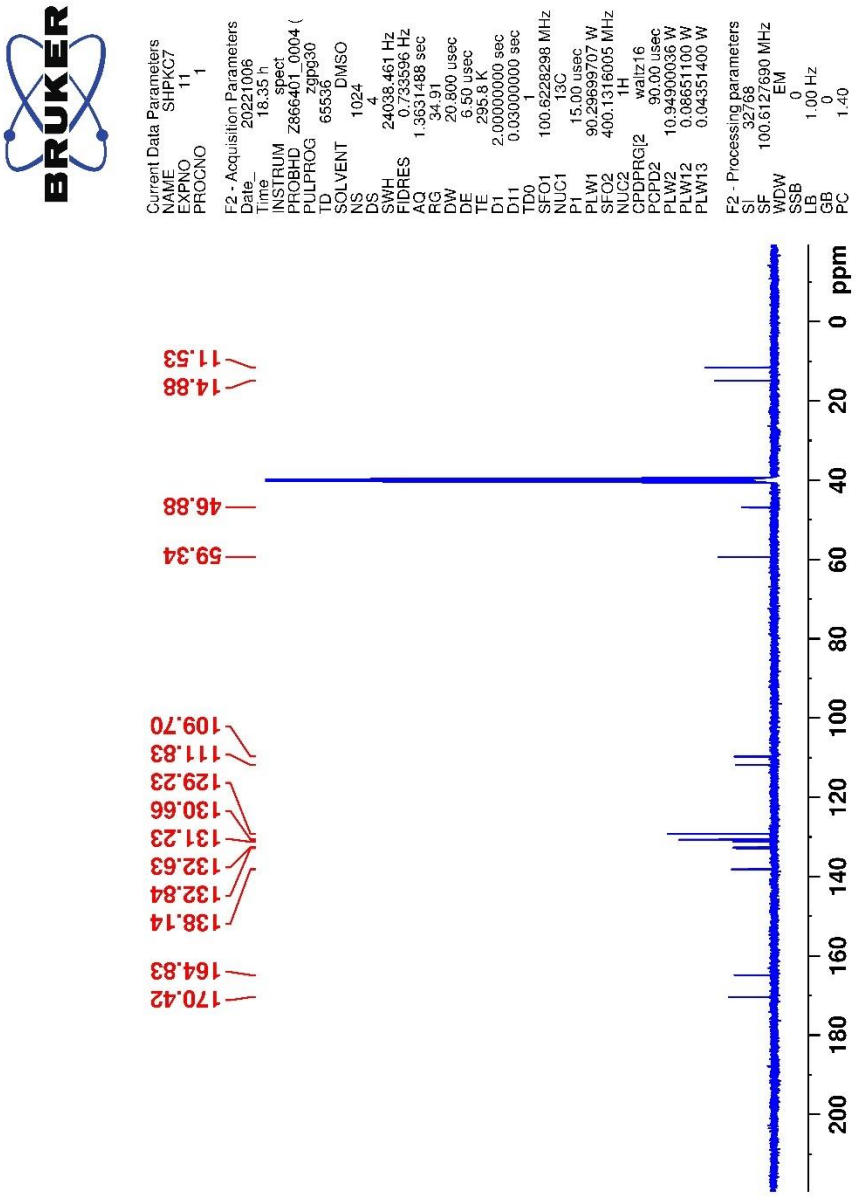

Figure 5.22. *^{13}C-NMR spectrum of the compound **4d***

Formula Predictor Report - SHPKC7_312.lcd

Page 1 of 1

Data File: C:\LabSolutions\Data\Analiz\Asaf\SHPKC7_312.lcd

Elmt	Val.	Min	Max	Elmt	Val.	Min	Max	Elmt	Val.	Min	Max	Elmt	Val.	Min	Max	Use Adduct
H	1	0	30	O	2	0	5	Cl	1	1	1	I	3	0	0	H
B	3	0	0	F	1	0	0	Br	1	0	0					
C	4	0	32	P	3	0	0	Ru	2	0	0					
N	3	0	6	S	2	0	0	Pd	2	0	0					

Error Margin (ppm): 5
HC Ratio: unlimited
Max Isotopes: 3
MSn Iso RI (%): 10.00

DBE Range: 5.0 - 25.0
Apply N Rule: yes
Isotope RI (%): 1.00
MSn Logic Mode: AND

Electron Ions: odd
Use MSn Info: yes
Isotope Res: 9000
Max Results: 50

Event#: 1 MS(E+) Ret. Time : 3.013 Scan# : 453

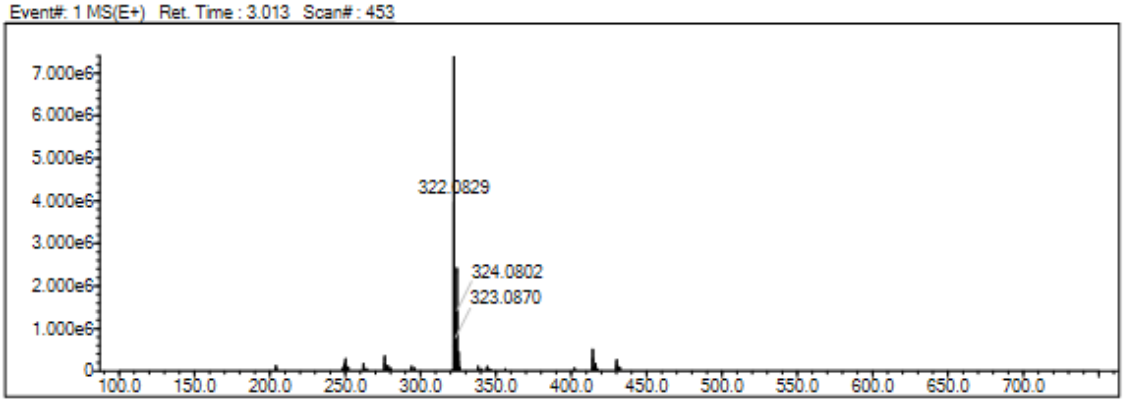

Measured region for 322.0829 m/z

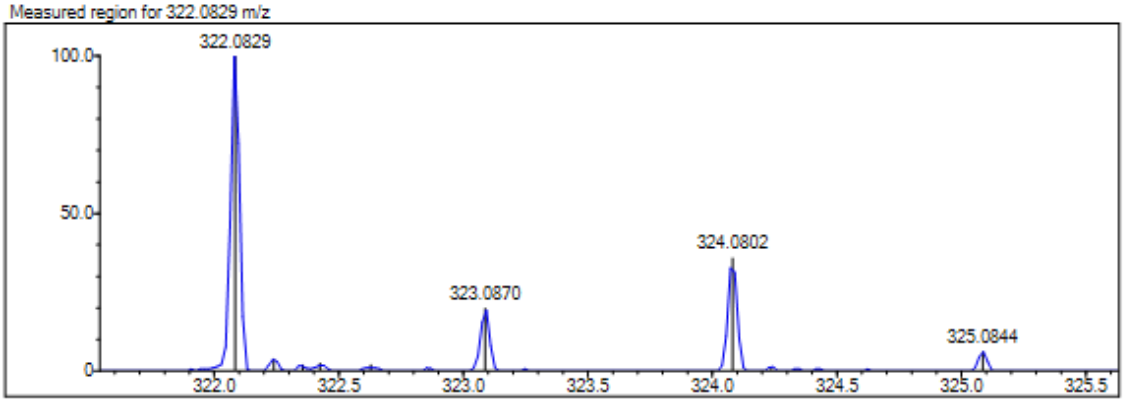

C16 H16 N O4 Cl [M+H]+ : Predicted region for 322.0841 m/z

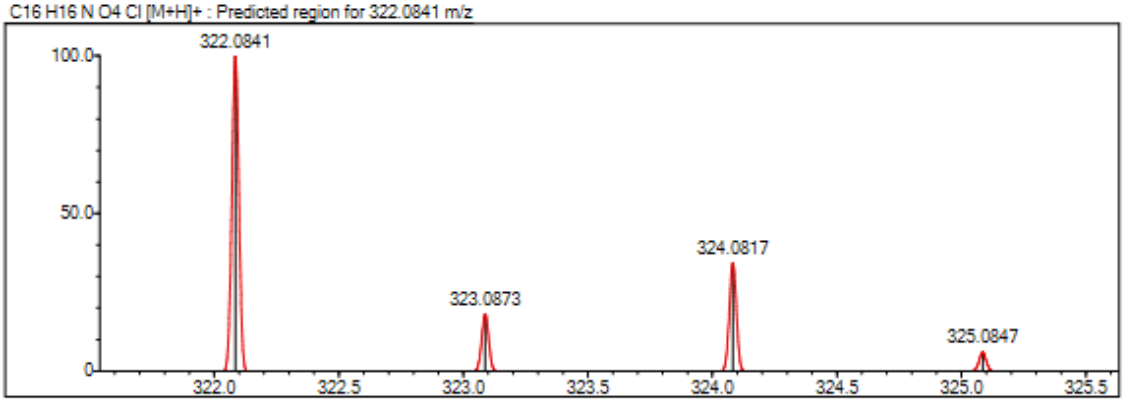

Rank	Score	Formula (M)	Ion	Meas. m/z	Pred. m/z	Df. (mDa)	Df. (ppm)	Iso	DBE
1	81.40	C16 H16 N O4 Cl	[M+H]+	322.0829	322.0841	-1.2	-3.73	87.36	9.0

Figure 5.23. *Mass spectrum of the compound* ***4d***

5.2.2.5. 2-[5-(4-Cyanophenyl)-3-(ethoxycarbonyl)-2-methyl-1H-pyrrol-1-yl]acetic acid

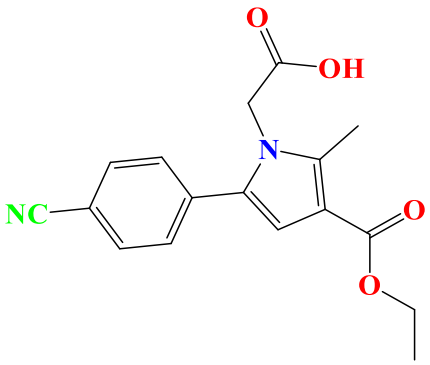

Figure 5.24. *Molecular structure of compound **4e***

Synthesized according to method **D**, experimental melting point: 185-186ºC, 70% yield percent.

^{1}H-NMR (400 MHz, DMSO-d_6; δ, ppm):): 1.26 (3H, t, *J*= 7.06 Hz, -CH_2-**CH_3**), 2.46 (3H, s, pyrrole-**CH_3**), 4.19 (2H, q, J_1=7.05 Hz, J_2= 14.14 Hz, -**CH_2**-CH_3), 4.71 (2H, s, **CH_2**-COOH), 6.61 (1H, s, **CH**-pyrrole), 7.50 (2H, d, *J*= 8.09 Hz, Ar-**$H_{3,5}$**), 7.88 (2H, d, *J*= 8.10 Hz, Ar-**$H_{2,6}$**).

^{13}C-NMR (100 MHz, DMSO-d_6; δ, ppm) 11.54 (-pyrrole-**C**H_3), 14.85 (-CH_2-**C**H_3), 46.83 (-**C**H_2-COOH), 59.50 (-**C**H_2-CH_3), 110.22 (Pyrrole-**C_4**), 111.27 (Pyrrole-**C_3**), 112.44 (Phenyl-**C_4**), 119.22 (-**C**N),129.15 (Phenyl-**$C_{2,6}$**), 132.36 (Phenyl-**$C_{3,5}$**), 133.20 (Phenyl-**C_1**), 136.82 (Pyrrole-**C_2**), 139.39 (Pyrrole-**C_5**), 164.64 (**C**O-O-Et), 170.33 (**C**OOH).

HRMS (-m/z): $[M+H]^+$: For $C_{17}H_{16}N_2O_4$ calculated molecular weight: 313.1186, found: 313.1183.

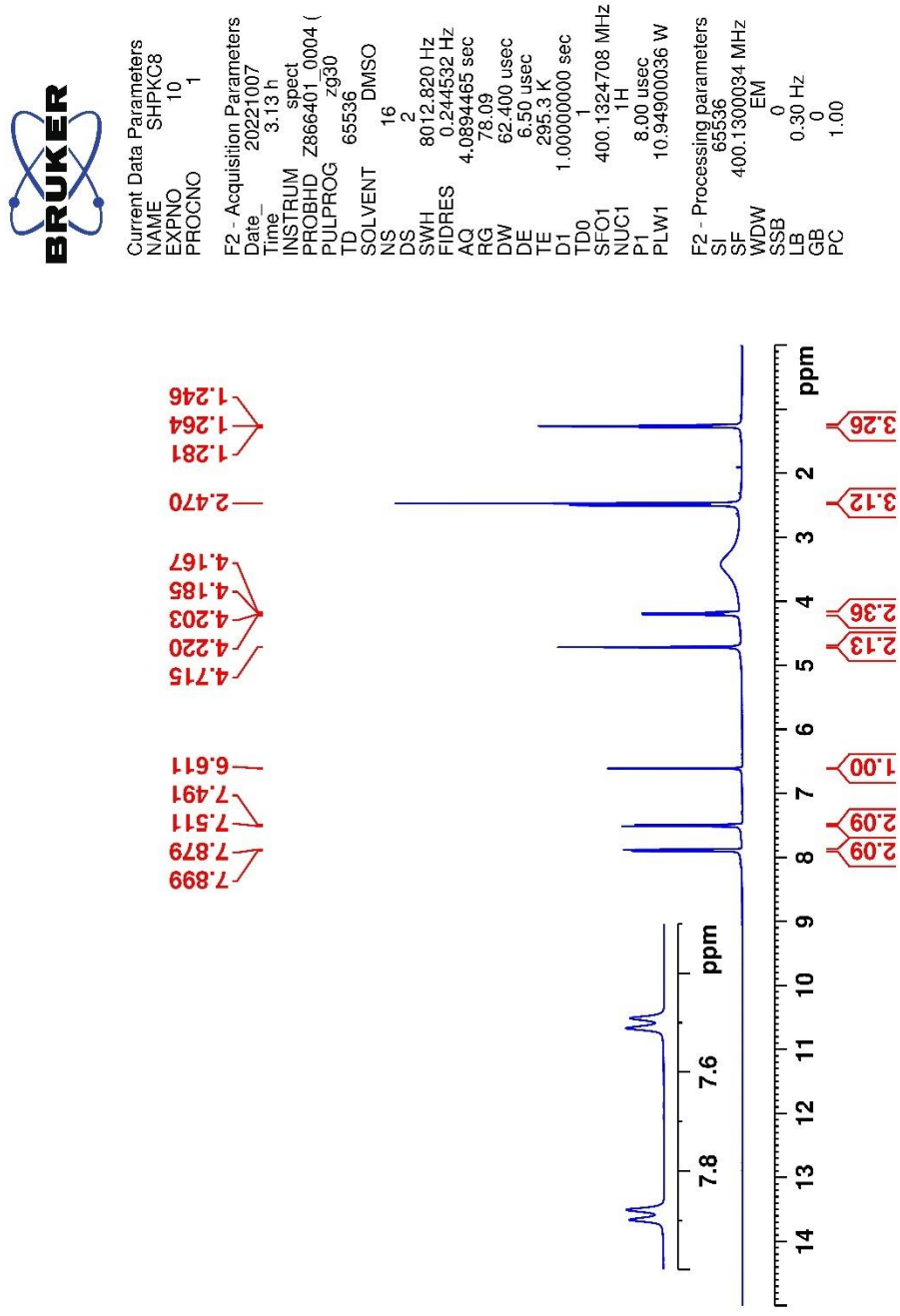

Figure 5.25. *^{1}H-NMR spectrum of the compound* ***4e***

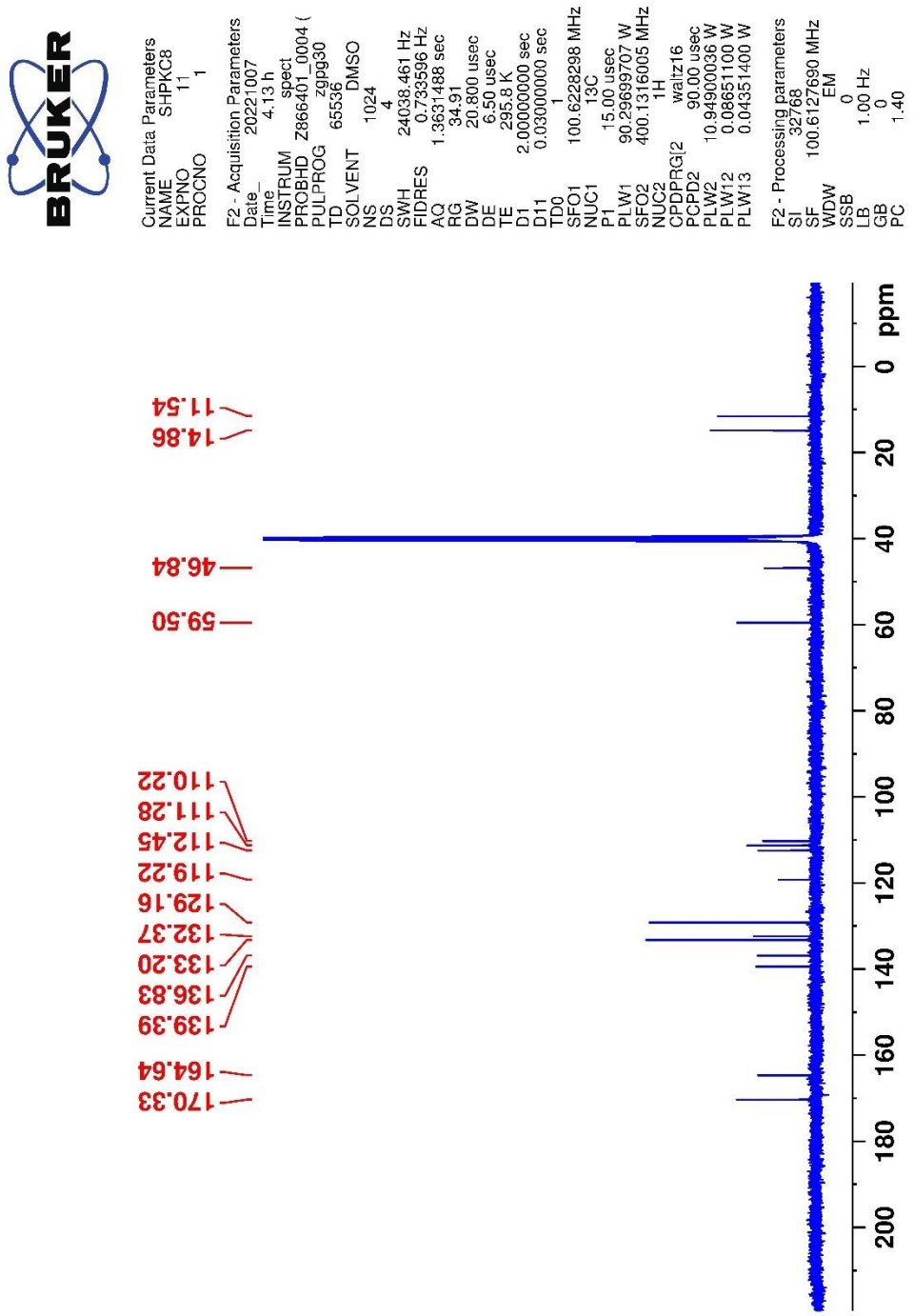

Figure 5.26. *^{13}C-NMR spectrum of the compound **4e***

Formula Predictor Report - SHPKC-8_06.lcd

Page 1 of 1

Data File: C:\LabSolutions\Data\Analiz\Asaf\SHPKC-8_06.lcd

Elmt	Val.	Min	Max	Elmt	Val.	Min	Max	Elmt	Val.	Min	Max	Elmt	Val.	Min	Max	Use Adduct
H	1	0	25	O	2	1	10	Cl	1	0	0	I	3	0	0	H
B	3	0	0	F	1	0	0	Br	1	0	0					
C	4	0	35	P	3	0	0	Ru	2	0	0					
N	3	0	5	S	2	0	0	Pd	2	0	0					

Error Margin (ppm): 10
HC Ratio: unlimited
Max Isotopes: 3
MSn Iso RI (%): 10.00

DBE Range: 5.0 - 25.0
Apply N Rule: yes
Isotope RI (%): 1.00
MSn Logic Mode: AND

Electron Ions: both
Use MSn Info: yes
Isotope Res: 9000
Max Results: 50

Event#: 1 MS(E+) Ret. Time : 2.307 -> 2.307 Scan# : 347 -> 347

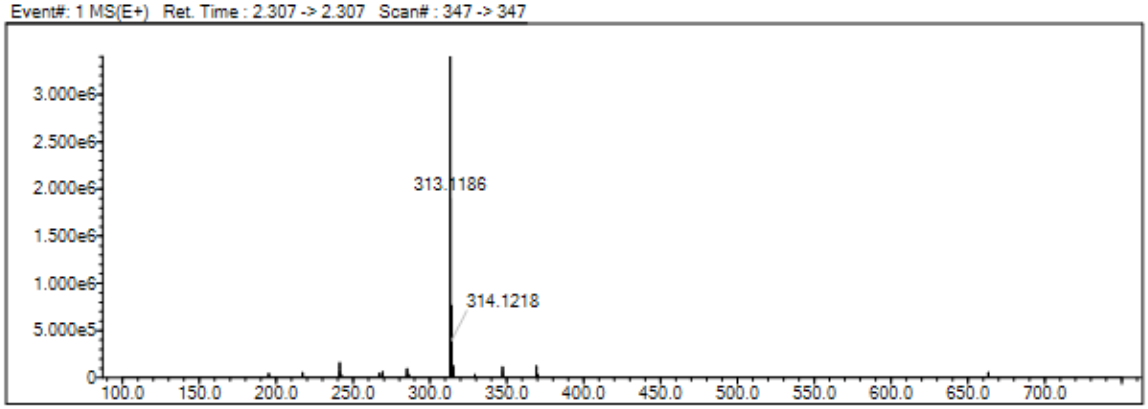

Measured region for 313.1186 m/z

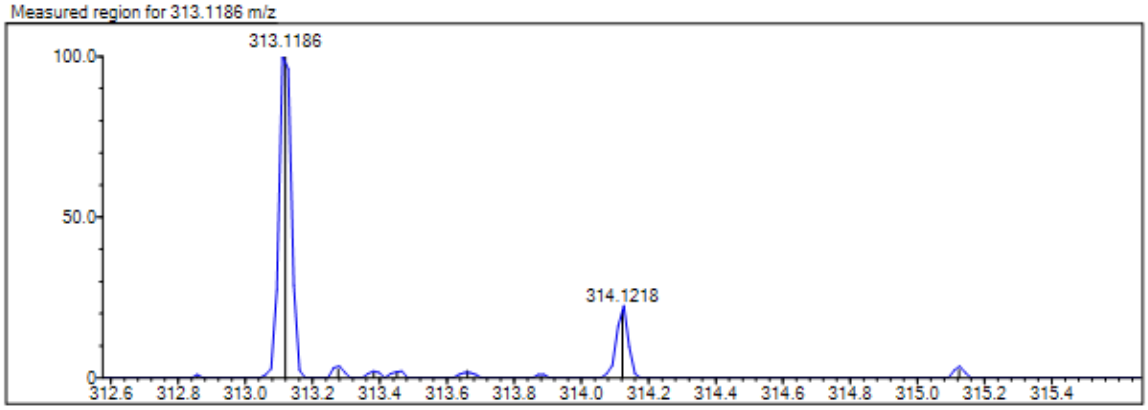

C17 H16 N2 O4 [M+H]+ : Predicted region for 313.1183 m/z

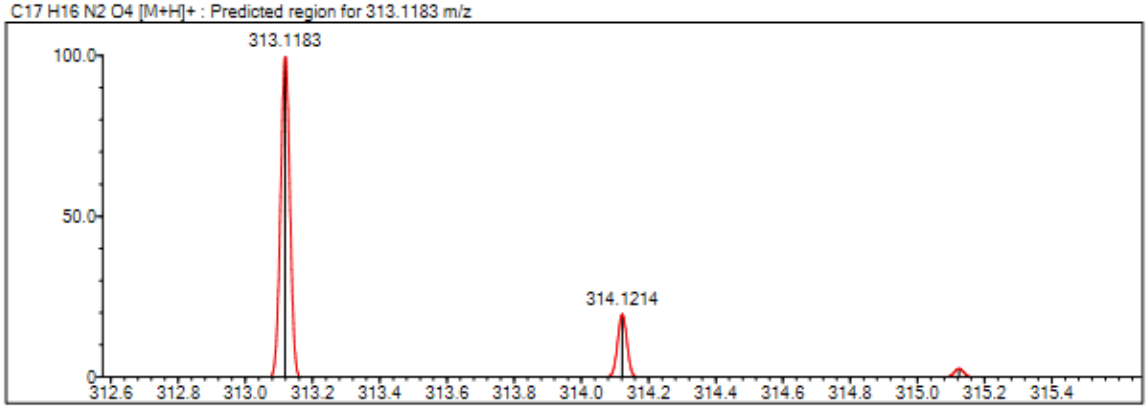

Rank	Score	Formula (M)	Ion	Meas. m/z	Pred. m/z	Df. (mDa)	Df. (ppm)	Iso	DBE
1	100.00	C17 H16 N2 O4	[M+H]+	313.1186	313.1183	0.3	0.96	100.00	11.0

Figure 5.27. *Mass spectrum of the compound* ***4e***

5.2.2.6. 2-[3-(Ethoxycarbonyl)-2-methyl-5-(4-nitrophenyl)-1H-pyrrol-1-yl]acetic acid

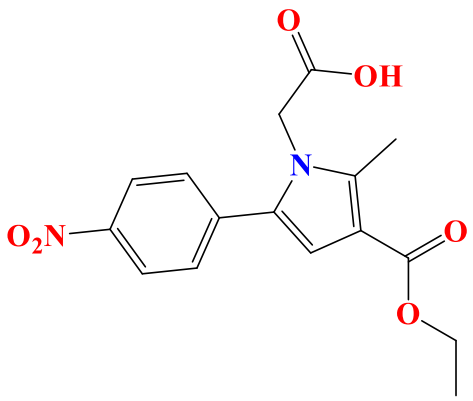

Figure 5.28. *Molecular structure of compound* ***4f***

Synthesized according to method **D**, experimental melting point 155-156ºC, 55% yield percent.

^{1}H-NMR (400 MHz, DMSO-*d*$_6$; δ, ppm): 1.26 (3H, t, *J*= 7.06 Hz, -CH_2-**$\underline{CH_3}$**), 2.47 (3H, s, pyrrole-**$\underline{CH_3}$**), 4.20 (2H, q, J_1=7.08 Hz, J_2= 14.12 Hz, -**$\underline{CH_2}$**-CH_3), 4.73 (2H, s, **$\underline{CH_2}$**-COOH), 6.67 (1H, s, **$\underline{CH}$**-pyrrole), 7.59 (2H, d, *J*= 8.37 Hz, Ar-**$\underline{H_{2,6}}$**), 8.26 (2H, d, *J*= 8.36 Hz, Ar-**$\underline{H_{3,5}}$**).

^{13}C-NMR (100 MHz, DMSO-*d*$_6$; δ, ppm) 11.57 (-pyrrole-**$\underline{C}$**H_3), 14.85 (-CH_2-**$\underline{C}$**H_3), 47.05 (-**$\underline{C}$**H_2-COOH), 59.54 (-**$\underline{C}$**H_2-CH_3), 111.83 (Pyrrole-**$\underline{C_4}$**), 112.59 (Pyrrole-**$\underline{C_3}$**), 124.52 (Phenyl-**$\underline{C_{3,5}}$**), 129.25 (Phenyl-**$\underline{C_{2,6}}$**), 132.00 (Phenyl-**$\underline{C_1}$**), 138.80 (Pyrrole-**$\underline{C_2}$**), 139.87 (Pyrrole-**$\underline{C_5}$**),146.59 (Phenyl-**$\underline{C_4}$**), 164.59 (**$\underline{C}$**O-O-Et), 170.26 (**$\underline{C}$**OOH).

HRMS (-m/z): $[M+H]^+$: For $C_{16}H_{16}N_2O_6$ calculated molecular weight: 333.1090; found: 333.1081.

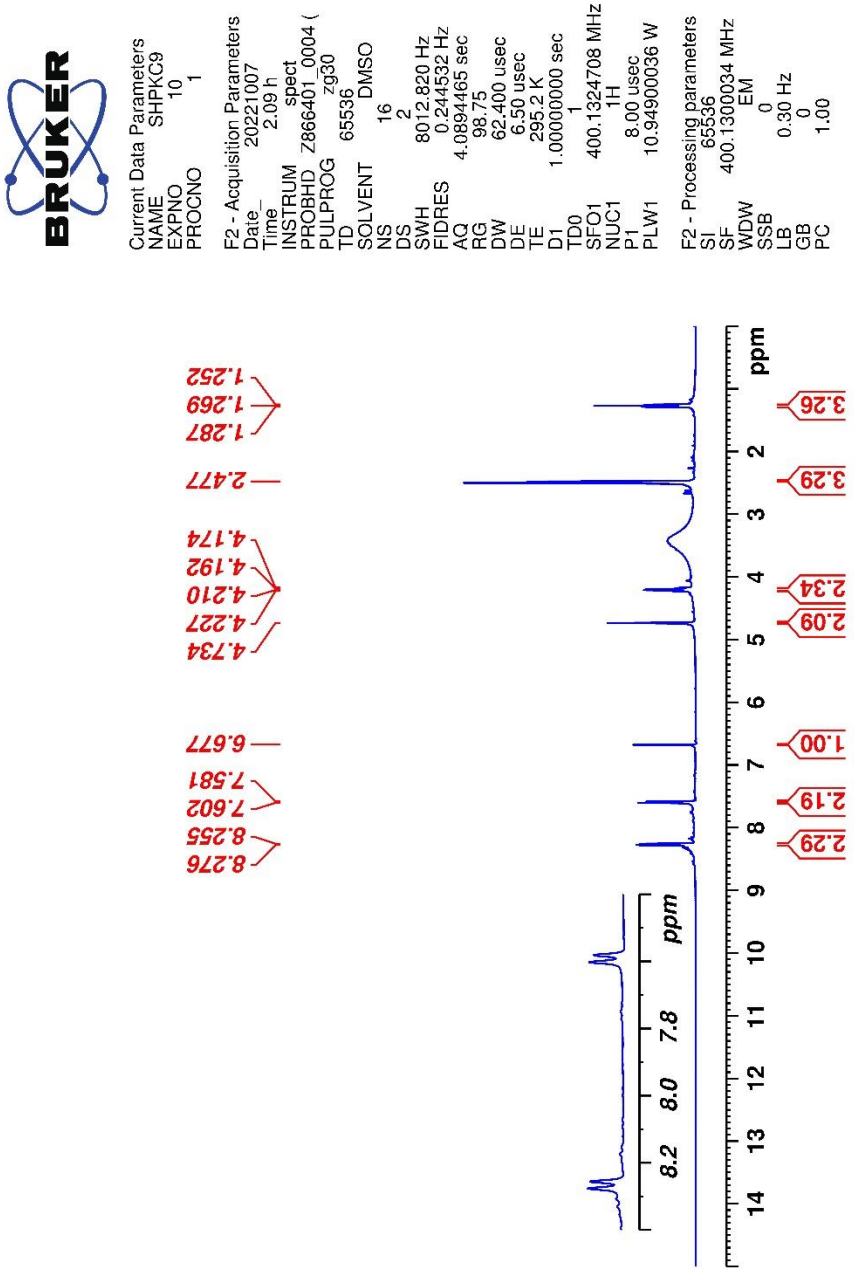

Figure 5.29. *^{1}H-NMR spectrum of the compound **4f***

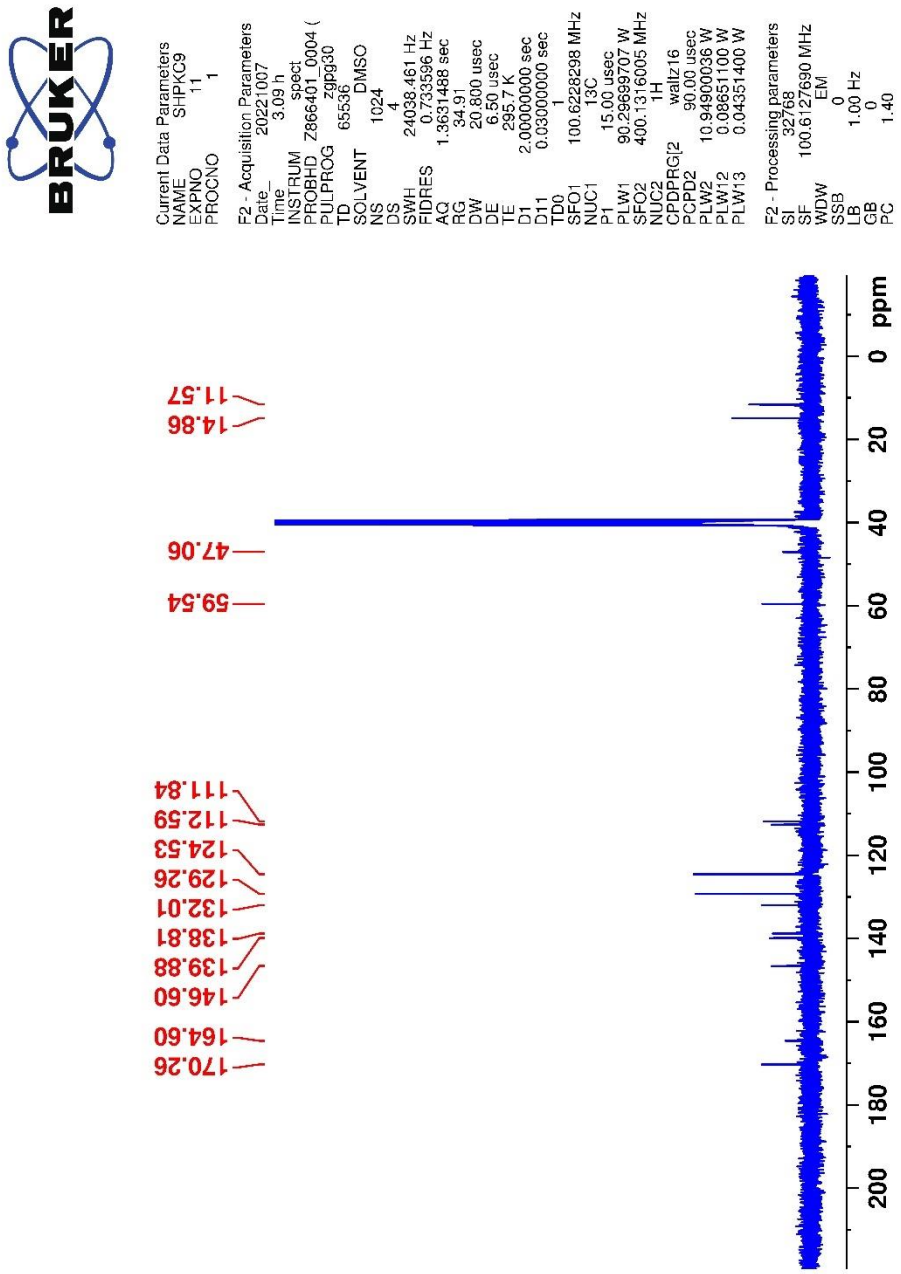

Figure 5.30. *^{13}C-NMR spectrum of the compound **4f***

Formula Predictor Report - SHPKC-9_07.lcd

Page 1 of 1

Data File: C:\LabSolutions\Data\Analiz\Asaf\SHPKC-9_07.lcd

Elmt	Val.	Min	Max	Elmt	Val.	Min	Max	Elmt	Val.	Min	Max	Elmt	Val.	Min	Max	Use Adduct
H	1	0	25	O	2	1	10	Cl	1	0	0	I	3	0	0	H
B	3	0	0	F	1	0	0	Br	1	0	0					
C	4	0	35	P	3	0	0	Ru	2	0	0					
N	3	0	5	S	2	0	0	Pd	2	0	0					

Error Margin (ppm): 10
HC Ratio: unlimited
Max Isotopes: 3
MSn Iso RI (%): 10.00

DBE Range: 5.0 - 25.0
Apply N Rule: yes
Isotope RI (%): 1.00
MSn Logic Mode: AND

Electron Ions: both
Use MSn Info: yes
Isotope Res: 9000
Max Results: 50

Event#: 1 MS(E+) Ret. Time : 2.480 -> 2.480 Scan# : 373 -> 373

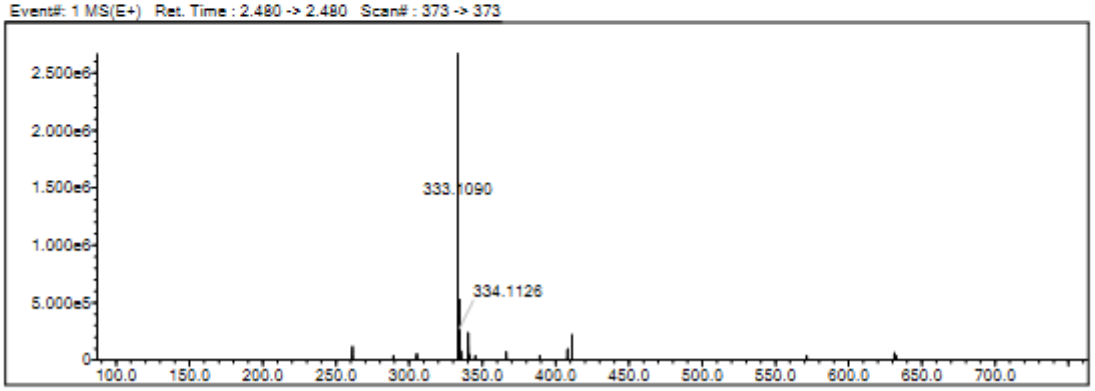

Measured region for 333.1090 m/z

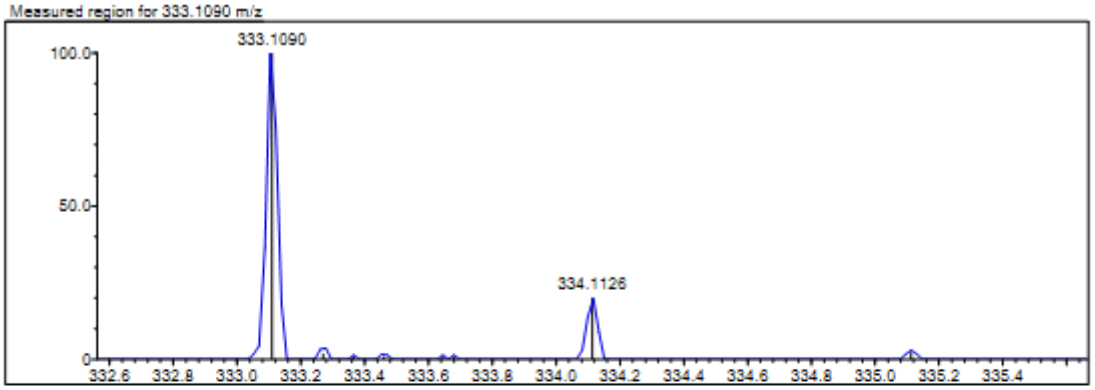

C16 H16 N2 O6 [M+H]+ : Predicted region for 333.1081 m/z

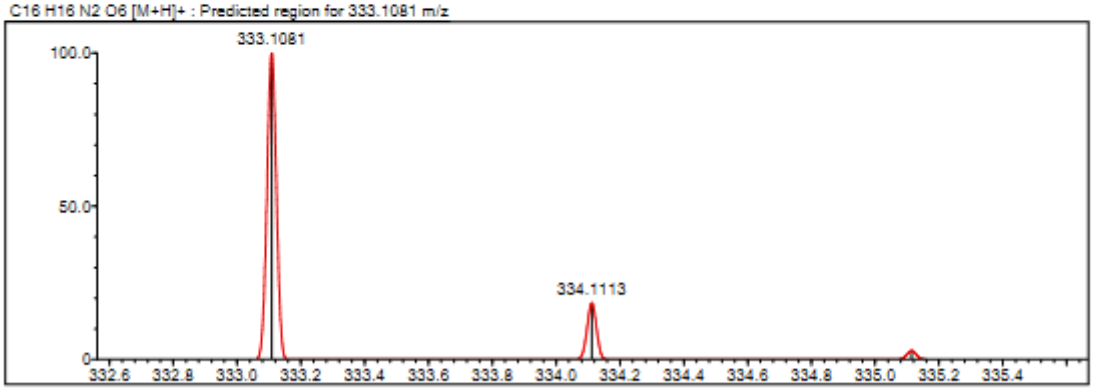

Rank	Score	Formula (M)	Ion	Meas. m/z	Pred. m/z	Df. (mDa)	Df. (ppm)	Iso	DBE
1	85.96	C16 H16 N2 O6	[M+H]+	333.1090	333.1081	0.9	2.70	89.78	10.0

Figure 5.31. *Mass spectrum of the compound* ***4f***

5.2.2.7. 2-[5-(2,6-Dimethoxyphenyl)-3-(ethoxycarbonyl)-2-methyl-1H-pyrrol-1yl]acetic acid.

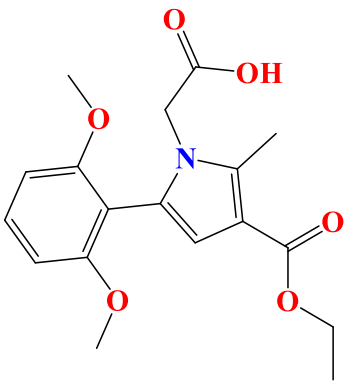

Figure 5.32. *Molecular structure of compound* ***4g***

Synthesized according to method **D**, experimental melting point 159-205ºC, 68% yield percent.

^{1}H-NMR (400 MHz, DMSO-*d*$_6$; δ, ppm): 1.24 (3H, t, *J*= 7.06 Hz, -CH_2-**$\underline{CH_3}$**), 2.44 (3H, s, pyrrole-**$\underline{CH_3}$**), 3.60 (3H, s, -O**$\underline{CH_3}$**), 3.69 (3H, s, -O**$\underline{CH_3}$**), 4.16 (2H, q, J_1=7.04 Hz, J_2= 14.12 Hz, -**$\underline{CH_2}$**-CH_3), 4.39 (2H, s, **$\underline{CH_2}$**-COOH), 6.29 (1H, s, **$\underline{CH}$**-pyrrole), 6.69 (1H, d, *J*= 8.37 Hz, Ar-**$\underline{H}$**), 6.94 (1H, dd, J_1= 8.37 Hz, J_2= 8.86 Ar-**$\underline{H}$**), 6.99 (1H, d , *J*= 8.97 Hz, Ar-**$\underline{H}$**).

^{13}C-NMR (100 MHz, DMSO-*d*$_6$; δ, ppm) 11.66 (-pyrrole-**$\underline{C}$**H_3), 14.93 (-CH_2-**$\underline{C}$**H_3), 46.49 (-**$\underline{C}$**H_2-COOH), 55.84 (-O**$\underline{C}$**H_3), 59.17 (-**$\underline{C}$**H_2-CH_3), 109.72 (Pyrrole-**$\underline{C_4}$**), 112.77 (Phenyl-**$\underline{C_1}$**), 115.18 (Phenyl-**$\underline{C_3}$**), 117.94 (Phenyl-**$\underline{C_5}$**), 121.58 (pyrrole-**$\underline{C_3}$**), 130.52 (Phenyl-**$\underline{C_4}$**), 137.43 (Pyrrole-**$\underline{C_5}$**), 151.43 (Pyrrole-**$\underline{C_2}$**),153.43 (Phenyl-**$\underline{C_{2,6}}$**), 164.94 (**$\underline{C}$**O-O-Et), 169.89 (**$\underline{C}$**OOH).

HRMS (-m/z): $[M+H]^+$: For $C_{18}H_{21}NO_6$ calculated molecular weight: 348.1438; found: 348.1442.

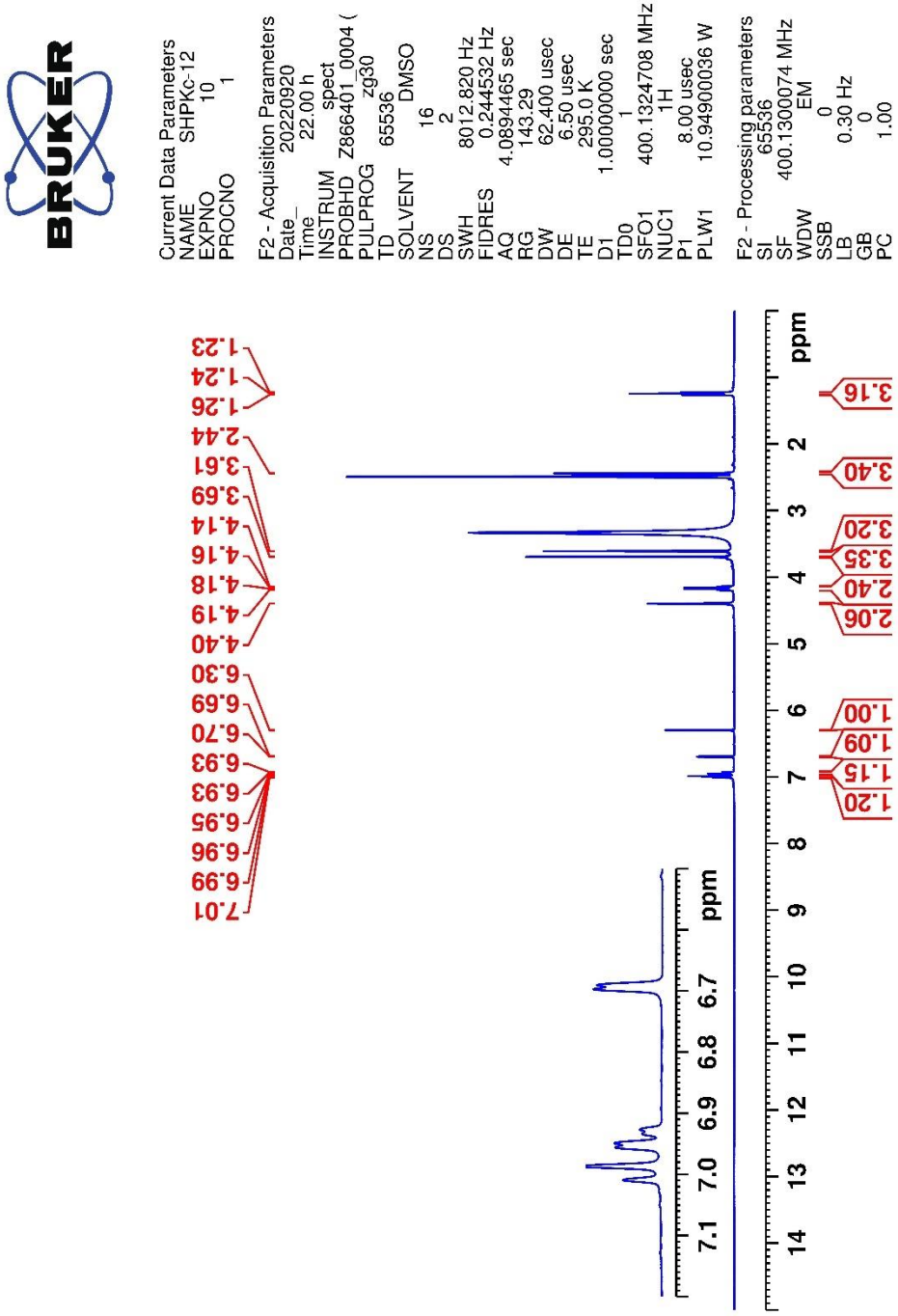

Figure 5.33. *^{1}H-NMR spectrum of the compound **4g***

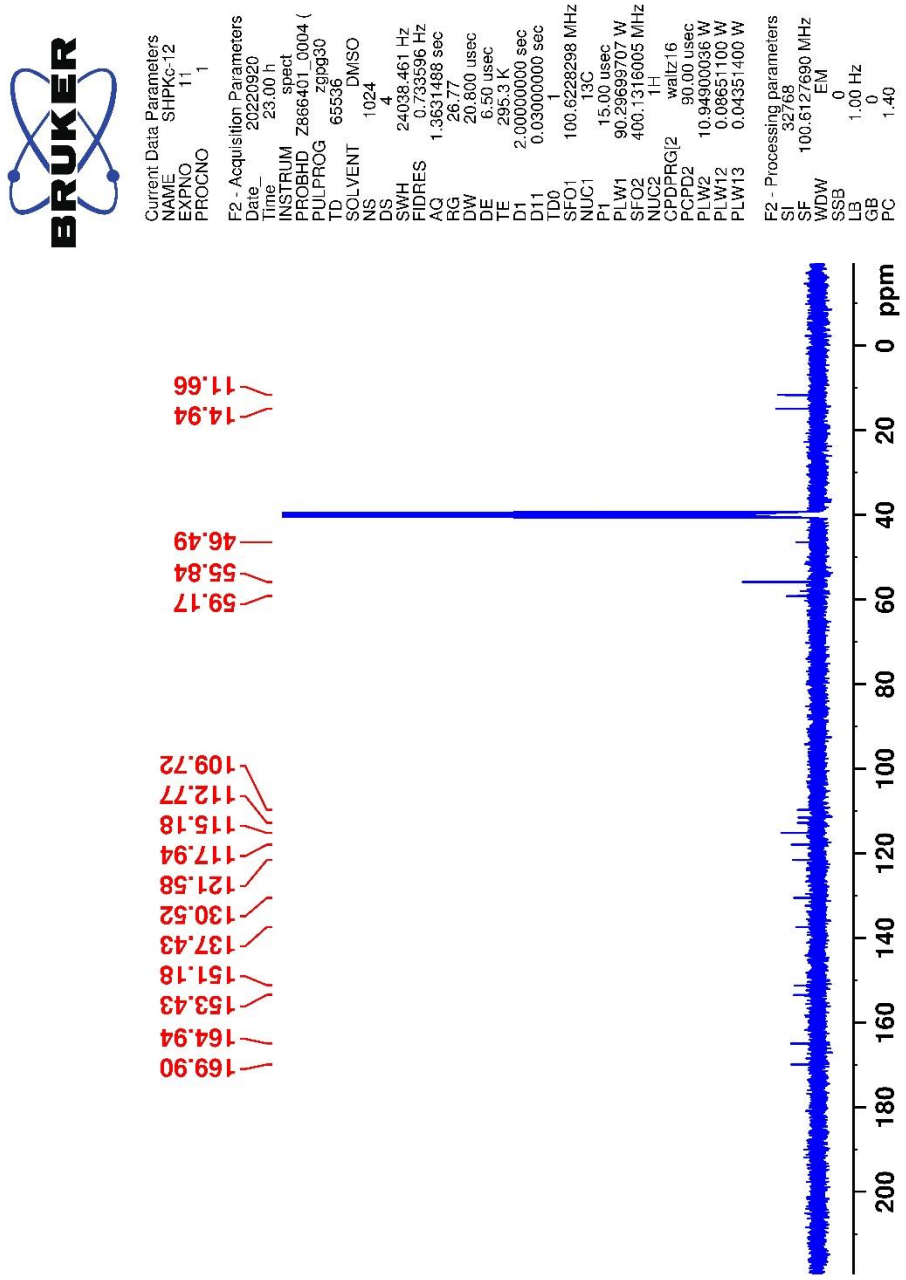

Figure 5.34. *^{13}C-NMR spectrum of the compound **4g***

Formula Predictor Report - SH-PKC-B12_271.lcd

Page 1 of 1

Data File: C:\LabSolutions\Data\Analiz\Asaf\SH-PKC-B12_271.lcd

Elmt	Val.	Min	Max	Elmt	Val.	Min	Max	Elmt	Val.	Min	Max	Elmt	Val.	Min	Max	Use Adduct
H	1	6	46	O	2	0	6	S	2	0	0	Ru	2	0	0	H
C	4	5	36	F	1	0	0	Cl	1	0	0	Pd	2	0	0	Na
N	3	0	6	P	3	0	0	Br	1	0	0	I	3	0	0	

Error Margin (ppm): 5
HC Ratio: unlimited
Max Isotopes: 3
MSn Iso RI (%): 10.00

DBE Range: 0.0 - 30.0
Apply N Rule: yes
Isotope RI (%): 1.00
MSn Logic Mode: AND

Electron Ions: both
Use MSn Info: yes
Isotope Res: 9000
Max Results: 50

Event#: 1 MS(E+) Ret. Time : 2.387 -> 2.400 Scan# : 359 -> 361

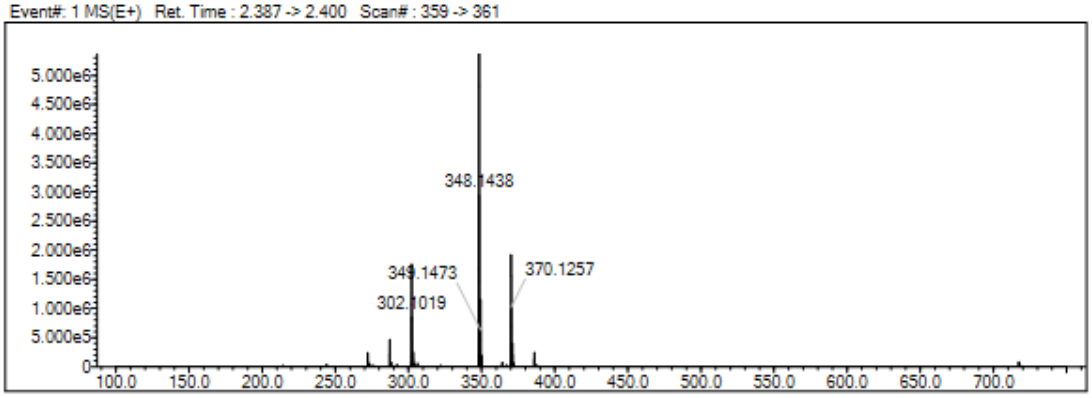

Measured region for 348.1438 m/z

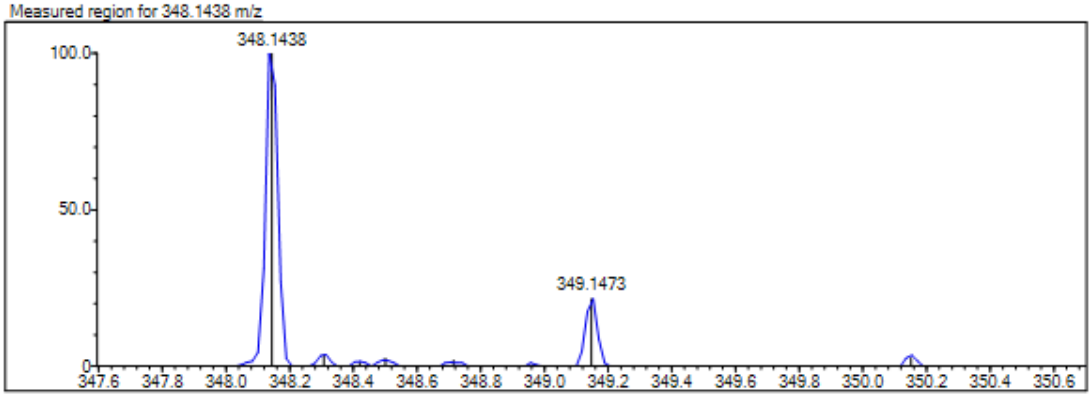

C18 H21 N O6 [M+H]+ : Predicted region for 348.1442 m/z

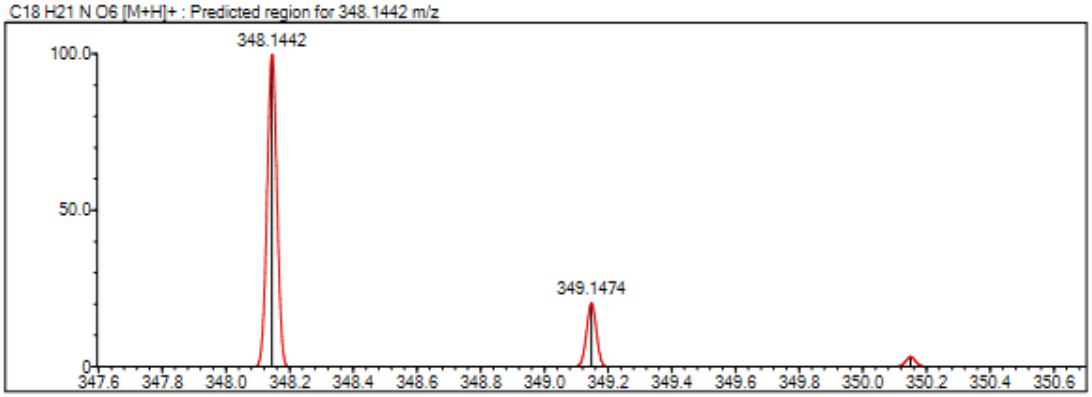

Rank	Score	Formula (M)	Ion	Meas. m/z	Pred. m/z	Df. (mDa)	Df. (ppm)	Iso	DBE
1	94.82	C18 H21 N O6	[M+H]+	348.1438	348.1442	-0.4	-1.15	95.18	9.0

Figure 5.35. *Mass spectrum of the compound* ***4g***

5.2.2.8. 2-(5-([1,1'-Biphenyl]-4-yl)-3-(ethoxycarbonyl)-2-methyl-1H-pyrrol-1-yl)acetic acid

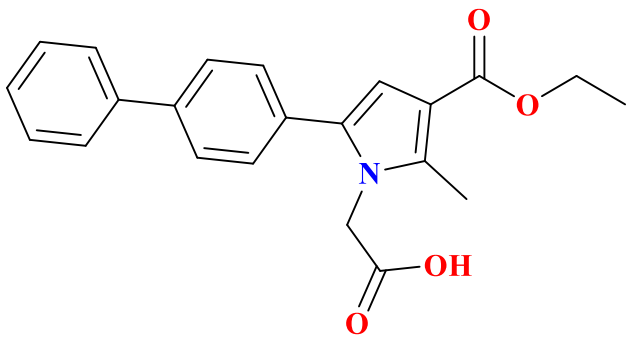

Figure 5.36. *Molecular structure of compound* ***4h***

Synthesized according to method **D**, experimental melting point: 190-212ºC, 79% yield percent.

IR (ATR) ν_{max} (cm^{-1}): 3493 (O-H stretching), 3433 (aromatic C-H stretching band), 1722 and 1681 (C=O stretching band).

^{1}H-NMR (400 MHz, DMSO-d_6; δ, ppm): 1.27 (3H, t, *J*= 7.07 Hz, -CH_2-**CH_3**), 2.47 (3H, s, pyrrole-**CH_3**), 4.19 (2H, q, J_1=7.04 Hz, J_2= 15.41 Hz, -**CH_2**-CH_3), 4.66 (2H, s, **CH_2**-COOH), 6.48 (1H, s, **CH**-pyrrole), 7.39 (3H, t, *J*= 5.45, Ar-**H**), 7.47 (2H, t, *J*= 7.52 Hz, Ar-**H**), 7.72 (4H, t, *J*= 8.61 Hz, Ar-**H**).

^{13}C-NMR (100 MHz, DMSO-d_6; δ, ppm) 11.56 (-pyrrole-**C**H_3), 14.90 (-CH_2-**C**H_3), 46.92 (-**C**H_2-COOH), 59.33 (-**C**H_2-CH_3), 109.42, 111.85, 127.05, 127.43, 128.07, 129.39, 129.46, 131.39, 133.54, 138.03, 139.64, 139.87, 164.91(**C**O-O-Et), 170.48 (**C**OOH).

HRMS (-m/z): $[M+H]^+$: For $C_{22}H_{21}NO_4$ calculated molecular weight: 364.1535; found: 364. 1543.

DOPNALAB

Item	Value
Acquired Date&Time	22.05.2023 15:20:38
Acquired by	System Administrator
Filename	C:\Users\dopnalab\Desktop\MASAUSTU\LEYLA YURTDAŞ\Yeni klasör\SHPKC15.1.ispd
Spectrum name	SHPKC15.1
Sample name	SHPKC15
Sample ID	
Option	
Comment	
No. of Scans	15
Resolution	4 [cm-1]
Apodization	Happ-Genzel

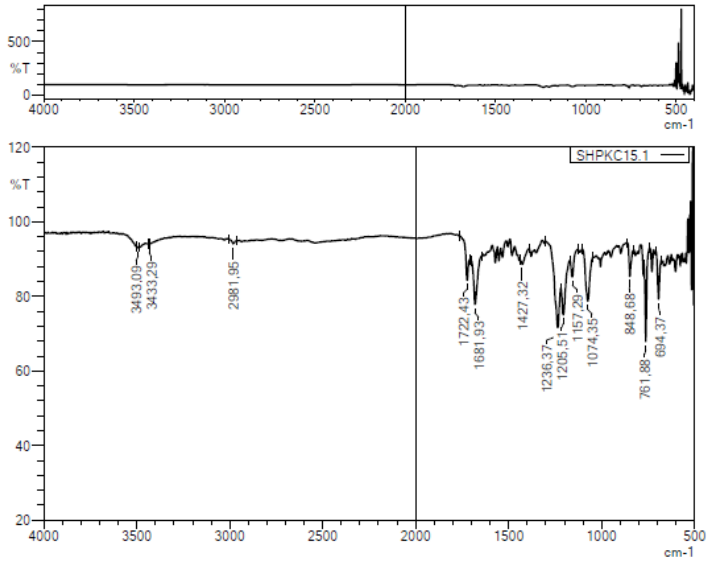

Figure 5.37. *IR spectrum of the compound* ***4h***

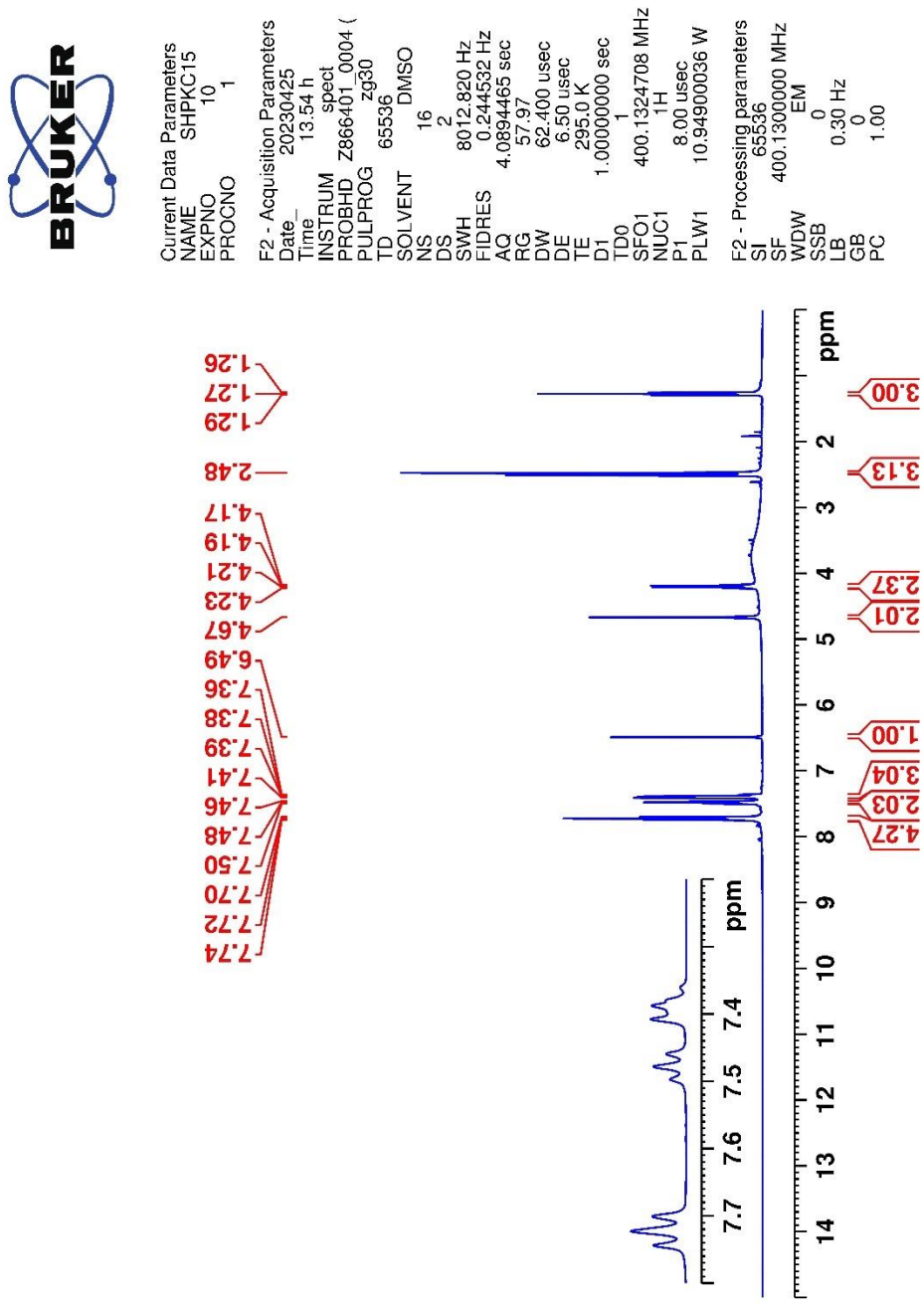

Figure 5.38. *^{13}C-NMR spectrum of the compound **4h***

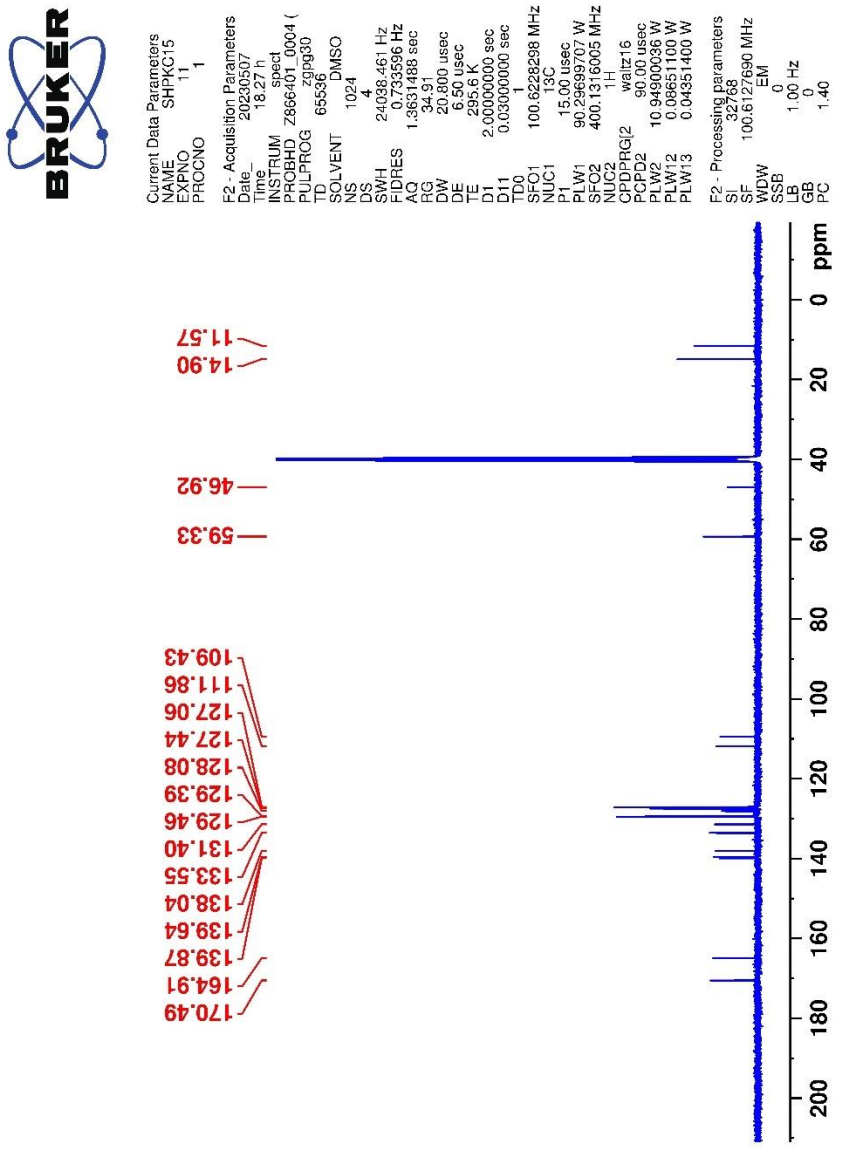

Figure 5.39. *^{13}C-NMR spectrum of the compound **4h***

Formula Predictor Report - SHPKC15_455.lcd

Page 1 of 1

Data File: C:\LabSolutions\Data\Analiz\Asaf\SHPKC15_455.lcd

Elmt	Val.	Min	Max	Elmt	Val.	Min	Max	Elmt	Val.	Min	Max	Elmt	Val.	Min	Max	Use Adduct
H	1	6	46	O	2	0	5	S	2	0	0	Ru	2	0	0	H
C	4	5	36	F	1	0	0	Cl	1	0	2	Pd	2	0	0	
N	3	0	5	P	3	0	0	Br	1	0	0	I	3	0	0	

Error Margin (ppm): 5
HC Ratio: unlimited
Max Isotopes: 3
MSn Iso RI (%): 10.00

DBE Range: 5.0 - 30.0
Apply N Rule: yes
Isotope RI (%): 1.00
MSn Logic Mode: AND

Electron Ions: both
Use MSn Info: yes
Isotope Res: 9000
Max Results: 50

Event#: 1 MS(E+) Ret. Time : 9.133 -> 9.133 Scan# : 1371 -> 1371

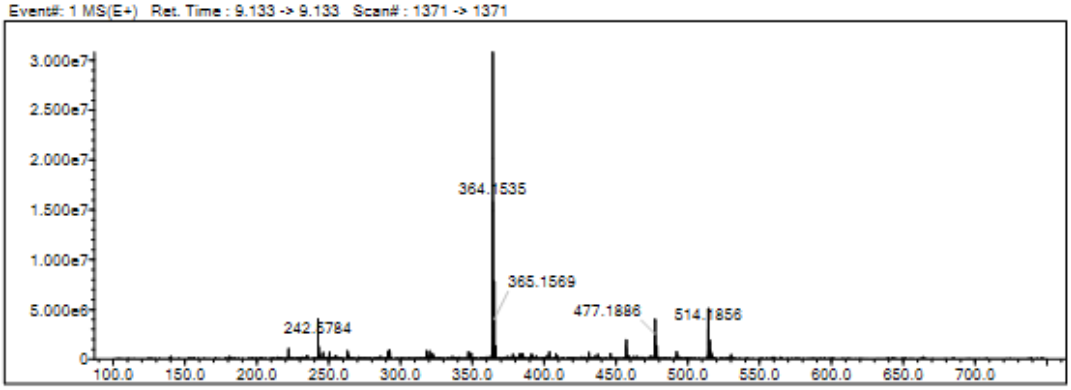

Measured region for 364.1535 m/z

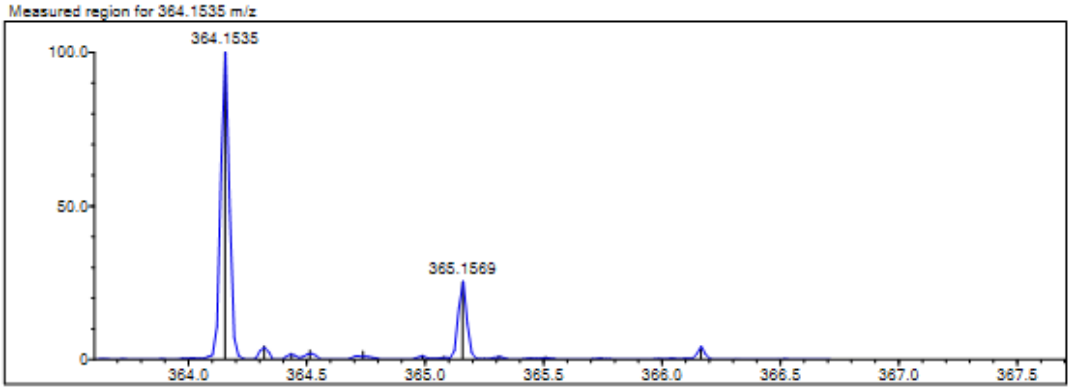

C22 H21 N O4 [M+H]+ : Predicted region for 364.1543 m/z

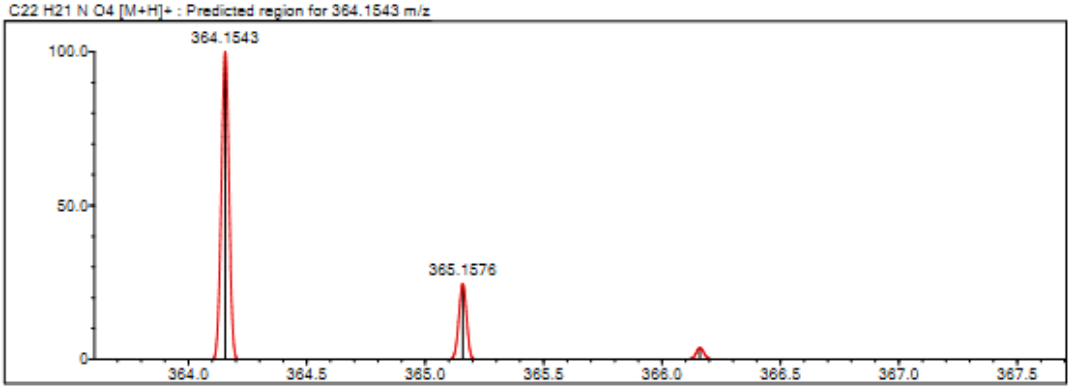

Rank	Score	Formula (M)	Ion	Meas. m/z	Pred. m/z	Df. (mDa)	Df. (ppm)	Iso	DBE
1	97.00	C22 H21 N O4	[M+H]+	364.1535	364.1543	-0.8	-2.20	100.00	13.0

Figure 5.40. *Mass spectrum of the compound **4h***

5.2.2.9. 2-(3-(Ethoxycarbonyl)-2-methyl-5-(naphthalen-2-yl)-1H-pyrrol-1-yl)acetic acid

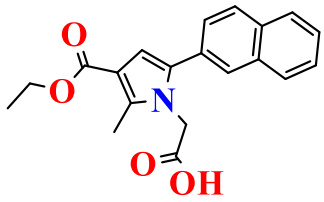

Figure 5.41. *Molecular structure of compound* ***4i***

Synthesized according to method **D**, experimental melting point: 145-146ºC, 80% yield percent.

^{1}H-NMR (400 MHz, DMSO-d_6; δ, ppm): 1.28 (3H, t, *J*= 7.04 Hz, -CH_2-**CH_3**), 2.50 (3H, s, pyrrole-**CH_3**), 4.21 (2H, q, J_1=7.04 Hz, J_2= 15.51 Hz, -**CH_2**-CH_3), 4.72 (2H, s, **CH_2**-COOH), 6.55 (1H, s, **CH**-pyrrole), 7.45 (1H, d, *J*= 5.45, Ar-**H**), 7.47 (2H, t, *J*= 8.45 Hz, Ar-**H**), 7.55 (2H, t, J_1= 4.05 Hz, Ar-**H**), 7.85 (1H, s, Ar-**H)**, 7.91 (1H, t, *J*= 4.48 Hz, Ar-**H**), 7.96 (2H, t, *J*= 8.08 Hz, Ar-**H**).

^{13}C-NMR (100 MHz, DMSO-d_6; δ, ppm) 11.57 (-pyrrole-**C**H_3), 14.90 (-CH_2-**C**H_3), 46.74 (-**C**H_2-COOH), 59.36 (-**C**H_2-CH_3), 109.87, 111.93, 126.84, 126.93, 127.10, 127.66, 128.05, 128.39, 128.71, 129.75, 132.54, 133.37, 133.87, 138.11, 164.91(**C**O-O-Et), 170.48 (**C**OOH).

HRMS (-m/z): $[M+H]^+$: For $C_{20}H_{19}NO_4$ calculated molecular weight: 338.1380; found: 338. 1387.

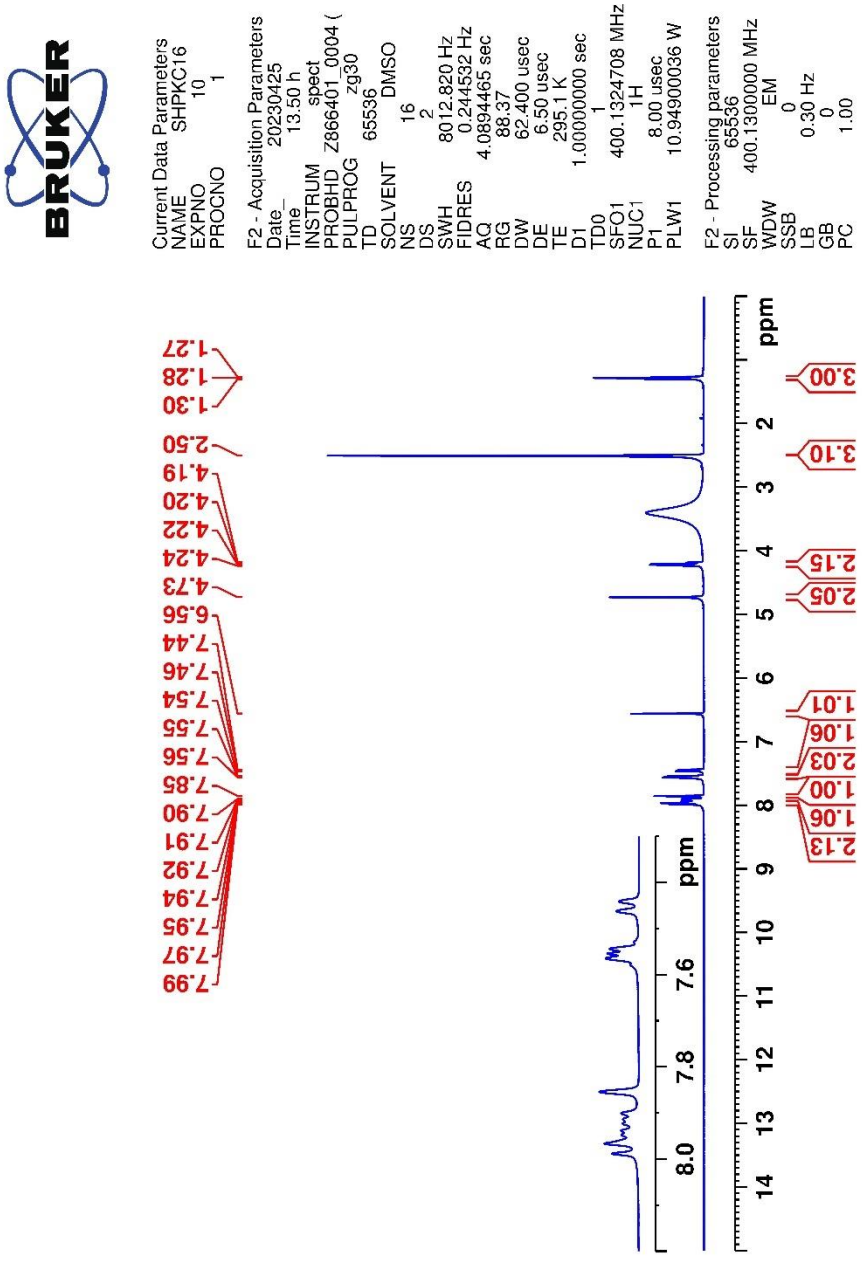

Figure 5.42. *^{1}H-NMR spectrum of the compound* ***4i***

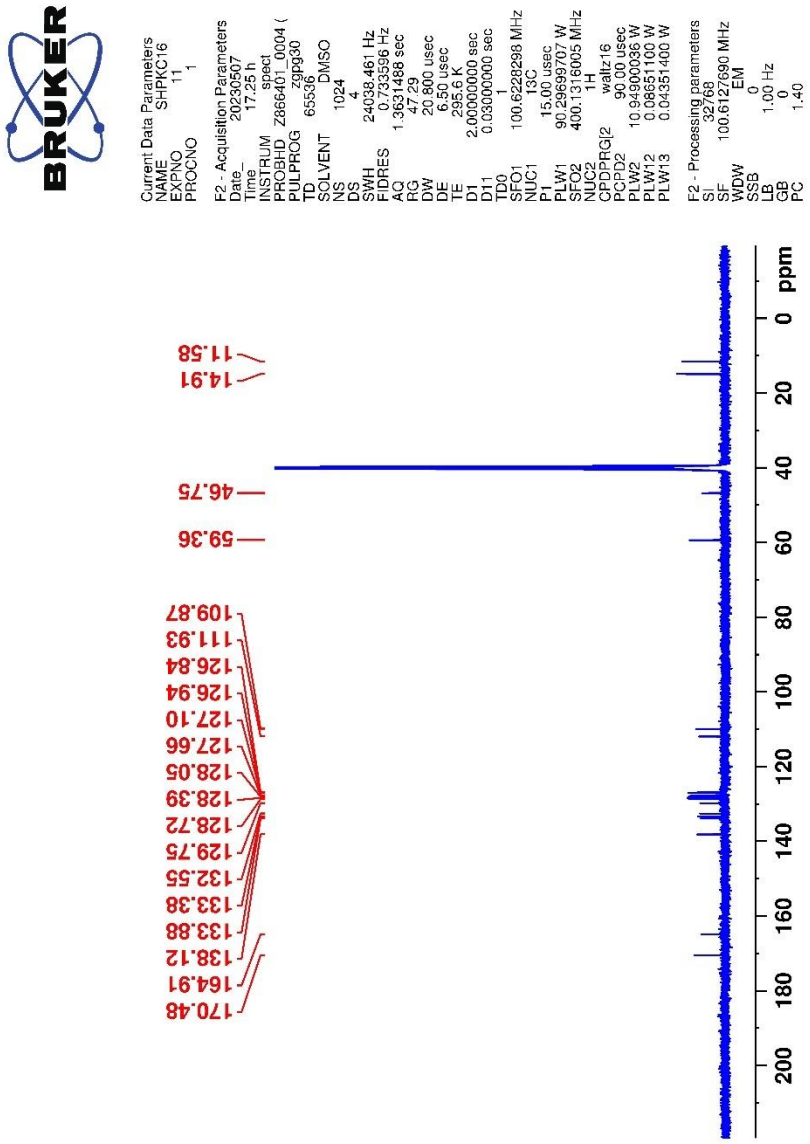

figure 5.43. *^{13}C-NMR spectrum of the compound **4i***

Formula Predictor Report - SHPKC16_451.lcd

Page 1 of 1

Data File: C:\LabSolutions\Data\Analiz\Asaf\SHPKC16_451.lcd

Elmt	Val.	Min	Max	Elmt	Val.	Min	Max	Elmt	Val.	Min	Max	Elmt	Val.	Min	Max	Use Adduct
H	1	6	46	O	2	0	6	S	2	0	2	Ru	2	0	0	H
C	4	5	36	F	1	0	0	Cl	1	0	2	Pd	2	0	0	Na
N	3	0	6	P	3	0	0	Br	1	0	0	I	3	0	0	

Error Margin (ppm): 5
HC Ratio: unlimited
Max Isotopes: 3
MSn Iso RI (%): 10.00

DBE Range: 0.0 - 30.0
Apply N Rule: yes
Isotope RI (%): 1.00
MSn Logic Mode: AND

Electron Ions: both
Use MSn Info: yes
Isotope Res: 9000
Max Results: 50

Event#: 1 MS(E+) Ret. Time : 6.827 Scan# : 1025

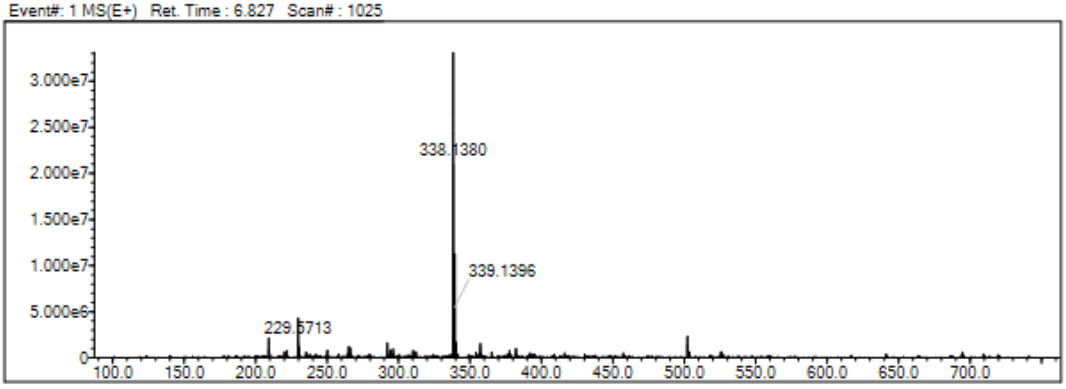

Measured region for 338.1380 m/z

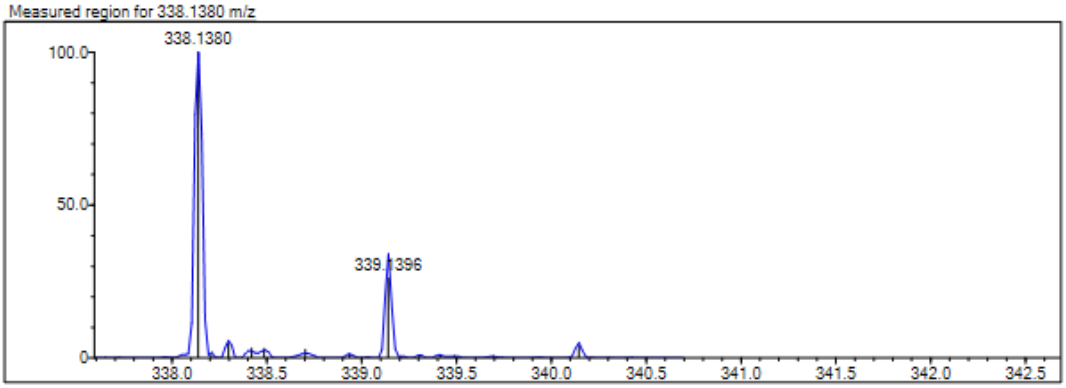

C20 H19 N O4 [M+H]+ : Predicted region for 338.1387 m/z

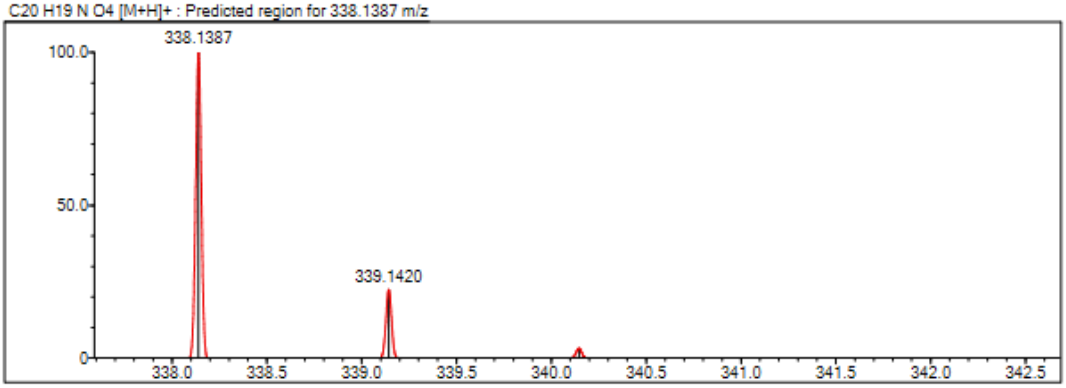

Rank	Score	Formula (M)	Ion	Meas. m/z	Pred. m/z	Df. (mDa)	Df. (ppm)	Iso	DBE
1	75.09	C20 H19 N O4	[M+H]+	338.1380	338.1387	-0.7	-2.07	77.15	12.0

Figure 5.44. *Mass spectrum of the compound* ***4i***

5.2.2.10. 2-[5-(3,4-Dichloroyphenyl)-3-(ethoxycarbonyl)-2-methyl-1H-pyrrol-1yl]acetic acid

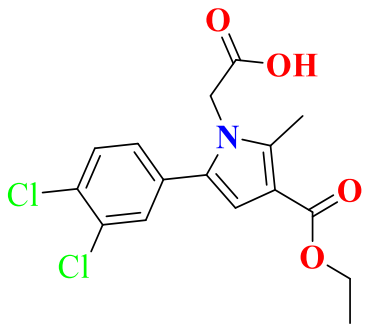

Figure 5.45. *Molecular structure of compound* ***4k***

Synthesized according to method **D**, experimental melting point: 280-282ºC, 76% yield percent.

^{1}H-NMR (400 MHz, DMSO-d_6; δ, ppm): 1.29 (3H, t, *J*= 7.07 Hz, -CH_2-**CH_3**), 2.49 (3H, s, pyrrole-**CH_3**), 4.22 (2H, q, J_1=7.04 Hz, J_2= 14.11 Hz, -**CH_2**-CH_3), 4.73 (2H, s, **CH_2**-COOH), 6.58 (1H, s, **CH**-pyrrole), 7.32 (1H, dd, J_1= 3.44, J_2= 8.44 Hz, Ar-**H**), 7.58 (1H, d, *J*= 1.88 Hz, Ar-**H**), 7.73 (1H, d, *J*= 8.34 Hz, Ar-**H**), 13.38 (1H, br-s, COO**H**).

^{13}C-NMR (100 MHz, DMSO-d_6; δ, ppm) 11.71 (-pyrrole-**C**H_3), 14.91 (-CH_2-**C**H_3), 49.82 (-**C**H_2-COOH), 59.15 (-**C**H_2-CH_3), 109.75, 111.14, 128.38, 130.01, 130.22, 132.02, 131.59, 133.71, 138.62, 164.99 (**C**O-O-Et), 173.13 (**C**OOH).

HRMS (-m/z): $[M+H]^+$: For $C_{16}H_{15}Cl_2NO_4$ calculated molecular weight: 356.0440; found: 356. 0451.

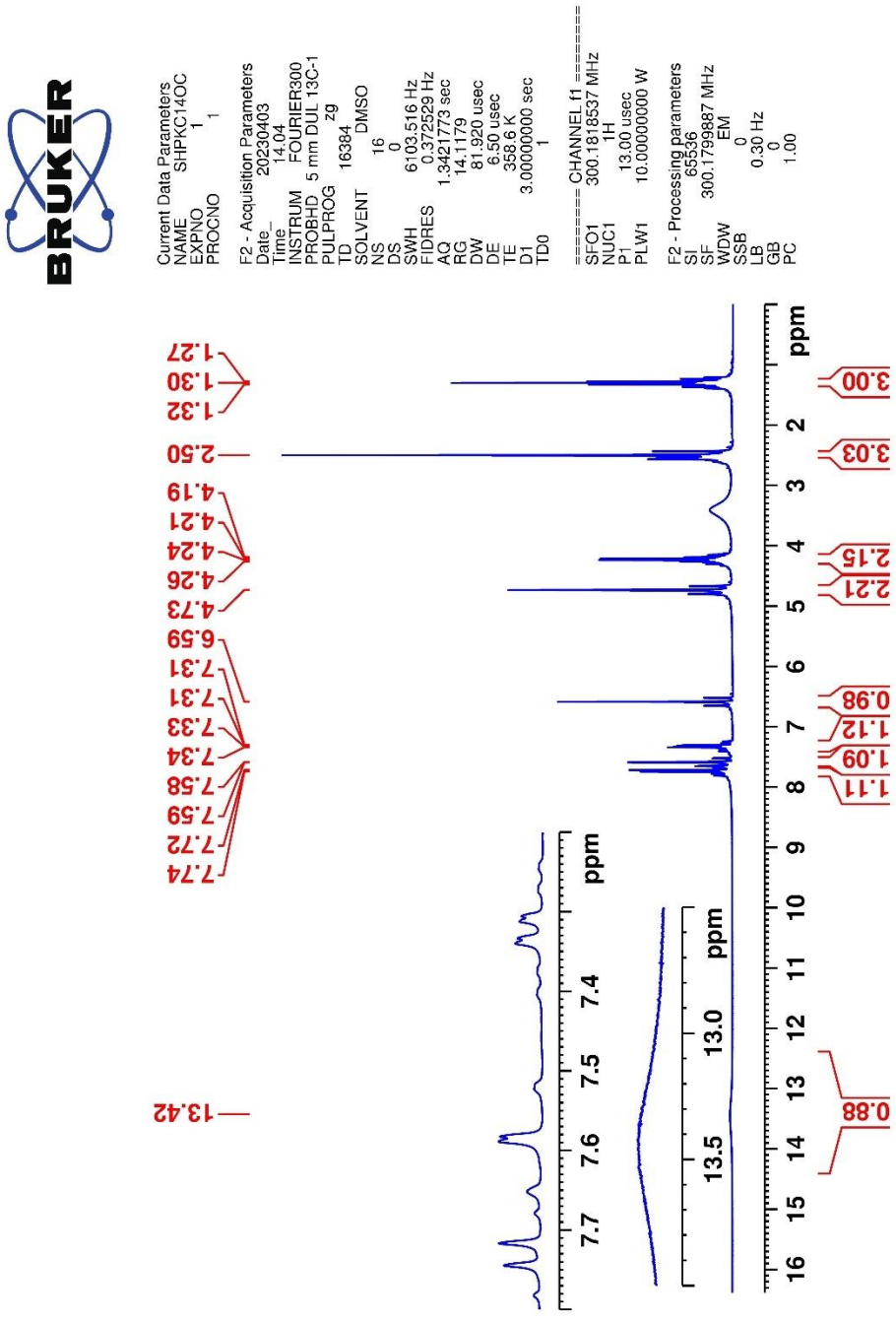

Figure 5.46. *[1]H-NMR spectrum of the compound **4k***

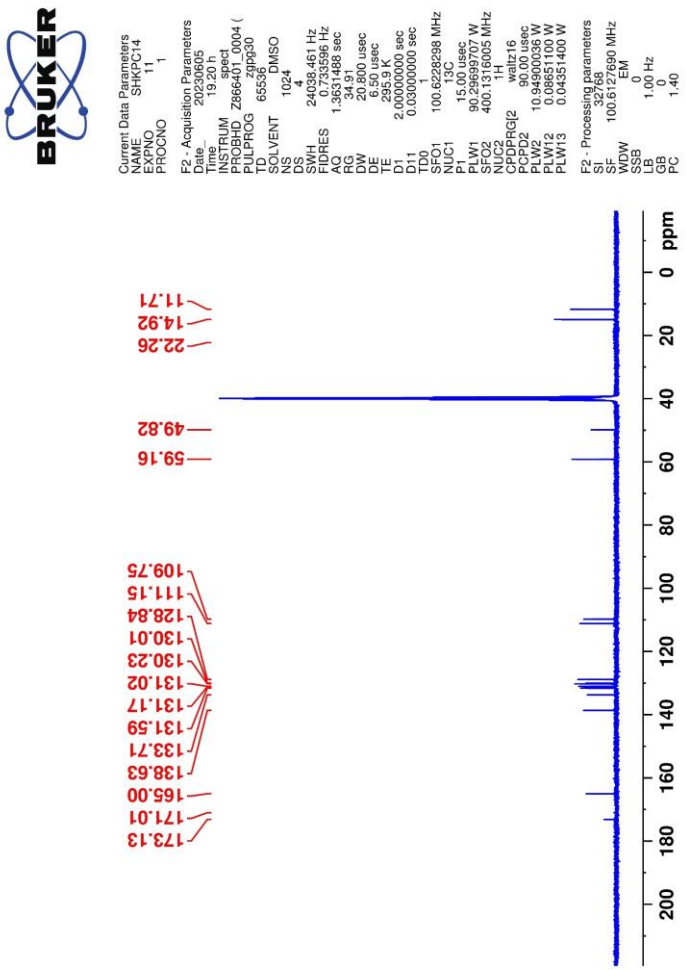

Figure 5.47. *^{13}C-NMR spectrum of the compound **4k***

Formula Predictor Report - SHPKC14-9C_7.lcd

Page 1 of 1

Data File: C:\LabSolutions\Data\Analiz\Asaf\SHPKC14-9C_7.lcd

Elmt	Val.	Min	Max	Elmt	Val.	Min	Max	Elmt	Val.	Min	Max	Elmt	Val.	Min	Max	Use Adduct
H	1	6	46	O	2	0	5	S	2	0	2	Ru	2	0	0	H
C	4	5	36	F	1	0	0	Cl	1	0	2	Pd	2	0	0	
N	3	0	5	P	3	0	0	Br	1	0	0	I	3	0	0	

Error Margin (ppm): 5
HC Ratio: unlimited
Max Isotopes: 3
MSn Iso RI (%): 10.00

DBE Range: 5.0 - 30.0
Apply N Rule: yes
Isotope RI (%): 1.00
MSn Logic Mode: AND

Electron Ions: both
Use MSn Info: yes
Isotope Res: 9000
Max Results: 50

Event#: 1 MS(E+) Ret. Time : 7.707 -> 8.120 Scan# : 1157 -> 1219

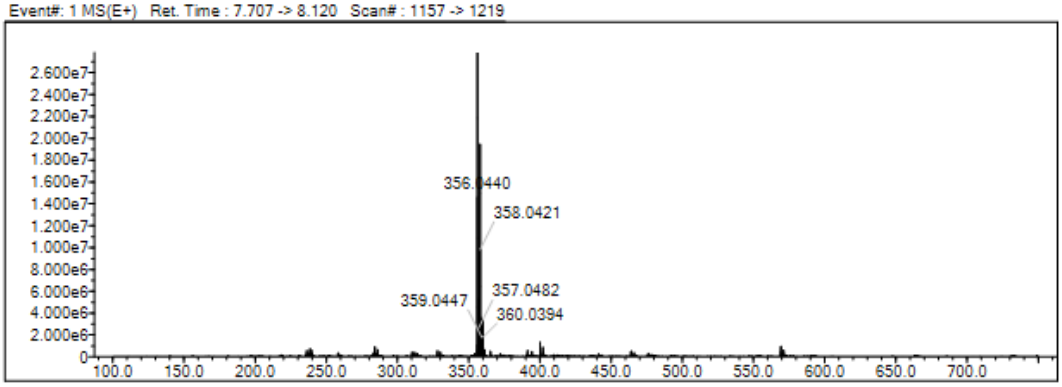

Measured region for 356.0440 m/z

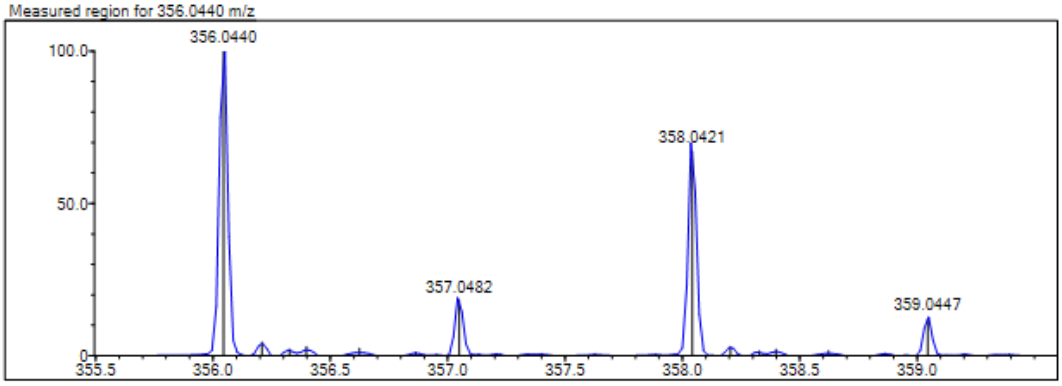

C16 H15 N O4 Cl2 [M+H]+ : Predicted region for 356.0451 m/z

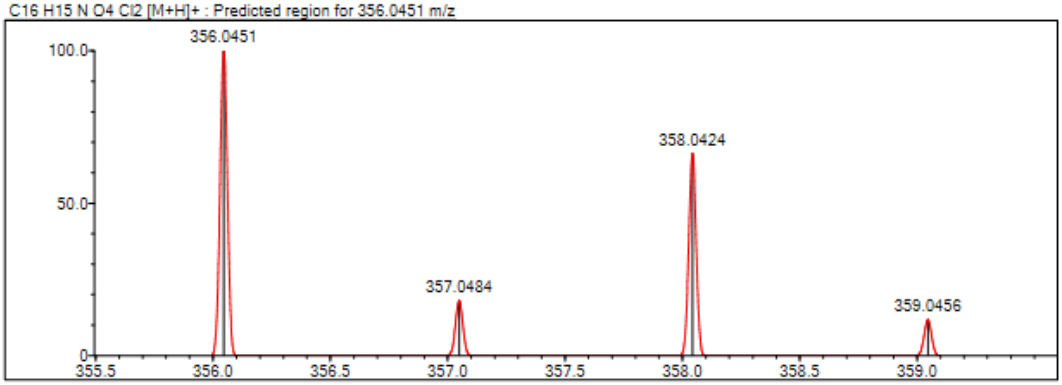

Rank	Score	Formula (M)	Ion	Meas. m/z	Pred. m/z	Df. (mDa)	Df. (ppm)	Iso	DBE
1	89.29	C16 H15 N O4 Cl2	[M+H]+	356.0440	356.0451	-1.1	-3.09	94.22	9.0

Figure 5.48. *Mass spectrum of the compound* ***4k***

5.2.2.11. 2-[5-(3-Chloroyphenyl)-3-(ethoxycarbonyl)-2-methyl-1H-pyrrol-1yl]acetic acid

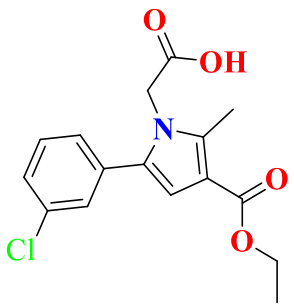

Figure 5.49. *Molecular structure of compound* ***4l***

Synthesized according to method **D**, experimental melting point: 100-102ºC, 65% yield percent.

^{1}H-NMR (400 MHz, DMSO-*d*$_6$; δ, ppm): 1.25 (3H, t, *J*= 7.08 Hz, -CH_2-**$\underline{CH_3}$**), 2.45 (3H, s, pyrrole-**$\underline{CH_3}$**), 4.18 (2H, q, J_1=7.08 Hz, J_2= 14.09 Hz, -**$\underline{CH_2}$**-CH_3), 4.64 (2H, s, **$\underline{CH_2}$**-COOH), 6.49 (1H, s, **$\underline{CH}$**-pyrrole), , 7.26 (1H, dt, *J*= 4.31 Hz, Ar-**$\underline{H}$**), 7.36 (1H, dt, J_1= 1.82 Hz, J_2= 1.87 Hz, Ar-**$\underline{H}$**), 7.42(1H, t, J_1= 1.87 Hz, Ar-**$\underline{H}$**), 7.45(1H, s, Ar-**$\underline{H}$**).

^{13}C-NMR (100 MHz, DMSO-*d*$_6$; δ, ppm) 11.50 (-pyrrole-**$\underline{C}$**H_3), 14.87 (-CH_2-**$\underline{C}$**H_3), 46.74 (-**$\underline{C}$**H_2-COOH), 59.40 (-**$\underline{C}$**H_2-CH_3), 110.15, 111.97, 127.50, 127.97, 128.48, 131.08, 132.38, 133.81, 134.34, 138.36, 164.77 (**$\underline{C}$**O-O-Et), 170.44 (**$\underline{C}$**OOH).

HRMS (-m/z): [M+H]$^+$: For $C_{16}H_{16}ClNO_4$ calculated molecular weight: 322.0838; found: 322. 0841.

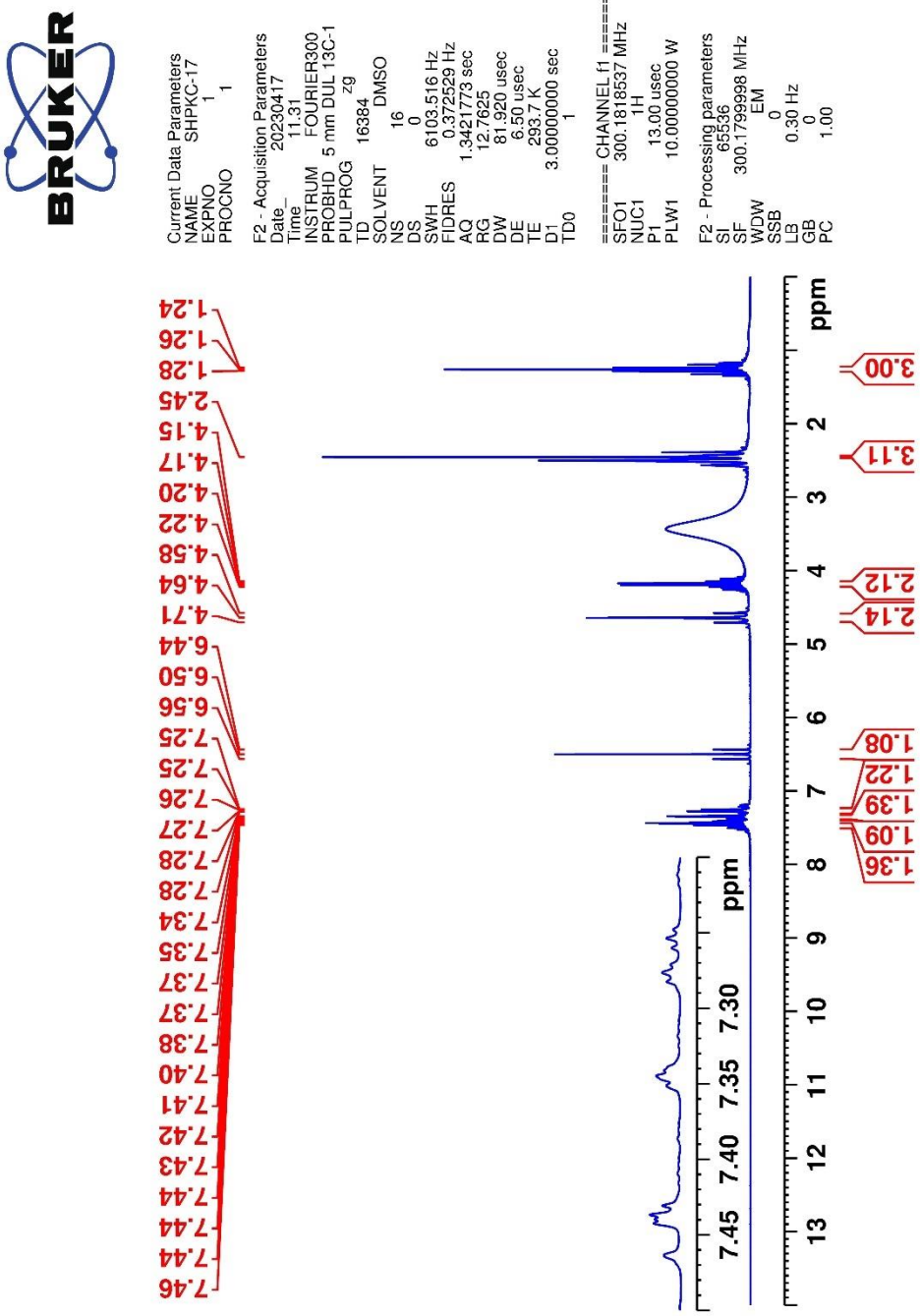

Figure 5.50. *^{1}H-NMR spectrum of the compound **4l***

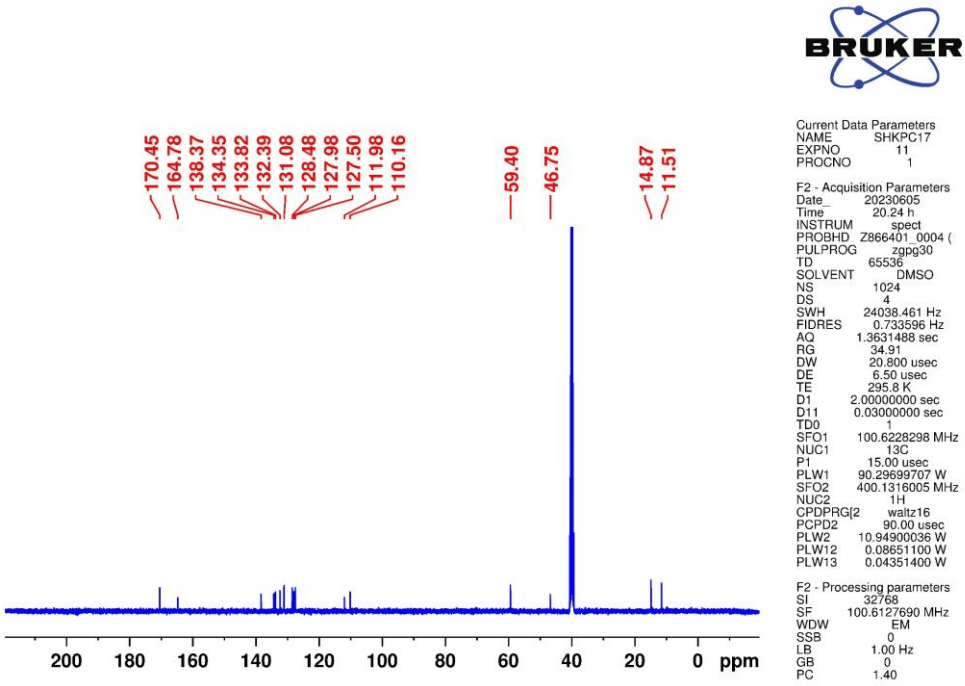

Figure 5.51. *^{13}C-NMR spectrum of the compound **4l***

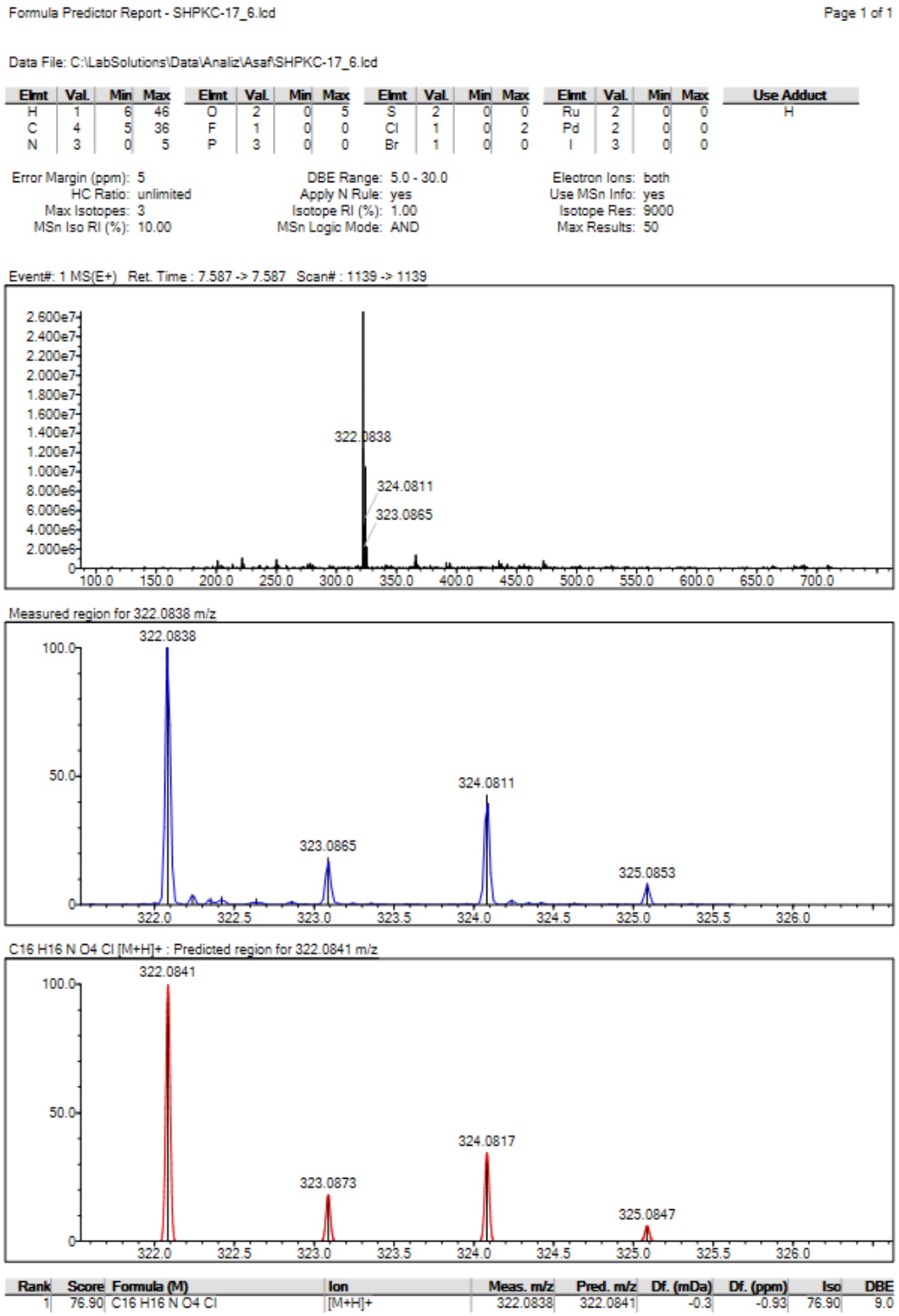

Figure 5.52. *Mass spectrum of the compound* ***4l***

5.2.2.12. 2-(3-(Ethoxycarbonyl)-2-methyl-5-(thiophen-2-yl)-1H-pyrrol-1-yl)acetic acid

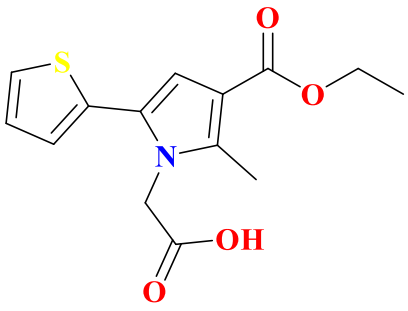

Figure 5.53. *Molecular structure of compound* ***4m***

Synthesized according to method **D**, experimental melting point: 90-95ºC, 55% yield percent.

^{1}H-NMR (400 MHz, DMSO-*d*$_6$; δ, ppm):): 1.25 (3H, t, *J*= 7.08 Hz, -CH_2-**$\underline{CH_3}$**), 2.45 (3H, s, pyrrole-**$\underline{CH_3}$**), 4.19 (2H, q, J_1=7.05 Hz, J_2= 14.14 Hz, -**$\underline{CH_2}$**-CH_3), 4.73 (2H, s, **$\underline{CH_2}$**-COOH), 6.51 (1H, s, **$\underline{CH_4}$**-pyrrole), 7.01 (1H, dd, J_1= 1.55 Hz, J_2= 3.66 Hz , thiophen-**$\underline{H}$**), 7.12 (1H, q, J_1= 2.91 Hz, J_2= 5.93 Hz , thiophen-**$\underline{H}$**), 7.57 (1H, dd, *J*= 2.08 Hz , thiophen-**$\underline{H}$**).

HRMS (-m/z): $[M+H]^+$: For $C_{14}H_{15}NO_4S$ calculated molecular weight: 294.0782, found: 294.0795.

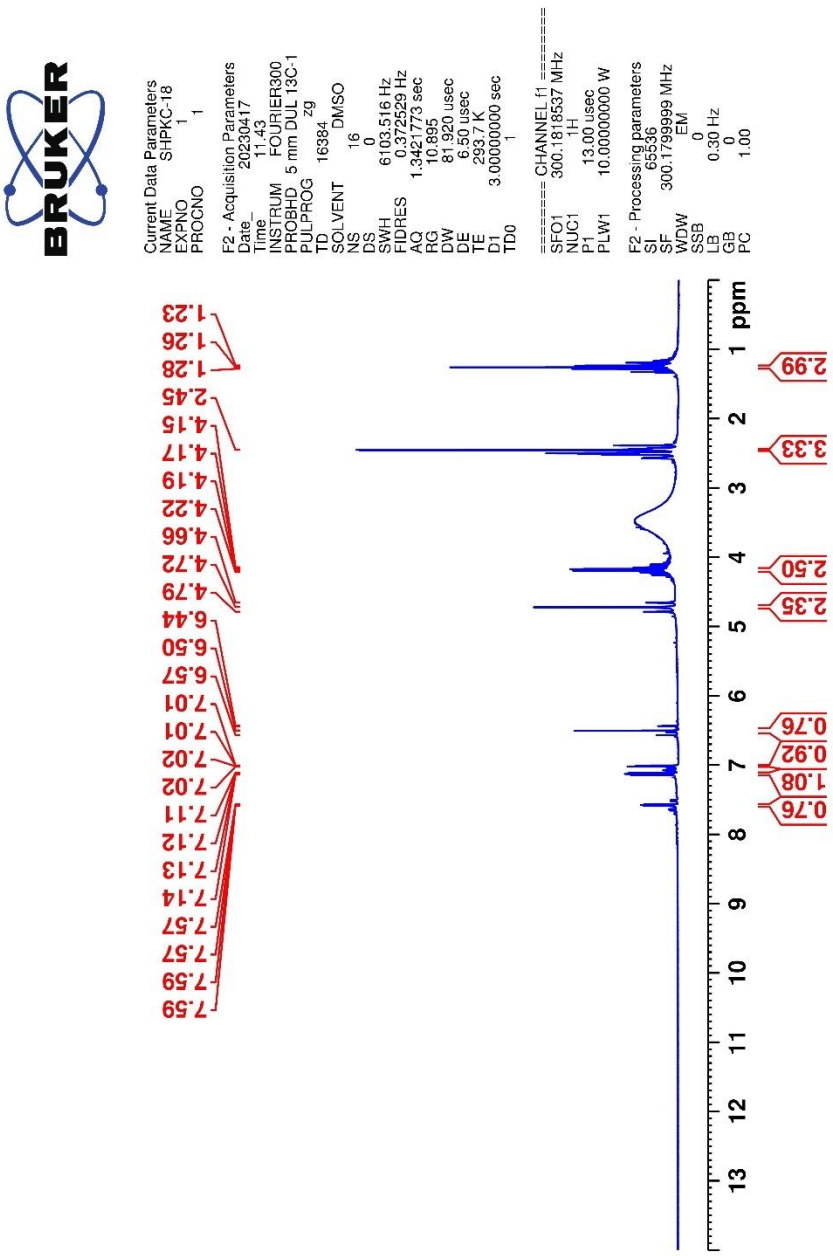

Figure 5.54. *[1]H-NMR spectrum of the compound **4m***

Formula Predictor Report - SHPKC-18_5.lcd

Page 1 of 1

Data File: C:\LabSolutions\Data\Analiz\Asaf\SHPKC-18_5.lcd

Elmt	Val.	Min	Max	Elmt	Val.	Min	Max	Elmt	Val.	Min	Max	Elmt	Val.	Min	Max	Use Adduct
H	1	6	46	O	2	0	4	S	2	1	1	Ru	2	0	0	H
C	4	5	36	F	1	0	0	Cl	1	0	0	Pd	2	0	0	
N	3	0	6	P	3	0	0	Br	1	0	0	I	3	0	0	

Error Margin (ppm): 5
HC Ratio: unlimited
Max Isotopes: 3
MSn Iso RI (%): 10.00

DBE Range: 5.0 - 30.0
Apply N Rule: yes
Isotope RI (%): 1.00
MSn Logic Mode: AND

Electron Ions: both
Use MSn Info: yes
Isotope Res: 9000
Max Results: 50

Event#: 1 MS(E+) Ret. Time : 6.253 Scan# : 939

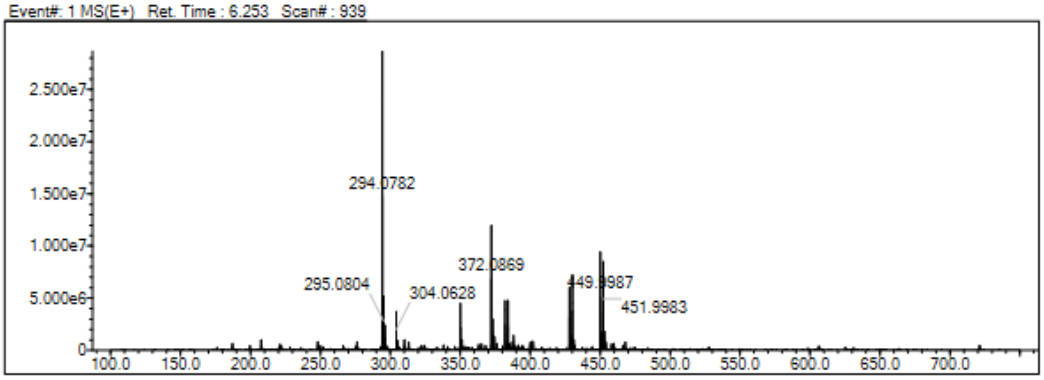

Measured region for 294.0782 m/z

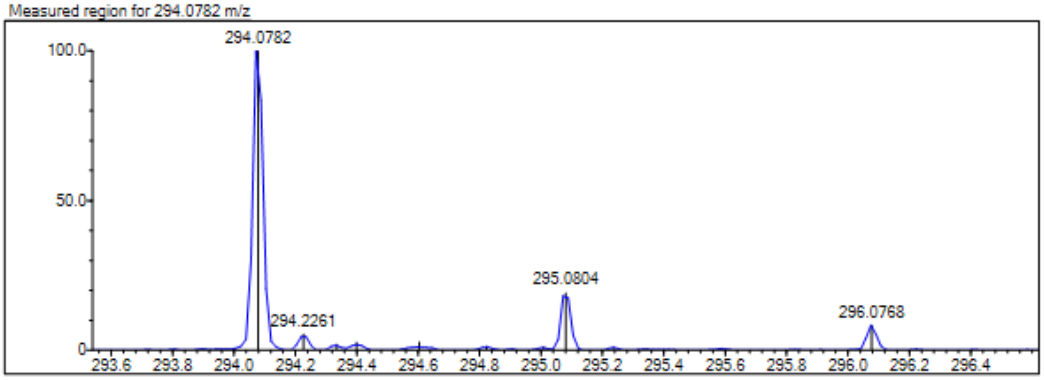

C14 H15 N O4 S [M+H]+ : Predicted region for 294.0795 m/z

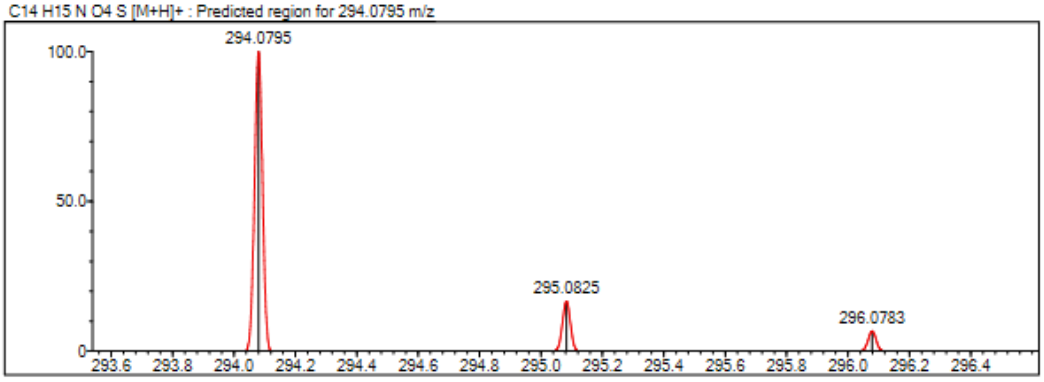

Rank	Score	Formula (M)	Ion	Meas. m/z	Pred. m/z	Df. (mDa)	Df. (ppm)	Iso	DBE
1	69.77	C14 H15 N O4 S	[M+H]+	294.0782	294.0795	-1.3	-4.42	76.29	8.0

Figure 5.55. *Mass spectrum of the compound* ***4m***

5.2.2.13. 2-(3-(Ethoxycarbonyl)-2-methyl-5-(3,4,5-trichlorophenyl)-1H-pyrrol-1-yl) acetic acid

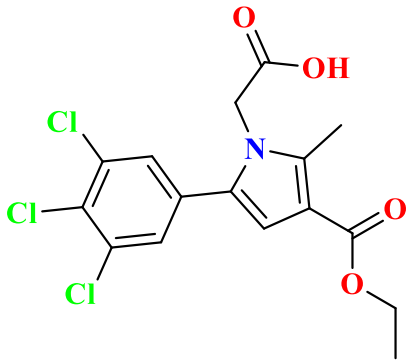

Figure 5.56. *Molecular structure of compound **4n***

Synthesized according to method **D**, experimental melting point: 101-105ºC, 62% yield percent.

^{1}H-NMR (400 MHz, DMSO-d_6; δ, ppm): 1.26 (3H, t, *J*= 7.07 Hz, -CH_2-**CH_3**), 2.46 (3H, s, pyrrole-**CH_3**), 4.19 (2H, q, J_1=7.04 Hz, J_2= 14.07 Hz, -**CH_2**-CH_3), 4.51 (2H, s, **CH_2**-COOH), 6.44 (1H, s, **CH**-pyrrole), 7.28 (1H, d, *J*= 8.36 Hz, Ar-**H**), 7.72 (1H, d, *J*= 8.36 Hz, Ar-**H**).

^{13}C-NMR (100 MHz, DMSO-d_6; δ, ppm) 11.49 (-pyrrole-**C**H_3), 14.87 (-CH_2-**C**H_3), 46.34 (-**C**H_2-COOH), 59.42 (-**C**H_2-CH_3), 110.97, 111.89, 129.03, 129.25, 131.36, 132.10, 132.16, 133.76, 137.75, 164.96 (**C**O-O-Et), 169.81 (**C**OOH).

HRMS (-m/z): $[M+H]^+$: For $C_{16}H_{14}Cl_3NO_4$ calculated molecular weight: 390.0045; found: 390. 0061.

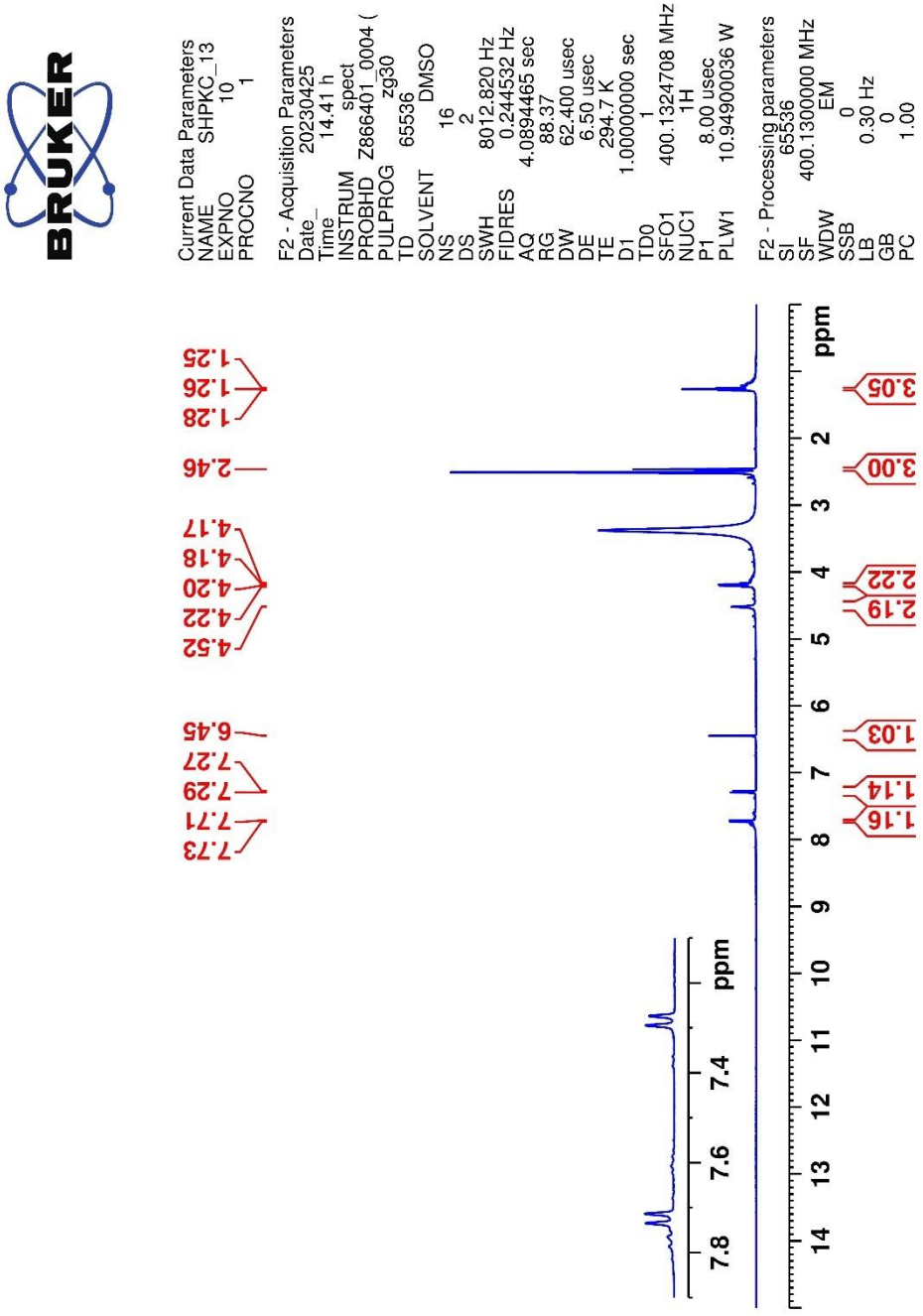

Figure 5.57. *[1]H-NMR spectrum of the compound* ***4n***

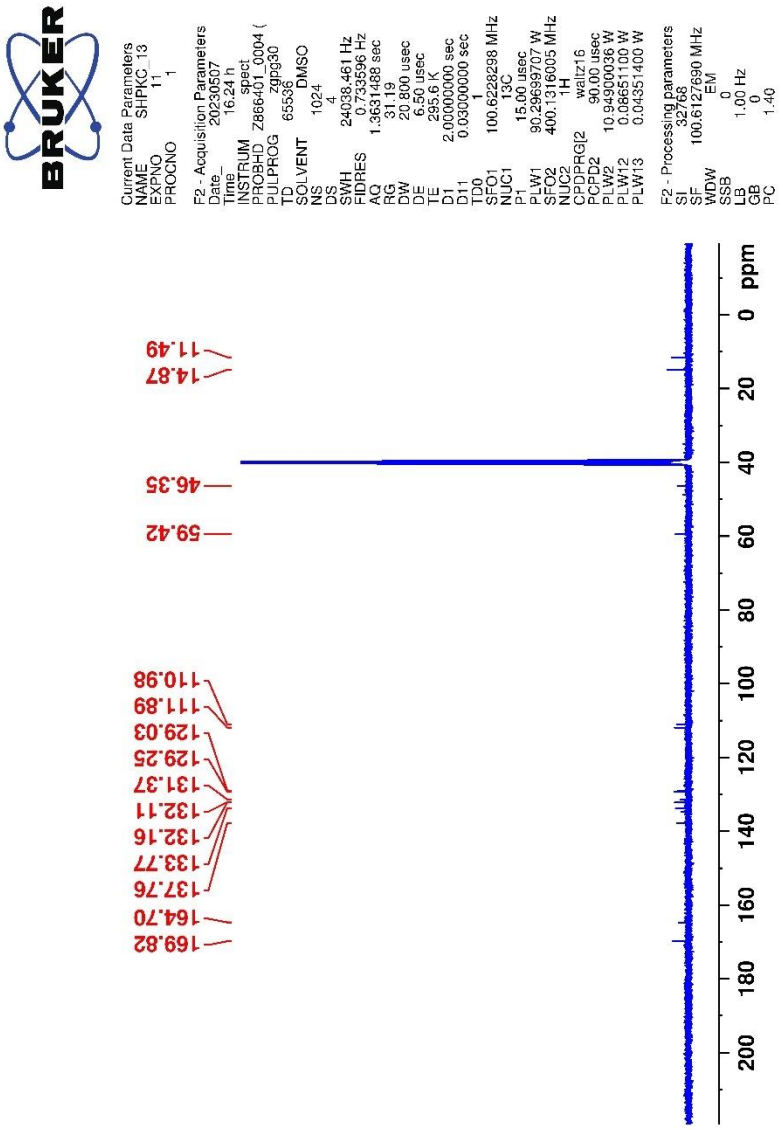

figure 5.58. *^{13}C-NMR spectrum of the compound **4n***

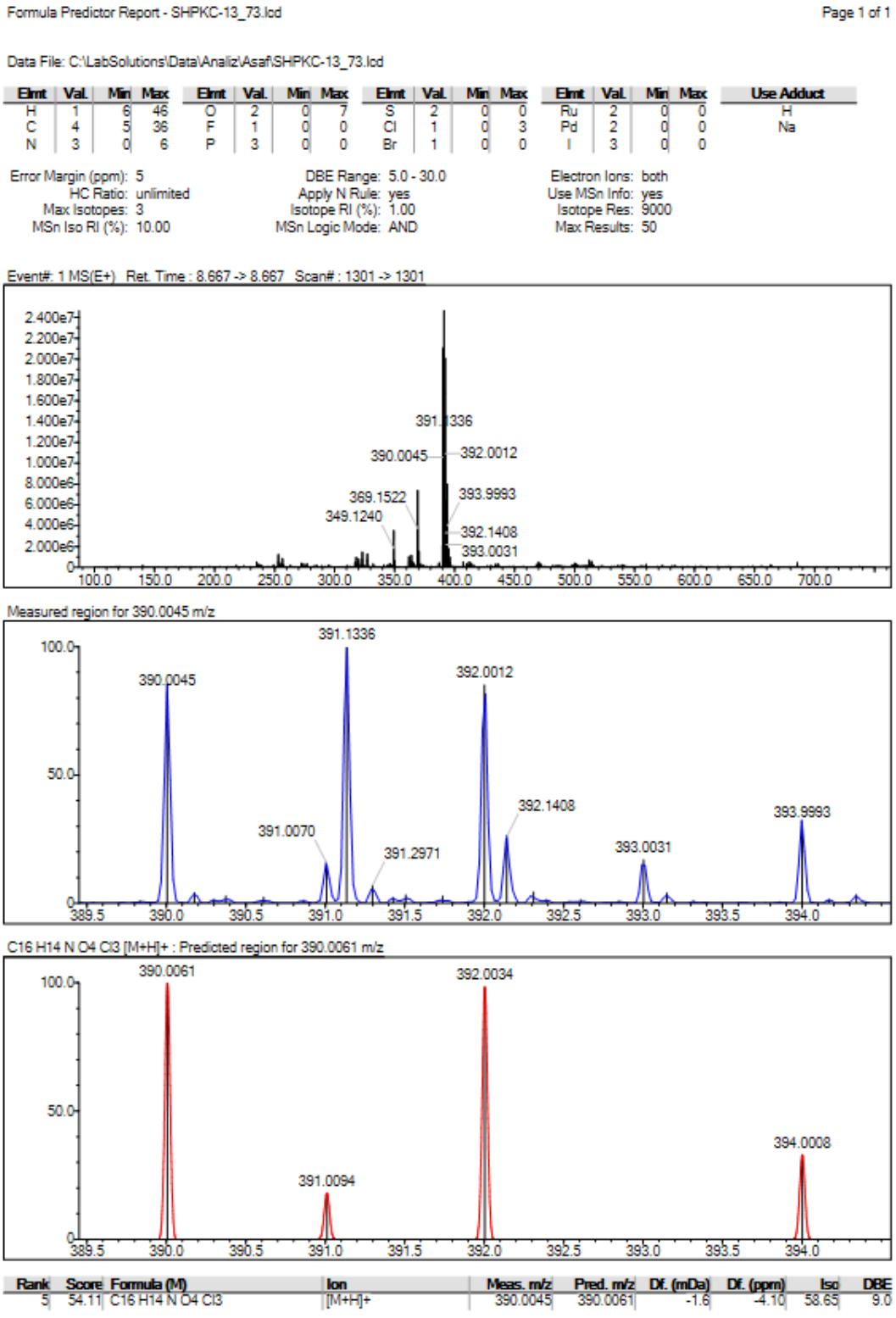

Figure 5.59. Mass *spectrum of the compound* ***4n***

5.2.2.14. 2-(3-(Ethoxycarbonyl)-2-methyl-5-(p-tolyl)-1H-pyrrol-1-yl)acetic acid

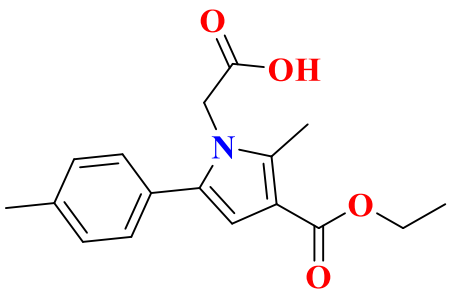

Figure 5.60. *Molecular structure of compound* ***4o***

Synthesized according to method **D**, experimental melting point: 125-127ºC, 79% yield percent.

^{1}H-NMR (400 MHz, DMSO-d_6; δ, ppm): 1.26 (3H, t, *J*= 7.07 Hz, -CH_2-**CH_3**), 2.33 (3H, s, pyrrole-**CH_3**), 4.18 (2H, q, J_1=7.06 Hz, J_2= 14.08 Hz, -**CH_2**-CH_3), 4.60 (2H, s, **CH_2**-COOH), 6.37 (1H, s, **CH**-pyrrole), , 7.17 (2H, d, *J*= 7.87 Hz, Ar-**$H_{3,5}$**), 7.24 (2H, d, *J*= 7.90 Hz, Ar-**$H_{2,6}$**).

^{13}C-NMR (100 MHz, DMSO-d_6; δ, ppm) 11.51 (-pyrrole-**C**H_3), 14.89 (-CH_2-**C**H_3), 21.20 (**C**H_3-Ph), 46.46 (-**C**H_2-COOH), 59.28 (-**C**H_2-CH_3), 108.93, 111.67, 128.96, 129.41, 129.80, 133.92, 137.52, 137.59, 164.92 (**C**O-O-Et), 170.44 (**C**OOH).

HRMS (-m/z): $[M+H]^+$: For $C_{17}H_{19}NO_4$ calculated molecular weight: 302.1400; found: 302. 1387.

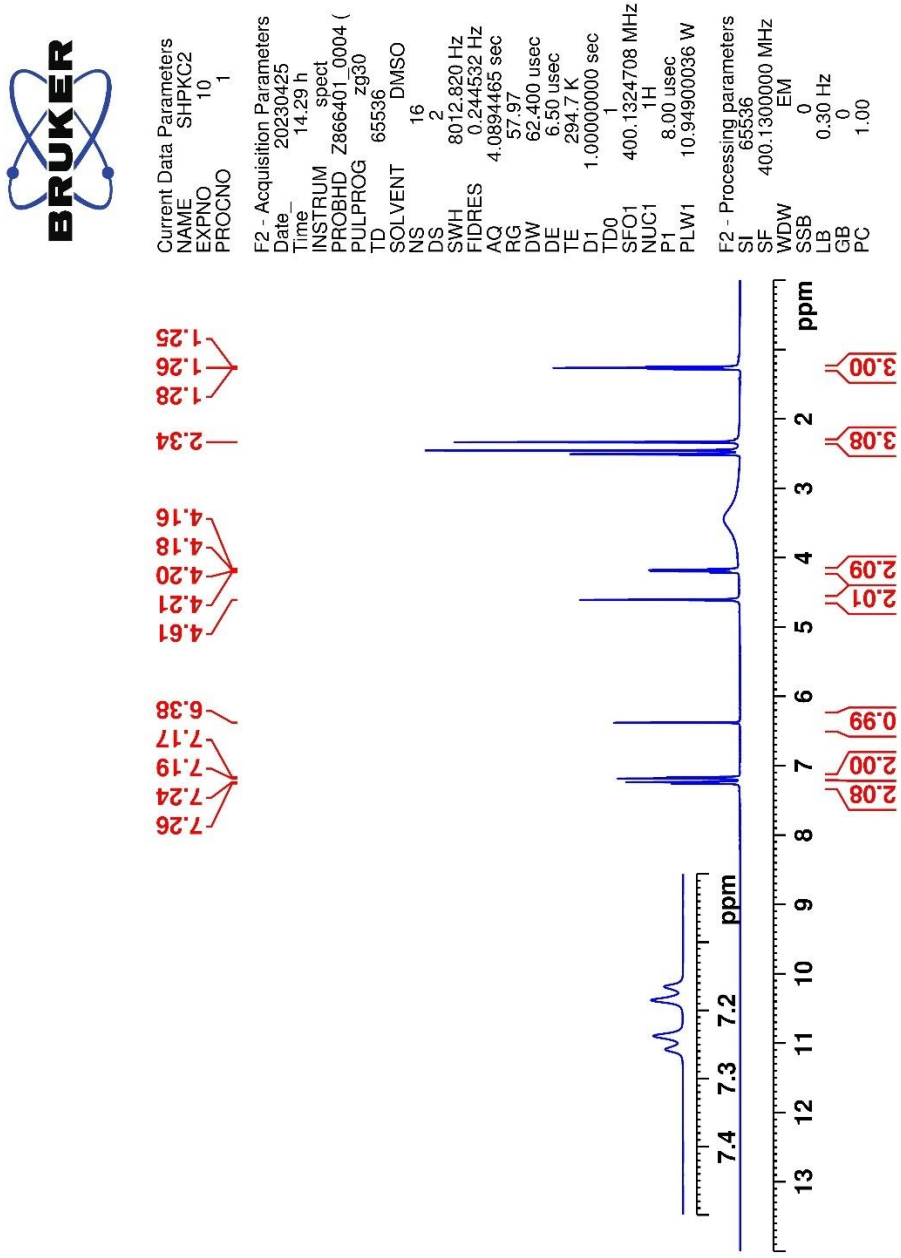

Figure 5.61. *[1]H-NMR spectrum of the compound* ***4o***

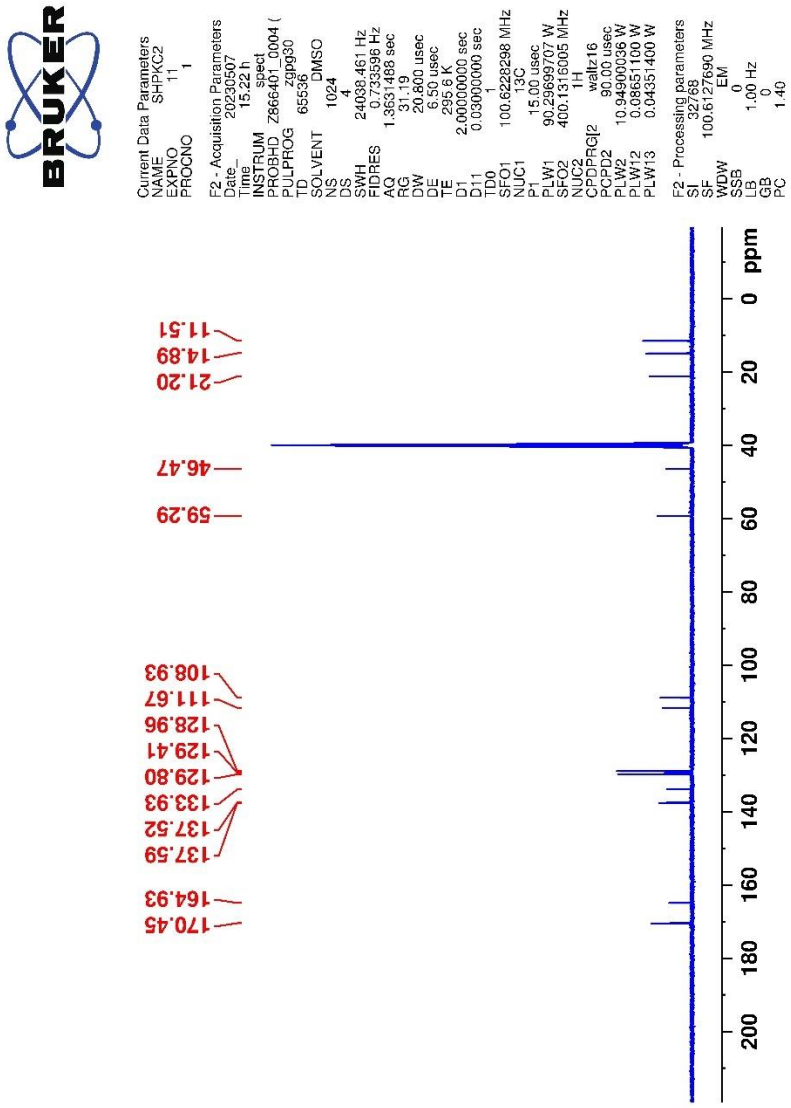

Figure 5.62. *^{13}C-NMR spectrum of the compound* ***4o***

Formula Predictor Report - SHPKC2_460.lcd

Page 1 of 1

Data File: C:\LabSolutions\Data\Analiz\Asaf\SHPKC2_460.lcd

Elmt	Val.	Min	Max	Elmt	Val.	Min	Max	Elmt	Val.	Min	Max	Elmt	Val.	Min	Max	Use Adduct
H	1	6	46	O	2	0	7	S	2	0	0	Ru	2	0	0	H
C	4	5	36	F	1	0	0	Cl	1	0	0	Pd	2	0	0	
N	3	0	6	P	3	0	0	Br	1	0	0	I	3	0	0	

Error Margin (ppm): 10
HC Ratio: unlimited
Max Isotopes: 3
MSn Iso RI (%): 10.00

DBE Range: 5.0 - 30.0
Apply N Rule: yes
Isotope RI (%): 1.00
MSn Logic Mode: AND

Electron Ions: both
Use MSn Info: yes
Isotope Res: 9000
Max Results: 50

Event#: 1 MS(E+) Ret. Time : 7.333 Scan# : 1101

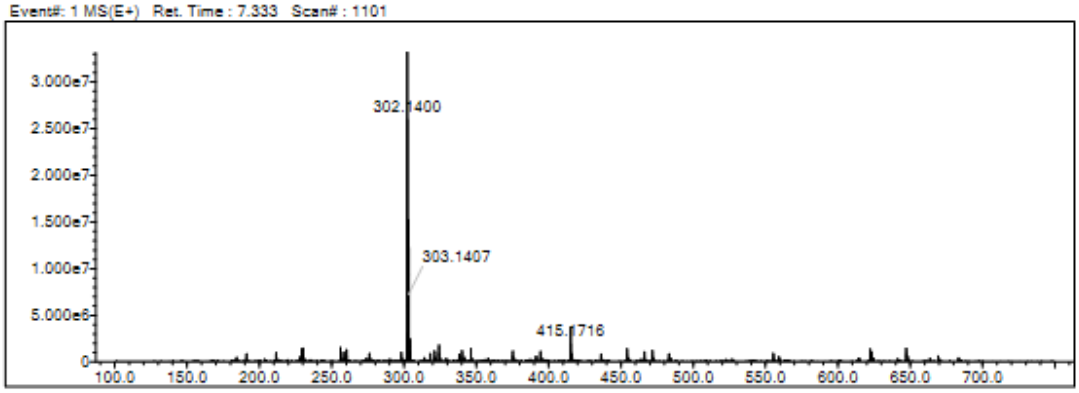

Measured region for 302.1400 m/z

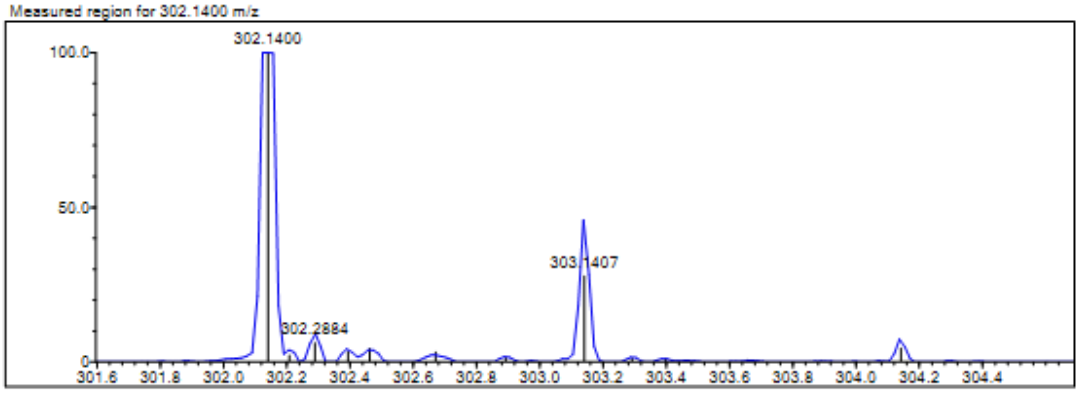

C17 H19 N O4 [M+H]+ : Predicted region for 302.1387 m/z

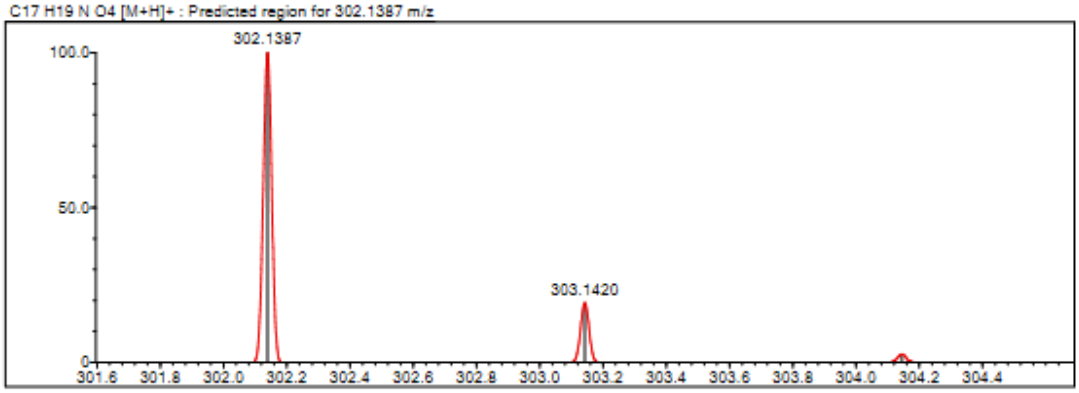

Rank	Score	Formula (M)	Ion	Meas. m/z	Pred. m/z	Df. (mDa)	Df. (ppm)	Iso	DBE
2	42.20	C17 H19 N O4	[M+H]+	302.1400	302.1387	1.3	4.30	46.00	9.0

Figure 5.63. *Mass spectrum of the compound* ***4o***

5.2.2.15. 2-(3-(Ethoxycarbonyl)-2-methyl-5-(3-nitrophenyl)-1H-pyrrol-1-yl)acetic acid

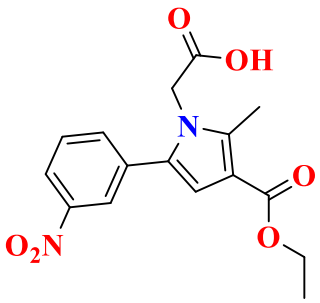

Figure 5.64. *Molecular structure of compound* ***4p***

Synthesized according to method **D**, experimental melting point 120-122ºC, 75% yield percent.

^{1}H-NMR (400 MHz, DMSO-*d*$_6$; δ, ppm): 1.27 (3H, t, *J*= 7.07 Hz, -CH_2-**$\underline{CH_3}$**), 2.48 (3H, s, pyrrole-**$\underline{CH_3}$**), 4.20 (2H, q, J_1=7.06 Hz, J_2= 14.11 Hz, -**$\underline{CH_2}$**-CH_3), 4.72 (2H, s, **$\underline{CH_2}$**-COOH), 6.62 (1H, s, **$\underline{CH}$**-pyrrole), 7.74 (1H, t, *J*= 7.39 Hz, Ar-**$\underline{H}$**), 7.79 (1H, d, *J*= 7.63 Hz, Ar-**$\underline{H}$**), 8.09 (1H, s, Ar-**$\underline{H}$**), 8.20 (1H, d, *J*= 7.63 Hz, Ar-**$\underline{H}$**).

^{13}C-NMR (100 MHz, DMSO-*d*$_6$; δ, ppm) 11.50 (-pyrrole-**$\underline{C}$**H_3), 14.85 (-CH_2-**$\underline{C}$**H_3), 46.70 (-**$\underline{C}$**H_2-COOH), 59.49 (-**$\underline{C}$**H_2-CH_3), 110.83, 112.25, 122.70, 123.06, 123.38, 130.87, 131.69, 133.69, 135.26, 138.83, 148.45, 164.68 (**$\underline{C}$**O-O-Et), 170.51 (**$\underline{C}$**OOH).

HRMS (-m/z): [M+H]$^+$: For $C_{16}H_{16}N_2O_6$ calculated molecular weight: 333.1090; found: 333.1081.

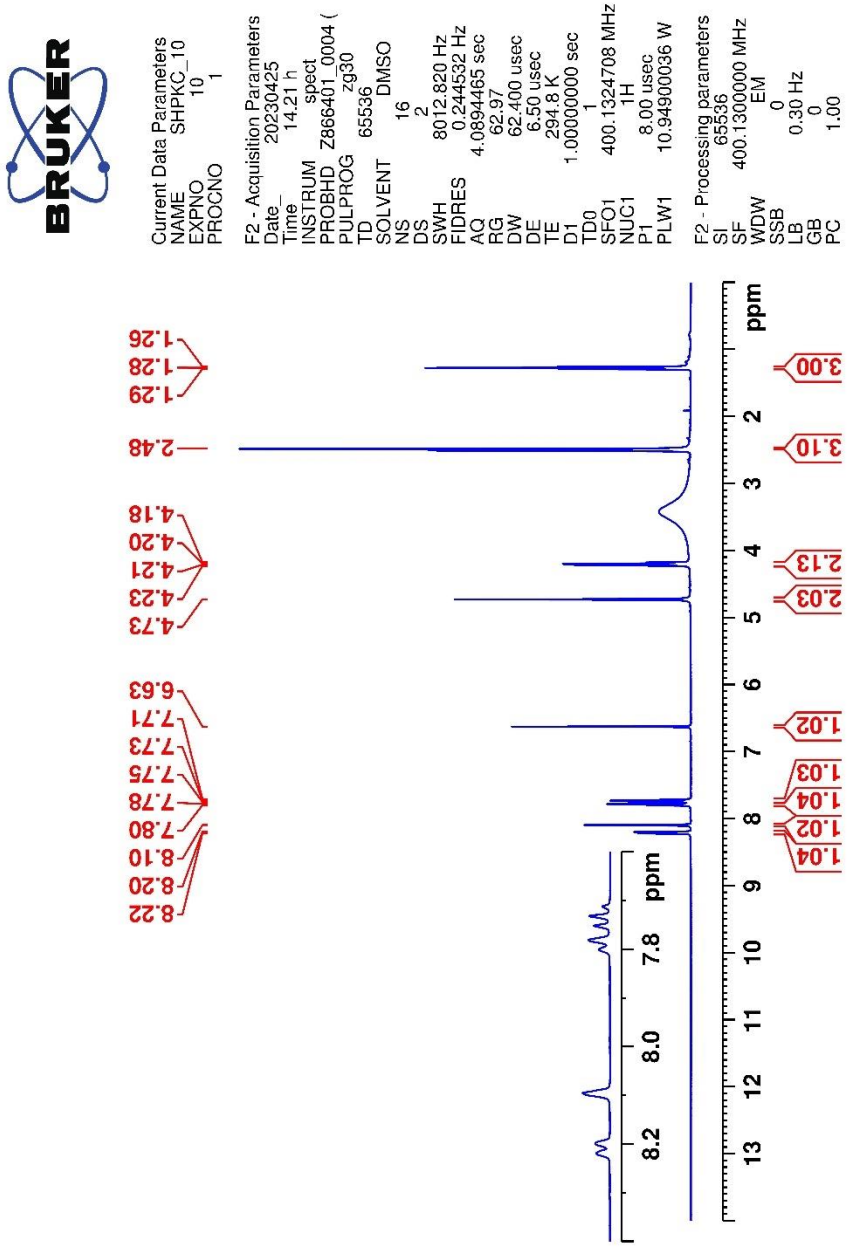

Figure 5.65. *[1]H-NMR spectrum of the compound* ***4p***

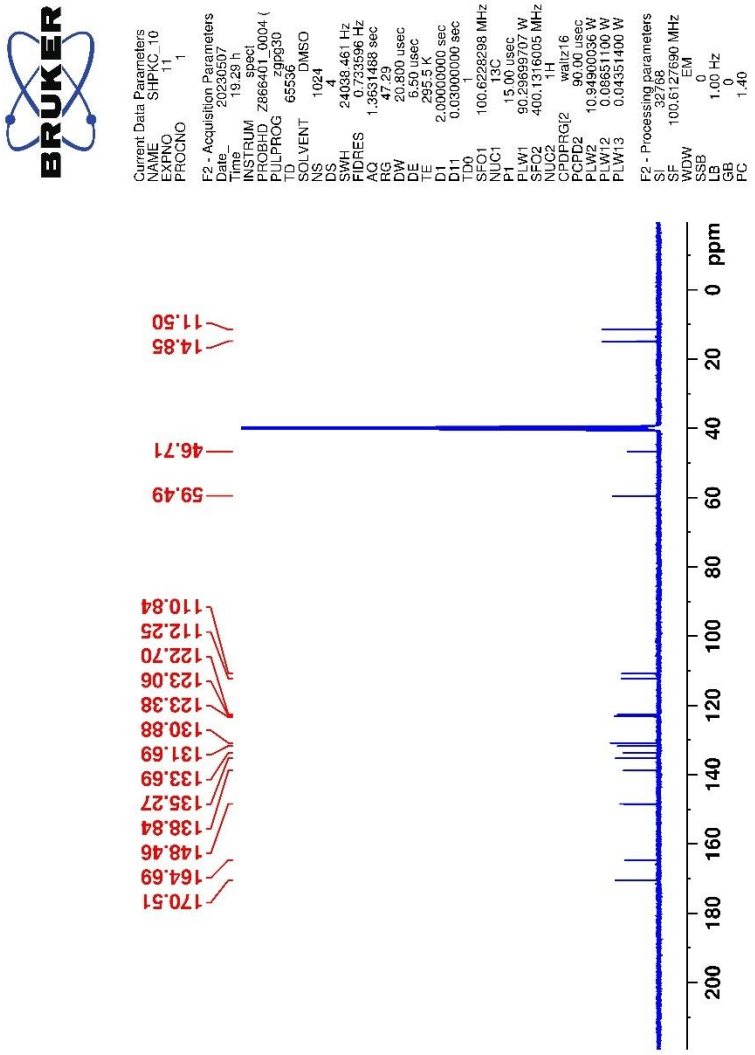

Figure 5.66. *^{13}C-NMR spectrum of the compound **4p***

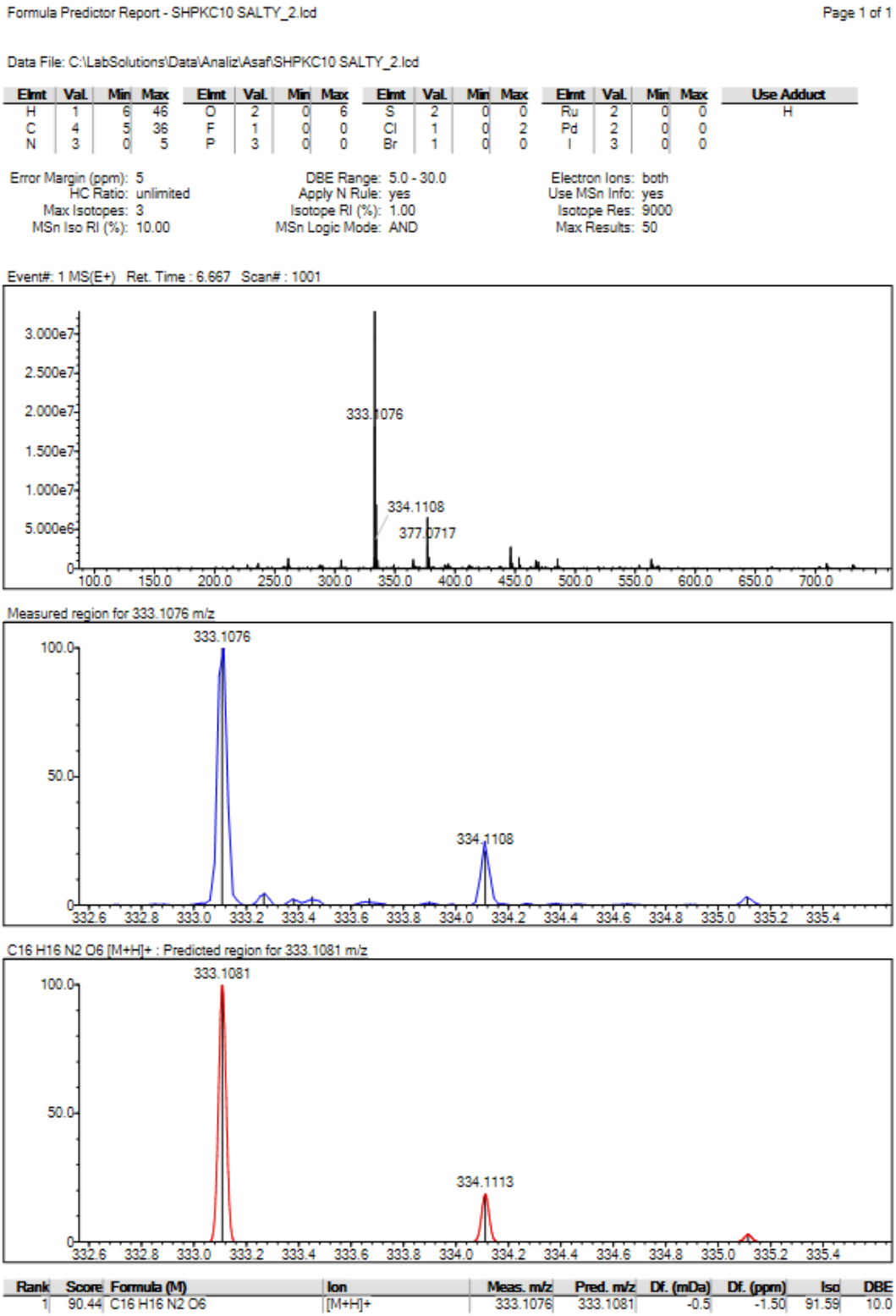

Figure 5.67. *Mass spectrum of the compound* ***4p***

5.2.2.16. 3-(5-(3,4-Dichlorophenyl)-3-(ethoxycarbonyl)-2-methyl-1H-pyrrol-1-yl)-4-methoxybenzoic acid

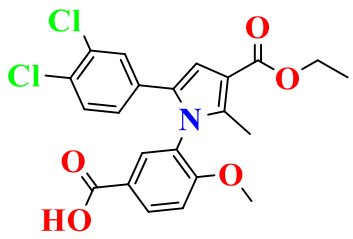

Figure 5.68. *Molecular structure of compound* ***5a***

Synthesized according to method **D**, experimental melting point 205-106ºC, 65% yield percent.

^{1}H-NMR (400 MHz, DMSO-*d*$_6$; δ, ppm):): 1.28 (3H, t, *J*= 7.08 Hz, -CH_2-**CH_3**), 2.21 (3H, s, pyrrole-**CH_3**),), 3.78 (3H, s, pyrrole-**OCH_3**), 4.22 (2H, q, J_1=7.08 Hz, J_2= 14.16 Hz, -**CH_2**-CH_3), 6.82 (1H, s, **CH**-pyrrole), 6.94 (1H, dd, J_1= 2.11, J_2= 8.42 Hz, Ar-**H**), 7.27 (1H, d, *J*= 2.05 Hz, Ar-**H**), 7.35 (1H, d, *J*= 8.87 Hz, Ar-**H**), 7.43 (1H, d, *J*= 8.43 Hz, Ar-**H**), 7.64 (1H, d, *J*= 2.12 Hz, Ar-**H**) 8.07 (1H, dd, J_1= 3.61, J_2= 9.17 Hz, Ar-**H**), 12.95 (1H, br-s, COO**H**).

^{13}C-NMR (100 MHz, DMSO-*d*$_6$; δ, ppm) 12.06 (-pyrrole-**C**H_3), 14.89 (-CH_2-**C**H_3), 56.88 (-O**C**H_3), 59.63 (-**C**H_2-CH_3), 110.98, 112.94, 113.31, 124.10, 125.81, 127.48, 129.11, 129.74, 130.89, 131.24, 131.38, 132.80, 133.00, 139.30, 159.04, 164.65 (**C**O-O-Et), 166.58 (**C**OOH).

HRMS (-m/z): [M+H]$^{+}$: For $C_{22}H_{19}NO_5Cl_2$ calculated molecular weight: 448.0710, found: 448.0713.

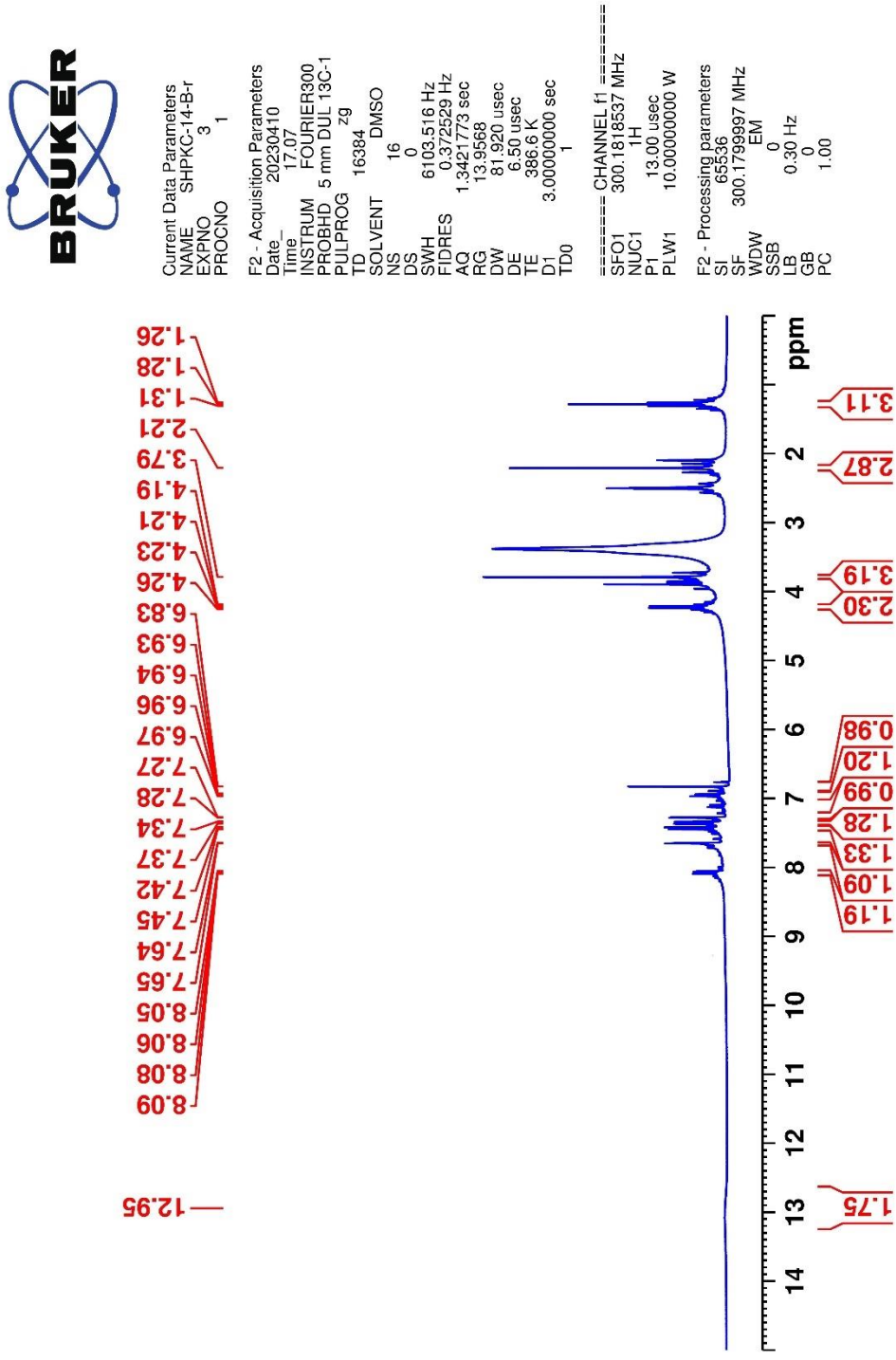

Figure 5.69. *[1]H-NMR spectrum of the compound **5a***

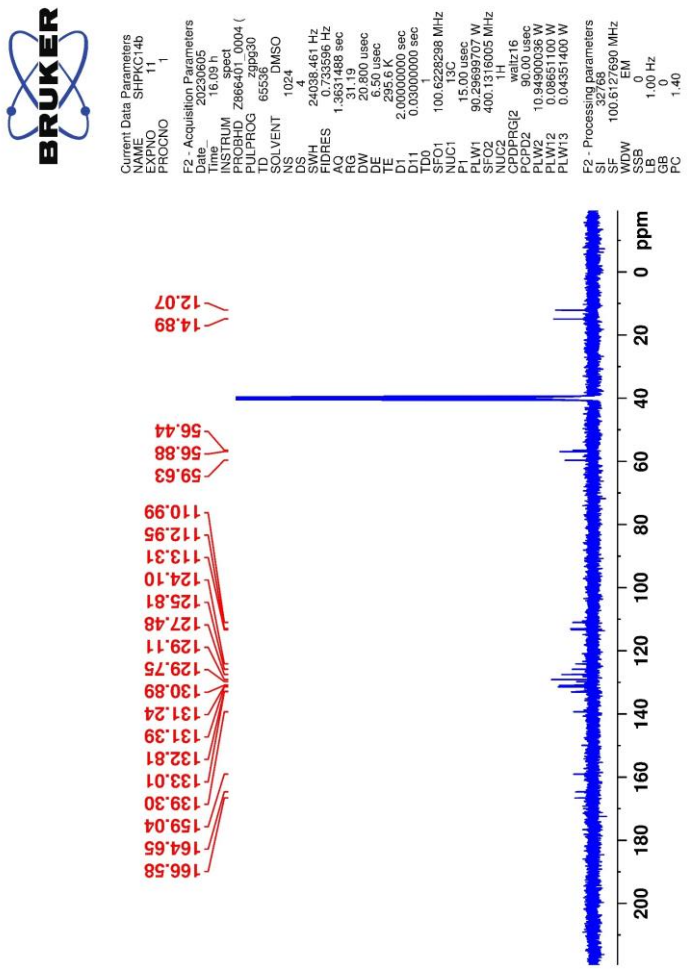

Figure 5.70. *^{13}C-NMR spectrum of the compound **5a***

Formula Predictor Report - 14-B_61.lcd

Page 1 of 1

Data File: C:\LabSolutions\Data\Analiz\Asaf\14-B_61.lcd

Elmt	Val.	Min	Max	Elmt	Val.	Min	Max	Elmt	Val.	Min	Max	Elmt	Val.	Min	Max	Use Adduct
H	1	6	46	O	2	0	5	S	2	0	0	Ru	2	0	0	H
C	4	5	36	F	1	0	0	Cl	1	0	2	Pd	2	0	0	
N	3	0	5	P	3	0	0	Br	1	0	0	I	3	0	0	

Error Margin (ppm): 5
HC Ratio: unlimited
Max Isotopes: 3
MSn Iso RI (%): 10.00

DBE Range: 5.0 - 30.0
Apply N Rule: yes
Isotope RI (%): 1.00
MSn Logic Mode: AND

Electron Ions: both
Use MSn Info: yes
Isotope Res: 9000
Max Results: 50

Event#: 1 MS(E+) Ret. Time : 9.320 -> 9.320 Scan# : 1399 -> 1399

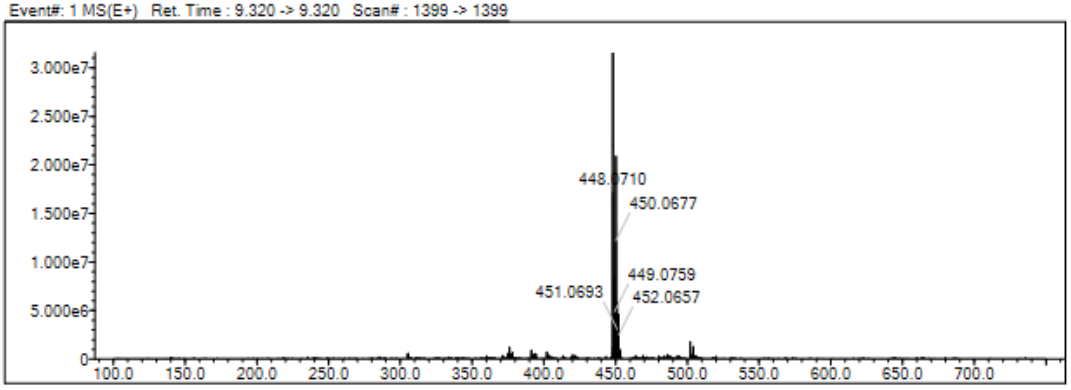

Measured region for 448.0710 m/z

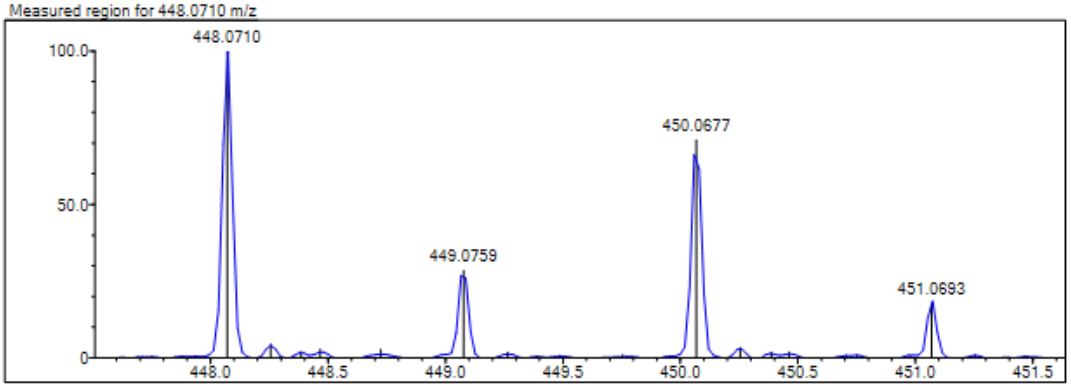

C22 H19 N O5 Cl2 [M+H]+ : Predicted region for 448.0713 m/z

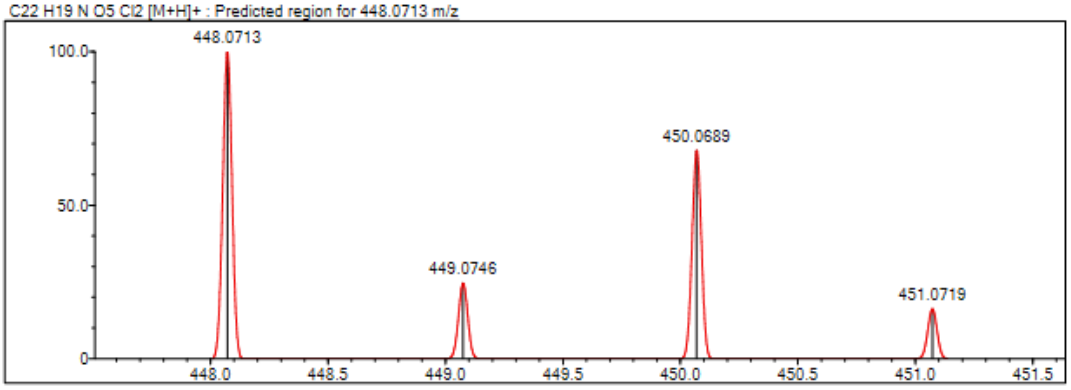

Rank	Score	Formula (M)	Ion	Meas. m/z	Pred. m/z	Df. (mDa)	Df. (ppm)	Iso	DBE
2	88.74	C22 H19 N O5 Cl2	[M+H]+	448.0710	448.0713	-0.3	-0.67	88.74	13.0

Figure 5.71. *Mass spectrum of the compound* ***5a***

5.2.2.17. 3-(5-(3,4-Dichlorophenyl)-3-(ethoxycarbonyl)-2-methyl-1H-pyrrol-1-yl)-4-hydroxybenzoic acid

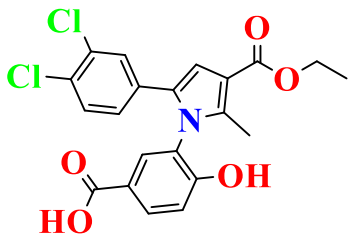

Figure 5.72. *Molecular structure of compound* ***5b***

Synthesized according to method **D**, experimental melting point 165-166ºC, 55% yield percent.

^{1}H-NMR (400 MHz, DMSO-*d*$_6$; δ, ppm):): 1.28 (3H, t, *J*= 7.06 Hz, -CH_2-**CH_3**), 2.23 (3H, s, pyrrole-**CH_3**),), 4.22 (2H, q, J_1=7.05 Hz, J_2= 14.11 Hz, -**CH_2**-CH_3), 6.83 (1H, s, **CH**-pyrrole), 7.02 (1H, dd, J_1= 3.43 Hz, J_2= 8.68 Hz, Ar-**H**), 7.12 (1H, d, *J*= 1.38, Ar-**H**), 7.30 (1H, d, *J*= 1.76 Hz, Ar-**H**), 7.45 (1H, d, *J*= 8.44 Hz, Ar-**H**), 7.56 (1H, d, *J*= 1.83 Hz, Ar-**H**), 7.91 (1H, dd, J_1= 3.48, J_2= 9.58 Hz, Ar-**H**), 11.21 (1H, br-s, O**H**), 12.80 (1H, br-s, COO**H**).

^{13}C-NMR (100 MHz, DMSO-*d*$_6$; δ, ppm) 12.08 (-pyrrole-**C**H_3), 14.90 (-CH_2-**C**H_3), 59.58 (-**C**H_2-CH_3), 110.97, 112.81, 117.14, 122.66, 124.62, 127.42, 128.96, 129.63, 130.89, 131.32, 131.40, 131.67, 132.70, 133.00, 139.49, 158.29, 164.67 (**C**O-O-Et), 166.73 (**C**OOH).

HRMS (-m/z): [M+H]$^+$: For $C_{21}H_{17}NO_5Cl_2$ calculated molecular weight: 434.0552, found: 434.0557.

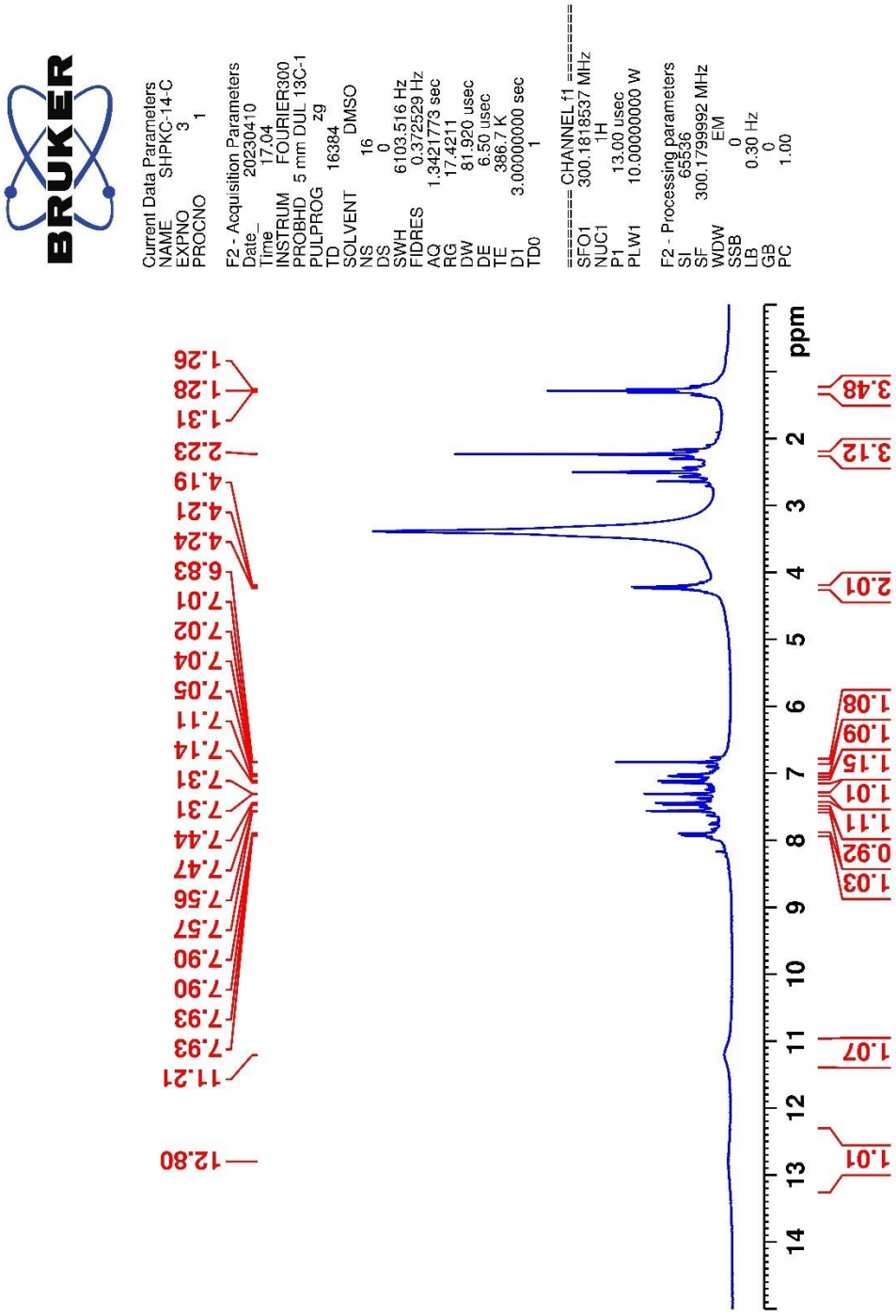

Figure 5.73. *[1]H-NMR spectrum of the compound **5b***

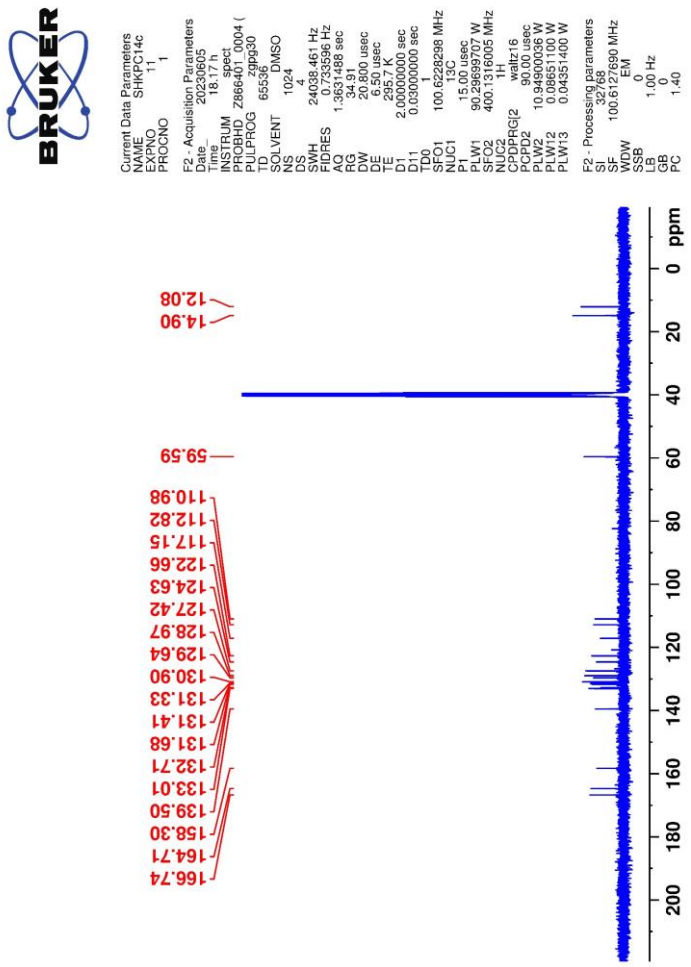

Figure 5.74. *^{13}C-NMR spectrum of the compound **5b***

Formula Predictor Report - 14-C_60.lcd

Page 1 of 1

Data File: C:\LabSolutions\Data\Analiz\Asaf\14-C_60.lcd

Elmt	Val.	Min	Max	Elmt	Val.	Min	Max	Elmt	Val.	Min	Max	Elmt	Val.	Min	Max	Use Adduct
H	1	6	46	O	2	0	5	S	2	0	0	Ru	2	0	0	H
C	4	5	36	F	1	0	0	Cl	1	0	2	Pd	2	0	0	
N	3	0	5	P	3	0	0	Br	1	0	0	I	3	0	0	

Error Margin (ppm): 5
HC Ratio: unlimited
Max Isotopes: 3
MSn Iso RI (%): 10.00

DBE Range: 5.0 - 30.0
Apply N Rule: yes
Isotope RI (%): 1.00
MSn Logic Mode: AND

Electron Ions: both
Use MSn Info: yes
Isotope Res: 9000
Max Results: 50

Event#: 1 MS(E+) Ret. Time : 6.653 -> 6.653 Scan# : 999 -> 999

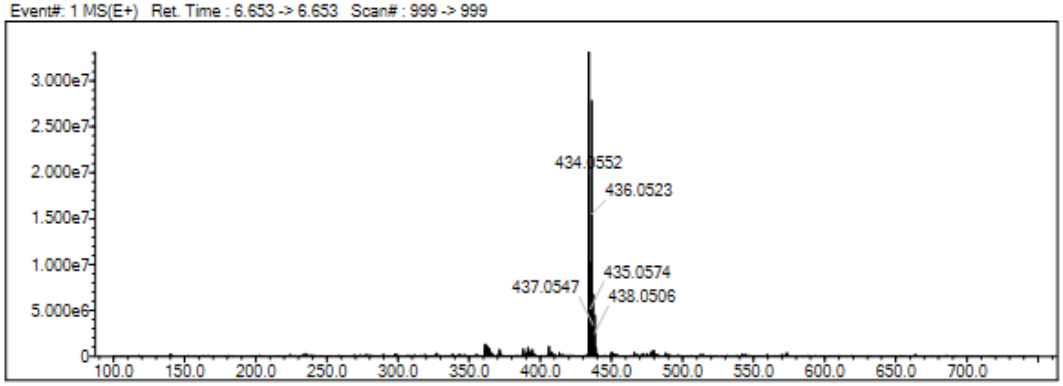

Measured region for 434.0552 m/z

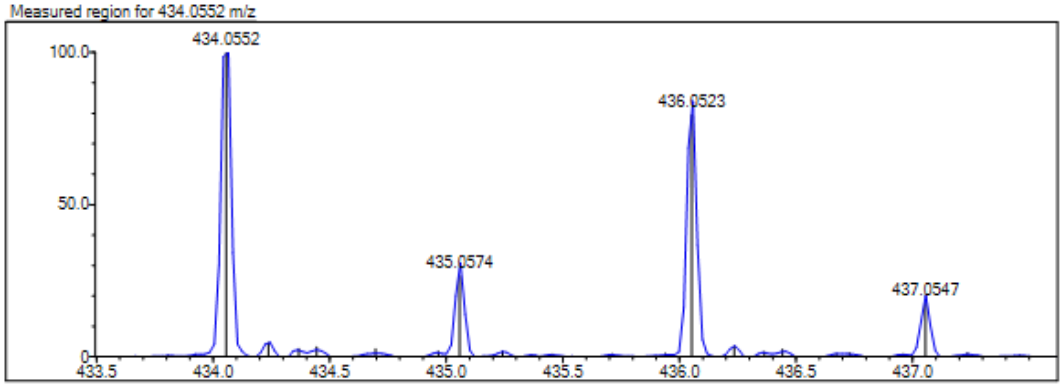

C21 H17 N O5 Cl2 [M+H]+ : Predicted region for 434.0557 m/z

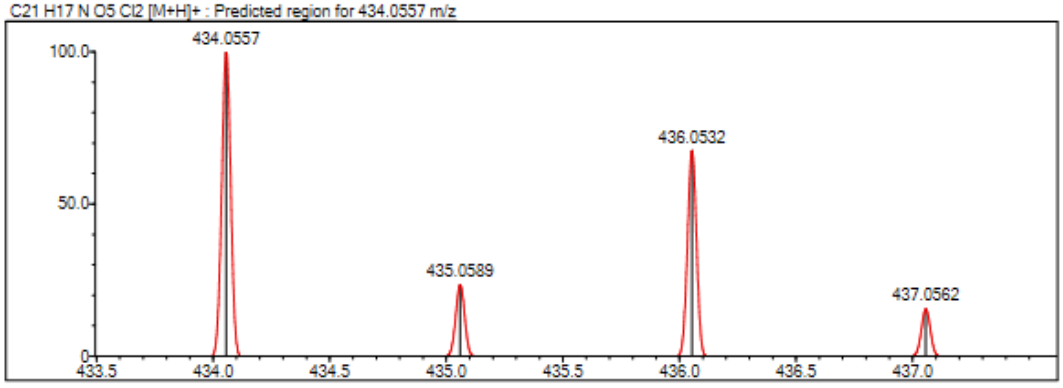

Rank	Score	Formula (M)	Ion	Meas. m/z	Pred. m/z	Df. (mDa)	Df. (ppm)	Iso	DBE
1	68.71	C21 H17 N O5 Cl2	[M+H]+	434.0552	434.0557	-0.5	-1.15	68.97	13.0

Figure 5.75. *Mass spectrum of the compound* ***5b***

5.2.2.18. 3-(5-(3,4-Dichlorophenyl)-3-(ethoxycarbonyl)-2-methyl-1H-pyrrol-1-yl)benzoic acid

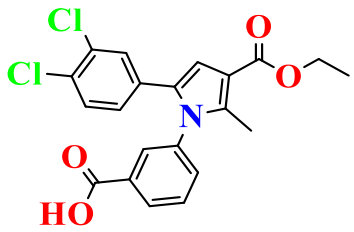

Figure 5.76. *Molecular structure of compound* ***5c***

Synthesized according to method **D**, experimental melting point 233-235ºC, 65% yield percent.

^{1}H-NMR (400 MHz, DMSO-*d*$_6$; δ, ppm):): 1.28 (3H, t, *J*= 7.08 Hz, -CH_2-**$\underline{CH_3}$**), 2.05 (3H, s, pyrrole-**C$\underline{H_3}$**),), 4.23 (2H, q, J_1=7.07 Hz, J_2= 14.14 Hz, **-$\underline{CH_2}$**-CH_3), 6.87 (1H, s, **$\underline{CH}$**-pyrrole), 7.29 (1H, d, *J*= 2.08 Hz, Ar-**$\underline{H}$**), 7.42 (1H, dd, J_1= 8.45 Hz, J_2= 8.61 Hz, Ar-**$\underline{H}$**), 7.60 (1H, d, *J*= 7.77 Hz, Ar-**$\underline{H}$**), 7.45 (1H, d, *J*= 8.44 Hz, Ar-**$\underline{H}$**), 7.59 (1H, d, *J*= 7.77 Hz, Ar-**$\underline{H}$**), 7.67 (1H, d, *J*= 7.73 Hz, Ar-**$\underline{H}$**), 8.04 (1H, d, *J*= 7.45 Hz, Ar-**$\underline{H}$**), 13.09 (1H, br-s, Ar-COO**$\underline{H}$**).

HRMS (-m/z): $[M+H]^+$: For $C_{21}H_{17}NO_4Cl_2$ calculated molecular weight: 418.0587, found: 418.0607.

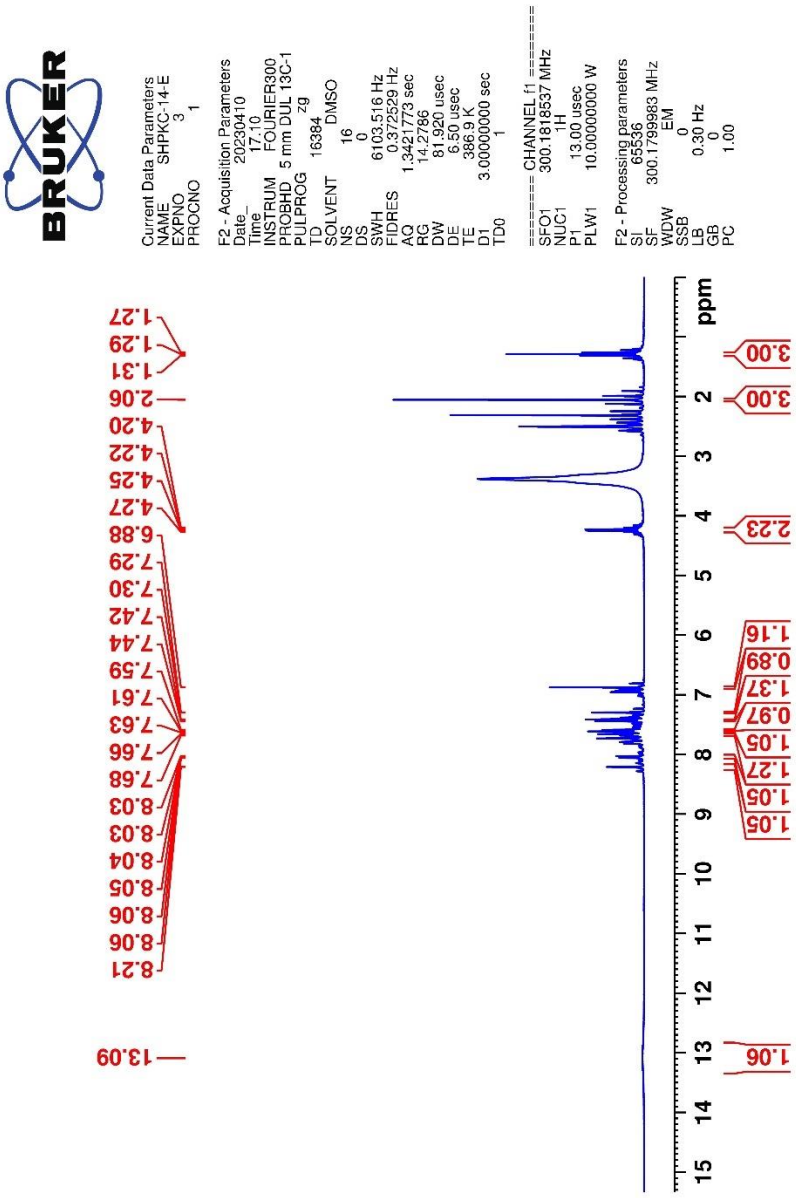

Figure 5.77. *[1]H-NMR spectrum of the compound* ***5c***

Formula Predictor Report - 14-C_60.lcd

Page 1 of 1

Data File: C:\LabSolutions\Data\Analiz\Asaf\14-C_60.lcd

Elmt	Val.	Min	Max	Elmt	Val.	Min	Max	Elmt	Val.	Min	Max	Elmt	Val.	Min	Max	Use Adduct
H	1	6	46	O	2	0	5	S	2	0	0	Ru	2	0	0	H
C	4	5	36	F	1	0	0	Cl	1	0	2	Pd	2	0	0	
N	3	0	5	P	3	0	0	Br	1	0	0	I	3	0	0	

Error Margin (ppm): 5
HC Ratio: unlimited
Max Isotopes: 3
MSn Iso RI (%): 10.00

DBE Range: 5.0 - 30.0
Apply N Rule: yes
Isotope RI (%): 1.00
MSn Logic Mode: AND

Electron Ions: both
Use MSn Info: yes
Isotope Res: 9000
Max Results: 50

Event#: 1 MS(E+) Ret. Time : 0.080 -> 0.080 Scan# : 13 -> 13

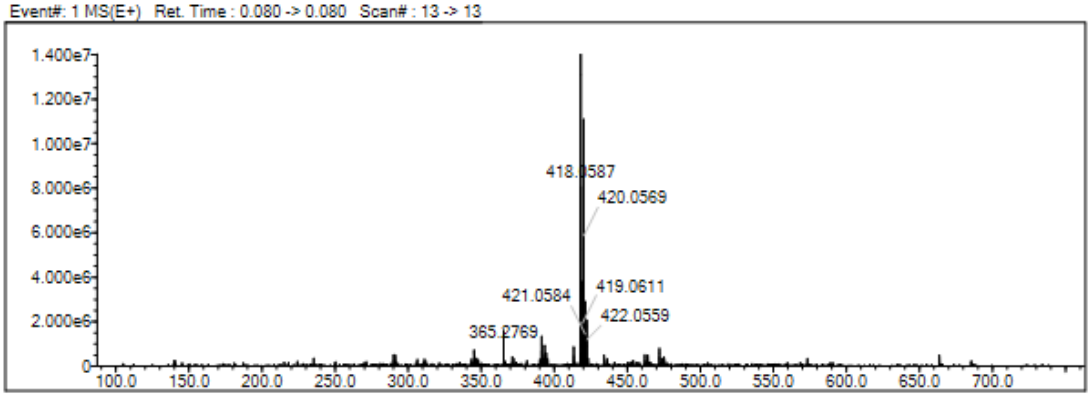

Measured region for 418.0587 m/z

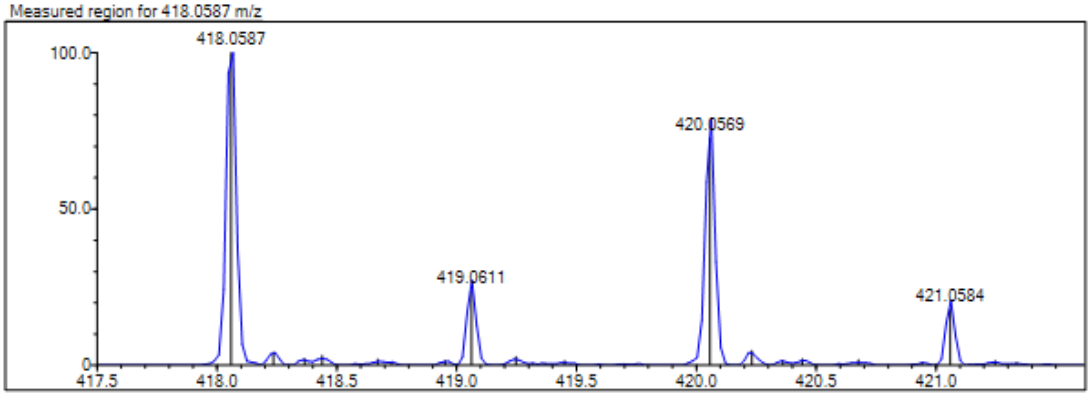

C21 H17 N O4 Cl2 [M+H]+ : Predicted region for 418.0607 m/z

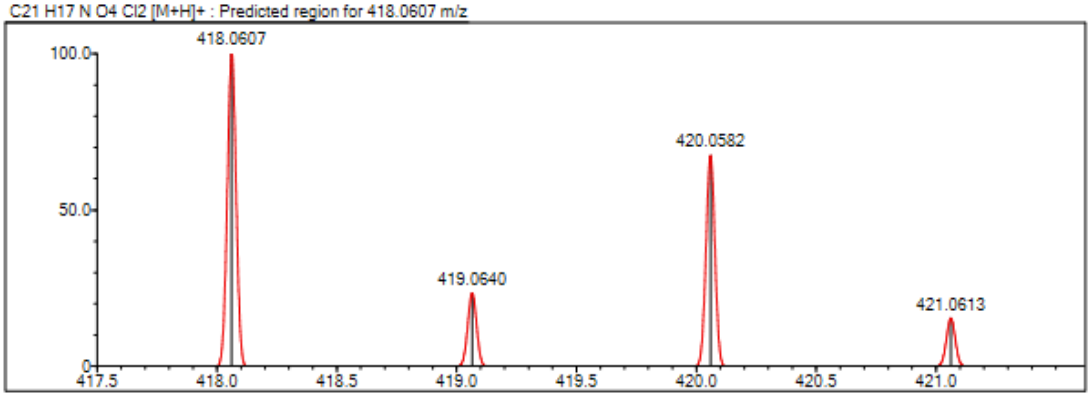

Rank	Score	Formula (M)	Ion	Meas. m/z	Pred. m/z	Df. (mDa)	Df. (ppm)	Iso	DBE
1	67.14	C21 H17 N O4 Cl2	[M+H]+	418.0587	418.0607	-2.0	-4.78	74.14	13.0

Figure 5.78. *Mass spectrum of the compound* ***5c***

5.2.2.19. 4-Chloro-3-(5-(3,4-dichlorophenyl)-3-(ethoxycarbonyl)-2-methyl-1H-pyrrol-1-yl)benzoic acid

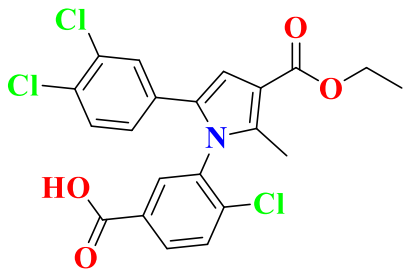

Figure 5.79. *Molecular structure of compound* ***5d***

Synthesized according to method **D**, experimental melting point 230-232ºC, 50% yield percent.

^{1}H-NMR (400 MHz, DMSO-*d*$_6$; δ, ppm):): 1.29 (3H, t, *J*= 7.07 Hz, -CH_2-**CH_3**), 2.25 (3H, s, pyrrole-**CH_3**),), 4.24 (2H, q, J_1=7.08 Hz, J_2= 14.13 Hz, -**CH_2**-CH_3), 6.98 (1H, s, **CH**-pyrrole), 6.93 (1H, dd, J_1= 2.64 Hz, J_2= 8.31 Hz Ar-**H** 7.32 (1H, d, *J*= 1.69 Hz, Ar-**H**), 7.54 (1H, d, *J*= 8.44 Hz, Ar-**H**), 7.60 (1H, d, *J*= 8.36 Hz, Ar-**H**), 7.80 (1H, d, *J*= 8.36 Hz, Ar-**H**), 9.67 (1H, br-s, O**H**).

^{13}C-NMR (100 MHz, DMSO-*d*$_6$; δ, ppm) 12.08 (-pyrrole-**C**H_3), 14.83 (-CH_2-**C**H_3), 59.83 (-**C**H_2-CH_3), 111.38, 113.47, 126.99, 127.58, 129.28, 130.11, 130.20, 130.49, 131.03, 131.39, 131.55, 131.94, 132.34, 135.25, 135.66, 136.96, 138.88, 164.56 (**C**O-O-Et), 169.43 (**C**OOH).

HRMS (-m/z): [M+H]$^+$: For $C_{21}H_{16}NO_4Cl_3$ calculated molecular weight: 452.0214, found: 452.0218.

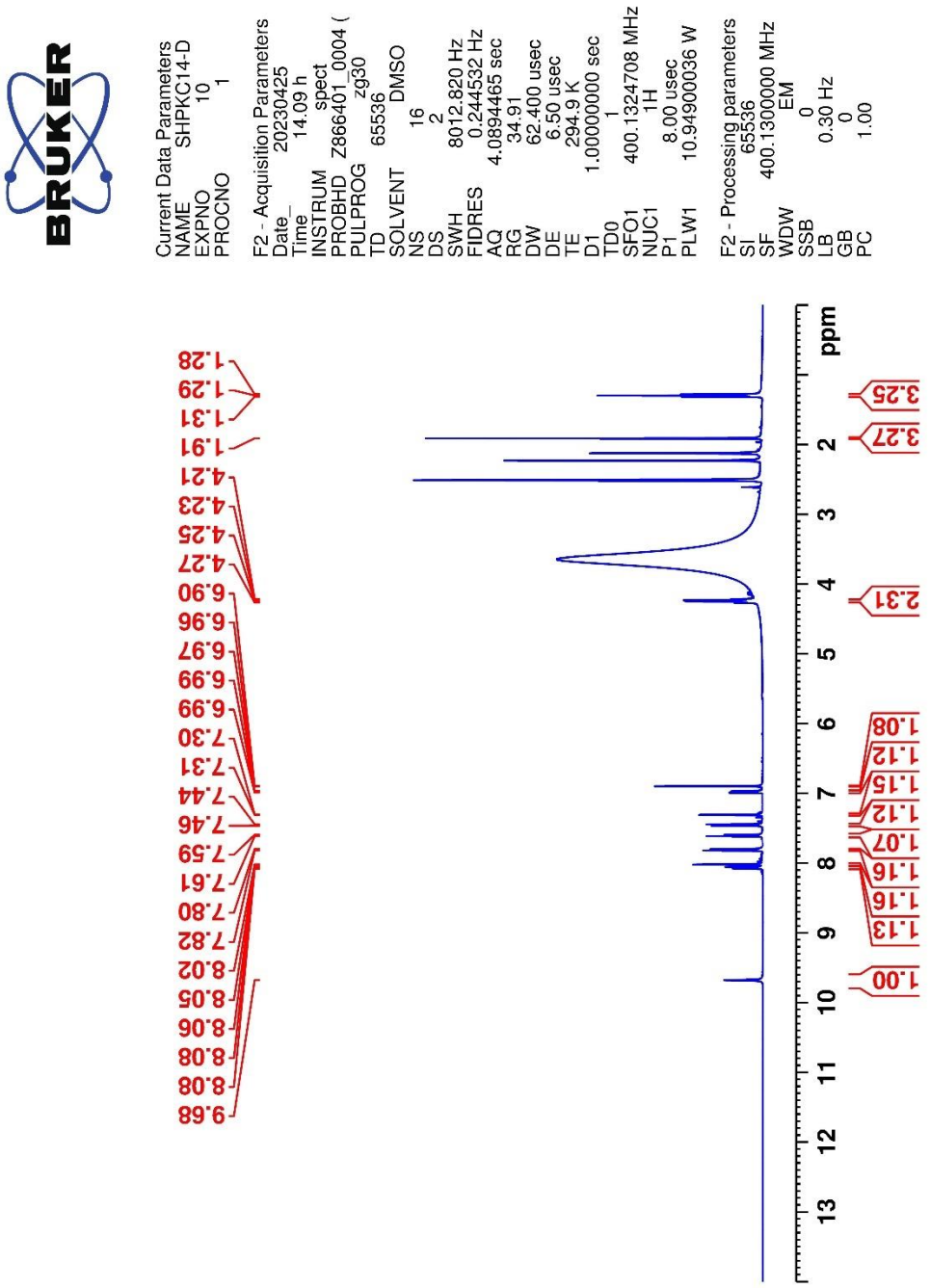

Figure 5.80. *^{1}H-NMR spectrum of the compound **5d***

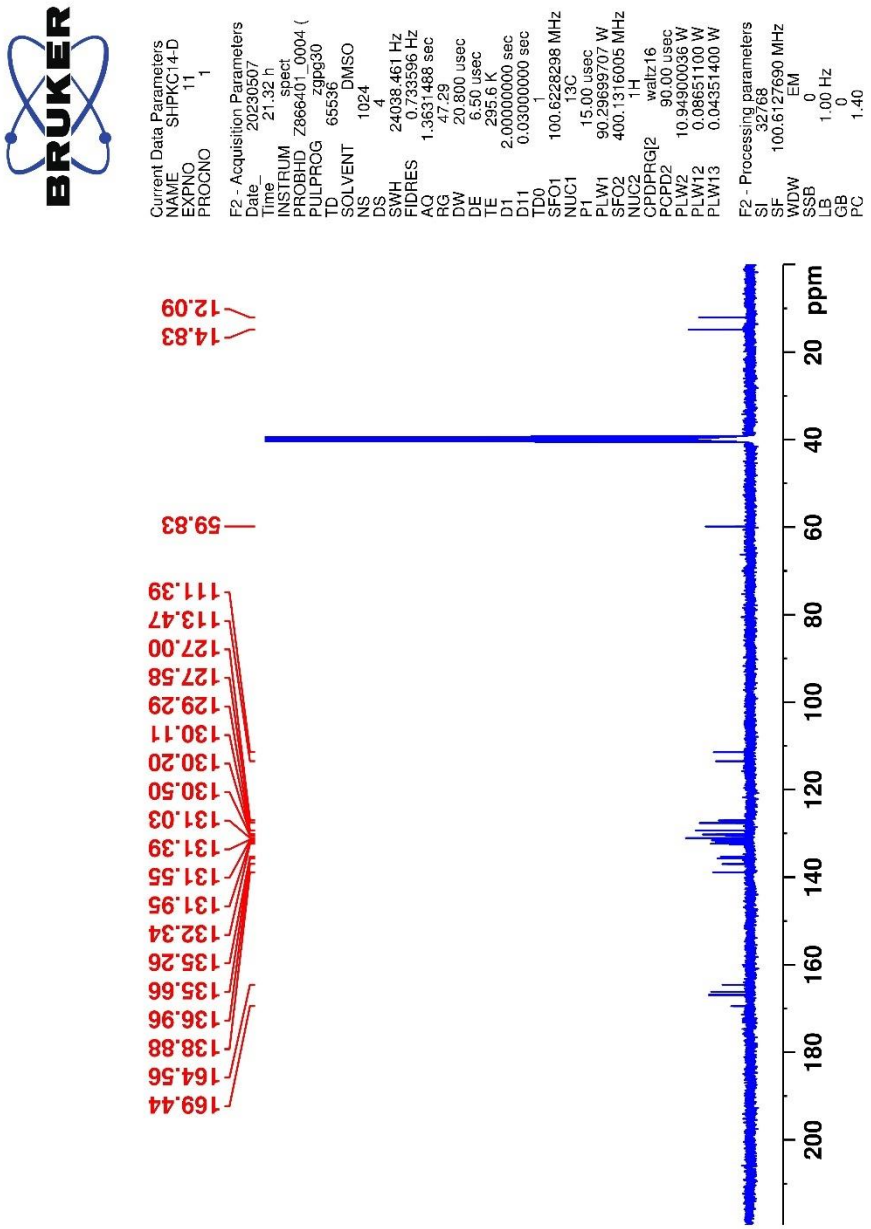

Figure 5.81. *^{13}C-NMR spectrum of the compound **5d***

Formula Predictor Report - SHPKC-10C_72.lcd

Page 1 of 1

Data File: C:\LabSolutions\Data\Analiz\Asaf\SHPKC-10C_72.lcd

Elmt	Val.	Min	Max	Elmt	Val.	Min	Max	Elmt	Val.	Min	Max	Elmt	Val.	Min	Max	Use Adduct
H	1	6	46	O	2	0	7	S	2	0	0	Ru	2	0	0	H
C	4	5	36	F	1	0	0	Cl	1	0	3	Pd	2	0	0	Na
N	3	0	6	P	3	0	0	Br	1	0	0	I	3	0	0	

Error Margin (ppm): 5
HC Ratio: unlimited
Max Isotopes: 3
MSn Iso RI (%): 10.00

DBE Range: 5.0 - 30.0
Apply N Rule: yes
Isotope RI (%): 1.00
MSn Logic Mode: AND

Electron Ions: both
Use MSn Info: yes
Isotope Res: 9000
Max Results: 50

Event#: 1 MS(E+) Ret. Time : 2.920 Scan# : 439

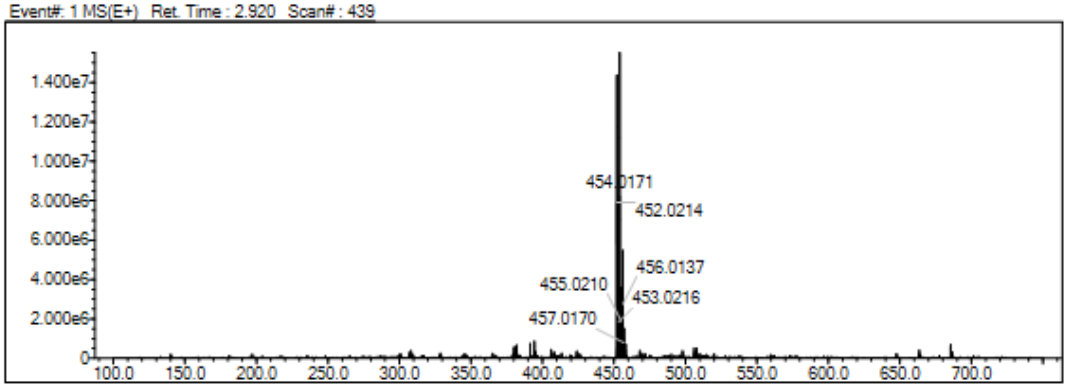

Measured region for 452.0214 m/z

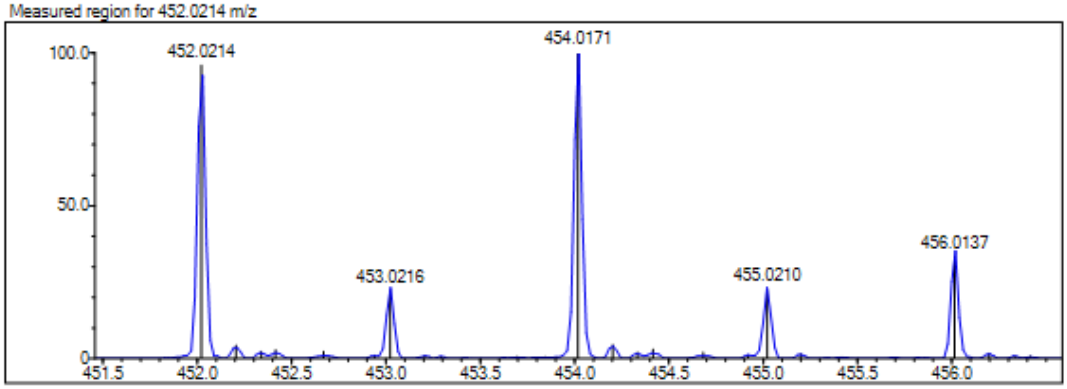

C21 H16 N O4 Cl3 [M+H]+ : Predicted region for 452.0218 m/z

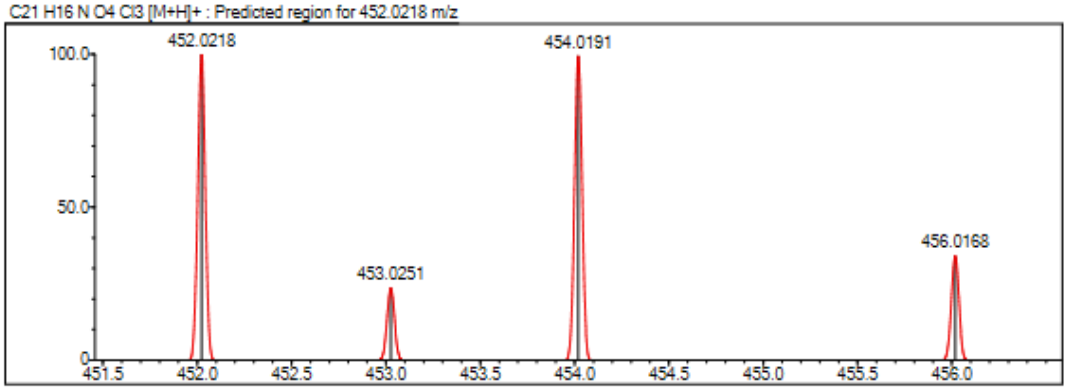

Rank	Score	Formula (M)	Ion	Meas. m/z	Pred. m/z	Df. (mDa)	Df. (ppm)	Iso	DBE
1	76.70	C21 H16 N O4 Cl3	[M+H]+	452.0214	452.0218	-0.4	-0.88	76.70	13.0

Figure 5.82. *Mass spectrum of the compound* ***5d***

5.2.2.20. 3-(3-(Ethoxycarbonyl)-2-methyl-5-(4-nitrophenyl)-1H-pyrrol-1-yl)-4-hydroxybenzoic acid

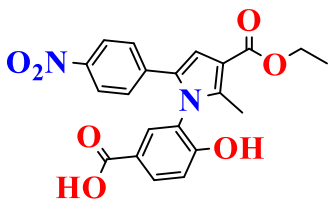

Figure 5.83. *Molecular structure of compound* ***5e***

Synthesized according to method **D**, experimental melting point 280-286ºC, 68% yield percent.

^{1}H-NMR (400 MHz, DMSO-d_6; δ, ppm):): 1.29 (3H, t, *J*= 7.08 Hz, -CH_2-**CH_3**), 2.25 (3H, s, pyrrole-**CH_3**),), 4.24 (2H, q, J_1=7.08 Hz, J_2= 14.13 Hz, -**CH_2**-CH_3), 6.98 (1H, s, **CH**-pyrrole), 6.93 (1H, m, *J*= 2.64 Hz, Ar-**H**), 7.12 (1H, d, *J*= 8.59 Hz, Ar-**H**), 7.31 (1H, d, *J*= 2.06 Hz, Ar-**H**), 7.33 (1H, d, *J*= 2.02 Hz, Ar-**H**), 7.58 (1H, d, *J*= 2.15 Hz, Ar-**H**), 7.92 (1H, dd, J_1= 3.58 Hz, J_2= 8.75 Hz, Ar-**H**), 8.03 (1H, d, *J*= 2.07 Hz, Ar-**H**), 8.06 (1H, d, *J*= 2.01 Hz, Ar-**H**), 11.19 (1H, br-s, O**H**).

HRMS (-m/z): $[M+H]^+$: For $C_{21}H_{18}N_2O_7$ calculated molecular weight: 411.1194, found: 411.1187.

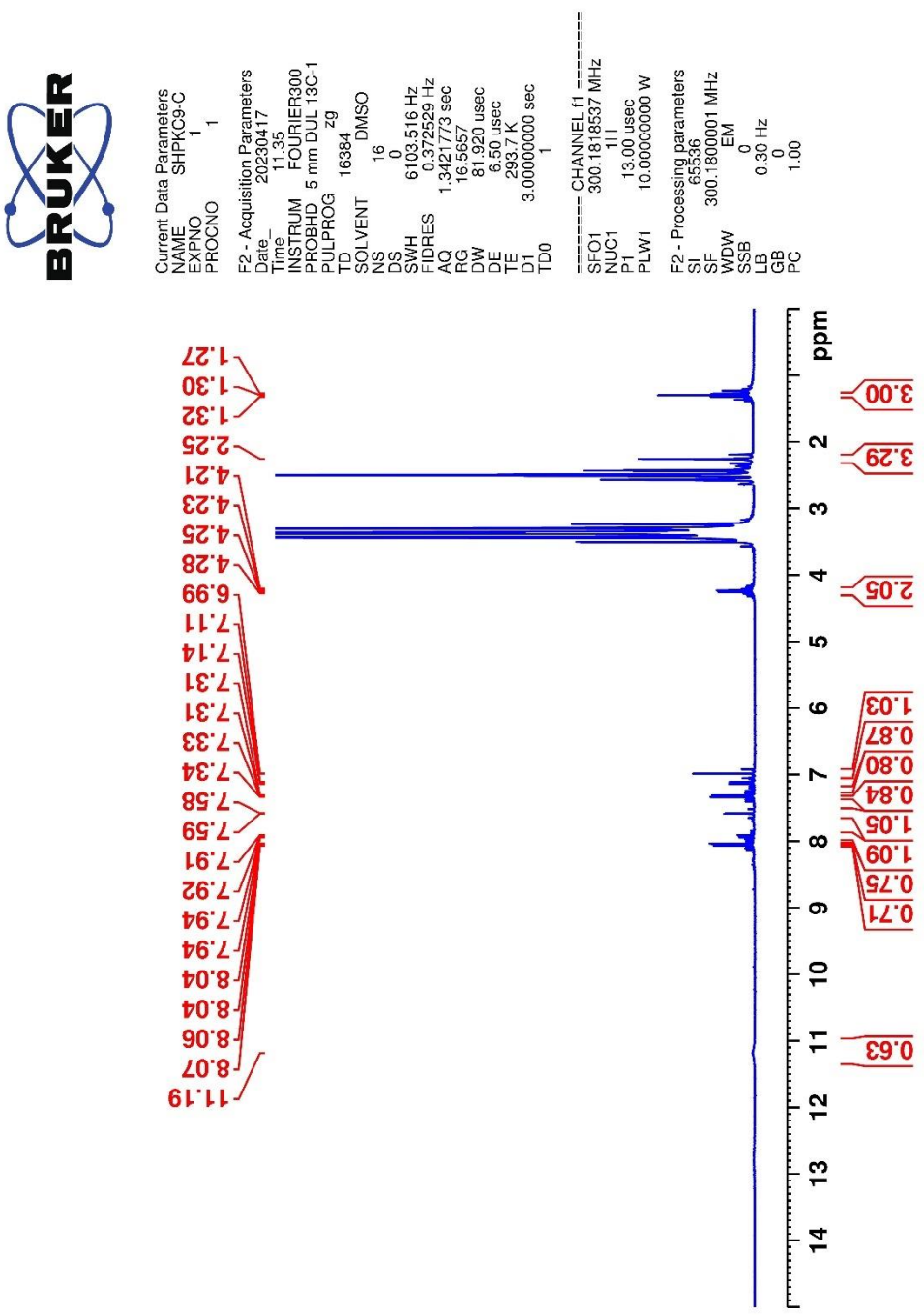

Figure 5.84. *^{1}H-NMR spectrum of the compound **5e***

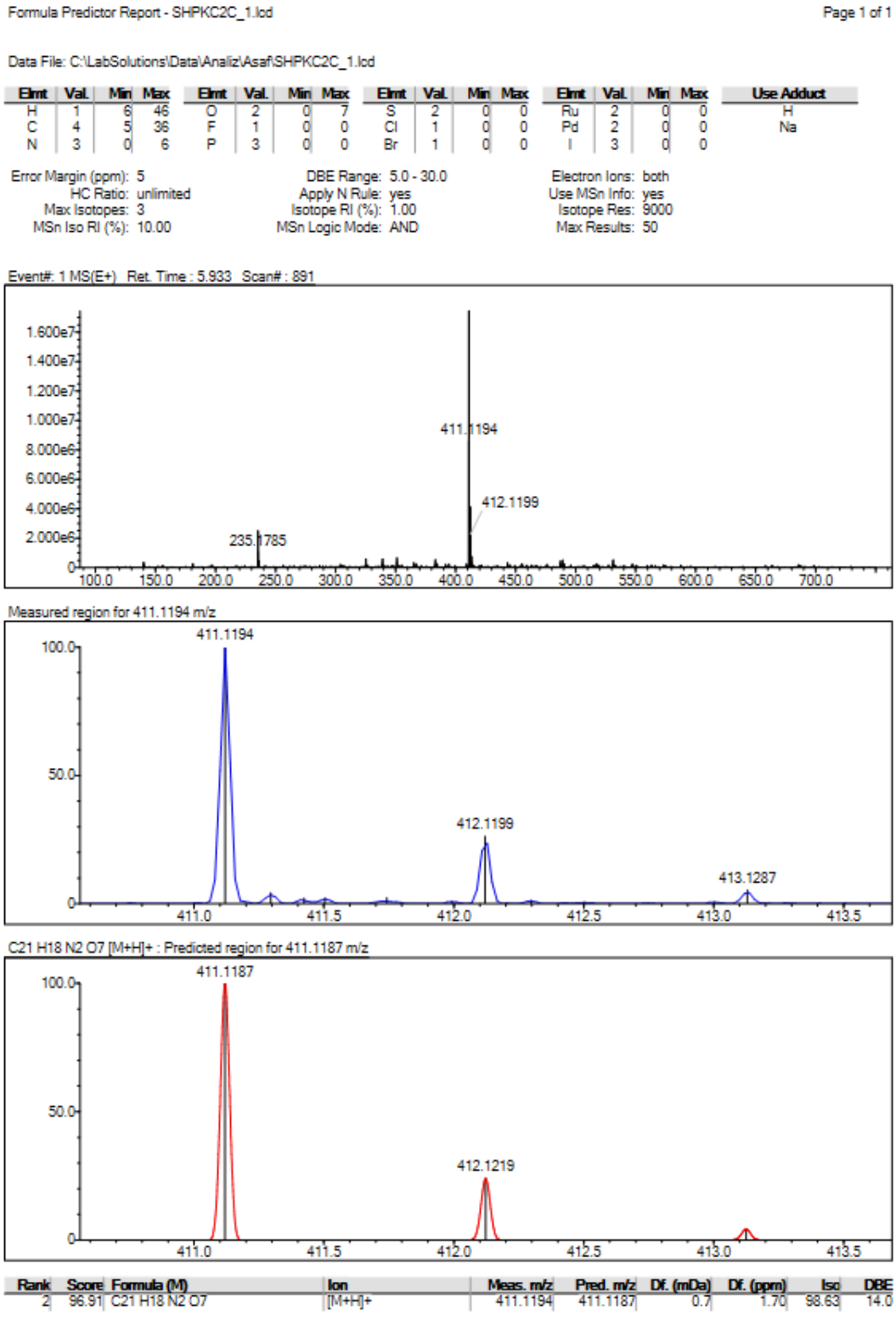

Figure 5.85. *Mass spectrum of the compound* ***5e***

5.2.2.21. 3-(3-(Ethoxycarbonyl)-2-methyl-5-(4-nitrophenyl)-1H-pyrrol-1-yl)-4-methoxybenzoic acid

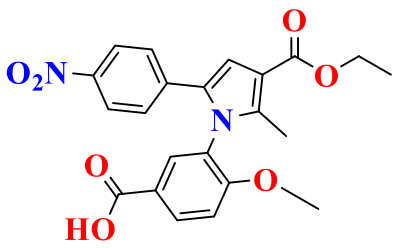

Figure 5.86. *Molecular structure of compound* ***5f***

Synthesized according to method **D**, experimental melting point 255-256ºC, 69% yield percent.

^{1}H-NMR (400 MHz, DMSO-*d*$_6$; δ, ppm):): 1.28 (3H, t, *J*= 7.08 Hz, -CH_2-**CH_3**), 2.09 (3H, s, pyrrole-**CH_3**), 3.78 (3H, s, O-**CH_3**), 4.23 (2H, q, J_1=7.06 Hz, J_2= 14.14 Hz, -**CH_2**-CH_3), 6.93 (1H, m, *J*= 2.64 Hz, Ar-**H**), 6.96 (1H, s, **CH**-pyrrole), 7.10 (1H, d, *J*= 8.66 Hz, Ar-**H**), 7.26 (1H, d, *J*= 8.93 Hz, Ar-**H**), 7.35 (1H, d, *J*= 8.84 Hz, Ar-**H**), 7.65 (1H, d, *J*= 2.17 Hz, Ar-**H**), 8.02 (1H, d, *J*= 8.95 Hz, Ar-**H**), 8.08 (1H, dd, J_1= 2.72, J_2= 8.75 Hz, Ar-**H**), 8.55 (1H, d, *J*= 1.83, Ar-**H**), 12.89 (1H, br-s, Ar-COO**H**).

^{13}C-NMR (100 MHz, DMSO-*d*$_6$; δ, ppm) 12.11 (-pyrrole-**C**H_3), 14.87 (-CH_2-**C**H_3), 56.43 (-O**C**H_3), 56.89 (-**C**H_2-CH_3), 111.07, 112.63, 113.67, 123.02, 123.35, 124.15, 126.61, 127.64, 127.77, 131.08, 138.75, 140.08, 145.92, 153.41, 160.12, 164.53 (**C**O-O-Et), 167.53 (**C**OOH).

HRMS (-m/z): $[M+H]^+$: For $C_{22}H_{20}N_2O_7$ calculated molecular weight: 425.1348, found: 425.1343.

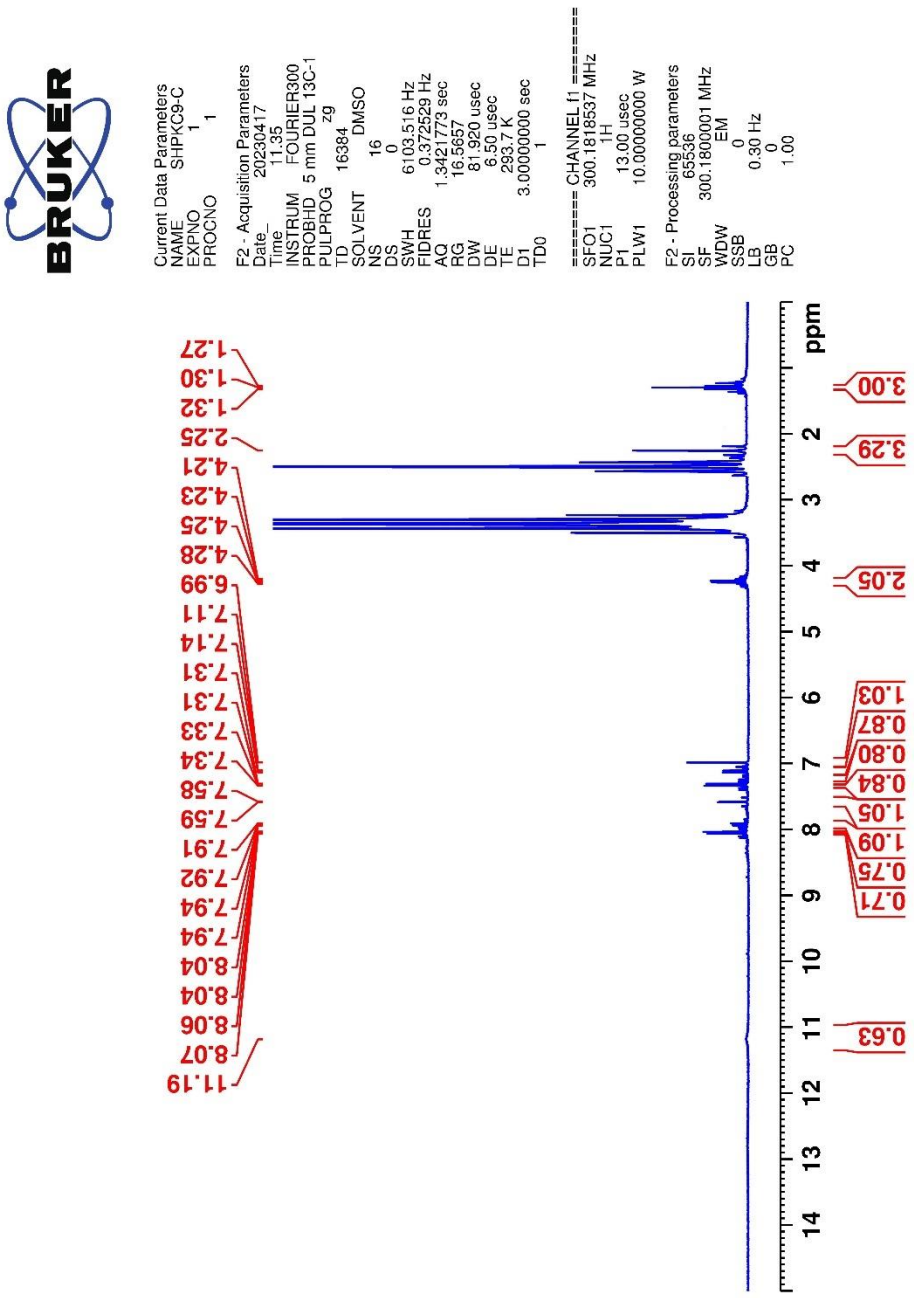

Figure 5.87. *[1]H-NMR spectrum of the compound **5f***

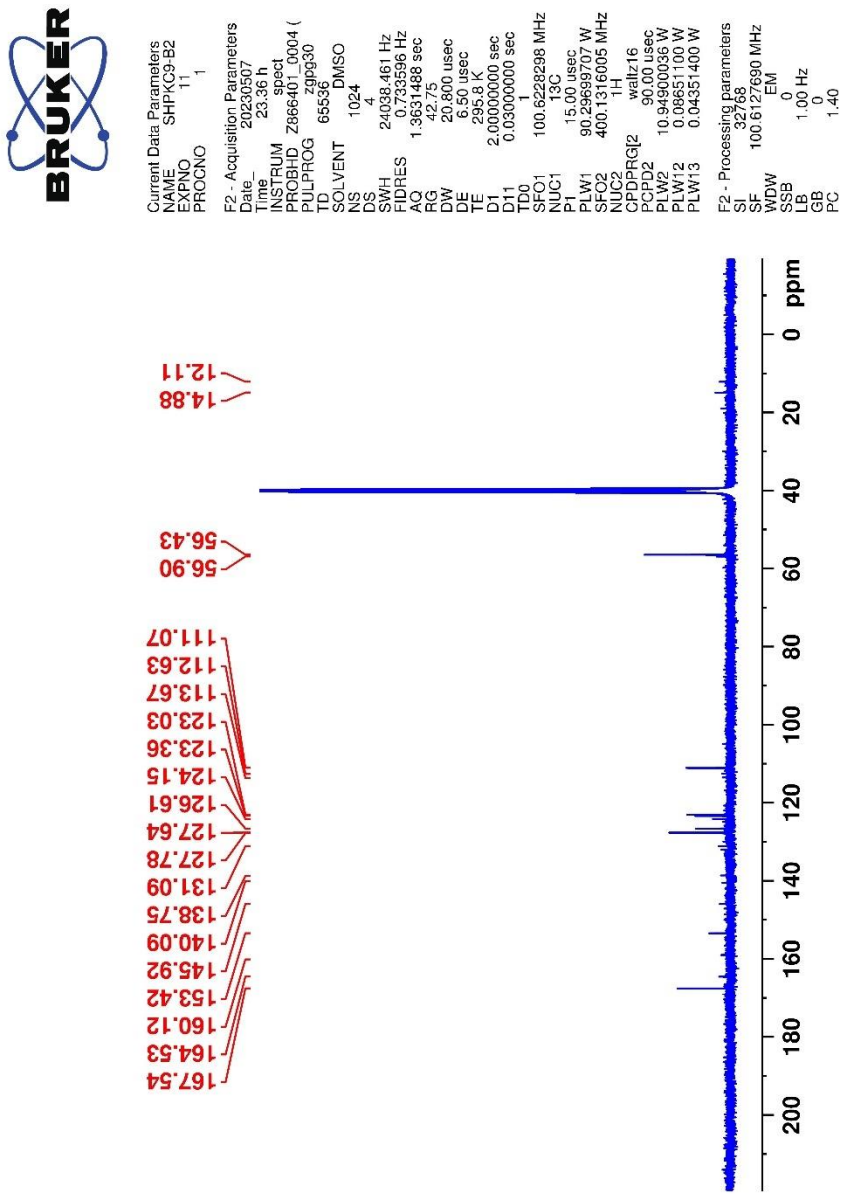

Figure 5.88. *^{13}C-NMR spectrum of the compound **5f***

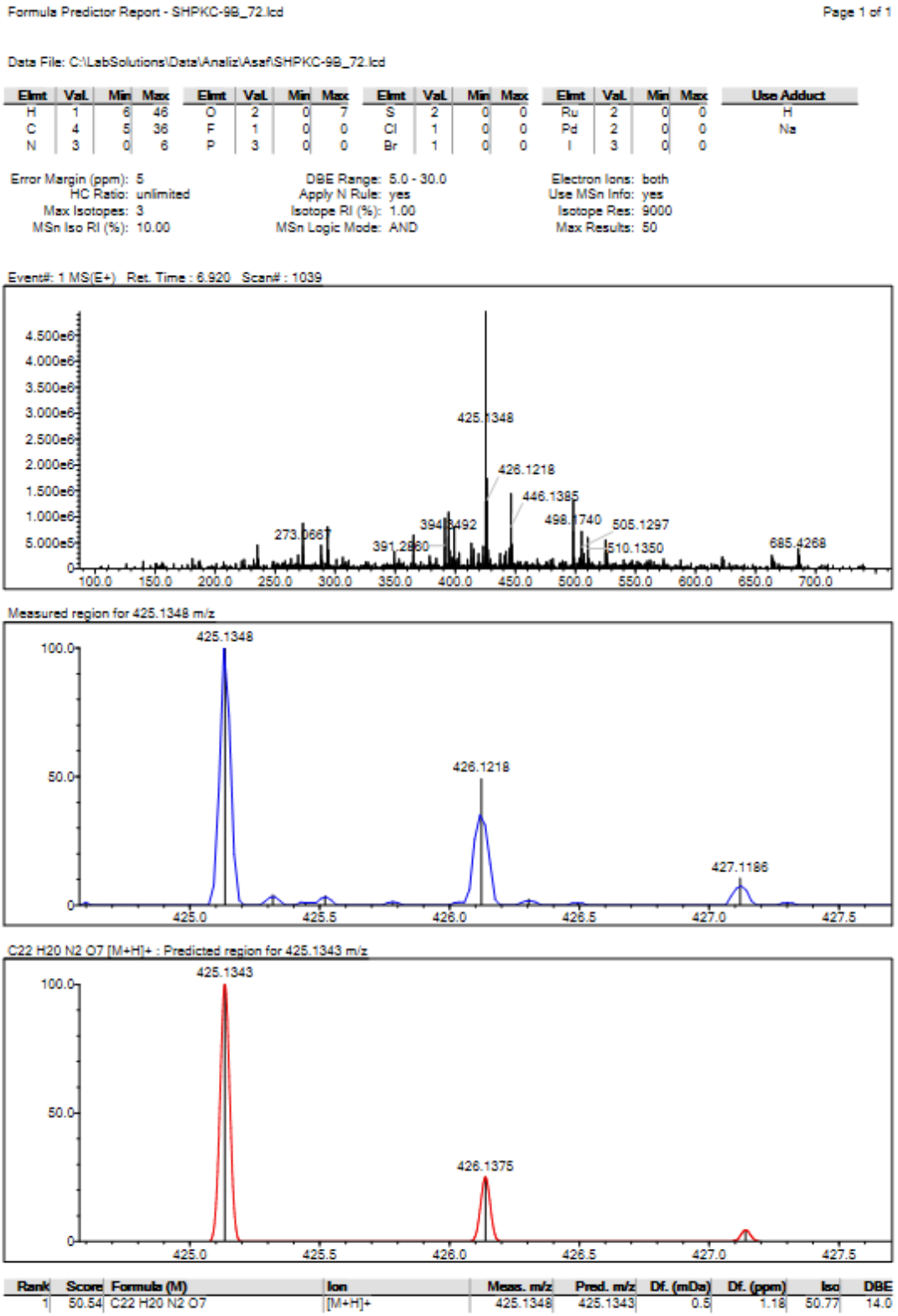

Figure 5.89. *Mass spectrum of the compound* ***5f***

5.2.2.22. 4-Chloro-3-(3-(ethoxycarbonyl)-2-methyl-5-(4-nitrophenyl)-1H-pyrrol-1-yl)benzoic acid

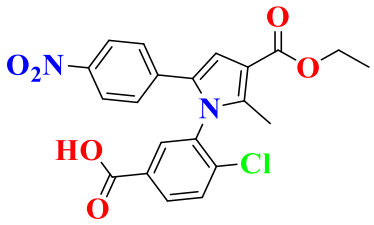

Figure 5.90. *Molecular structure of compound* ***5g***

Synthesized according to method **D**, experimental melting point 240-245ºC, 79% yield percent.

^{1}H-NMR (400 MHz, DMSO-*d*$_6$; δ, ppm):): 1.31 (3H, t, *J*= 7.06 Hz, -CH_2-**$\underline{CH_3}$**), 2.24 (3H, s, pyrrole-**C$\underline{H_3}$**), 4.26 (2H, q, J_1=6.97 Hz, J_2= 15.14 Hz, -**$\underline{CH_2}$**-CH_3), 7.05 (1H, s, **$\underline{CH}$**-pyrrole), 7.30 (1H, d, *J*= 8.50 Hz, Ar-**$\underline{H}$**), 7.68 (1H, d, *J*= 8.18 Hz, Ar-**$\underline{H}$**), 7.86 (1H, Ar-**$\underline{H}$**), 7.65 (1H, d, *J*= 2.17 Hz, Ar-**$\underline{H}$**), 8.03 (2H, t, *J*= 10.59 Hz, Ar-**$\underline{H}$**), 8.26 (2H, m, *J*= 16.61 Hz, Ar-**$\underline{H}$**).

HRMS (-m/z): [M+H]$^+$: For $C_{21}H_{17}N_2O_6Cl$ calculated molecular weight: 429.0828, found: 429.0848.

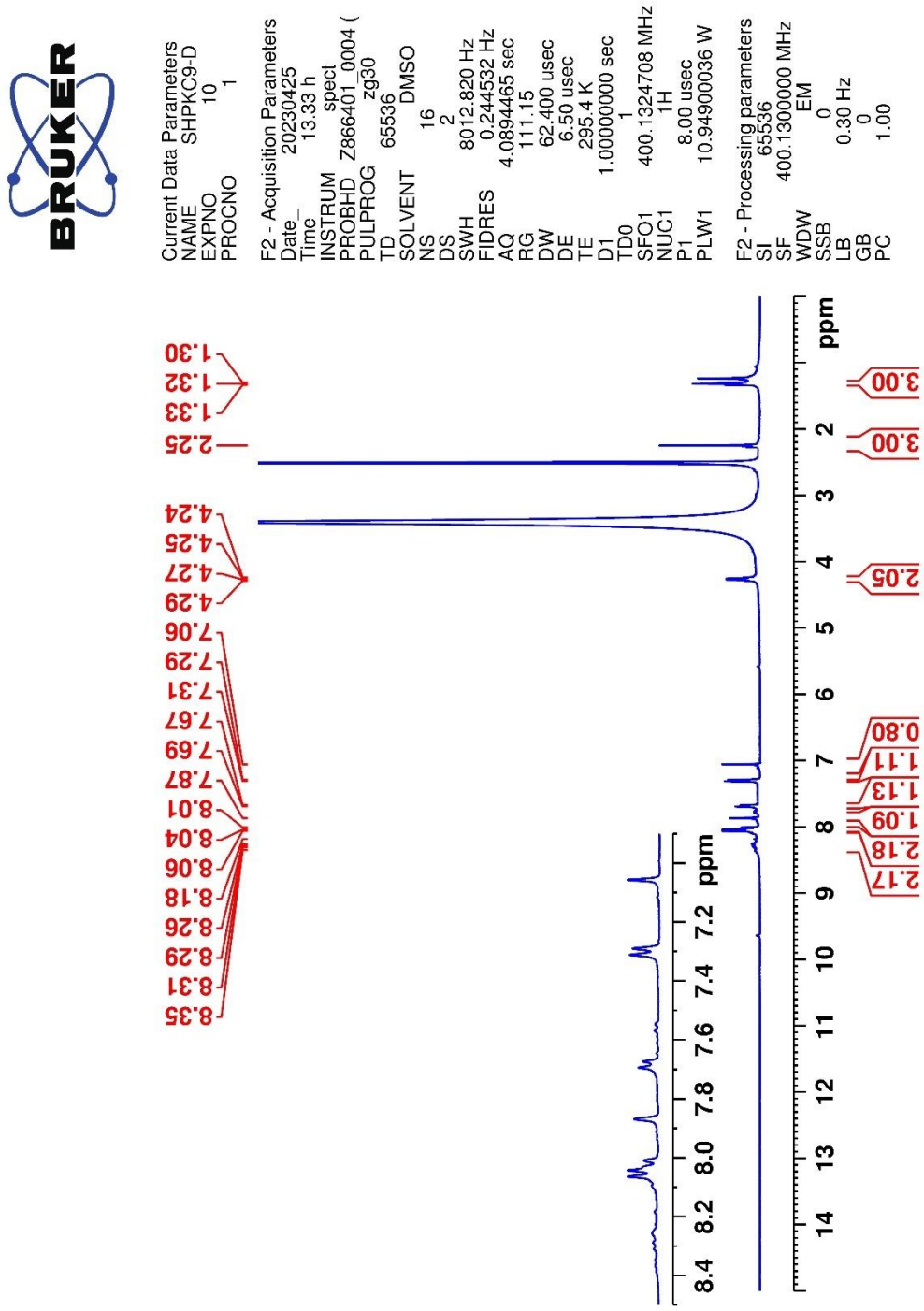

Figure 5.91. *[1]H-NMR spectrum of the compound **5g***

Formula Predictor Report - SHPKC-9D-2_72.lcd

Page 1 of 1

Data File: C:\LabSolutions\Data\Analiz\Asaf\SHPKC-9D-2_72.lcd

Elmt	Val.	Min	Max	Elmt	Val.	Min	Max	Elmt	Val.	Min	Max	Elmt	Val.	Min	Max	Use Adduct
H	1	6	46	O	2	0	7	S	2	0	0	Ru	2	0	0	H
C	4	5	36	F	1	0	0	Cl	1	0	3	Pd	2	0	0	Na
N	3	0	6	P	3	0	0	Br	1	0	0	I	3	0	0	

Error Margin (ppm): 5
HC Ratio: unlimited
Max Isotopes: 3
MSn Iso RI (%): 10.00

DBE Range: 5.0 - 30.0
Apply N Rule: yes
Isotope RI (%): 1.00
MSn Logic Mode: AND

Electron Ions: both
Use MSn Info: yes
Isotope Res: 9000
Max Results: 50

Event#: 1 MS(E+) Ret. Time : 8.400 -> 8.400 Scan# : 1261 -> 1261

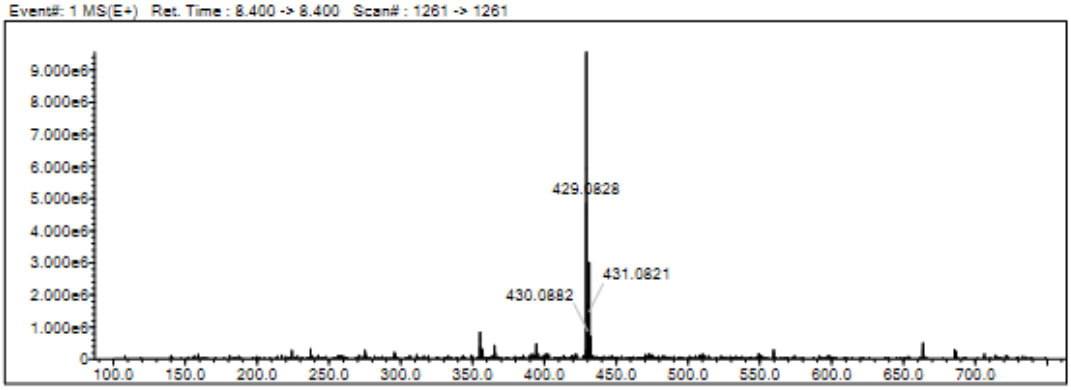

Measured region for 429.0828 m/z

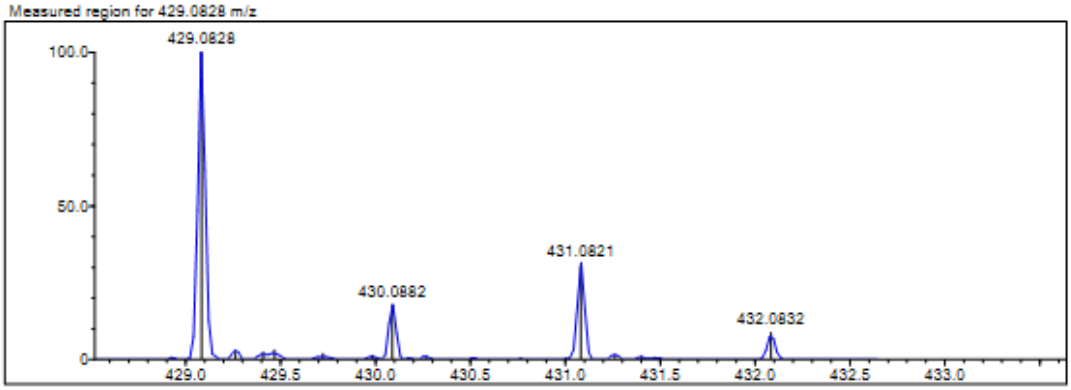

C21 H17 N2 O6 Cl [M+H]+ : Predicted region for 429.0848 m/z

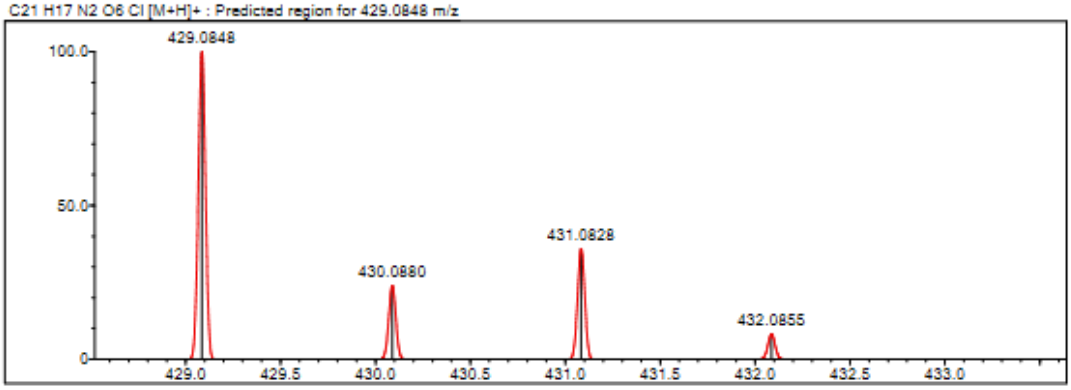

Rank	Score	Formula (M)	Ion	Meas. m/z	Pred. m/z	Df. (mDa)	Df. (ppm)	Iso	DBE
3	70.69	C21 H17 N2 O6 Cl	[M+H]+	429.0828	429.0848	-2.0	-4.66	77.81	14.0

Figure 5.92. *Mass spectrum of the compound* ***5g***

5.3. Evaluation of Synthetic Methods

After determining the skeleton of our targeted compound, which was generated from the FB-QSAR model as described in **subsection 5.1**, we made the decision to utilize 1,2,3,5-tetrasubstituted pyrrole derivatives as our selected compounds.

The synthetic procedure for the compounds utilized in this study was carefully designed using a four-step pathway that employed the Paal-Knorr synthesis technique. This methodology enabled the successful synthesis of pyrrole by utilizing a 1,4-dicarbonyl compound as a precursor for the formation of the pyrrole ring, along with a substituted amine, followed by dehydrative condensation. The process began with ethyl 3-oxobutanoate as the starting material, and anhydrous sodium metal was added as a reducing agent, catalyzing a series of transformations that resulted in the formation of radical intermediates denoted as compound **(1)**. These intermediates displayed notable nucleophilic properties, functioning as carbanions to search for suitable chemical partners. Subsequently, bromoacetophenone derivatives were introduced, where the carbonyl groups acted as electrophiles, leading to the generation of compound **3**, namely Ethyl 2-acetyl-4-oxo-4- (substituted phenyl) butanoate. Compound **3** exhibited enhanced complexity and sophistication compared to its precursor, reflecting the progression of the synthesis process.

The synthesis journey then continued with the introduction of an amino-substituted compound, which underwent cyclization in the presence of acidic conditions, specifically glacial acetic acid, resulting in the formation of a pyrrole ring. This pivotal step added an elegant dimension to the synthesis, bringing the target compound closer to fruition. The synthesis was eventually concluded by quenching the reaction with iced water, causing the desired target compound (**4**) to precipitate out of the solution, while undesirable compounds such as NaBr remained in the water phase. This final step ensured the isolation of the target compounds and marked the successful completion of the synthesis process. To verify the authenticity of the synthesized compounds, ^{1}HNMR, ^{13}CNMR and HRMS spectral methods were rigorously employed to confirm the structures of the obtained derivatives of 2-[3-(Ethoxycarbonyl)-2-methyl-5-(substituted phenyl)-1*H*-pyrrol-1-yl] substituted carboxylic acid Figure 5.89.

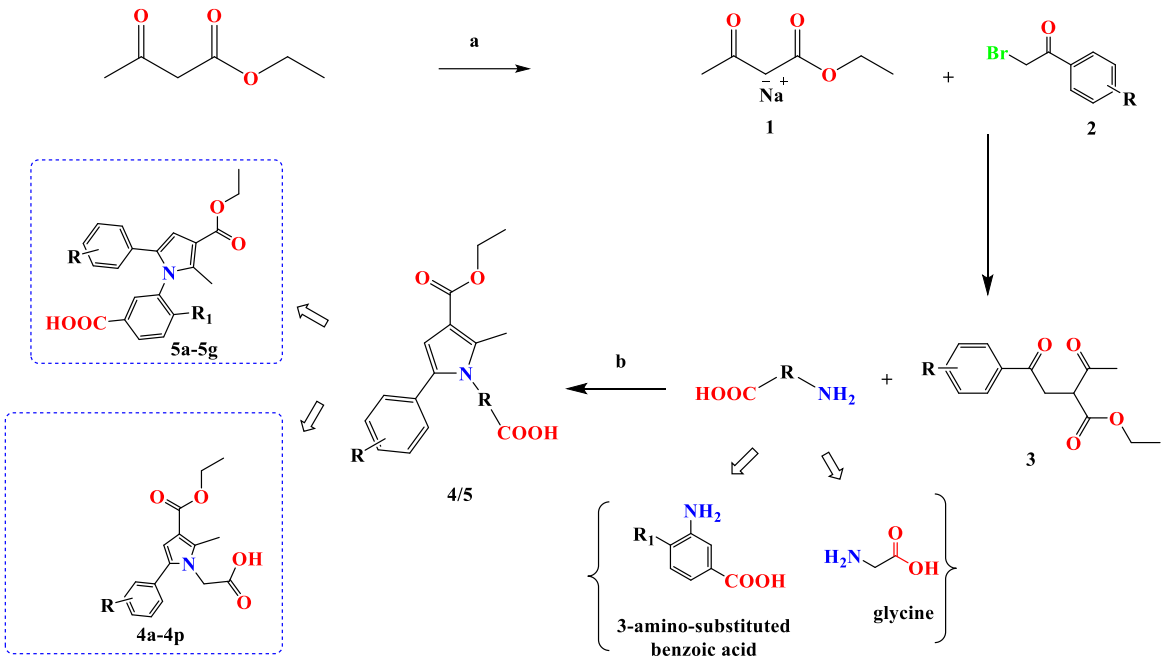

Figure 5.93. *Schematic representation of the synthetic pathways*

Reaction conditions: a) Metalic sodium, anhydrous toluene, r.t; b) glacial acetic acid, reflux

The main objective of the experiment was to synthesize compounds capable of inhibiting both COX-1 and COX-2 enzymes, which play a crucial role in the inflammatory processes of the body. To achieve this, a strategic approach was employed that took into account the structural differences between the active sites of COX-1 and COX-2. The design involved incorporating N-pyrrole, linked with glycine, to increase the chances of binding to COX-1, which has a smaller active site. In contrast, larger groups such as amino benzoic substitutes were employed to enhance the probability of binding to the larger active site of COX-2. However, throughout the design process, it was ensured that the synthesized compounds retained the essential chemical properties required for the desired pharmacological activity. Specifically, the presence of an aryl group at position 5 and a methyl group at position 2 was maintained in all the designed compounds. This approach aimed to produce novel compounds with potent dual inhibition activity against both COX-1 and COX-2 enzymes.

5.4. Evaluation of Chemical Spectral Data

5.4.1. Mass spectrometry

Mass spectrometry was employed to evaluate the final compounds synthesized in the experiment. High resolution mass spectrometry, utilizing the electrospray ionization (ESI) method, was utilized to obtain the mass spectra of all synthesized compounds. The obtained mass spectra were analyzed to determine the molecular weights of the compounds, with the peak of the M+1 ion being detected in the mass spectra of all synthesized compounds. This peak corresponds to the molecular ion of the compounds with an additional hydrogen atom, indicating the presence of protonation in the molecules. The detection of this peak confirms the authenticity of the synthesized compounds and ensures that the expected molecular weight was achieved during the synthesis process. The utilization of high resolution mass spectrometry and the detection of the M+1 ion peak adds to the credibility and reliability of the synthesized compounds, as it confirms the molecular formula of the compounds and provides essential data for the structural elucidation of the compounds [100].

5.4.2. ^{1}H-NMR analysis results

The ^{1}H-NMR data was analyzed using the Bruker UltraShield 400 MHz instrument after dissolving all samples in DMSO-d_6. In all spectra, a quintet at 2.5 ppm was observed, corresponding to the DMSO solvent signal. Additionally, a strong singlet at around 3.5 ppm indicated the presence of water protons in all compounds.

The basic building block was pyrrole carboxylic acid, with an ethoxy carbonyl group attached at the third position. Different derivatives were obtained by modifying the groups attached to the substituted phenyl ring at position 5 of the pyrrole ring.

The ^{1}H-NMR spectra revealed specific chemical shifts for various protons. The methyl group attached at position 2 of the pyrrole ring exhibited a singlet peak in the range of 2.35-2.58 ppm. The C_4-H protons of the pyrrole ring appeared as a singlet peak within the range of 6.25-6.67 ppm.

The adjacent methyl group to the ester group, which was the first methyl group for the ethoxy carbonyl attached at position 3 on the pyrrole ring, appeared as a quartet at 4.15-4.26 ppm. In contrast, the terminal methyl group was observed as a triplet at 1.24-1.38 ppm. This difference in chemical shifts can be attributed to the influence of the

carbonyl group's electronegativity, resulting in an increased chemical shift for the adjacent methyl group compared to the terminal methyl group.

In the first group (**4a-4p**), where N-pyrrole was attached to an aliphatic carboxylic acid group (in this study, acetic acid), the signal of the methyl proton in acetic acid appeared as a singlet peak in the range of 4.05-4.73 ppm. This chemical shift value corresponded to the same observed in the adjacent methyl of the ester group. The similarity in chemical shift can be attributed to the presence of the carbonyl group in both the ester and carboxylic acid moieties, causing the signals to appear in the downfield region.

In the second group (**5a-5g**), where N-pyrrole was attached to aromatic carboxylic acid groups (in this study, 4-Substituted-3-amino benzoic acids), specific substituents (-OCH_3 and -OH) were associated with singlet peaks at 3.78 ppm and broad singlet peaks at 11.21 ppm, respectively. The COOH group exhibited a singlet broad peak within the range of 11.19-13.09 ppm. The ^{1}H-NMR values of these common scaffolds are summarized in Figure 5.94.

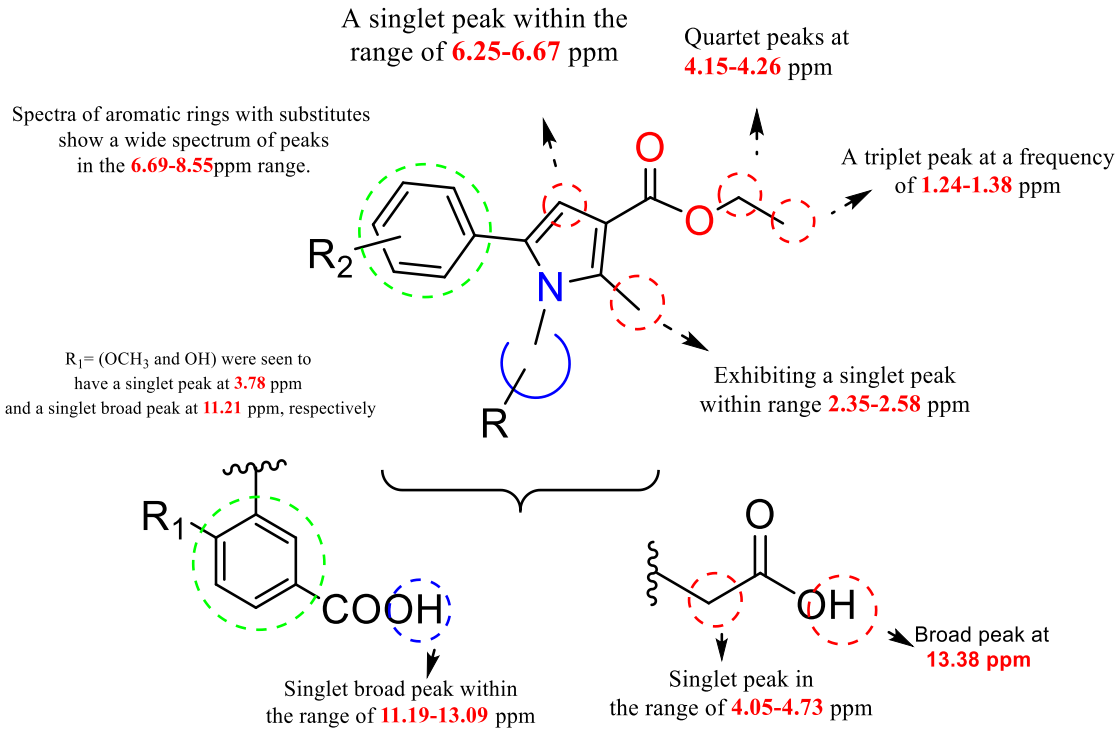

Figure 5.94. *Characterizing ^{1}H-NMR chemical shift values for common scaffolds in targeted compounds*

5.4.3. ^{13}C-NMR analysis results

^{13}C-NMR analysis was conducted on a Bruker UltraShield instrument using DMSO-d_6 as the solvent at a frequency of 100 MHz. The septet peak of the solvent appeared at approximately 39.95 ppm. Each sample was subjected to a one-hour analysis. Among all the compounds, the carbonyl carbon exhibited the most significant deshielding effect. The carbonyl carbon of the ester group appeared in the range of (164.59-164.96) ppm, while in the acetic acid groups, it was deshielded to (169.89-170.52) ppm. All pyrrole carbons were observed within the range of 107.57-138.80 ppm.

The methyl group at position 2 was situated in the upfield region, appearing at (11.5-11.79) ppm. Similarly, the terminal methyl carbons of the ester group were positioned in the upfield region at (14.85-14.99) ppm. Conversely, the methyl groups adjacent to both the acetic acid and ester groups were located in the downfield region, ranging from (46.34-49.86) ppm and (58.88-59.50) ppm, respectively. These downfield shifts can be attributed to the influence of the electronegative carbonyl group, which induces an increase in the chemical shift due to its electron-withdrawing nature.

All aromatic carbons at position 5 were identified within the range of (112.44-158.85) ppm. Substitutions in the phenyl ring were observed, including the methoxy group carbon in compounds **4b** and **4g** at (55.55-55.84) ppm, the nitrile group carbon in compound **4e** at 119.22 ppm, and the methyl group in compound **4o** at 21.20 ppm. The ^{13}C-NMR values of these common scaffolds are summarized in Figure 5.95.

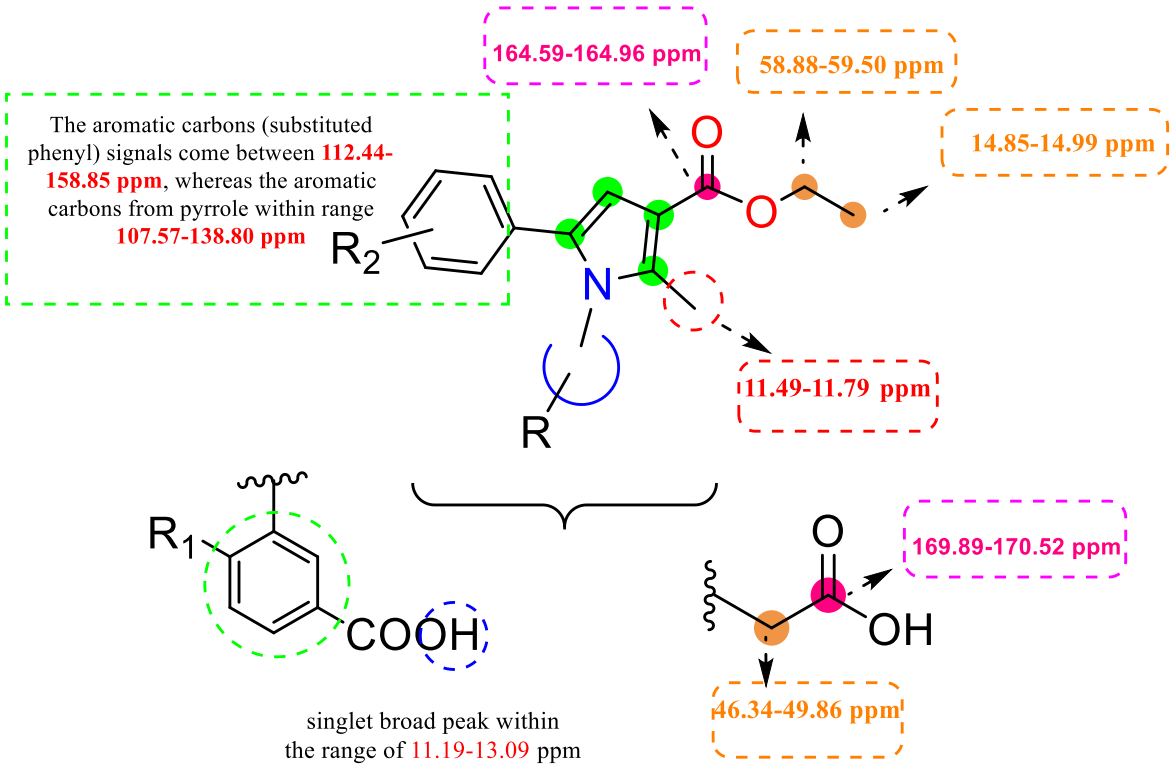

Figure 5.95. *Characterizing ^{13}C-NMR chemical shift values for common scaffolds in targeted compounds*

5.5. Evaluation of Pharmacokinetic Profile

Absorption, distribution, metabolism, excretion, and toxicity (ADMET) property prediction *in-silico* is essential for prioritizing the most promising molecules for development. QikProp was used to make predictions of the pharmacokinetic properties of the chosen structures, including absorption, distribution, metabolism, and elimination. Ten criteria (see Table 5.4), all of which are connected to the inflammatory process and to the reference compound indomethacin, were used to make this assessment. The #star parameter checks the obtained results against the properties of drugs already present in the QikProp software's database [101]. When a result is outside the 95% confidence interval of values that are comparable to commercially available drugs, an alert is generated. Some of the characteristics considered by this parameter are the following: molecular weight (MW), dipole moment, number of rotatable bonds (#rotor), number of hydrogen bond donor groups (HBD), number of hydrogen bond acceptor groups (HBA), predicted water/gas partition coefficient (QPlogPw), predicted octanol/water, partition coefficient (QPlogPo/w), predicted aqueous solubility (logS), prediction of binding to human, predicted brain/blood partition coefficient (QPlogBB) [102]. These tabulated below are the outcomes for the chosen compounds (Table 5.4).

QplogPo/w, which stands for the apparent permeability between octanol and water, is a crucial parameter utilized in drug design to predict solubility, membrane permeability, and bioavailability of compounds [103]. The calculated values regarding QlogPo/w for 4n, 4i, 4h and 5b are higher than the value found for indomethacin (QplogPo/w = 4.267). For the remaining compounds values ranged from 2.695 ≥ QlogPo/w ≥ 4.306, considered more lipophilic compounds (logPo/w ≥ 0). Therefore, it can be inferred that the new compounds are primarily absorbed through passive transcellular mechanisms in the intestine [104]. Subsequently, the CNS activity of the chosen compounds was predicted using a parameter that ranges from -2 (inactive) to +2 (active). Similar to our pivot compound indomethacin, we found **4p, 4b, 4c, 4m, 4i, 4n, 5g, 5**c and **5a** exhibited values equal to (-1), typically indicate a lower level of activity compared to the maximum activity level. It could suggest that the CNS is somewhat less active than the optimal or desired level, but not completely inactive [102].

Percent Human Oral Absorption (PHOA): This parameter predicts the potential oral absorption of a compound on a scale of 0 to 100%. It is calculated using a quantitative multiple linear regression model. PHOA is closely correlated with Human Oral Absorption, as they measure the same property. A value above 80% indicates high predicted oral absorption, while a value below 25% suggests poor predicted oral absorption [102]. Among the compounds analyzed, all of them exhibit values higher than 80%, indicating a high predicted oral absorption. Notably, the most absorbable compounds include **4n** (96.06%), **5d** (93.35%), **4i** (93.04%), **4g** (91.71%), and **4k** (91.13%). Remarkably, compounds **4n**, **5d**, and **4i** demonstrate higher values than indomethacin (91.87%), which is commonly known for its oral absorption efficiency.

Some of the characteristics used in Lipinski's (RO5) evaluation are molecular weight (MW), lipophilicity (as shown by the partition coefficient, LogP), and hydrophilicity (as shown by the number of hydrogen bond donor and acceptor groups). The rate of drug uptake and translocation across a cell membrane is quantified by its relative oral bioavailability (RO5) [105]. The predicted values indicate that , The MW and log P for the compounds fall between (287 and 452) and (2.695 - 5.834) respectively. The HBD and HBA are both ≤ 2, with the HBA ≤ 5.75. Therefore, the number of rotatable bonds in all compounds contained in our own datasets was less than seven, as required by Lipinski's Rule of Five. These results suggest that the synthetic compounds can be manipulated therapeutically and could be used in oral drug delivery systems..

Except for **5c** and **5g**, no compounds in this study exhibited RO5 violations, suggesting that these two compounds would likely render the drug orally active in humans. Since indomethacin is taken orally, its properties don't run afoul of the Lipinski rule (RO5). This finding is suggestive of a similarity to an orally-administered biological activity [106]. When compared to indomethacin, the new COX (1&2) inhibitors may be judged to have superior pharmacokinetic performance without compromising any of their descriptors or molecular properties.

Table 5.4. Pharmacokinetic parameters and drug likness based on Lipinski parameters of the synthesized compounds.

Compounds	**Physicochemical parameters**					**Pharmacokinetic properties**					**RO5**
	#stars	**Mw[a] ≤500**	**HBA**	**HBD**	**No. rotar**	**PHOA**	**QPlogPo/w**	**QLogS**	**QPPCaco**	**CNS[h]**	
5a	1	448.30	4.75	1	4	78.64	5.505	-7.142	90.539	-1	0
5b	1	434.27	4.75	2	4	87.55	4.882	-7.148	43.471	-2	0
5d	1	452.72	4	1	3	93.35	5.834	-7.923	43.72	-2	0
5c	2	418.27	4	1	3	82.98	5.531	-7.28	89.126	-1	1
5g	1	428.82	5	1	4	66.58	4.199	-6.713	110.15	-1	1
5e	1	410.38	5.75	2	5	62.64	3.273	-5.993	10.63	-2	0
5f	0	424.40	5.75	1	5	66.41	3.925	-6.128	5.198	-2	0
4o	0	301.34	4	1	4	92.73	3.719	-4.935	7.342	-2	0
4g	0	347.36	5.5	1	6	91.71	3.895	-5.099	14.559	-2	0
4k	0	305.30	4	1	4	91.13	3.726	-4.896	16.218	-2	0
4d	0	321.76	4	1	4	89.70	3.977	-5.27	115.592	-2	0
4e	0	312.32	5.5	1	5	70.57	2.66	-5.316	157.905	-2	0
4b	0	317.34	4.75	1	5	87.76	3.587	-4.768	132.788	-1	0
4p	0	332.31	5	1	5	65.72	2.784	-4.69	130.961	-1	0
4a	0	287.31	4	1	4	84.61	3.256	-4.673	24.305	-2	0
4l	0	321.76	4	1	4	87.103	3.999	-5.264	15.591	-2	0
4c	0	305.30	4	1	4	87.37	3.765	-4.955	151.381	-1	0
4h	0	363.41	4	1	5	86.60	4.585	-5.91	68.146	-2	0
4m	0	293.33	4	1	4	85.62	3.323	-4.193	155.256	-1	0
4i	0	337.37	4	1	4	93.04	4.406	-5.544	130.692	-1	0
4n	1	390.65	4	1	4	96.06	4.932	-6.408	177.173	-1	0
4f	1	330.29	5	1	6	67.27	2.695	-4.522	131.241	-2	0
Indomethacin	0	357.79	5.75	1	4	91.87	4.267	-5.122	162.164	-1	0

(HBA: Hydrogen bond acceptors, **HBD:** Hydrogen bond donors, **Mw:** Molecular weight g/mol, **PHOA**: Percent Human Oral Absorption, **QplogPo/w**: apparent permeability of compound between octanol/water, **CNS[h]** activity in the central nervous system, **QPPCaco**: permeability of the diferentiated cells of intestinal epithelium Caco-2, Q**Log S:** aqueous solubility (highly soluble > 0 > very soluble > −2 > soluble > −4 > moderately soluble > −6 > poorly soluble > −10 > insoluble), **RO5**: rule of five).

5.6. Evaluation of COX Inhibition Assay

In order to evaluate the COX-1 and COX-2 inhibitory properties of the pyrrole carboxylic acid derivatives, an *in-vitro* study was conducted. Table 5.5 presents the results, showing that all compounds and reference drugs exhibited over 50% inhibition activity at concentrations of 1 μM and 10 μM. The fluorometric inhibitor screening kits were employed following the protocol outlined in **Subsection 4.6**. In this thesis, a higher inhibition profile was observed for both COX-1 and COX-2 with all of the synthesized compounds in the concentration range (1 μM and 10 μM).

Compounds containing the acetic acid group at position 1 (**4g, 4h, 4k, 4l**) exhibited the highest activity against both COX-2 and COX-1. Their IC_{50} values indicated greater activity compared to celecoxib (92.327±1.425 and 85.485±1.303) at concentrations of 10 μM and 1 μM. Specifically, compound **4k** and **4h** demonstrated IC_{50} values of (94.674 ±2.123 and 88.055 ±1.927) and (95.374 ±2.046 and 90.521 ±2.459) against COX-2 and COX-1, respectively.

Moreover, compound **4h** and **4g** exhibited higher inhibition against COX-1, with IC_{50} values of (96.628 ±2.020 and 92.710 ±2.674) and (92.366 ±2.731 and 84.517 ±2.036), respectively, which were comparable to the activity of Ibuprofen (98.152 ±1.058 and 89.361 ±1.245) at concentrations of 10 μM and 1 μM, respectively. Conversely, compounds containing a hydroxy benzoic acid substitute at position 1 (**5e** and **5b**) exhibit the most active against COX-1 with IC_{50} (93.185 ±2.031 and 86.799 ±1.879) and (95.766 ±2.012 and 91.499 ±1.547) at concentrations 10 μM and 1 μM respectively. One noteworthy observation is that the existence of a small acidic group at position 1 provides effectiveness against both COX-1 and COX-2 for all synthesized compounds. However, if a larger group is introduced, the activity becomes biased towards COX-1 more than COX-2. Additionally, the compounds containing acetic acid moieties at position 1, along with a lipophilic and bulkier group such as phenyl or methoxy on the phenyl ring at position 5, play a significant role in making the compound active against both COX-1 and COX-2 simultaneously, as observed in compounds **4g** and **4h**. Conversely, when a lipophilic but smaller group, such as a chloro group, is substituted, the activity favors COX-2 inhibition, as seen in compounds **4k** and **4l**. However, if the bulkiness is increased at a different site (position 1) and the acetic group is replaced with a more substantial acidic group (benzoic acid group), the activity shifts back towards favoring COX-1 more than COX-2.

Overall, the study shows that small changes in the chemical structure of pyrrole carboxylic acid derivatives can significantly affect their COX-1 and COX-2 inhibitory activities. The findings of this study provide insight into the design and development of more effective COX inhibitors with improved selectivity and reduced side effects. Future research could focus on further optimizing the structure of pyrrole carboxylic acid derivatives to enhance their therapeutic potential.

Table 5.5. Values for IC_{50} (μM) and percent inhibition at 10 and 1 μM for both synthesized compounds and reference drugs against COX-1 and COX-2.

Compounds	COX-1 % Inhibition		COX-1	COX-2 % Inhibition		COX-2
	10 μM	1 μM	IC_{50} (μM)	10 μM	1 μM	IC_{50} (μM)
4c	46.122 ±0.822	32.720 ±0.957	>10	79.429 ±2.056	38.749 ±0.848	>1
4d	63.568 ±1.390	39.447 ±1.055	>1	47.036 ±0.961	29.642 ±0.722	>10
4e	74.919 ±1.862	43.367 ±1.677	>1	80.441 ±1.837	48.320 ±0.836	>1
4g	92.366 ±2.731	84.517 ±2.036	0.117 ±0.005	90.967 ±2.022	83.033 ±1.878	0.188 ±0.008
4n	41.552 ±0.921	28.627 ±0.745	>10	38.748 ±1.057	21.590 ±0.967	>10
4k	86.461 ±1.716	46.378 ±1.501	>1	94.674 ±2.123	88.055 ±1.927	0.108 ±0.004
4h	96.628 ±2.020	92.710 ±2.674	0.068 ±0.003	95.374 ±2.046	90.521 ±2.459	0.091 ±0.004
4i	82.275 ±2.355	48.367 ±2.157	>1	87.759 ±1.936	38.521 ±2.241	>1
4l	41.326 ±1.057	34.587 ±0.836	>10	91.579 ±2.458	82.602 ±2.061	0.143 ±0.006
4m	46.259 ±0.923	26.874 ±0.755	>10	38.626 ±0.861	30.855 ±0.858	>10
5f	71.737 ±1.839	43.330 ±0.874	>1	79.761 ±1.963	48.237 ±1.064	>1
5e	93.185 ±2.031	86.799 ±1.879	0.129 ±0.005	74.618 ±1.884	37.217 ±0.936	>1
5g	85.418 ±2.416	41.218 ±1.036	>1	89.176 ±1.822	37.418 ±0.874	>1
5a	88.038 ±2.856	47.611 ±1.802	>1	41.366 ±1.631	38.044 ±1.161	>10
5b	95.766 ±2.012	91.499 ±1.547	0.082 ±0.003	83.403 ±2.784	40.498 ±1.634	>1
5d	40.369 ±0.861	30.748 ±1.058	>10	48.317 ±1.361	25.679 ±0.963	>10
5c	48.513 ±1.236	48.513 ±1.236	>10	79.501 ±1.922	79.501 ±1.922	>1
SC560	99.076 ±2.165	96.274 ±1.864	0.006 ± 0.0002	-	-	-
Ibuprofen	98.152 ±1.058	89.361 ±1.245	2.450 ±0.135	98.234 ±1.208	88.155 ±1.348	5.326 ±0.218
Celecoxib	-	-		92.327 ±1.425	85.485 ±1.303	0.132 ±0.005
Nimesulide	-	-		97.821 ±1.214	89.575 ±1.049	1.684 ±0.079

5.7. Evaluation of Computional Studies

5.7.1. Docking protocol

Understanding the structure of cyclooxygenase protein and distinguishing between its isoforms is crucial for the development of novel and highly selective inhibitors of COX-1 and COX-2. The active site of COX is characterized by a long hydrophobic channel and a narrow opening near the membrane-binding domain. While their active sites are similar, COX-2 has a larger binding cavity than COX-1 does (Figure 5.96) [107]. Because of this discrepancy, scientists have been working hard to create selective COX-1 and COX-2 inhibitors. Three distinct regions of the enzyme's active site govern the selectivity of these inhibitors: the entrance region containing Arg120/Tyr355, the hydrophobic pocket located just below the hem group, and the side pocket.

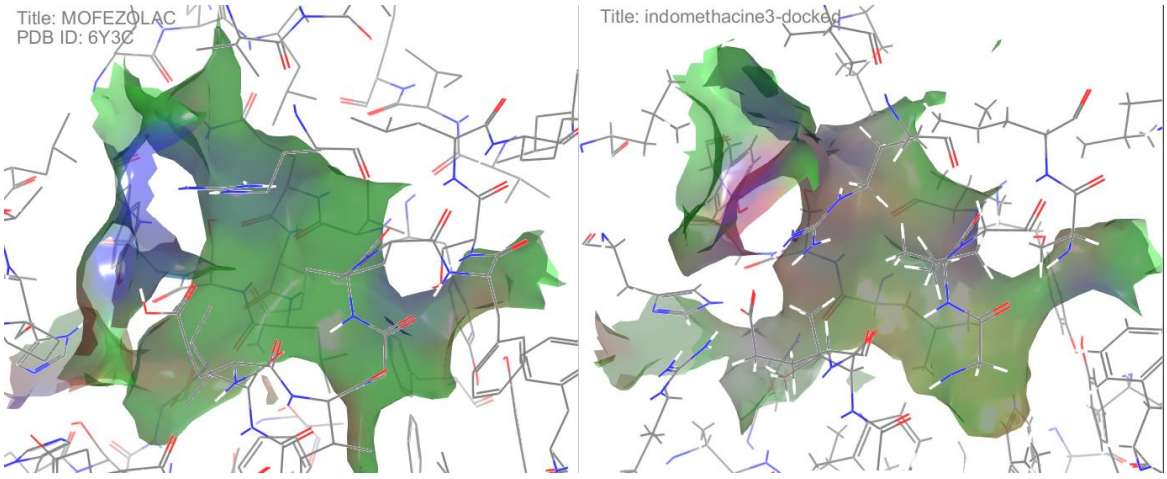

Figure 5.96. *Schematic shape of COX-1(1) and COX-2 (2) active site*

COX-1 and COX-2 share similar active sites, but COX-2 is distinguished by a side pocket above the entrance to the binding site (Arg120 and Tyr355). This side pocket is formed by a single amino acid residue variation at position 523, close to Arg120, and is absent in COX-1. To be more precise, changing the isoleucine (Ile) at position 523 of COX-2 to valine (Val) creates a gap in the binding site's lining, allowing drugs or inhibitors to enter the side pocket [108]. The selectivity of COX-2 inhibitors stems from their ability to interact with a specific, non-conserved region in the COX-2 enzyme. This region's variation allows these drugs to selectively target COX-2, laying the groundwork

for the development of novel and highly selective COX-2 inhibitors. Additional interactions with Arg513 (which replaces His513 in COX-1) are made possible by the side pocket, which further increases COX-2 selectivity. The orientation of Leu384 is also important for COX-2 selectivity. Phe503 directs the Leu384 side chain into the active site of COX-1. However, in COX-2, Leu503's reduced size permits Leu384 to relocate away from the active site, thereby expanding the binding site's accessibility [109]. Important insights for the design of novel and selective COX-2 inhibitors are provided by the relative positions of Arg513 and Leu384 in COX-2 and COX-1, respectively (Figure 5.97).

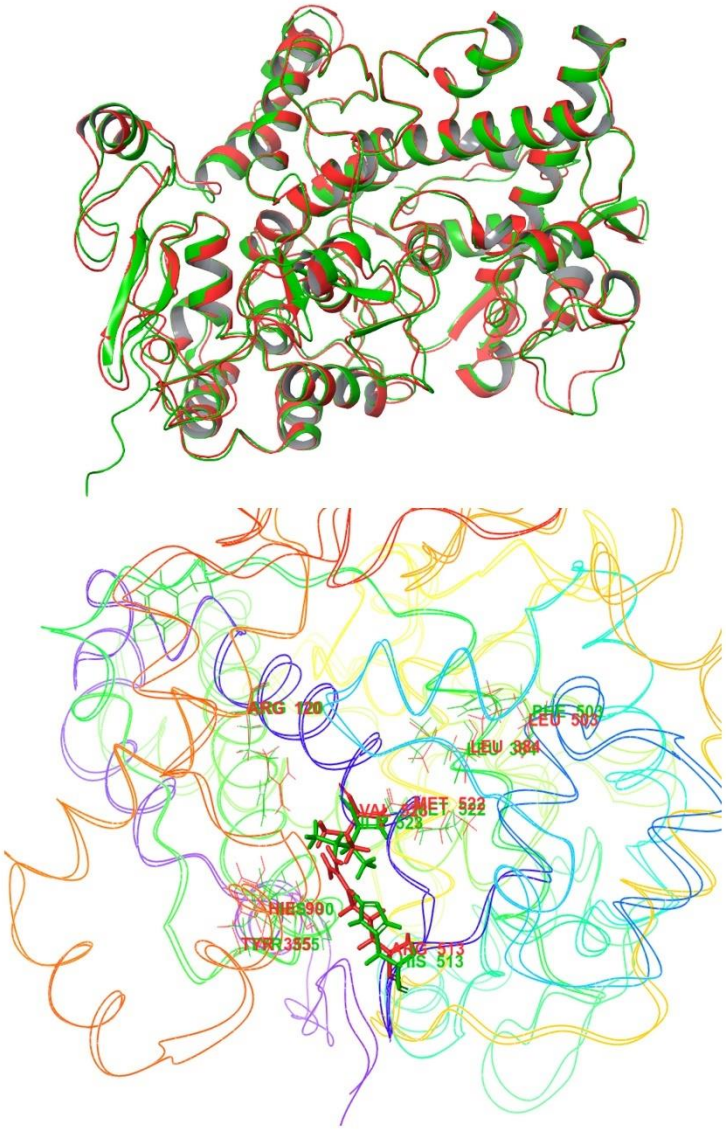

Figure 5.97. *Aligment of COX-1 and COX-2 binding site: (5-F1a) represent COX-2 in red color and (6-Y3C) represent COX-1 in green color*

5.7.2. Validation of docking protocol

In previous studies, the Protein Data Bank did not have the three-dimensional structure of human COX-1 available, so in the previous research, homology modeling was used to generate a structural model for COX-1[110]. However, a recent finding (PDB ID: 6-Y3C) has provided a human COX-1 crystal structure that can now be used for further studies [89, 111]. On the other hand, the crystal structure of human COX-2 complexed with salicylic acid (PDB entry: 5-F1a, resolution 2.38 Å) was selected as the receptor for docking experiments to investigate compounds with selectivity towards COX-2 protein. In order to test the accuracy of the molecular docking process, the ligand's crystallographic structure was repositioned in the hCOX-2 protein (5-F1a). The RMSD value obtained by repositioning the ligand and comparing its binding pose in the complex was 0.1857A˚. This value was calculated by superimposing all atoms. It is possible to visualize the comparison between the crystallographic ligand and the predicted docking pose by observing the overlap of the ligand in both structures Figure 5.98.

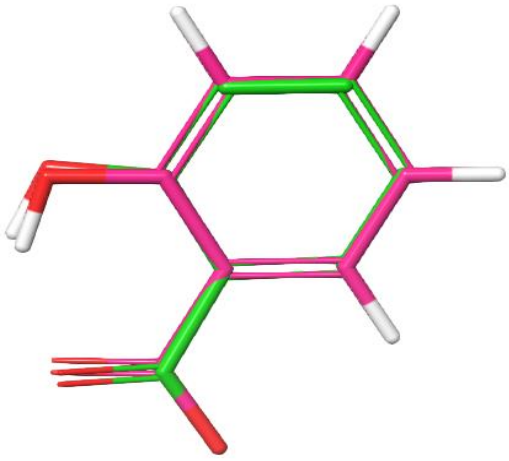

Figure 5.98. Overlapping *of the crystallographic ligand (green) and the conformation obtained by re-docking (Pink)*

Then the inhibitor's structure (salicylic acid) was extracted from the enzyme COX-2 complex and re-docked into the enzyme's binding site. Finally, as can be seen in Figure 5.99, there is excellent agreement between the calculated (via docking simulations, ΔG = -7.467 kcal/mol) and experimental (via the crystallographic complex, ΔG = -7.58 kcal/mol) coordinates of saliysic acid. Therefore, once the interaction affinity value was close to what was observed experimentally, our protocol performed satisfactorily in

predicting the interaction conformation. Specifically, it is suggested that the predicted binding mode of 5-F1a proteins is similar to the experimental one if RMSD value between the two is less than 2 A˚ [112] . This demonstrates the reliability of the binding site prediction made by the re-docking protocol. Overall, this supports the idea that 5-F1a proteins are biologically significant, as their predicted binding mode is highly similar to the experimentally determined one.

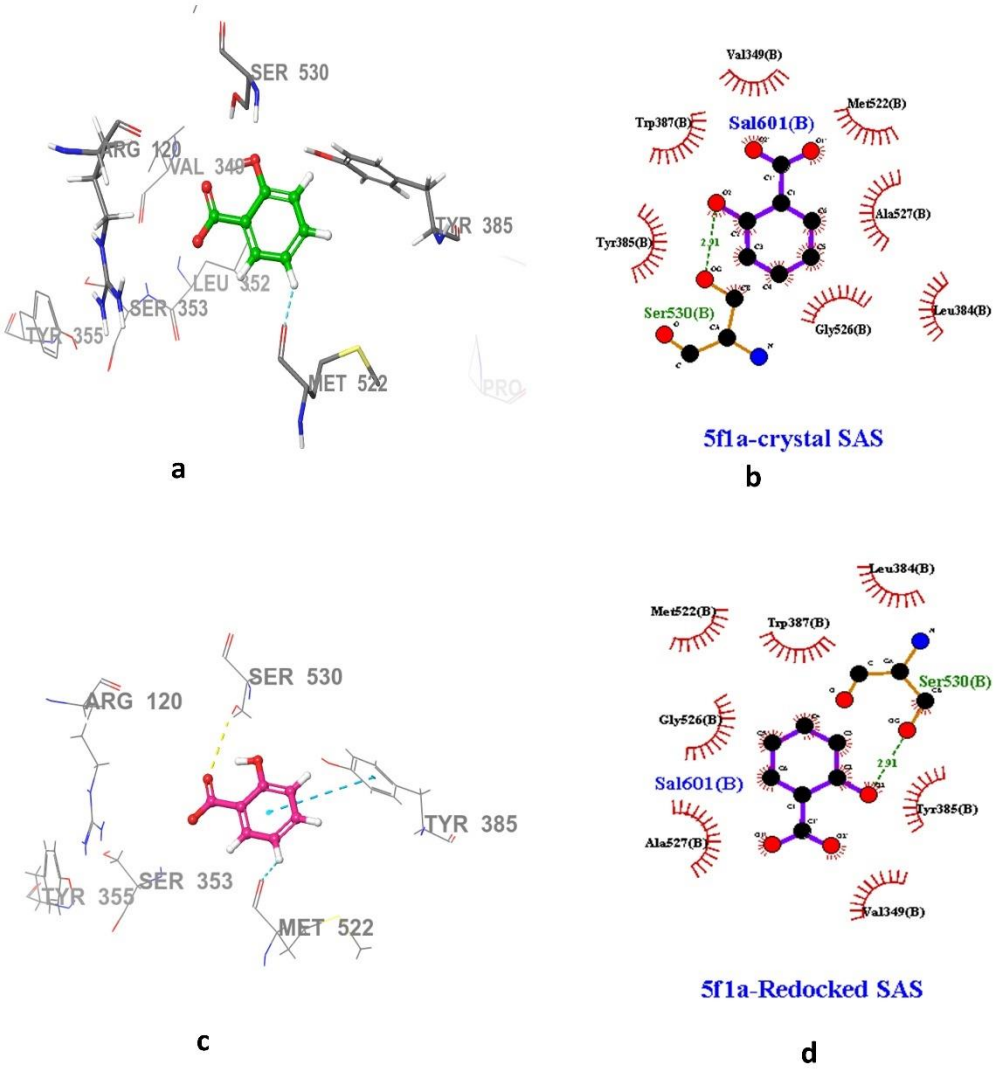

Figure 5.99. *The 3D interacting mode of the crystal structure salysic acid (green color) and after redocking (purpule color) in COX-2 active region (PDB ID: 5-F1a)*

5.7.3. Evaluation of induced fit docking protocols

As indomethacin is commonly used as a reference ligand in our synthesized compound, we conducted an IFD simulation to gain a comprehensive understanding of the protein-ligand interactions. Figure 5.100 visually illustrates the docked indomethacin molecule and its interactions with various types of grids, including normal and IFD protocols. The IFD simulation provides a more detailed and nuanced picture of the molecular interactions and conformations of indomethacin, allowing for a better understanding of its behavior in the binding site. This information is derived from our extensive database and enhances our understanding of the synthesized compound's behavior. The hydrogen bond interaction between Arg120 and Tyr355 is preserved by the carboxylic acid group of indomethacin in both protocols, as well as the carbonyl group of acyl phenyl with Ser530. However, in contrast to the standard docking protocol, the methoxy substitute in the phenyl ring in IFD forms a hydrogen bond interaction with His90, which is absent in the standard docking protocol. Additionally, unlike the standard docking protocol, the acyl aryl group is found throughout the entire protein binding site in an IFD simulation Figure 5.101.

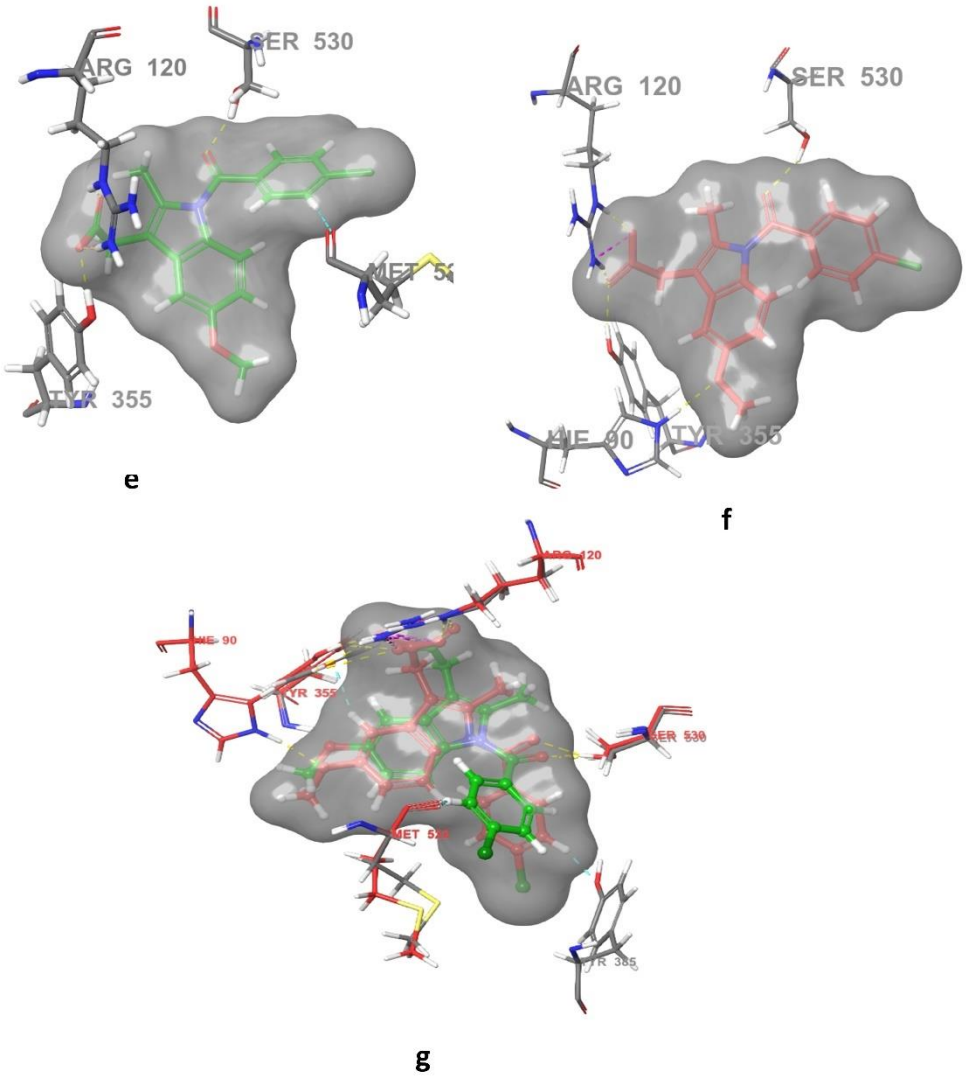

Figure 5.100. *e) The 3D interacting mode of the indomethacin with normal docking protocol, f) the 3D interacting mode of the indomethacin with IFD protocol, g) Comparison of Ligand Alignment in Indomethacin using Normal Docking and Induced Fit Protocols*

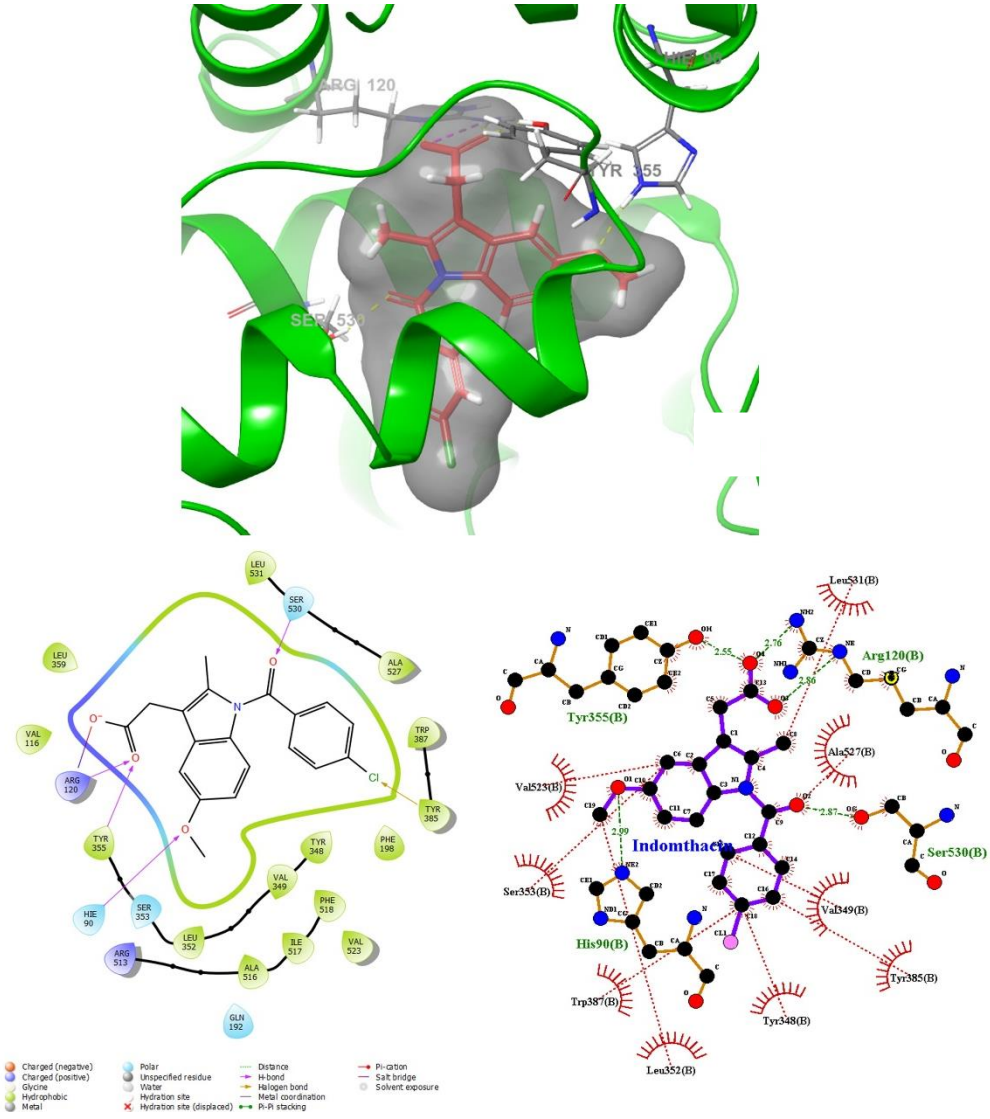

Figure 5.101. *Docked pose of indomethacin in the binding site on the stem region (PDB ID: 5F1a) induced-fit docking (docking score:-11.380 kcal/mol)*

In the case of the 6Y3C PDB protein (10.2210/pdb6Y3C/pdb), it does not have a crystal structure with a bound ligand, so we have used IFD to predict the binding mode of Mofezolac (IC_{50}= 5 μM for COX-1, PIC_{50}=5.3010) within the protein. The IFD protocol will use the available structural information on the unbound protein to predict conformational change in response to ligand binding and the ligand (mofezolac) is docked in this site. IFD simulation results can shed light on the mode of binding and affinity of Mofezolac to the 6Y3C protein (Figure 5.102), The simulation shows that upon binding, the protein undergoes significant conformational changes, including movement of key residues, changes in its overall shape, and the formation of new interactions with the

ligand. which can then be validated experimentally, if possible, to ensure that the predicted binding mode is biologically plausible. By comparing the unbound and bound structures, key differences in conformation are highlighted, elucidating their impact on the protein's function and binding affinity. Figure 5.103 displays the interactions formed by the reported ligand (mofezolac, docking score -9.324): two HB and salt bridge with Arg120; three AHB with Tyr355; and one AHB with both Sere530 and Met522. As mentioned previously, mofezolac has been shown to have a higher affinity for COX-1 compared to COX-2 inhibitor proteins, and it interacts with Arg120 and Tyr355, which are considered key residues in evaluating COX activity [113]. However, mofezolac does not interact with Arg513, which may indicate that it is not selective towards COX-2 and is considered to be more selective towards COX-1 inhibition.

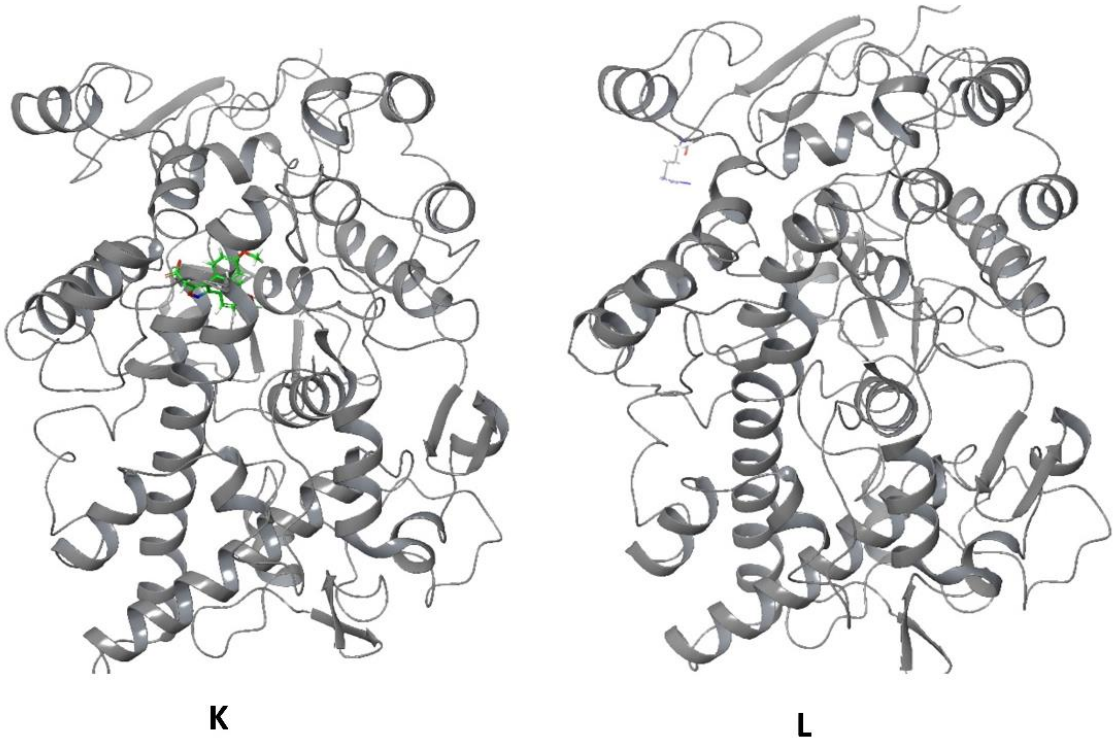

Figure 5.102. *k) The 6Y3C protein structure in complex with mofezolac: A Snapshot of the protein in its induced conformation. l) Protein structure: A snapshot of the protein in its native conformation*

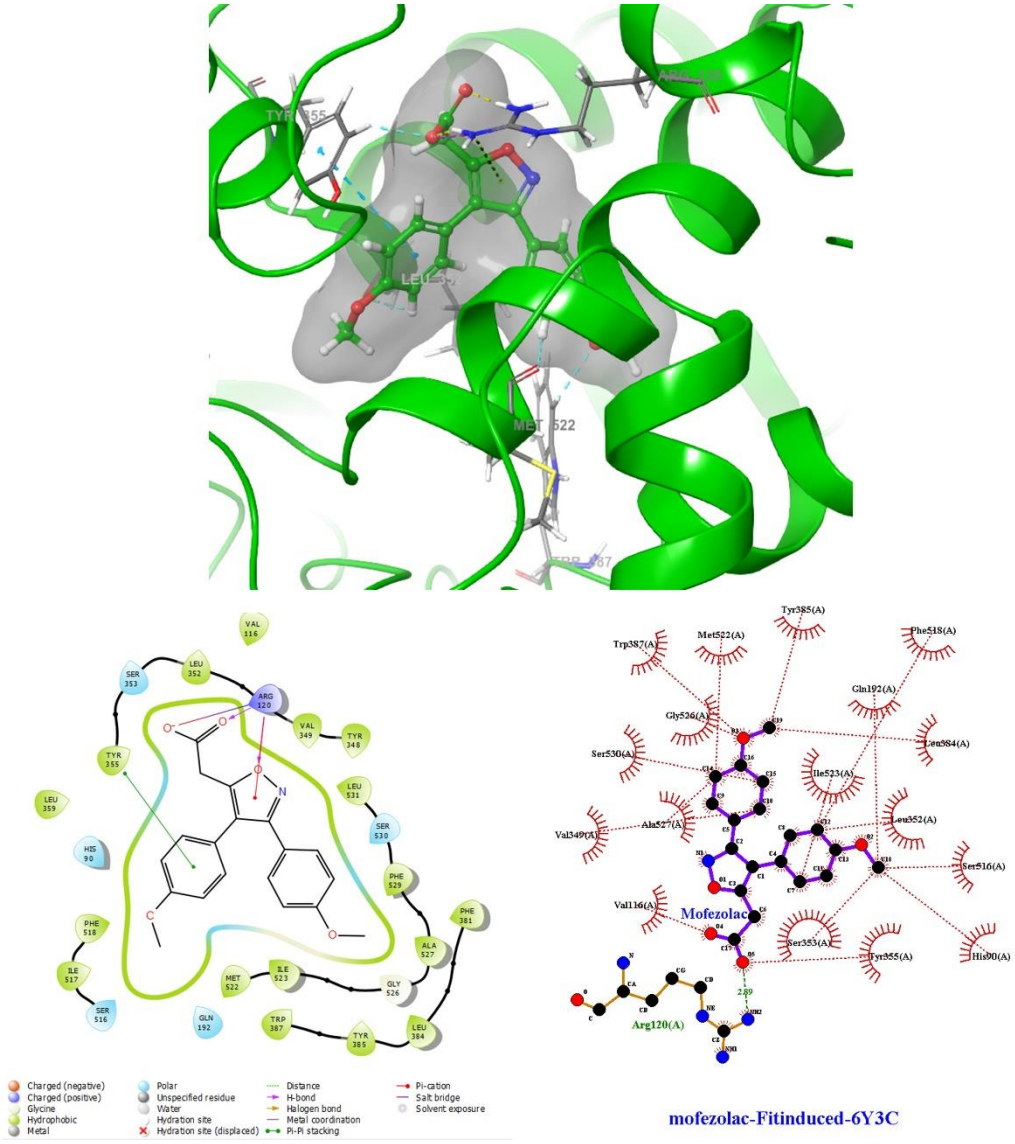

Figure 5.103. *Docked pose of mofezolac in the binding site on the stem region (PDB ID: 6Y3C) induced-fit docking (docking score:-9.324 kcal/mol)*

5.7.4. Exploring the *In-Silico* Studies of Highly Active Compounds

5.7.4.1. Molecular docking analysis of most active compounds (4h, 4g, 4k, 4l, 5a, 5e)

All of the designed compounds' modes of binding to the primary binding sites of both enzymes were predicted using molecular docking simulations. The results were displayed in Figures 5.104, 5.105, 5.106, 5.107. Compounds **4g** and **4h** were selected for docking studies after displaying significant dual COX-1/COX-2 inhibitory activity in the biological assay. The GLIDE software was used to dock these compounds into the COX-1 and COX-2 active sites. While these compounds were identified as "COX-2-favoring inhibitors" similar to meloxicam, etodolac, and nimesulide, their inhibitory activities and

binding energy for COX activities were relatively lower compared to Celecoxib. Notably, compound **4h** demonstrated superior biological activity compared to Celecoxib. This heightened activity can be attributed to its unique ability to simultaneously interact with Arg120 and His90, while effectively occupying the lipophilic pocket with its bi-phenyl group, leading to enhanced binding affinity (see Figure 5.104). Furthermore, we conducted docking studies of **4h** in the COX-1 (6-Y3C) protein, revealing interactions with Arg120 and Tyr355 (as depicted in Figure 5.105). The presence of the bi-phenyl group plays a significant role in augmenting the activity towards both COX-1 and COX-2. Additionally, the inclusion of small and electrostatic groups at positions 1 and 3 facilitates the occupation of the bi-phenyl moiety within the active site, facilitating interactions with essential amino acids crucial for COX-1 and COX-2 activity.In Figure 5.106, the docking results revealed that the benzene ring and ethoxy carbonyl of **4k** and **4l** were oriented in a similar manner and situated within two of the three key binding pockets of the COX-2 binding site, suggesting their potential more toward COX-2 inhibitors. The acetic acid pyrrole derivatives **4k** and **4l**, which contained 3,4-dichlorophenyl and 3-chlorophenyl moieties at position 5, respectively, showed similarities in their orientation to the co-crystallized inhibitor, indomethacin. However, the carbonyl on the ethoxy carbonyl group of **4k** and **4l** formed hydrogen bonding interactions with His 90, while the methoxy group in indomethacin formed the same interaction with this residue. In addition, the carboxyl group at position 1 of **4k** and **4l** and position 3 of indomethacin formed a salt bridge and HB interactions with Arg120. The methyl substituent at position 2 of the pyrrole ring was positioned in a polar pocket between the side chains of Arg120 and His90. The corresponding 3-hydroxy benzoic acid derivatives, compounds **5e** and **5b**, showed a shift in activity towards COX-1 due to the different interactions formed by the carboxyl group on the benzoic acid and the substituted phenyl group at position 5. The pyrrole ring interacted through Pi-cation interaction with Arg120, while the substituted phenyl group occupied the hydrophobic pocket like COX-2 inhibitors. Compound **5e**, which contained a nitro group, was responsible for hydrogen bonding interaction with Phe518, while both phenyl groups in **5e** and **5b** formed asymmetric hydrogen bonds with Tyr355, His90, and Leu352 (see Figure 5.107). Overall, compounds **4h** ,**4k** and **4l** exhibited significant COX-1/COX-2 inhibitory activity and a high potential for effective binding with the COX-2 enzyme, making them potential candidates for the development of new selective COX-2 inhibitors.

Although they were "preferential COX-2 inhibitors," their inhibitory activities and binding energy were still noteworthy compared to highly selective COX-2 inhibitors like Celecoxib. These findings provide insight into the molecular mechanisms underlying COX-1/COX-2 inhibition and suggest promising avenues for the development of more effective anti-inflammatory drugs.

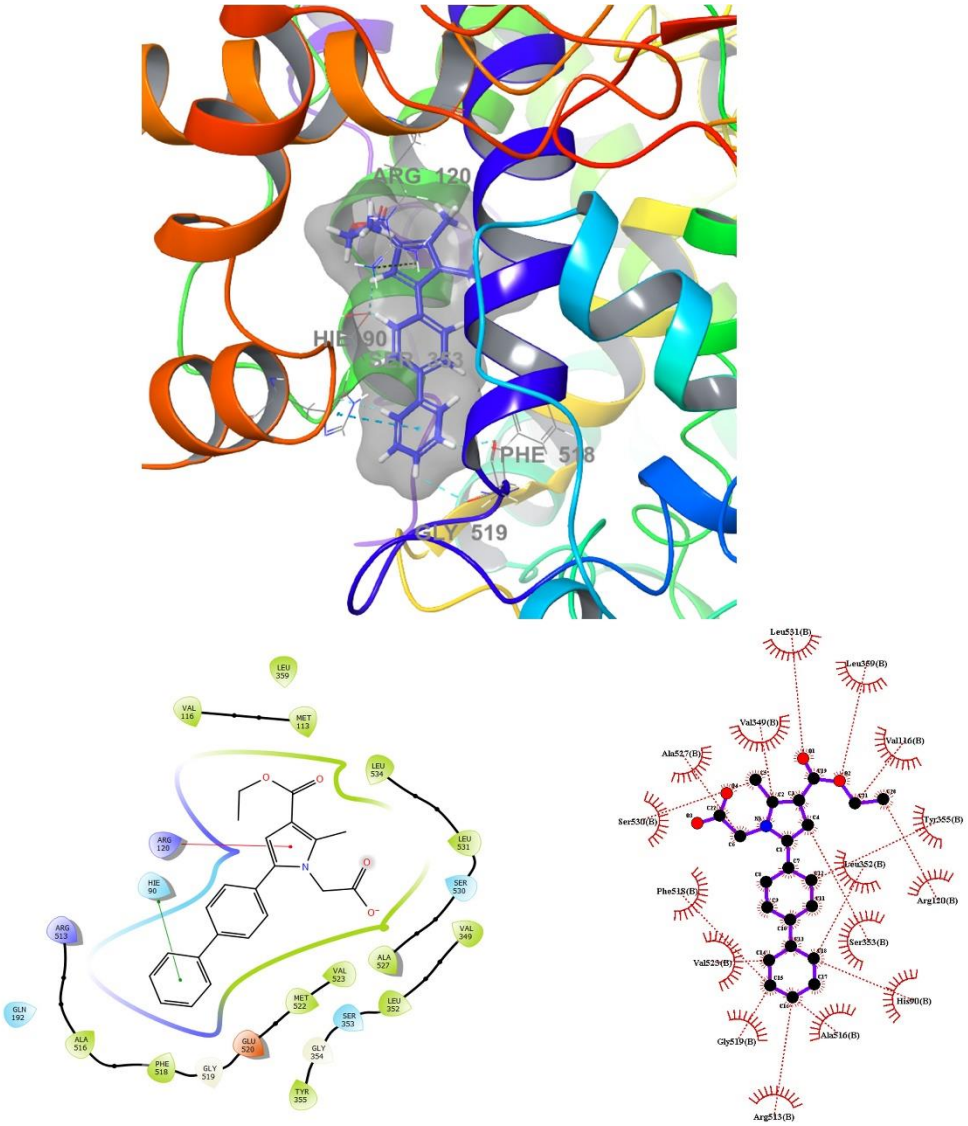

Figure 5.104. *Superimposition pose and 2D interacting mode of **4h** in the active region of COX-2 (5-F1a)*

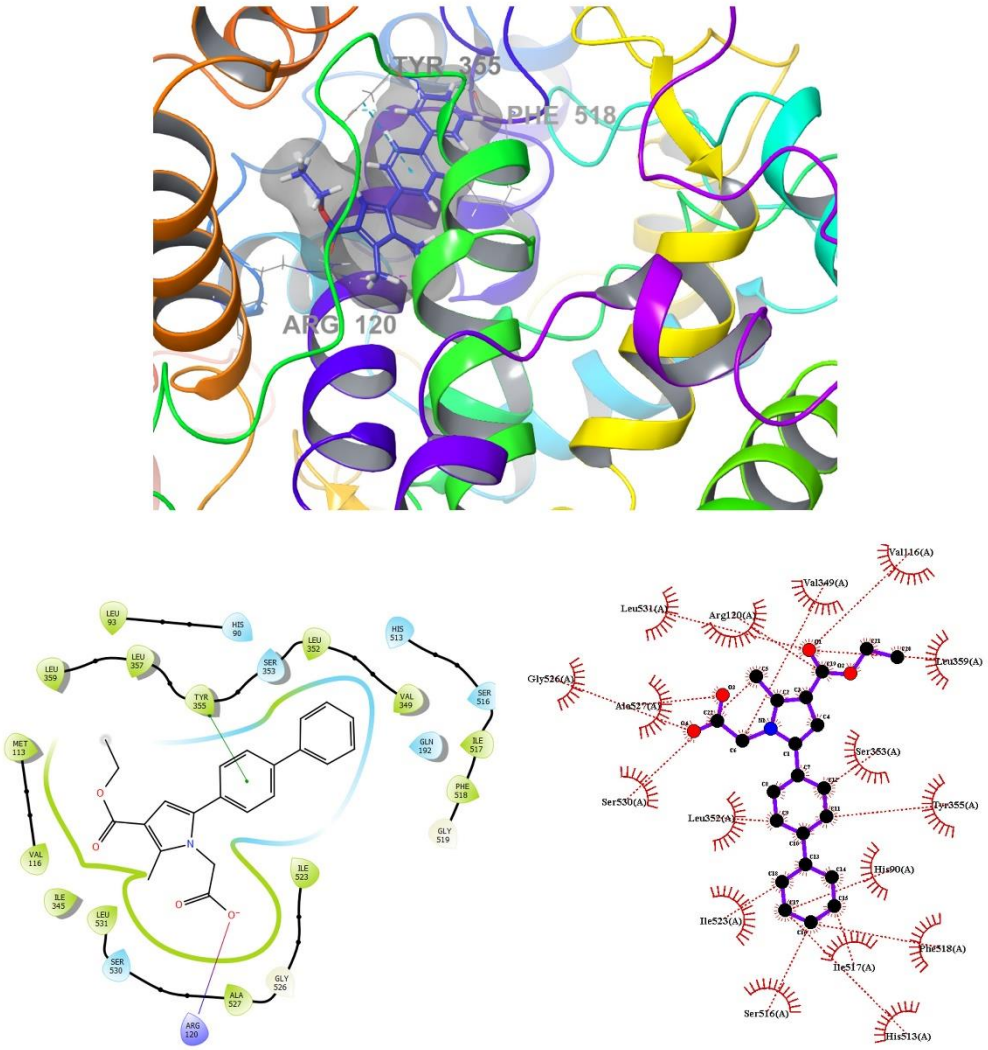

Figure 5.105. *Superimposition pose and 2D interacting mode of* ***4h*** *in the active region of COX-1 (6-Y3C)*

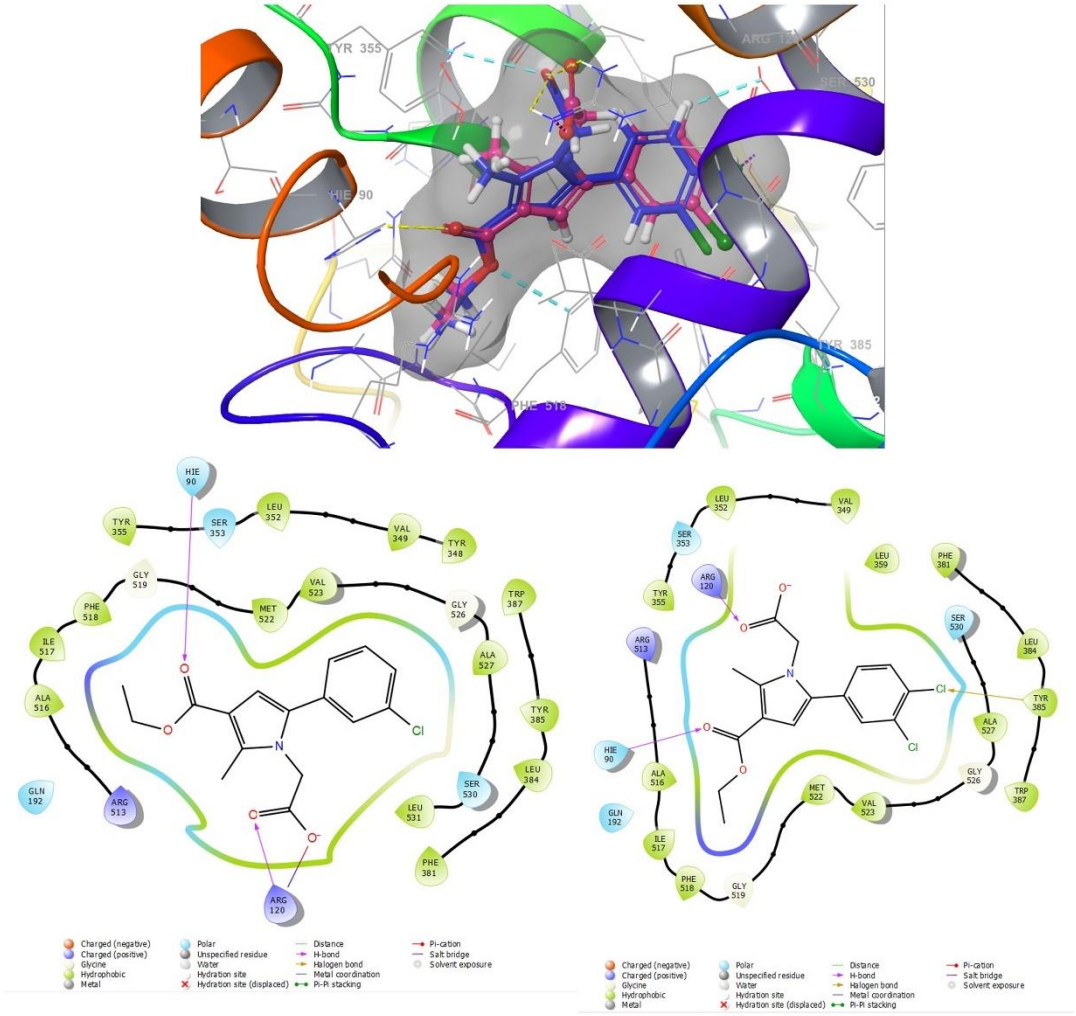

Figure 5.106. *Superimposition pose and 2D interacting mode of* ***4k*** *and* ***4l*** *in the active region of COX-2 (5-F1a)*

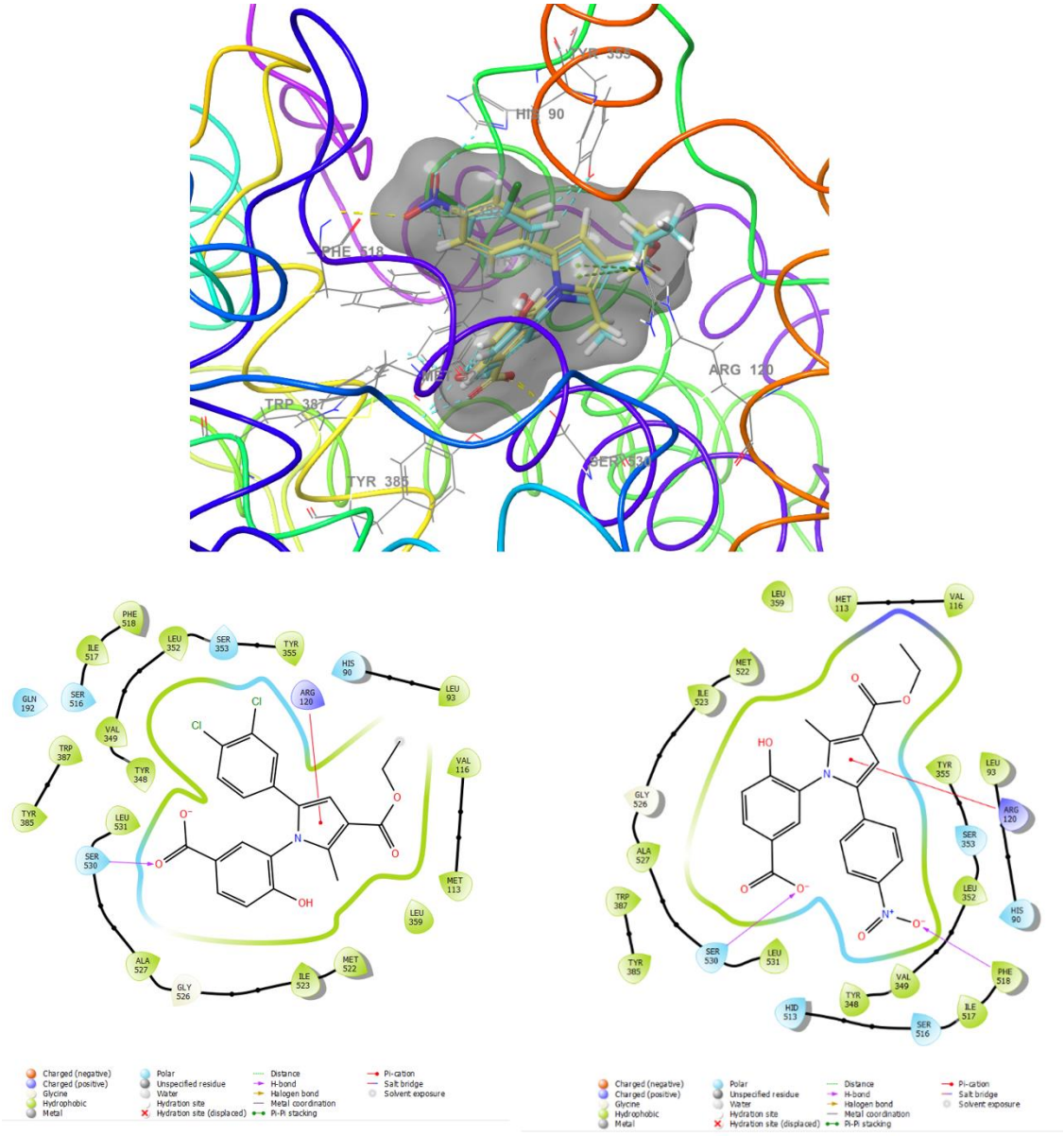

Figure 5.107. *Superimposition pose and 2D interacting mode of* ***5e*** *and* ***5b*** *in the active region of COX-1 (6-Y3C)*

5.7.4.2. In-Depth FB-QSAR analysis of the highly active compounds (4h)

To identify the most active compounds, we performed *in-vivo* experiments and synthesized several compounds with different chemical structures. Subsequently, we utilized the FB-QSAR model to forecast the activity of these compounds. Interestingly, the model accurately predicted the activity of the most potent compound identified through in vivo studies, thus demonstrating its reliability and utility. Our future plans involve applying the FB-QSAR model to predict the activity of additional compounds

that have been synthesized with modified chemical structures. The insights obtained from this model will enhance our comprehension of the factors influencing COX-2 inhibitor activity. Furthermore, it will assist us in the rational design of novel and more potent inhibitors with improved selectivity and therapeutic efficacy.

The findings indicated that a biphenyl ring can be configured at position 4 with small lipophilic groups, instead of potential HBA or HBD groups. Additionally, the terminal phenyl group can be replaced with a bioisosteric alternative such as pyridine, which would enhance the electrostatic interaction in that region. Moreover, in the acetic acid group, the contour map revealed the presence of a small lipophilic group in that area. The carboxyl group exhibited good electrostatic interaction that aligned with the contour map generated from FB-QSAR. The small methyl group in the acetic acid should not possess any HBA or HBD groups either. Although the biphenyl substitution acts as a steric hindrance group and may impede the compound from entering the COX-1 pocket (which is smaller than COX-2), the biological activity demonstrated that the **4h** compound also exhibited good activity in COX-1 (see Figure 5.108). This suggests that the presence of the bi-phenyl group facilitates the compound's flat or planar shape, enabling easy access to the COX-1 active site. Consequently, this QSAR model can be employed to identify novel and existing pyrrole carboxylic acid derivatives with COX-2 inhibition activity. Furthermore, it can serve as a valuable intermediary model for developing new QSAR hypotheses for dual inhibitors of both COX-1 and COX-2 enzyme isomers.

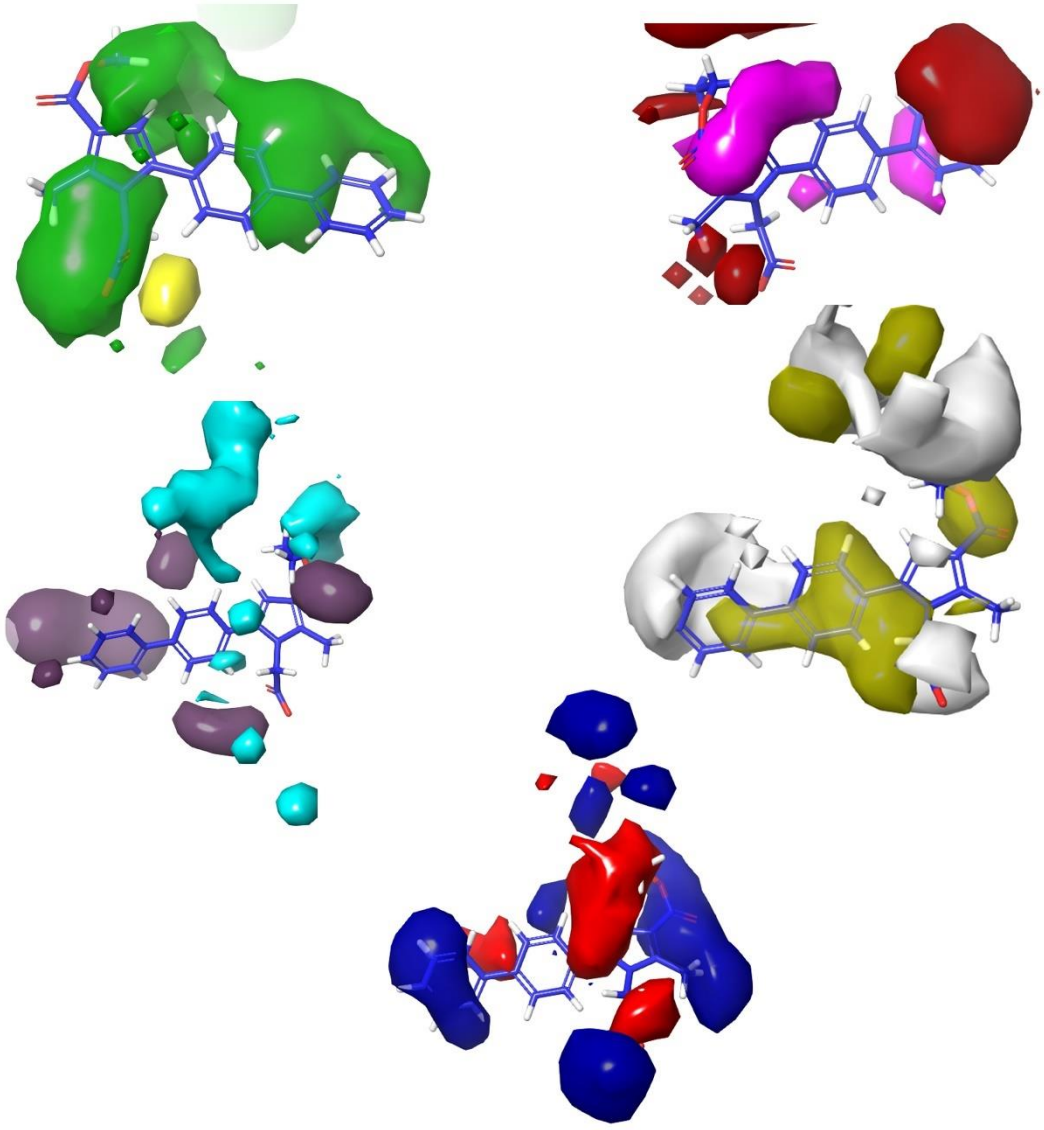

Figure 5.108. *3D visualizations of **4h** contour maps: steric (positive effect (+): green, negative effect (_): yellow), electrostatic (+: blue, -: red), hydrophobic (+: yellow, -: white), HBA (+:red, -:magenta), and HBD (+:blue-violet, -: cyan), respectively.*

5.7.4.3. Exploring the MDS of Compound (4h) in COX Isomers Complex

The analysis focused on evaluating the stability and structure-activity relationship (SAR) of the **4h** ligand within the 6-Y3C and 5-F1a protein complexes. The stability of the complexes was examined using MDS, and the results, as shown in Figure 5.109, indicated that both complexes exhibited values within an acceptable range. The simulation also revealed that there were no significant changes in the Rg plots, suggesting the overall stability of the complexes. The RMSD values for COX-1 and COX-2 remained below 3 Å, indicating minimal fluctuations in the crucial structural elements such as the

alpha-helix (red areas) and beta-strand (blue areas). Overall, the complexes demonstrated a protective effect on their stability. Further analysis using RMSF plots highlighted the positive impact of interactions with loop amino acids (green line in the white area), leading to reduced fluctuation intensity. This finding indicates that both complexes effectively stabilized their ligand-protein interactions during the simulation. Following the confirmation of complex stability, Figure 5.110 presented an evaluation of the interaction types, their continuity, and their strength. The hydrophobic interactions between **4h** and specific amino acid residues, such as His90, Met113, Val116, Leu117, Arg120, Ile345, Val349, Leu352, Tyr355, Leu359, Arg513, Arg518, Val523, Ala527, Leu531, and Leu534, were observed in both protein complexes. Additionally, 5-F1a protein formed hydrogen bonds (HBs) with Tyr348, Tyr385, and Ser530, while 6-Y3C protein formed HBs with Arg120, Tyr355, Tyr385, and Ser353. Water-mediated hydrogen bonds were detected in 5-F1a with Arg120, Ile345, Tyr348, Tyr355, Tyr385, Val523, Ser530, and Met535, while in 6-Y3C protein, they were observed with His90, Arg120, Leu352, Ser353, and Ile523. Furthermore, ionic interactions were noted with Arg120 in 6-Y3C protein. Notably, the ligand exhibited intensive interactions with specific residues, including Arg120, Tyr248, Val349, Tyr385, Val523, and Ser530 in 5-F1a protein, and Arg120, Ser353, Tyr355, and Tyr385 in 6-Y3C protein.

In video-1 and video-2, the focus was specifically on highlighting the aromatic hydrogen bonds (AHBs) and hydrophobic interactions involving the 5-F1a protein complex. These interactions were visually represented as faded teal dashes and blue dashes, respectively, while other types of interactions were hidden to improve clarity. Notably, AHBs, hydrogen bonds (HBs), ionic interactions, and water mediated HBs were observed between the 4h ligand and specific amino acids, Ty355 and Arg120. These interactions indicate the stability of the bonds within the active site, without any breakage or loss.

The interaction continuity analysis revealed that in the 5-F1a complex, the interaction between 4h and Arg120 displayed H-bond strengths of 43%, while in the 6-Y3C complex, the corresponding interaction with Arg120 exhibited a higher H-bond strength of 96%. Additionally, in the 6-Y3C complex, the interactions between 4h and Tyr385, Tyr355, and Ser352 demonstrated interaction strengths of 99%, 85%, and 71%, respectively. These findings provide insights into the persistence and strength of the interactions between **4h** and specific residues within the complexes.

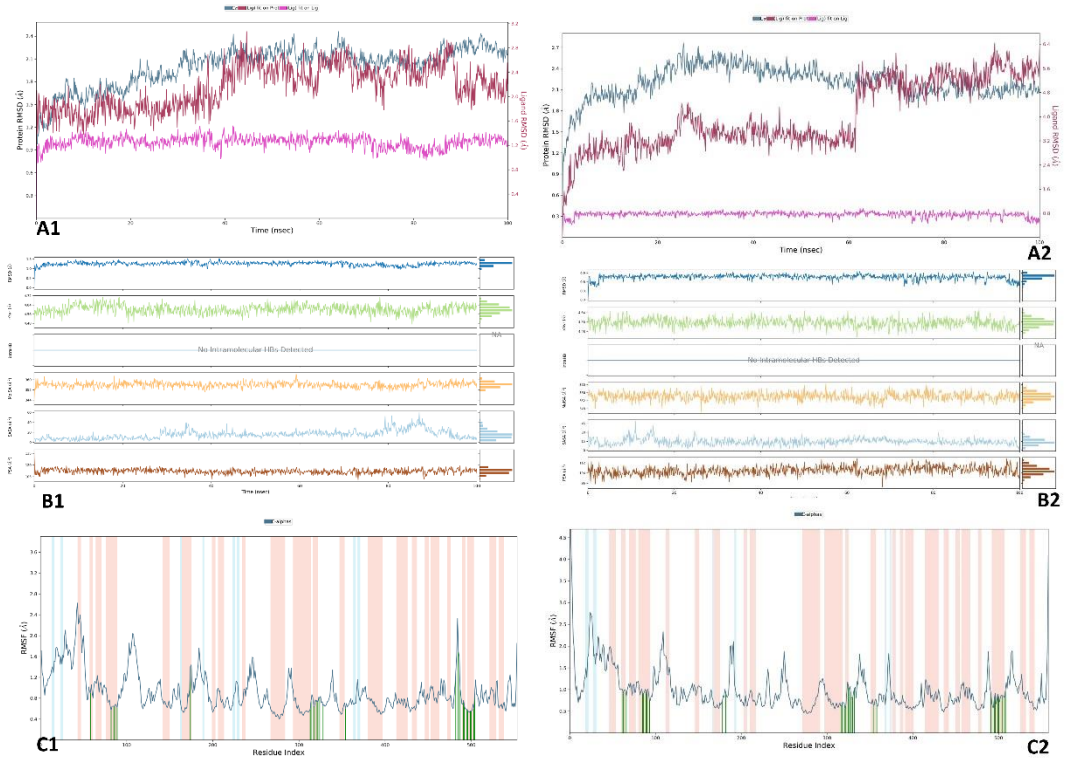

Figure 5.109. *The stability diagrams and ligand properties (RMSD, Rg, MolSA, SASA, PSA) of complexes **4h**, 6-Y3C-complex (A2, B2, C2), 5-F1a-complex (A1, B1, C1), and RMSF analysis*

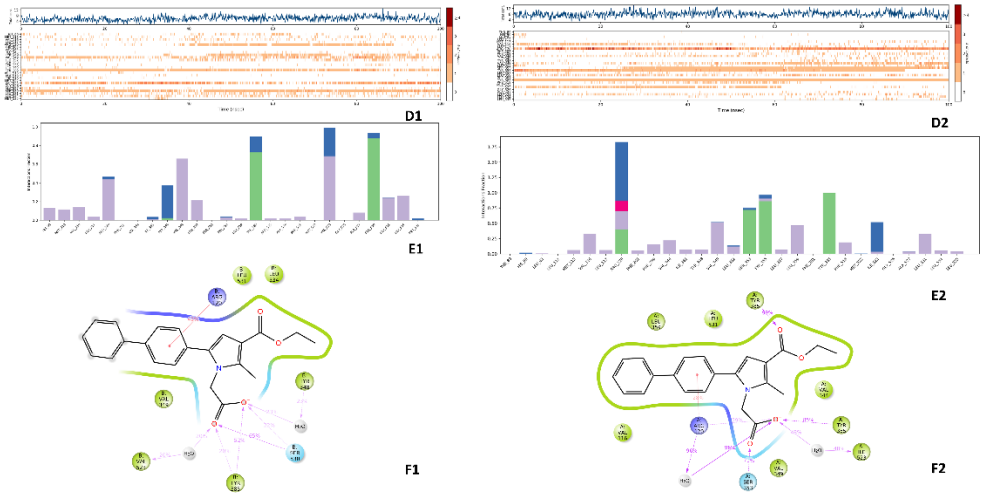

Figure 5.110. *The interaction diagrams of the complexes of 5-F1a (left) and 6-Y3C (right). D1, D2: The plot of total bond number-amino acid fraction during the simulation time; E1,E2: Types of interactions with the amino acids and their fraction graphic; F1,F2: The bond strength (cutoff=20%), respectively*

5.8. Structure-Activity Relationship Evaluation

Our study employed in vivo assays, FB-QSAR and molecular docking to elucidate the structure-activity relationship of our synthesized compounds. Our findings highlight the significant role of carboxylic acid in the activity of the compounds. This is due to its ability to form hydrogen bonds and salt bridges with essential amino acids like Arg120, Arg513, Tyr385, His90, Ser353, and Ser530 within the COX-1 and COX-2 enzyme active site. For instance, the acetic acid group at position 1 forms a hydrogen bond with Arg120, whereas the benzoic acid group at the same position forms a hydrogen bond with Ser530. Consequently, we observed that compounds with benzoic acid groups worked more effectively in COX-1, while those with acetic acid groups showed greater efficacy in COX-2. Moreover, the introduction of a withdrawing group on the phenyl ring at position 5 reduced the activity of the compounds against both COX-1 and COX-2, as observed in compounds **4f** and **4g**. Furthermore, our findings revealed that the inclusion of a hydroxy group at position 4 of hydroxybenzoic acid significantly enhances the potency of the compounds towards COX-1, as observed in compounds **5b** and **5e**. This increased potency can be attributed to the additional possibility of forming hydrogen bond interactions within the COX-1 active site. Conversely, when larger and more lipophilic groups such as OMe and Cl are introduced, as seen in compounds **5a**, **5f**, **5d**, and **5g**, the participate in hydrophobic interactions within the active site. Our investigation revealed that the most active compounds had large hydrophobic substitutes on the phenyl ring, such as phenyl substitution at position 4 in **4h** compound, OMe substitution at position 2 and 6 in **4g** compound, Cl substitution at position 3 and 4 in **4k**, naphthyl group in compound **4l**, all of which worked more effectively in COX-2 than COX-1. In contrast, withdrawing groups at position 4 such as NO_2 in compound **5e** and Cl group in compound **5b** made the compounds work more effectively in COX-1, likely due to their retention of hydrophobic character in the presence of benzoic acid substitution at position 1. Our study provides valuable insights into the factors that impact COX-2 inhibitor activity, aiding in the rational design of more potent inhibitors with improved selectivity and therapeutic efficacy. The SAR of synthetic compounds is summarized in Figure 5.111.

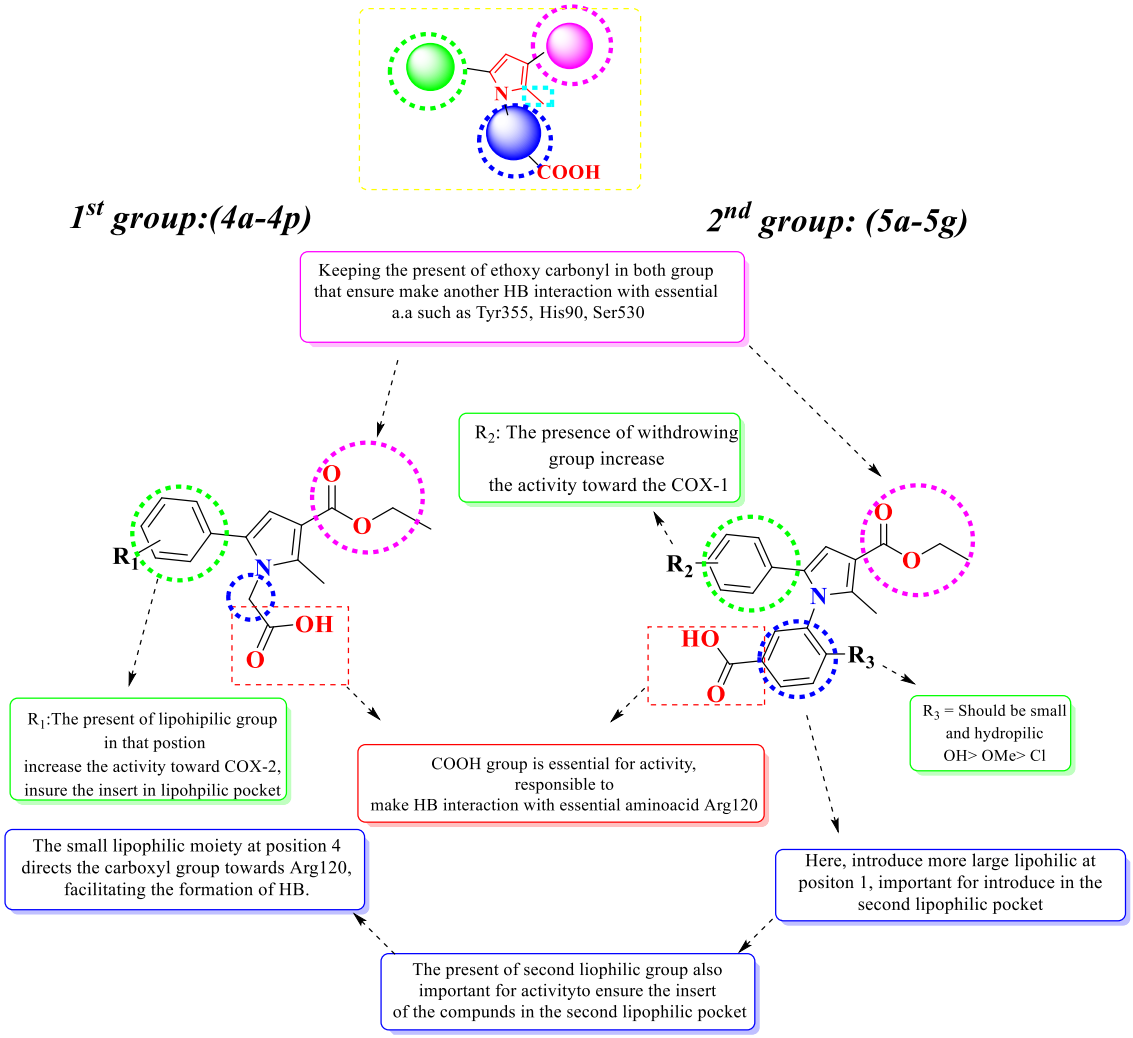

Figure 5.111. *Summery of the structure-activity relationship of synthesized compounds*

6. CONCLUSION AND FURTHER RECOMMENDATIONS

The present study involves the development of novel compounds based on pyrrole nucleus with potential anti-inflammatory activity. Inflammation is a biological response of the body to harmful stimuli such as pathogens, toxins, and damaged cells. However, uncontrolled or chronic inflammation can lead to the development of various diseases such as cancer, arthritis, and cardiovascular diseases. One of the key enzymes involved in the inflammatory response is cyclooxygenase (COX), which catalyzes the conversion of arachidonic acid to prostaglandins, which are important mediators of inflammation.

The aim of this study was to construct a bank of synthesizable compounds consisting of alkyl and aryl carboxylic acid derivatives with a pyrrole nucleus, and to screen them for potential anti-inflammatory activity using in vitro assays. The compounds were designed based on the structure-activity relationship (SAR) of known COX inhibitors and FB-QSAR techniques. The molecules bank was constructed by synthesizing different alkyl and aryl carboxylic acid derivatives of pyrrole nucleus using standard synthetic procedures. The synthesized compounds were then analyzed using various spectroscopic techniques such as HRMS, ^{1}H-NMR, and ^{13}C-NMR, to determine their structures and impurities. Next, the bank of molecules was screened using various QSAR parameters such as molecular weight, logP, and topological polar surface area (TPSA), to identify hit molecules and their analogues. The hit molecules were then synthesized and subjected to further spectroscopic analysis to determine their purity and structures. To evaluate the anti-inflammatory activity of the synthesized compounds, an inhibition study was carried out on COX enzymes. The study revealed that two compounds, **4g** and **4h**, inhibited both COX subtypes without selectivity, while **5e** and **5b** selectively inhibited COX-1, and **4k** and **4l** selectively inhibited COX-2. In general, the first group of compounds, which have acetic acid substitution in the first positions, exhibit activity in both COX-1 and COX-2. When the steric and lipophilicity of the group at position 5 are increased, as observed in compounds **4h**, **4g**, **4k**, and **4i**, the activity is enhanced towards COX-2. Conversely, when a hydrophilic group, such as in compound **4c**, is introduced, the activity decreases. As for the second group of compounds with substituted benzoic acid groups at position 1, these compounds tend to display higher activity towards COX-1. The presence of a small, hydrophilic group in the para position of the benzoic acid enhances the activity, especially if the group has a tendency to form hydrogen bonds. This trend can be observed in the compounds **5b**, **5e**, **5a**, and **5f**, where

the activity increases in that order. Similarly, at position 5, a more lipophilic and sterically bulky group leads to increased activity. This can be seen in the comparison of the 3,4-dichloro phenyl analogs (**5b, 5a, 5d**) and the 4-nitro phenyl analogs (**5e, 5f, 5g**), where the former exhibits higher activity. The findings of the study were further evaluated using molecular docking and dynamic simulation techniques. The results of the molecular docking studies revealed the binding modes of the compounds in the active site of COX enzymes and provided insights into the structure-activity relationship of the compounds. In conclusion, this study provides valuable insights into the potential of synthesizable compounds based on pyrrole nucleus as inhibitors of COX enzymes. The findings of this study could be useful in the development of new anti-inflammatory drugs with improved selectivity and efficacy. Furthermore, the methods used in this study, including QSAR and molecular docking, can be applied to the design and development of other bioactive compounds.

REFERENCES

[1] Feghali, C.A., Wright, T.M. (1997). Cytokines in acute and chronic inflammation. *Frontiers in Bioscience-Landmark,* 2 (4), 12-26.

[2] Mak, T.W., Saunders, M.E., Jett, B.D. (2013). *Primer to the immune response*. Newnes.

[3] Ahmed, A.U. (2011). An overview of inflammation: mechanism and consequences. *Frontiers in Biology,* 6 (4), 274.

[4] Allison, M.C., Howatson, A.G., Torrance, C.J., Lee, F.D., Russell, R.I. (1992). Gastrointestinal damage associated with the use of nonsteroidal antiinflammatory drugs. *New England Journal of Medicine,* 327 (11), 749-754.

[5] Fu, J.-Y., Masferrer, J., Seibert, K., Raz, A., Needleman, P. (1990). The induction and suppression of prostaglandin H2 synthase (cyclooxygenase) in human monocytes. *Journal of Biological Chemistry,* 265 (28), 16737-16740.

[6] Kujubu, D.A., Herschman, H. (1992). Dexamethasone inhibits mitogen induction of the TIS10 prostaglandin synthase/cyclooxygenase gene. *Journal of Biological Chemistry,* 267 (12), 7991-7994.

[7] Ristimäki, A., Garfinkel, S., Wessendorf, J., Maciag, T., Hla, T. (1994). Induction of cyclooxygenase-2 by interleukin-1 alpha. Evidence for post-transcriptional regulation. *Journal of Biological Chemistry,* 269 (16), 11769-11775.

[8] Everts, B., Währborg, P., Hedner, T. (2000). COX-2-Specific inhibitors–the emergence of a new class of analgesic and anti-inflammatory drugs. *Clinical rheumatology,* 19, 331-343.

[9] Brune, K., Patrignani, P. (2015). New insights into the use of currently available non-steroidal anti-inflammatory drugs. *Journal of pain research,* 105-118.

[10] McGettigan, P., Henry, D. (2006). Cardiovascular risk and inhibition of cyclooxygenase: a systematic review of the observational studies of selective and nonselective inhibitors of cyclooxygenase 2. *Jama,* 296 (13), 1633-1644.

[11] McGettigan, P., Henry, D. (2011). Cardiovascular risk with non-steroidal anti-inflammatory drugs: systematic review of population-based controlled observational studies. *PLoS medicine,* 8 (9), e1001098.

[12] Consalvi, S., Alfonso, S., Di Capua, A., Poce, G., Pirolli, A., Sabatino, M., Ragno, R., Anzini, M., Sartini, S., La Motta, C. (2015). Synthesis, biological evaluation and docking analysis of a new series of methylsulfonyl and sulfamoyl acetamides and ethyl acetates as potent COX-2 inhibitors. *Bioorganic & Medicinal Chemistry,* 23 (4), 810-820.

[13] Dannhardt, G., Kiefer, W. (2001). Cyclooxygenase inhibitors – current status and future prospects. *European Journal of Medicinal Chemistry,* 36 (2), 109-126.

[14] Lipsky, P. (1999). Specific COX-2 inhibitors in arthritis, oncology, and beyond: where is the science headed? *The Journal of rheumatology. Supplement,* 56, 25-30.

[15] Martelli, A., Breschi, M.C., Calderone, V. (2009). Pharmacodynamic hybrids coupling established cardiovascular mechanisms of action with additional nitric oxide releasing properties. *Current pharmaceutical design,* 15 (6), 614-636.

[16] Ali, S.L. (1982). Phenylbutazone, *Analytical profiles of drug substances* içinde (s. 483-521). Elsevier.

[17] Otterness, I.G. (1995). The discovery of drugs to treat arthritis: a historical view. *The search for anti-inflammatory drugs: case histories from concept to clinic*, 1-26.

[18] Rainsford, K. (2015). History and development of ibuprofen. *Ibuprofen: Discovery, Development and Therapeutics*, 1-21.
[19] Davis, A., Robson, J. (2016): The dangers of NSAIDs: look both ways. British Journal of General Practice, pp. 172-173.
[20] Luong, C., Miller, A., Barnett, J., Chow, J., Ramesha, C., Browner, M.F. (1996). Flexibility of the NSAID binding site in the structure of human cyclooxygenase-2. *Nature structural biology,* 3 (11), 927-933.
[21] Dogné, J.-M., Supuran, C.T., Pratico, D. (2005). Adverse cardiovascular effects of the coxibs. *Journal of medicinal chemistry,* 48 (7), 2251-2257.
[22] Han, W.B., Zhang, A.H., Deng, X.Z., Lei, X., Tan, R.X. (2016). Curindolizine, an Anti-Inflammatory Agent Assembled via Michael Addition of Pyrrole Alkaloids Inside Fungal Cells. *Organic letters,* 18 (8), 1816-1819.
[23] Bhattacharyya, P., Kishore Kumar, M., Narasu, L., Gundla, R., Samanta, S., Cuthbertson, C., Neamati, N. (2016). Designing novel MEK1 inhibitors as anticancer agents. *Int. J. Life Sci. Pharm. Res,* 6, 23-33.
[24] Dannhardt, G., Kiefer, W., Krämer, G., Maehrlein, S., Nowe, U., Fiebich, B. (2000). The pyrrole moiety as a template for COX-1/COX-2 inhibitors. *European Journal of Medicinal Chemistry,* 35 (5), 499-510.
[25] Tintori, C., Magnani, M., Schenone, S., Botta, M. (2009). Docking, 3D-QSAR studies and in silico ADME prediction on c-Src tyrosine kinase inhibitors. *Eur J Med Chem,* 44 (3), 990-1000.
[26] Nalamachu, S., Wortmann, R. (2014). Role of indomethacin in acute pain and inflammation management: a review of the literature. *Postgraduate medicine,* 126 (4), 92-97.
[27] Moore, M.E., Goldsmith, D.P. (1980). Nonsteroidal Anti-inflammatory Intolerance: An Anaphylactic Reaction to Tolmetin. *Archives of Internal Medicine,* 140 (8), 1105-1106.
[28] Bocheva, A., Bijev, A., Nankov, A. (2006). Further evaluation of a series of anti-inflammatory N-pyrrolylcarboxylic acids: effects on the nociception in rats. *Archiv der Pharmazie,* 339 (3), 141-144.
[29] Sammes, M.P., Katritzky, A.R. (1982). The 2H- and 3H-Pyrroles, A. R. Katritzky (Ed.), *Advances in Heterocyclic Chemistry* içinde (s. 233-284). Academic Press.
[30] Liberto, N.A., Simões, J.B., de Paiva Silva, S., da Silva, C.J., Modolo, L.V., de Fátima, Â., Silva, L.M., Derita, M., Zacchino, S., Zuñiga, O.M.P., Romanelli, G.P., Fernandes, S.A. (2017). Quinolines: Microwave-assisted synthesis and their antifungal, anticancer and radical scavenger properties. *Bioorganic & Medicinal Chemistry,* 25 (3), 1153-1162.
[31] Balme, G. (2004). Pyrrole syntheses by multicomponent coupling reactions. *Angewandte Chemie International Edition,* 43 (46), 6238-6241.
[32] Barton, D.H., Kervagoret, J., Zard, S.Z. (1990). A useful synthesis of pyrroles from nitroolefins. *Tetrahedron,* 46 (21), 7587-7598.
[33] Van Leusen, A., Siderius, H., Hoogenboom, B., van Leusen, D. (1972). A new and simple synthesis of the pyrrole ring system from Michael acceptors and tosylmethylisocyanides. *Tetrahedron Letters,* 13 (52), 5337-5340.
[34] Milgram, B.C., Eskildsen, K., Richter, S.M., Scheidt, W.R., Scheidt, K.A. (2007). Microwave-assisted Piloty− Robinson synthesis of 3, 4-disubstituted pyrroles. *The Journal of organic chemistry,* 72 (10), 3941-3944.
[35] Knorr, L. (1885): Ber. 1884, 17, 1635.(b) Paal, C. Ber.

[36] Wang, S.-F., Guo, C.-L., Cui, K.-k., Zhu, Y.-T., Ding, J.-X., Zou, X.-Y., Li, Y.-H. (2015). Lactic acid as an invaluable green solvent for ultrasound-assisted scalable synthesis of pyrrole derivatives. *Ultrasonics Sonochemistry,* 26, 81-86.
[37] Leonardi, M., Estévez, V., Villacampa, M., Menéndez, J.C. (2019). The Hantzsch pyrrole synthesis: Non-conventional variations and applications of a neglected classical reaction. *Synthesis,* 51 (04), 816-828.
[38] Amarnath, V., Anthony, D.C., Amarnath, K., Valentine, W.M., Wetterau, L.A., Graham, D.G. (1991). Intermediates in the Paal-Knorr synthesis of pyrroles. *The Journal of Organic Chemistry,* 56 (24), 6924-6931.
[39] Tzankova, D., Vladimirova, S., Peikova, L., Georgieva, M. (2018). Synthesis of pyrrole and substituted pyrroles. *Journal of Chemical Technology & Metallurgy,* 53 (3)
[40] Kurti, L., Czakó, B. (2005). *Strategic applications of named reactions in organic synthesis*. Elsevier.
[41] Ma, Z., Ma, Z., Zhang, D. (2018). Synthesis of multi-substituted pyrrole derivatives through [3+ 2] cycloaddition with tosylmethyl isocyanides (TosMICs) and electron-deficient compounds. *Molecules,* 23 (10), 2666.
[42] Jeelan Basha, N., Basavarajaiah, S., Shyamsunder, K. (2022). Therapeutic potential of pyrrole and pyrrolidine analogs: an update. *Molecular Diversity,* 26 (5), 2915-2937.
[43] Lang, K.D., Kaur, R., Arora, R., Saini, B., Arora, S. (2020). Nitrogen-Containing Heterocycles as Anticancer Agents: An Overview. *Anti-Cancer Agents in Medicinal Chemistry,* 20 (18), 2150-2168.
[44] Bürli, R.W., McMinn, D., Kaizerman, J.A., Hu, W., Ge, Y., Pack, Q., Jiang, V., Gross, M., Garcia, M., Tanaka, R., Moser, H.E. (2004). DNA binding ligands targeting drug-resistant Gram-positive bacteria. Part 1: Internal benzimidazole derivatives. *Bioorganic & Medicinal Chemistry Letters,* 14 (5), 1253-1257.
[45] Vieta, E., Montes, J.M. (2018). A Review of Asenapine in the Treatment of Bipolar Disorder. *Clinical Drug Investigation,* 38 (2), 87-99.
[46] de Wispelaere, M., Du, G., Donovan, K.A., Zhang, T., Eleuteri, N.A., Yuan, J.C., Kalabathula, J., Nowak, R.P., Fischer, E.S., Gray, N.S., Yang, P.L. (2019). Small molecule degraders of the hepatitis C virus protease reduce susceptibility to resistance mutations. *Nature Communications,* 10 (1), 3468.
[47] Toja, E., Selva, D., Schiatti, P. (1984). 3-Alkyl-2-aryl-3H-naphth[1,2-d]imidazoles, a novel class of nonacidic antiinflammatory agents. *Journal of Medicinal Chemistry,* 27 (5), 610-616.
[48] Fokoun, C., Serrier, H., Rabier, H., Goutelle, S., Tod, M., Bourguignon, L. (2021). Pharmacogenetic-guided glimepiride therapy in type-2 diabetes mellitus: a cost-effectiveness study. *The Pharmacogenomics Journal,* 21 (5), 559-565.
[49] Lehuédé, J., Fauconneau, B., Barrier, L., Ourakow, M., Piriou, A., Vierfond, J.-M. (1999). Synthesis and antioxidant activity of new tetraarylpyrroles. *European Journal of Medicinal Chemistry,* 34 (11), 991-996.
[50] Del Poeta, M., Schell, W.A., Dykstra, C.C., Jones, S., Tidwell, R.R., Czarny, A., Bajic, M., Bajic, M., Kumar, A., Boykin, D. (1998). Structure-in vitro activity relationships of pentamidine analogues and dication-substituted bis-benzimidazoles as new antifungal agents. *Antimicrobial agents and chemotherapy,* 42 (10), 2495-2502.
[51] Wang, S., Meng, X., Wang, Y., Liu, Y., Xia, J. (2019). HPO-Shuffle: an associated gene prioritization strategy and its application in drug repurposing for the treatment of canine epilepsy. *Bioscience Reports,* 39 (9)

[52] Januario, J.P., De Souza, T.B., Lavorato, S.N., Maiolini, T.C.S., Domingos, O.S., Baldim, J.L., Folquitto, L.R.S., Soares, M.G., Chagas-Paula, D.A., Dias, D.F., Dos Santos, M.H. (2018). Design and Synthesis of New Benzophenone Derivatives with In Vivo Anti-Inflammatory Activity through Dual Inhibition of Edema and Neutrophil Recruitment. *Molecules,* 23 (8), 1859.
[53] Khanum, S.A., Shashikanth, S., Deepak, A.V. (2004). Synthesis and anti-inflammatory activity of benzophenone analogues. *Bioorganic Chemistry,* 32 (4), 211-222.
[54] Küçükgüzel, Ş.G., Küçükgüzel, İ., Tatar, E., Rollas, S., Şahin, F., Güllüce, M., De Clercq, E., Kabasakal, L. (2007). Synthesis of some novel heterocyclic compounds derived from diflunisal hydrazide as potential anti-infective and anti-inflammatory agents. *European Journal of Medicinal Chemistry,* 42 (7), 893-901.
[55] Al Mekhlafi, S., Alkadi, H., El-Sayed, M.-I.K. (2015). Synthesis and anti-inflammatory activity of novel Ketoprofen and Ibuprofen derivatives. *J. Chem. Pharm. Res,* 7 (2), 503-510.
[56] Bekhit, A.A., Fahmy, H.T., Rostom, S.A., Baraka, A.M. (2003). Design and synthesis of some substituted 1H-pyrazolyl-thiazolo [4, 5-d] pyrimidines as anti-inflammatory–antimicrobial agents. *European journal of medicinal chemistry,* 38 (1), 27-36.
[57] Bandgar, B.P., Adsul, L.K., Chavan, H.V., Jalde, S.S., Shringare, S.N., Shaikh, R., Meshram, R.J., Gacche, R.N., Masand, V. (2012). Synthesis, biological evaluation, and docking studies of 3-(substituted)-aryl-5-(9-methyl-3-carbazole)-1H-2-pyrazolines as potent anti-inflammatory and antioxidant agents. *Bioorganic & medicinal chemistry letters,* 22 (18), 5839-5844.
[58] Zhang, Z., Cao, P., Fang, M., Zou, T., Han, J., Duan, Y., Xu, H., Yang, X., Li, Q.-S. (2021). Design, synthesis, and SAR study of novel 4,5-dihydropyrazole-Thiazole derivatives with anti-inflammatory activities for the treatment of sepsis. *European Journal of Medicinal Chemistry,* 225, 113743.
[59] Abdelall, E.K.A., Lamie, P.F., Ahmed, A.K.M., El-Nahass, E.L.S. (2019). COX-1/COX-2 inhibition assays and histopathological study of the new designed anti-inflammatory agent with a pyrazolopyrimidine core. *Bioorganic Chemistry,* 86, 235-253.
[60] Lynch, D.E., Hayer, R., Beddows, S., Howdle, J., Thake, C.D. (2006). Synthesis and activity of four (N, N-dimethylamino) benzamide nonsteroidal anti-inflammatory drugs based on thiazole and thiazoline. *Journal of heterocyclic chemistry,* 43 (1), 191-197.
[61] Ukrainets, I.V., Burian, A.A., Hamza, G.M., Voloshchuk, N.I., Malchenko, O.V., Shishkina, S.V., Sidorenko, L.V., Burian, K.O., Sim, G. (2019). Synthesis and Regularities of the Structure–Activity Relationship in a Series of N-Pyridyl-4-methyl-2,2-dioxo-1H-2λ6,1-benzothiazine-3-carboxamides. *Scientia Pharmaceutica,* 87 (2), 12.
[62] Szczęśniak-Sięga, B.M., Wiatrak, B., Czyżnikowska, Ż., Janczak, J., Wiglusz, R.J., Maniewska, J. (2021). Synthesis and biological evaluation as well as in silico studies of arylpiperazine-1,2-benzothiazine derivatives as novel anti-inflammatory agents. *Bioorganic Chemistry,* 106, 104476.
[63] Bergqvist, F., Morgenstern, R., Jakobsson, P.J. (2020). A review on mPGES-1 inhibitors: From preclinical studies to clinical applications. *Prostaglandins Other Lipid Mediat,* 147, 106383.
[64] Arhancet, G.B., Walker, D.P., Metz, S., Fobian, Y.M., Heasley, S.E., Carter, J.S., Springer, J.R., Jones, D.E., Hayes, M.J., Shaffer, A.F., Jerome, G.M., Baratta,

M.T., Zweifel, B., Moore, W.M., Masferrer, J.L., Vazquez, M.L. (2013). Discovery and SAR of PF-4693627, a potent, selective and orally bioavailable mPGES-1 inhibitor for the potential treatment of inflammation. *Bioorganic and Medicinal Chemistry Letters,* 23 (4), 1114-1119.
[65] Kim, M., Lee, S., Park, E.B., Kim, K.J., Lee, H.H., Shin, J.-S., Fischer, K., Koeberle, A., Werz, O., Lee, K.-T. (2016). Hit-to-lead optimization of phenylsulfonyl hydrazides for a potent suppressor of PGE2 production: Synthesis, biological activity, and molecular docking study. *Bioorganic & medicinal chemistry letters,* 26 (1), 94-99.
[66] Park, E.B., Kim, K.J., Jeong, H.R., Lee, J.K., Kim, H.J., Lee, H.H., Lim, J.W., Shin, J.-S., Koeberle, A., Werz, O., Lee, K.-T., Lee, J.Y. (2016). Synthesis, structure determination, and biological evaluation of phenylsulfonyl hydrazide derivatives as potential anti-inflammatory agents. *Bioorganic & Medicinal Chemistry Letters,* 26 (21), 5193-5197.
[67] Kamat, V., Santosh, R., Poojary, B., Nayak, S.P., Kumar, B.K., Sankaranarayanan, M., Faheem, Khanapure, S., Barretto, D.A., Vootla, S.K. (2020). Pyridine- and Thiazole-Based Hydrazides with Promising Anti-inflammatory and Antimicrobial Activities along with Their In Silico Studies. *ACS Omega,* 5 (39), 25228-25239.
[68] M, P.H., Al-Ostoot, F.H., Vivek, H.K., Khanum, S.A. (2022). Design, docking, synthesis, and characterization of novel N'(2-phenoxyacetyl) nicotinohydrazide and N'(2-phenoxyacetyl)isonicotinohydrazide derivatives as anti-inflammatory and analgesic agents. *Journal of Molecular Structure,* 1247, 131404.
[69] Sahu, S., Panda, S.S., Asiri, A.M., Katritzky, A.R. (2013). NSAID conjugates with carnosine and amino acids. *Synthesis,* 45 (24), 3369-3374.
[70] Mahfouz, N.M., Omar, F.A., Aboul-Fadl, T. (1999). Cyclic amide derivatives as potential prodrugs II: N-hydroxymethylsuccinimide- / isatin esters of some NSAIDs as prodrugs with an improved therapeutic index. *European Journal of Medicinal Chemistry,* 34 (7), 551-562.
[71] Hayashi, S., Ueno, N., Murase, A., Nakagawa, Y., Takada, J. (2012). Novel acid-type cyclooxygenase-2 inhibitors: Design, synthesis, and structure–activity relationship for anti-inflammatory drug. *European Journal of Medicinal Chemistry,* 50, 179-195.
[72] Reale, A., Brogi, S., Chelini, A., Paolino, M., Di Capua, A., Giuliani, G., Cappelli, A., Giorgi, G., Chemi, G., Grillo, A. (2019). Synthesis, biological evaluation and molecular modeling of novel selective COX-2 inhibitors: sulfide, sulfoxide, and sulfone derivatives of 1, 5-diarylpyrrol-3-substituted scaffold. *Bioorganic & Medicinal Chemistry,* 27 (19), 115045.
[73] Szczukowski, Ł., Krzyżak, E., Zborowska, A., Zając, P., Potyrak, K., Peregrym, K., Wiatrak, B., Marciniak, A., Świątek, P. (2020). Design, synthesis and comprehensive investigations of pyrrolo [3, 4-d] pyridazinone-based 1, 3, 4-oxadiazole as new class of selective cox-2 inhibitors. *International Journal of Molecular Sciences,* 21 (24), 9623.
[74] Harrak, Y., Rosell, G., Daidone, G., Plescia, S., Schillaci, D., Pujol, M. (2007). Synthesis and biological activity of new anti-inflammatory compounds containing the 1, 4-benzodioxine and/or pyrrole system. *Bioorganic & medicinal chemistry,* 15 (14), 4876-4890.
[75] Paprocka, R., Pazderski, L., Mazur, L., Wiese-Szadkowska, M., Kutkowska, J., Nowak, M., Helmin-Basa, A. (2022). Synthesis and Structural Study of Amidrazone

Derived Pyrrole-2,5-Dione Derivatives: Potential Anti-Inflammatory Agents. *Molecules,* 27 (9), 2891.
[76] Joseph, M., Muchowski, S., Unger, T., Ackrell, J., Cheung, P. (1985). Synthesis and anti-inflammatory and analgesic activity of 5-aroyl-1, 2-dihydro-3H-pyrrolo [1, 2-a] pyrrole-1-carboxylic acids and related compounds. *Med. Chem,* 28, 1037.
[77] Said Fatahala, S., Hasabelnaby, S., Goudah, A., Mahmoud, G.I., Helmy Abd-El Hameed, R. (2017). Pyrrole and Fused Pyrrole Compounds with Bioactivity against Inflammatory Mediators. *Molecules*, 22 (3), 461.
[78] Faudzi, S.M.M., Abdullah, M.A., Manap, M.R.A., Ismail, A.Z., Rullah, K., Aluwi, M.F.F.M., Ramli, A.N.M., Abas, F., Lajis, N.H. (2020). Inhibition of nitric oxide and prostaglandin E2 production by pyrrolylated-chalcones: Synthesis, biological activity, crystal structure analysis, and molecular docking studies. *Bioorganic Chemistry,* 94, 103376.
[79] Wilkerson, W.W., Galbraith, W., Gans-Brangs, K., Grubb, M., Hewes, W.E., Jaffee, B., Kenney, J., Kerr, J., Wong, N. (1994). Antiinflammatory 4, 5-diarylpyrroles: synthesis and QSAR. *Journal of medicinal chemistry,* 37 (7), 988-998.
[80] Wilkerson, W.W., Copeland, R.A., Covington, M., Trzaskos, J.M. (1995). Antiinflammatory 4, 5-diarylpyrroles. 2. Activity as a function of cyclooxygenase-2 inhibition. *Journal of medicinal chemistry,* 38 (20), 3895-3901.
[81] Khanna, I.K., Weier, R.M., Yu, Y., Collins, P.W., Miyashiro, J.M., Koboldt, C.M., Veenhuizen, A.W., Currie, J.L., Seibert, K., Isakson, P.C. (1997). 1, 2-Diarylpyrroles as potent and selective inhibitors of cyclooxygenase-2. *Journal of medicinal chemistry,* 40 (11), 1619-1633.
[82] Battilocchio, C., Poce, G., Alfonso, S., Porretta, G.C., Consalvi, S., Sautebin, L., Pace, S., Rossi, A., Ghelardini, C., Di Cesare Mannelli, L., Schenone, S., Giordani, A., Di Francesco, L., Patrignani, P., Biava, M. (2013). A class of pyrrole derivatives endowed with analgesic/anti-inflammatory activity. *Bioorganic & Medicinal Chemistry,* 21 (13), 3695-3701.
[83] Redzicka, A., Czyżnikowska, Ż., Wiatrak, B., Gębczak, K., Kochel, A. (2021). Design and synthesis of N-substituted 3, 4-pyrroledicarboximides as potential anti-inflammatory agents. *International journal of molecular sciences,* 22 (3), 1410.
[84] Salum, L.B., Andricopulo, A.D. (2010). Fragment-based QSAR strategies in drug design. *Expert Opinion on Drug Discovery,* 5 (5), 405-412.
[85] Chirico, N., Gramatica, P. (2011). Real External Predictivity of QSAR Models: How To Evaluate It? Comparison of Different Validation Criteria and Proposal of Using the Concordance Correlation Coefficient. *Journal of Chemical Information and Modeling,* 51 (9), 2320-2335.
[86] Biovision COX-1 Fluorescent Inhibitor Screening Kit (Catalog No: K548-100) manual.
[87] Schrödinger, Glide, Schrödinger, LLC, New York, NY, USA, 2020 .
[88] Maestro, Schrödinger, LLC: New York, NY, USA, (2020).
[89] Miciaccia, M., Belviso, B.D., Iaselli, M., Cingolani, G., Ferorelli, S., Cappellari, M., Loguercio Polosa, P., Perrone, M.G., Caliandro, R., Scilimati, A. (2021). Three-dimensional structure of human cyclooxygenase (hCOX)-1. *Scientific Reports,* 11 (1), 4312.
[90] Madhavi Sastry, G., Adzhigirey, M., Day, T., Annabhimoju, R., Sherman, W. (2013). Protein and ligand preparation: parameters, protocols, and influence on virtual screening enrichments. *Journal of Computer-Aided Molecular Design,* 27 (3), 221-234.

[91] Sherman, W., Day, T., Jacobson, M.P., Friesner, R.A., Farid, R. (2006). Novel Procedure for Modeling Ligand/Receptor Induced Fit Effects. *Journal of Medicinal Chemistry*, 49 (2), 534-553.
[92] Harmalkar, A., Mahajan, S.P., Gray, J.J. (2022). Induced fit with replica exchange improves protein complex structure prediction. *PLoS computational biology*, 18 (6), e1010124.
[93] Friesner, R.A., Murphy, R.B., Repasky, M.P., Frye, L.L., Greenwood, J.R., Halgren, T.A., Sanschagrin, P.C., Mainz, D.T. (2006). Extra Precision Glide: Docking and Scoring Incorporating a Model of Hydrophobic Enclosure for Protein−Ligand Complexes. *Journal of Medicinal Chemistry*, 49 (21), 6177-6196.
[94] Halgren, T.A., Murphy, R.B., Friesner, R.A., Beard, H.S., Frye, L.L., Pollard, W.T., Banks, J.L. (2004). Glide: A New Approach for Rapid, Accurate Docking and Scoring. 2. Enrichment Factors in Database Screening. *Journal of Medicinal Chemistry*, 47 (7), 1750-1759.
[95] Release, S. (2017). 3: Desmond molecular dynamics system, DE Shaw research, New York, NY, 2017. *Maestro-Desmond Interoperability Tools, Schrödinger, New York, NY*,
[96] DiMasi, J.A., Grabowski, H.G., Hansen, R.W. (2016). Innovation in the pharmaceutical industry: new estimates of R&D costs. *Journal of health economics*, 47, 20-33.
[97] van de Waterbeemd, H. (2009). Improving Compound Quality through in vitro and in silico Physicochemical Profiling. *Chemistry & Biodiversity*, 6 (11), 1760-1766.
[98] Sağlık, B.N., Osmaniye, D., Levent, S., Çevik, U.A., Çavuşoğlu, B.K., Özkay, Y., Kaplancıklı, Z.A. (2021). Design, synthesis and biological assessment of new selective COX-2 inhibitors including methyl sulfonyl moiety. *European Journal of Medicinal Chemistry*, 209, 112918.
[99] Osmaniye, D., Evren, A.E., Karaca, Ş., Özkay, Y., Kaplancıklı, Z.A. (2023). Novel thiadiazol derivatives; design, synthesis, biological activity, molecular docking and molecular dynamics. *Journal of Molecular Structure*, 1272, 134171.
[100] Glish, G.L., Vachet, R.W. (2003). The basics of mass spectrometry in the twenty-first century. *Nature reviews drug discovery*, 2 (2), 140-150.
[101] Ferreira, E.F.B., Silva, L.B., Costa, G.V., Costa, J.S., Fujishima, M.A.T., Leão, R.P., Ferreira, A.L.S., Federico, L.B., Silva, C.H.T.P., Rosa, J.M.C., Macêdo, W.J.C., Santos, C.B.R. (2019). Identification of New Inhibitors with Potential Antitumor Activity from Polypeptide Structures via Hierarchical Virtual Screening. *Molecules*, 24 (16), 2943.
[102] Press, S. (2012): QikProp 3.5 User Manual QikProp User Manual. Schrödinger Press: New York, NY, USA.
[103] Ogata, K., Hatakeyama, M., Nakamura, S. (2018). Effect of Atomic Charges on Octanol–Water Partition Coefficient Using Alchemical Free Energy Calculation. *Molecules*, 23 (2), 425.
[104] Bennion, B.J., Be, N.A., McNerney, M.W., Lao, V., Carlson, E.M., Valdez, C.A., Malfatti, M.A., Enright, H.A., Nguyen, T.H., Lightstone, F.C., Carpenter, T.S. (2017). Predicting a Drug's Membrane Permeability: A Computational Model Validated With in Vitro Permeability Assay Data. *The Journal of Physical Chemistry B*, 121 (20), 5228-5237.
[105] Lipinski, C.A., Lombardo, F., Dominy, B.W., Feeney, P.J. (2001). Experimental and computational approaches to estimate solubility and permeability in drug discovery and development settings1PII of original article: S0169-409X(96)00423-1. The article

was originally published in Advanced Drug Delivery Reviews 23 (1997) 3–25.1. *Advanced Drug Delivery Reviews*, 46 (1), 3-26.
[106] Chagas, C.M., Moss, S., Alisaraie, L. (2018). Drug metabolites and their effects on the development of adverse reactions: Revisiting Lipinski's Rule of Five. *International Journal of Pharmaceutics*, 549 (1), 133-149.
[107] Flower, R.J. (2003). The development of COX2 inhibitors. *Nature Reviews Drug Discovery*, 2 (3), 179-191.
[108] Gierse, J.K., McDonald, J.J., Hauser, S.D., Rangwala, S.H., Koboldt, C.M., Seibert, K. (1996). A single amino acid difference between cyclooxygenase-1 (COX-1) and− 2 (COX-2) reverses the selectivity of COX-2 specific inhibitors. *Journal of Biological Chemistry*, 271 (26), 15810-15814.
[109] Wong, E., Bayly, C., Waterman, H.L., Riendeau, D., Mancini, J.A. (1997). Conversion of prostaglandin G/H synthase-1 into an enzyme sensitive to PGHS-2-selective inhibitors by a double His513→ Arg and Ile523→ Val mutation. *Journal of Biological Chemistry*, 272 (14), 9280-9286.
[110] Shamsudin, Y., Gutiérrez-de-Terán, H., Boukharta, L., Åqvist, J. (2014). Toward an Optimal Docking and Free Energy Calculation Scheme in Ligand Design with Application to COX-1 Inhibitors. *Journal of Chemical Information and Modeling*, 54 (5), 1488-1499.
[111] Md Idris, M., Amin, S., Selvaraj, M., Jamari, H., Kek, T. (2018). High-throughput structure-based drug design of chalcones scaffolds as dual inhibitor of cyclooxygenase-2 and microsomal prostaglandin E synthase-1. *J Pharm Sci Emerg Drugs*, 6 (1), 1-14.
[112] Velázquez-Libera, J.L., Durán-Verdugo, F., Valdés-Jiménez, A., Núñez-Vivanco, G., Caballero, J. (2020). LigRMSD: a web server for automatic structure matching and RMSD calculations among identical and similar compounds in protein-ligand docking. *Bioinformatics*, 36 (9), 2912-2914.
[113] Lucido, M.J., Orlando, B.J., Vecchio, A.J., Malkowski, M.G. (2016). Crystal Structure of Aspirin-Acetylated Human Cyclooxygenase-2: Insight into the Formation of Products with Reversed Stereochemistry. *Biochemistry*, 55 (8), 1226-1238.